LNGS/EXP-01/04
March 2004

INFN

ANNUAL REPORT 2003

Laboratori Nazionali del Gran Sasso

Annual Report 2003

The Gran Sasso National Laboratory

The Gran Sasso National Laboratory (LNGS) is the largest underground laboratory in the world for experiments in particle and astroparticle physics. It is one of four INFN national laboratories and it is used as a worldwide facility by scientists (presently 750 in number) from 24 countries.
Its location is between the towns of L'Aquila and Teramo, about 120 km from Rome. The underground facilities are located on a side of the ten kilometres long freeway tunnel crossing the Gran Sasso Mountain. They consist of three large experimental halls, each about 100 m long, 20 m wide and 15 m high and service tunnels for a total volume of about 180,000 cubic metres.
The average 1400 m rock coverage gives a reduction factor of one million in the cosmic ray flux; moreover, the neutron flux is thousand times less than on the surface, thanks to the smallness of the Uranium and Thorium content of the dolomite rocks of the mountain.
The headquarters and the support facilities including the general electric and safety service, library and meeting halls, canteen, computing and networking services, mechanical, electronic and chemical shops, low activity service, assembly halls, offices and administration department are located on the surface. The mission of the Laboratory is to host experiments that require a low background environment in the field of astroparticle physics and nuclear astrophysics and other disciplines that can profit of its characteristics and of its infrastructures. The geographical location (inside the National Park of Gran Sasso - Monti della Laga) and the special operating conditions (underground, near a highway tunnel and in close proximity to water basins) demand that special attention is paid to the safety and environmental aspects of their activities.

Main research topics of the present scientific programme are: neutrino physics with neutrinos naturally produced in the Sun and in Supernova explosion and neutrino oscillations with a beam from CERN (CNGS program), search for neutrino mass in neutrino less double beta decays, dark matter search, nuclear reactions of astrophysical interest.

The activity in the year 2003 has been affected by the particular situation created by the accident of August 2002.
The history. On August 16^{th} 2002 the Borexino Group in the Hall C of LNGS by a series of unfortunate mistakes leaked 50 liters of pseudocumene in the external environment. The accident happened in the tense atmosphere of the extremely hot local debate about the safety tunnel project. No damage was caused but the potential damage was enough to rise juridical problems. In October 2002 the Borexino detector was sequestrated by the prosecuting magistrate of Teramo. In the mean time due to information which threw strong doubts upon the water-tightness of the draining system of the Gran Sasso laboratory the entire Hall C was placed under judicial attachment.

On June 17^{th} 2003, the competent Court of the city of Teramo indeed admitted the Infn request, allowing thus the restart of scientific activities within the underground Hall C. Researchers has been able to resume the preparation of the Opera experiment, aimed at the detection and study of the neutrino beam to be sent from Cern to the Gran Sasso Laboratories. The decision of the Court recognized the importance of the CNGS program.

Radical and urgent technical intervention decided by the government authorities at the end of July 2003 are enabling the continuation of the activities of the Laboratories, we hope in an atmosphere of total trust between researchers and nearby inhabitants.

Solar neutrino physics is one of the main research sectors of the laboratory. The GALLEX experiment, completed in 1997, has given fundamental results in particle physics and astrophysics, showing a relevant deficit in the solar electron neutrino flux at low energy unexplanable in terms of standard solar and subnuclear physics, an observation that contributed to the discovery of neutrino oscillations. This phenomenon implies that neutrinos have non-zero masses and that leptonic charges are not always conserved. For the first time we have evidence of new physics, beyond the standard model. GNO, the successor of GALLEX, with improved technique continues the measurement, gradually improving the resolution. GNO had collected 1713 days of live time pushing the systematic uncertainty to 4.0%.

Borexino is dedicated mainly to the measure of the Be line component of the solar neutrino spectrum. The construction of the main detector and of its ancillary facilities, almost completed at the moment of the August 2002 accident, is restarting now (beginning of 2004).

The solar models are based on data and extrapolations; in particular the thermonuclear cross sections of the involved reactions are not measured in the relevant energy range but rather extrapolated from higher energies. The direct measurements are made very difficult by the very low values of the cross sections. Using the new 400 kV accelerator, LUNA measured the cross section of the reaction ^{14}N $(p,\gamma)^{15}$O down to the energy of the nucleosynthesis in the stars. This is the slowest reaction in the CNO cycle and, as such determines the contribution of this cycle to solar burning and neutrino production. The LUNA results suggest a new estimate of age of the globular clusters, which are the oldest stars in the Galaxy.

The detection of low energy neutrinos from the gravitational collapse of galactic objects is the major purpose of the LVD (Large Volume Detector) experiment; the experiment is continuously monitoring the galaxies with its 1000 tons of liquid scintillator.

Elementary particles are different from their antiparticles because their charges - not only the electric one, but all of them - are opposite. The standard model assumes that neutrinos have only one charge, the lepton number. But, if this charge is not conserved, neutrinos and antineutrinos can be two states of the same particle. In this case well-specified nuclides would decay through the neutrino-less double beta channel. The Laboratory hosts experiments searching for these very rare decays, employing different and complementary techniques.

The Heidelberg-Moscow experiment with a sensitive mass of 11 kg of enriched ^{76}Ge is the most sensitive experiment in the world and has accumulated extremely interesting data until the end of november 2003.

The second most sensitive experiment on a different isotope in the world was MIBETA

that employed an array of 20 thermal detectors, based on TeO_2 crystals (340 g natural tellurium each). The experiment was completed in 2002 with a total exposure of 0.98 kg yr of ^{130}Te. Its place has been taken by CUORICINO, which employs larger TeO_2 bolometers (750 g natural tellurium each). The installation of the detectors was completed and data taking started in 2003.

From astronomical observations, we know that about 80% of the matter in the Universe is not made of nuclei and electrons as normal matter. It is called dark matter, because it does not emit light, and its nature is unknown. Probably, its constituents are not yet discovered elementary particles that interact only very weakly with the rest (they are called WIMPs). They are around us, invisible, waiting to be discovered. The search for WIMPs is very difficult and requires a very low background environment and the development of advanced background reduction techniques. The search is going on in many experiments worldwide. At Gran Sasso several experiments, using different techniques, are active.

DAMA employed NaI crystals to detect the WIMPs by means of the flash of light produced in the detector by an Iodine nucleus recoiling after having been hit by a WIMP, a very rare phenomenon. To distinguish these events from the background, DAMA searched for an annual modulation of the rate, a behaviour that has several aspects that are peculiar of the searched effect and not of the main backgrounds. With its about 100 kg sensitive mass DAMA was the only experiment world wide sensitive to the annual modulation signature. After the conclusion of the experiment, results were published confirming a signal of annual modulation. The larger experiment LIBRA, with 250 kg sensitive mass, has been preliminarly put in operation during 2003.

CRESST searches for WIMPs with a cryogenic technique, looking for a very tiny temperature increase in the detector, due to the energy deposited by nuclei hit by the WIMPs. After the final design of the CRESST2 $CaWO_2$ detector, it has been installed at the beginning of 2003. The GENIUS project proposes the use of one ton enriched Germanium with a strong reduction of the background for dark matter searches, double beta decay and other searches. A small test facility GENIUS-TF has been approved so far, with 40 kg of natural Germanium operated in liquid Nitrogen. Its installation has been completed.

One of the major commitments of the Gran Sasso laboratory in the next decennium will be the search of tau neutrino (and possibly electron neutrino) appearance on an artificial neutrino beam being built at CERN in Geneva, the CERN Neutrinos to Gran Sasso (CNGS) project. The beam will be directed through the Earth crust to two detector located in Gran Sasso at 732 km distance. Beam and experiments are foreseen to be ready in 2006.

The OPERA experiment is designed for the direct observation of tau neutrinos resulting from oscillations of the muon neutrino of the beam. This search requires both micrometer scale resolution, obtained with modern emulsion techniques and large sensitive mass (1800 t) obtained with Pb sheets interleaved by emulsion layers. In 2003 the installation in Hall C has started and proceedes regularly.

ICARUS is a general-purpose detector, with a broad physics programme, not limited to the CNGS project. It was proposed in 1985 based on the novel concept of the liquid Argon time-projection chamber. A first 300 t semi-module had been successfully operated on the

surface in Pavia in the summer 2001. After the development of the "definitive project" and of the risk analysis, completed in 2003, the 600 ton module is now ready for the installation in the LNGS.

GIGS is a laser interferometer for geophysical purposes operating since 1994. Strain data have been collected continuously in 2003 together with a new very-broad-band seismometer.

PULEX-2 was designed to investigate the effects of background radiation on metabolism and responses to external agents on cultured mammelian cells. The results suggest that background radiation can act as a priming dose capable of triggering an adaptive response.

The main activity of the theory group, staff and visitor scientists, has been focussed on astroparticle physics, including solar and Supernova neutrinos, massive neutrinos, ultra high energy cosmic rays, topological defects and relativistic astrophysics. Important activity took place also in particle phenomenology and computer simulations of Lattice Field Theories.

The Gran Sasso laboratory is one of the large European infrastructures as a "Low background facility for Particle Physics, Astrophysics, Nuclear Physics and Biology" (HPRI - CT- 2001-00149) in the action "Access to Research Infrastructures". This EU activity aims to maximise the impact of research infrastructures, facilities that provide essential services to Europe's research community in industry and academia. Another European contract (HPRP-CT-2001-00018), run in collaboration with the large European particle laboratories, CERN and DESY, aims to evaluate the effectiveness of their outreach actions.

Gran Sasso, March 10 2004

The Director of the Laboratory
Prof. Eugenio Coccia

Contents

BOREXINO. Solar Neutrino Physics

Borexino collaboration

H. Back[n], M. Balata[b], A. de Bari[e], T. Beau[o], A. de Bellefon[o], G. Bellini[a], J. Benziger[c], S. Bonetti[a], C. Buck[j], B. Caccianiga[a], L. Cadonati[d], F.P. Calaprice[d], G. Cecchet,[e], M. Chen,[r], O. Dadoune[o], A. Di Credico[b], D. D'Angelo[h], A. Derbin[m], A. Etenko[s], F. von Feilitzsch[h], R. Fernholz[d], R. Ford[b], D. Franco[a], B. Freudiger[j], C. Galbiati[d], S. Gazzana[b], M.G. Giammarchi[a], M. Göger-Neff[h], A. Goretti[a], C. Grieb[h], B. Harding[d], G. Heusser[j], A. Ianni,[d], A.M. Ianni[c], H. de Kerret[o], S. Kidner[d], J. Kiko[j], T. Kirsten[j], G. Korga[a], G. Korschinek[h], H. de Kerret[o], D. Kryn[o], M. Laubenstein[b], C. Lendvai[h], E. Litvinovich[s], P. Lombardi[a], I. Machulin[s], S. Malvezzi[a], J. Maneira[a], I. Manno[k], G. Manuzio[i], F. Masetti[g], U. Mazzucato[g], K. McCarty[d], E. Meroni[a], L. Miramonti[a], M.E. Monzani[a], V. Muratova[m], L. Niedermeier[h], L. Oberauer[h], M. Obolensky[o], F. Ortica[g], M. Pallavicini[i], L. Papp[a], L. Perasso[i], A. Pocar[d], R.S. Raghavan[l], G. Ranucci[a], A. Razeto[i], A. Sabelnikov[s], C. Salvo[i], S. Schönert[j], T. Shutt[d], H. Simgen[j], M. Skorokhvatov[s], O. Smirnov[m], A. Sotnikov[m], S. Sukhotin[s], Y. Suvorov[s], V. Tarasenkov[s], R. Tartaglia,[b], G. Testera[i], D. Vignaud[o], B. Vogelaar[n], V. Vyrodov[s], W. Wojcik[q], O. Zaimidoroga[m], G. Zuzel[q]

[a]Dip. di Fisica dell'Università and Infn Milano - Italy
[b]Laboratori Nazionali del Gras Sasso, Assergi (Aq) - Italy
[c]Dep.t of Chemical Engineering, Princeton University - NJ USA
[d]Dep.t of Physics, Princeton University - NJ USA
[e]Dip. di Fisica dell'Università and Infn Pavia - Italy
[f]Dep.t of Physics, Massachusetts Institute of Technology - MA USA
[g]Dip. di Chimica dell'Università and Infn Perugia - Italy
[h]Technische Universität München - Germany
[i]Dip. di Fisica dell'Università and Infn Genova - Italy
[j]Max Planck Inst. für Kernphysik, Heidelberg - Germany
[k]KFKI-RMKI Research Institute for Particle & Nuclear Physics, Budapest - Hungary
[l]Bell Laboratories, Lucent Technologies, Murray Hill - NJ USA
[m]J.I.N.R. Dubna - Russia
[n]Dep.t of Physics, Virginia Polytechnic Institute - VA USA
[o]Laboratoire de Physique Corpusculaire et Cosmologie, Paris - France
[p]I.R.M.M. - EURATOM, Geel - Belgium
[q]Institute of Physics, Jagellonian University, Kracov - Poland
[r]Dept. of Physics, Queen's University, Ontario - Canada
[s]RRC Kurchatov Institute, Moscow - Russia

Abstract

Borexino is a solar neutrino detector in construction phase in Hall C of LNGS. We summarize here the status of the construction, the assembling of the detector and the main achievements obtained in these years of technical development.

1 Introduction

Borexino is a real time experiment which plans to study the low energy (sub-MeV) solar neutrinos. The main experimental goal is the study of the 0.862 MeV ^{7}Be solar neutrino line through the neutrino-electron elastic scattering. The maximum energy of the recoiling electron is 664 KeV and the experimental design threshold will be at 250 KeV. The detection reaction will be observed in a large mass of well shielded liquid scintillator.
The main problem of a real time experiment with a so low energy threshold is the natural radioactivity which is present in any environment and in any material. As a consequence an intense R&D program has been carried out in the last ten years to develop methods for selecting low radioactivity materials and/or purify them. An effort in this field has to be accompanied by a comparably thorough research in the field of the detection system and measurement of ultralow radioactivity levels.
The development of purification methods has been focussed on the costituents of the , liquid scintillator. Four main methods have been developed and tested: distillation, water extraction, stripping with ultrapure N_2, solid gel column (Si gel, Al gel) adsorption. Significant results have been achieved by the Collaboration as for example: 10^{-16}-10^{-17} (g of contaminants/g of material) for ^{232}Th and ^{238}U family; few microBq of Rn in gases and liquids.
In addition the organic solvent selected by the collaboration shows a ^{14}C presence not exceeding 10^{-18} in its ratio to ^{12}C. This impurity is particularly important since it cannot be removed by ordinary chemical purification methods.
For the measurements of these ultralow radioactivity levels the Borexino Collaboration developed new methods. In addition to several small-scale techniques (such as Ge underground detectors installed in Rn free environment, Inductively Coupled Plasma Mass Spectometer, high sensitivity Neutron Activation, Atomic Absortion Spectroscopy etc...), a Counting Test Facility (CTF), has been constructed on purpose and operated in the Hall C of LNGS. The Counting Test Facility features 4 tonnes of liquid scintillator viewed by 100 photomultipliers and shielded by 1000 tons of ultrapure water.
In many of these fields many records have been achieved. The sensitivities reached are summarized below and correspond to the lowest radioactivity levels optained by the Borexino Collaboration, in preparation of the experiment:

- Bulk material radiopurities of 10^{-10} g/g for ^{238}U and ^{232}Th, $\sim 10^{-5}$ for ^{nat}K, few tenth of mBq/kg for ^{60}Co, have been measured with a Ge detector concerning construction materials as the Stainless Steel, metal and plastic gaskets, products for PMT sealing, etc...
- Radon emanations of 10 μBq/m^2 from plastic materials, 0.1 mBq/m^3 for Rn activity concentration in water and 1 mBq/m^3 for Ra, below 1 mBq/m^3 for the N_2 used for scintillator purification.
- Radiopurity levels of a few times 10^{-15} g/g ^{238}U, ^{232}Th and ^{40}K have been reached with the ICMPS in measuring the Borexino shielding water;
- few ppt for ^{238}U and ^{232}Th have been optained in the Nylon bulk measurements.
- The radiopurity of the scintillator itself was measured to be at the level of few 10^{-16} for ^{238}U, ^{232}Th and $\sim 10^{-18}$ for ^{14}C/^{12}C in the Counting Test Facility.
- Bulk radiopurity levels of 10^{-13} - 10^{-14} g/g for Au, Ba, Ce, Co, Cr, Cs, Ga, Hg, In,

Mo, Rb; less than few 10^{-15} g/g for Cd, Sb, Ta, W; 10^{-16} - 10^{-17} g/g for La, Lu, Re, Sc, Th; less than 1x10^{-17} g/g for U, have been reached by means of the Neutron Activation followed by a β-γ coincidence analysis selection applied to the scintillator.
These results were a milestone in the development of the Borexino detector and technique. Several of these concepts were incorporated in the construction of the auxiliary high-purity plants for the treatment of the most critical liquid, the scintillator of the experiment.

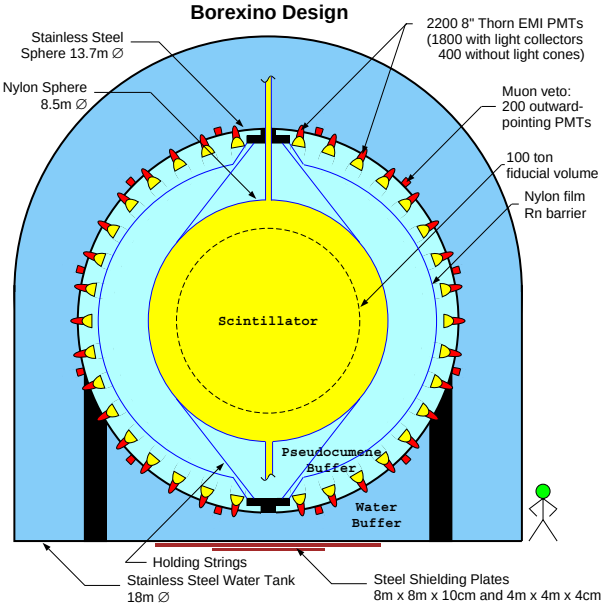

Figure 1: Schematic view of the Borexino detector.

2 The Borexino Detector

Borexino is an unsegmented liquid detector featuring 300 tonnes of well shielded ultrapure scintillator viewed by 2200 photomultipliers (fig. 1). The detector core is a transparent spherical vessel (Nylon Sphere, 100μm thick), 8.5 m of diameter, filled with 300 tonnes of liquid scintillator and surrounded by 1000 tonnes of high-purity buffer liquid. The scintillator mixture is PC and PPO (1.5 g/l) as a fluor, while the buffer liquid will be PC alone (with the addition of the light quencher, DMP). The photomultipliers are supported by the Stainless Steel Sphere (SSS), which also separates the inner part of the detector from the external shielding, provided by 2400 tonnes of pure water (water buffer).
An additional containment vessel (Nylon film Radon barrier) is interposed between the Scintillator Nylon Sphere and the photomultipliers, with the goal of reducing Radon diffusion towards the internal part of the detector.
The outer water shield is instrumented with 200 outward-pointing photomultipliers serving as a veto for penetrating muons, the only significant remaining cosmic ray background at the Gran Sasso depth (about 3500 meters of water equivalent). In addition the 2200

photomultipliers are equipped with light cones so that they see light only from the Nylon Sphere region, while the remaining 400 PMT's are sensitive to light originated in the whole volume of the Stainless Steel Sphere. This design greatly increases the capability of the system to identify muons crossing the PC buffer (and not the scintillator).
The BOREXINO design is based on the concept of a graded shield of progressively lower intrinsic radioactivity as one approaches the sensitive volume of the detector; this culminates in the use of 200 tonnes of the low background scintillator to shield the 100 tonnes innermost Fiducial Volume. In these conditions, the ultimate background will be dominated by the intrinsic contamination of the scintillator, while all backgrounds from the construction materials and external shieldings are negligible.
BOREXINO also features several external systems and apparatuses conceived to purify the experimental fluids (water, nitrogen and scintillator) and to keep clean conditions during the installation of the detector.

3 Status of the project

The Borexino detector is in an advanced stage of contruction. All the major detector components are already in place or very close to completion.
Among the installations to be still completed are a part of the muon system, a section of the PMT assembly and a part of the water distribution system. The completion of these parts is linked to the related installation of the Inner Vessel. The installation of the Inner Vessel has begun at the end of year 2003.

The experimental activity was relatively limited during year 2003 due to the legal investigations underway at LNGS. Significant progress has been made as regards the safety systems and the planning of a safety containment for all liquids of the experiment.

4 Borexino and Neutrino Physics

Borexino will be studying solar neutrino physics below the 1 MeV threshold, where the Large Mixing Angle suppresion pattern becomes vacuum dominated. This is in contrast with the "matter dominated" situation of the B-8 neutrinos, the only component observed in real-time up to now.
The expected Be-7 solar neutrino rates is close to 30 counts/day. With a sizeable number of real-time expected events, Borexino can also study several time-dependences of the solar neutrino signal, including day-night and seasonal variations.
Finally, a 10% accuracy measurement of the Be-7 line will be of great importance to measure the relative solar model parameter whose uncertainty is at present of the order of 50%.

Other physics topics can be investigated with high sensitivity with the Borexino detector, such as Supernova neutrinos, neutrino magnetic moment, terrestrial neutrinos...

Physics results already obtained with the Counting Test Facility, confirm the validity and the sensitivity of the Borexino technique.

5 List of articles published in year 2003

1. H.O. Back et al. *New limits on nucleon decays into invisible channels with the BOREXINO counting test facility.* Physics Letters B 563 (2003) 23.

2. H.O. Back et al. *Study of neutrino electromagnetic properties with the prototype of the Borexino detector.* Physics Letters B 563 (2003) 35.

3. H. O. Back et al. *New experimental limits on heavy neutrino mixing in B-8 Decay obtained with the Borexino Counting Test Facility.* JETP Letters 78 (2003) 261..

References

[1] G. Alimonti et al., *Science and technology of Borexino: a real-time detector for low energy solar neutrinos*, Astroparticle Physics 16 (2002) 205.

[2] C. Arpesella et al., *Measurements of extremely low radioactivity levels in BOREXINO*, Astroparticle Physics 18 (2002) 1.

CRESST. Dark Matter Search

W.Seidel for the CRESST collaboration

Abstract

The aim of CRESST (**C**ryogenic **R**are **E**vent **S**earch with **S**uperconducting **T**hermometers) is to search for particle Dark Matter and to contribute to the elucidation of its nature. The experiment is located at the 'Laboratori Nazionali del Gran Sasso' (LNGS), Italy, and it uses low background cryogenic detectors with superconducting phase transition thermometers for the direct detection of WIMP-nucleus scattering events. The CRESST experiment is a collaboration of the LNGS, the MPI für Physik München, the University of Oxford, and the Technische Universität München. The speaker of the collaboration is W. Seidel (MPI).

1 The Dark Matter Problem

The search for Dark Matter and the understanding of its nature is of central interest for particle physics, astronomy and cosmology. There is strong evidence for its existence on all scales, ranging from dwarf galaxies, through spiral galaxies like our own, to large scale structures. The history of the universe is difficult to reconstruct without Dark Matter, be it Big Bang Nucleosynthesis or structure formation.

Particle physics provides a well motivated candidate with the lightest SUSY-particle, the "neutralino". Generically, such particles are called WIMPs (Weakly Interacting Massive Particles). WIMPs are expected to interact with ordinary matter by elastic scattering on nuclei. All direct detection schemes have focused on this possibility.

Conventional methods for direct detection rely on the ionization or scintillation caused by the recoiling nucleus. This leads to certain limitations connected with the low ionization or scintillation efficiency of the slow recoil nuclei. The cryogenic detectors developed for the first phase of CRESST (CRESST-I) measure the deposited energy calorimetrically, independent of ionization, and allow a detection of much smaller recoil energies. When the cryogenic measurement of the deposited energy is combined with a measurement of scintillation light an extremely efficient discrimination of the nuclear recoil signals from radioactive background signals can be obtained. This type of detectors is beeing used in the upcoming phase CRESST-II.

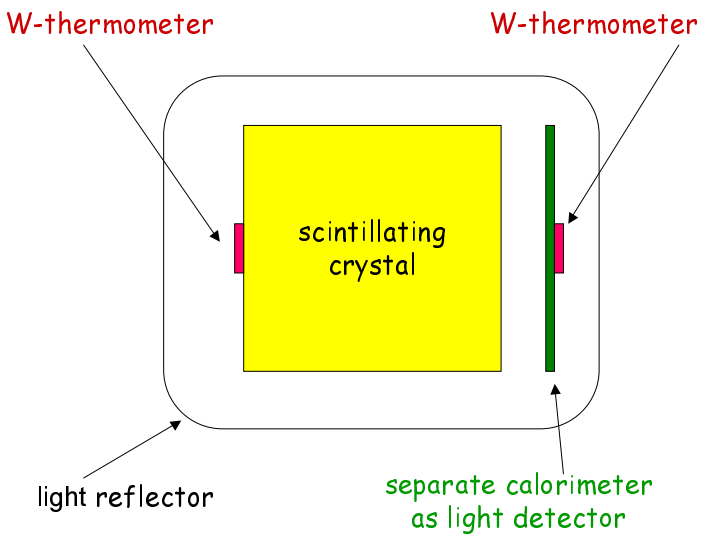

Figure 1: Sketch of the detector setup for the coincident detection of phonons and scintillation light. This novel concept will be used in CRESST-II. It allows to effieciently discriminate nuclear recoils signals from radioactive backgrounds.

2 Detection Principle

The low temperature calorimetric detectors consist of a target crystal, the so-called absorber, an extremely sensitive superconducting phase transition thermometer, and a weak thermal coupling to a heat bath to allow thermal relaxation of the system after an interaction. The thermometer is made of a tungsten film evaporated onto the absorber crystal. Its temperature is stabilized in the transition region from the superconducting to the normal conducting state, which occurs at termeratures of about 10 mK. A typical width of the transition region is about 1 mK. A small temperature rise (typically some μK), e.g. from a WIMP nucleus scattering event, leads to an increase of resistance, which is measured with a SQUID based readout. For the first phase of CRESST, which ended in Feb. 2001, 262 g sapphire detectors have been developed at the institute. These detectors provided an excellent energy resolution of 133 eV at 6 keV and a very low energy threshold of 600 eV.

In the upcoming second phase CRESST-II, we are using 300 g scintillating $CaWO_4$ crystals as absorbers. The scintillating crystal is equipped with a superconducting tungsten phase transition thermometer for the detection of the phonons created by particle interactions in the scintillating crystal. The scintillation light is measured in coincidence with a separate cryogenic detector, optimized for light detection. Fig. 1 schematically shows the setup of this composite detector. Starting with a proof of principle experiment in 1998, the technique of simultaneous measurement of phonons and scintillation light has been developed at the institue.

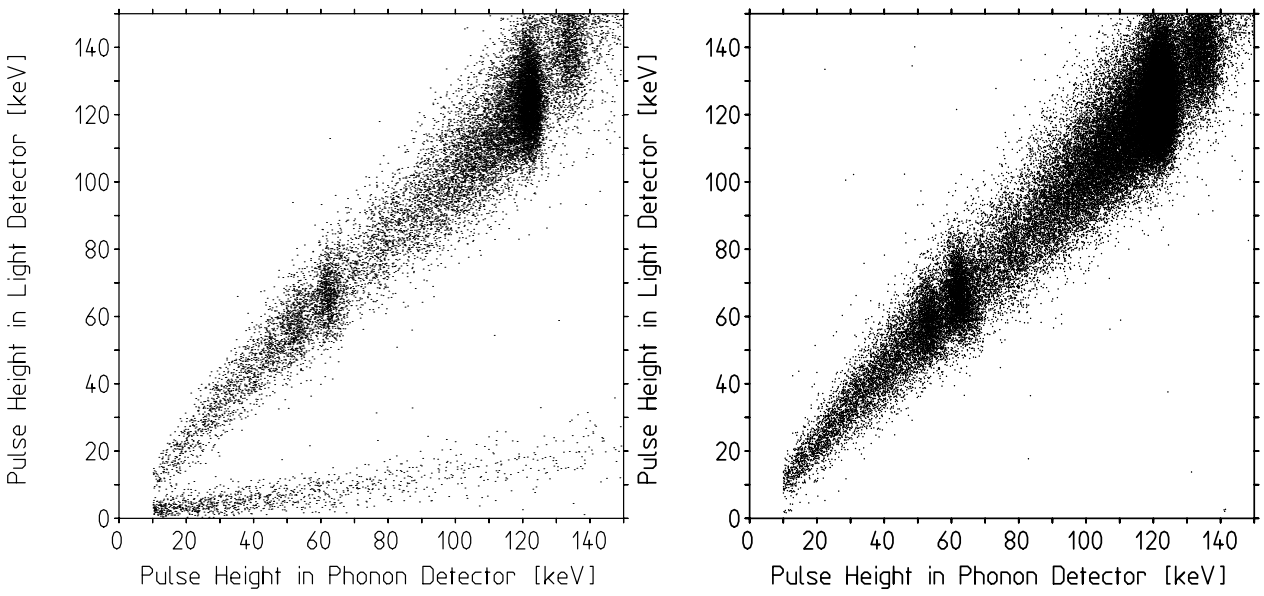

Figure 2: Coincident detection of phonons and scintillation light with a 6 g proof of principle $CaWO_4$ detector. Left fig.: The upper band of events is due to irradiation of the $CaWO_4$ crystal with electrons and gammas, whereas the lower band with lower light yield, is from nuclear recoils caused by a neutron source. Removing the neutron source (right fig.), confirms that there is no leakage of ionizing events into the nuclear recoil region.

The important advantage of the simultaneous detection of phonons and scintillation light is that it offers an extremely efficient suppression of the radioactive background. The ratio of the energy in the phonon channel and the energy in the light channel depends on the type of interaction. Nuclear recoils, such as WIMP or neutron scattering events, emit substantially less scintillation light than fully ionizing interactions, e.g. γ or β interactions do. As the overwhelming part of the backgroud consists of β and γ interactions, this phonon/light technique provides a very effective method of background suppression. Fig. 2 illustrates this novel detection method. With this proof of principle device, a 99.7 % suppression of ionizing background in the energy range from 15 and 25 keV , and 99.9 % at energies above 25 keV has been demonstrted.

Compared to the alternative approach of simultaneous measurement of phonons and charge in a semiconductor crystal, which is applied in the experiments CDMS and Edelweiss-II, the method developed for CRESST-II has the important advantage that it does not suffer from dead layers at the surface. A reduced charge collection for ionizing events occurring close to the surface in semiconducting crystals may lead to a false identification of low energetic γ's and β's as nuclear recoils. The result in Fig. 2, which was obtained with a gamma and beta source, confirms that the supression also works for low energy electrons impinging onto the crystal surface.

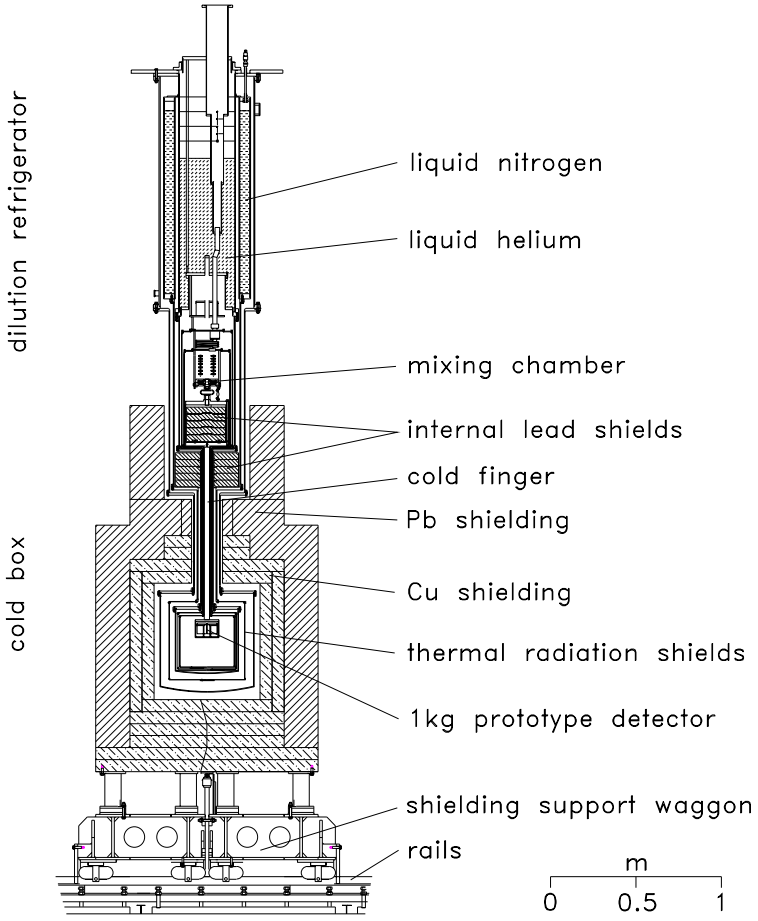

Figure 3: Layout of the CRESST ^{3}He/^{4}He dilution refrigerator and low background cold box with its shielding.

3 The CRESST Setup in Gran Sasso

The central part of the CRESST installation is the cryostat, sketched in figure 3. The low temperature generated in the mixing chamber of the dilution refrigerator is transferred into the radiopure cold box, which houses the detectors, via a 1.5 m long cold finger, protected by thermal radiation shields, all fabricated of low background copper. Two internal cold shields consisting of low level lead are attached to the mixing chamber and to a thermal radiation shield at liquid N_2 temperature, respectively, in order to block any line-of-sight from the non-radiopure parts of the dilution refrigerator to the detectors inside the cold box. The design completely avoids potentially contaminated cryogenic liquids inside the cold box.

An extensive passive shielding of low background copper and lead surrounds the cold box and serves to shield radioactivity from the surrounding rock. The entire shilding is inclosed inside a gas-tight radon box, that is flushed with boil of N_2 gas and maintained at a small overpressure. Special care has been taken to minimize above ground exposure of the construction materials of the cold box and the shielding to cosmic rays, in order to avoid activation.

Figure 4 schematically shows the CRESST experimental building. The cryostat is installed in a two level faraday cage to shield electromagnetic interference. The ground level inside

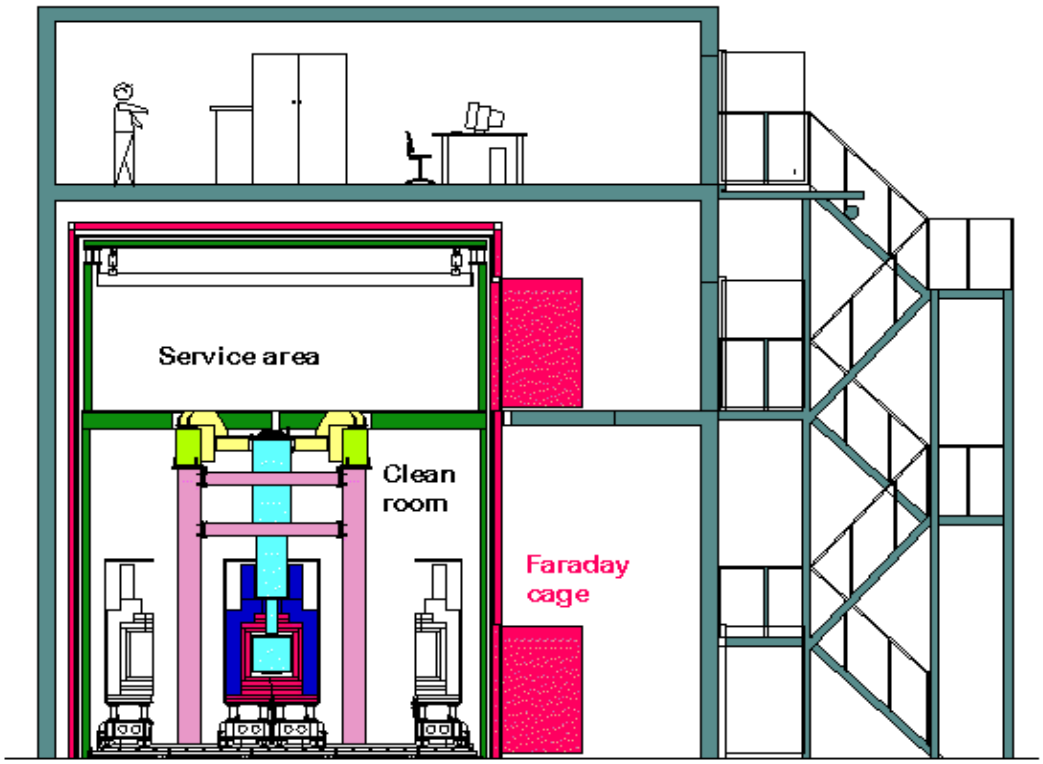

Figure 4: Schematic drawing of the three level CRESST building in hall B of the Gran Sasso Underground Laboratory.

the faraday cage is equipped as a class-100 clean room, in order to minimize contamination of the detectors and cold box during mounting. The head of the cryostat extends into the first floor of the farady cage, which is outside the clean room to simplify servicing of the cryostat. The first floor also houses the sensitive analog electronics. The gas handling system of the cryostat and the DAQ is outside the faraday cage. In the top floor, of the experimantal building a laminar flow work place is installed which serves to assemble and rebond detectors under clean conditions.

The setup is now beeing upgraded for the experimental program of CRESST-II, which will use 33 of such 300 g phonon/light detector modules. The upgrade includes the installation of a 66 channel SQUID readout system in the existing cryostat, the installation of a neutron shield and a muon veto and a new multichannel electronics and DAQ. The cryostat with the upgraded shielding is shown schematically in fig. 5. The upgrade will start in March 2004 with the installation of the SQUID system and will be completed in October 2004.

4 Preparations for CRESST-II

Starting in spring 2001, the CRESST set-up had to be moved from hall B to hall A within LNGS. After completion of this move the cryostat was still equipped with the four SQUID

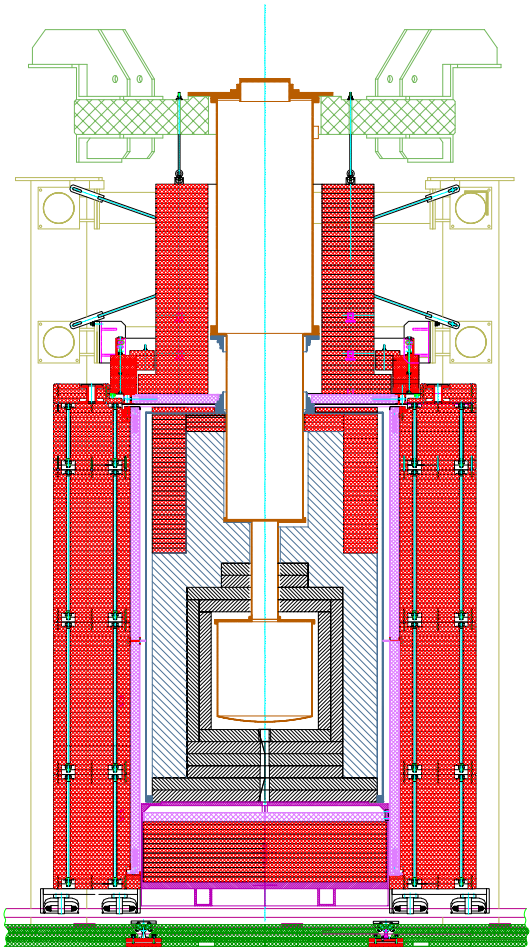

Figure 5: Dilution refrigerator and low background cold box with its shielding upgraded for CRESST-II. The gas tight radon box enclosing the Cu (shown in grey) and Pb (blue) shielding will be completely covered by a plastic scintillator μ-veto (pink) and 50 cm of poly ethylen (red).

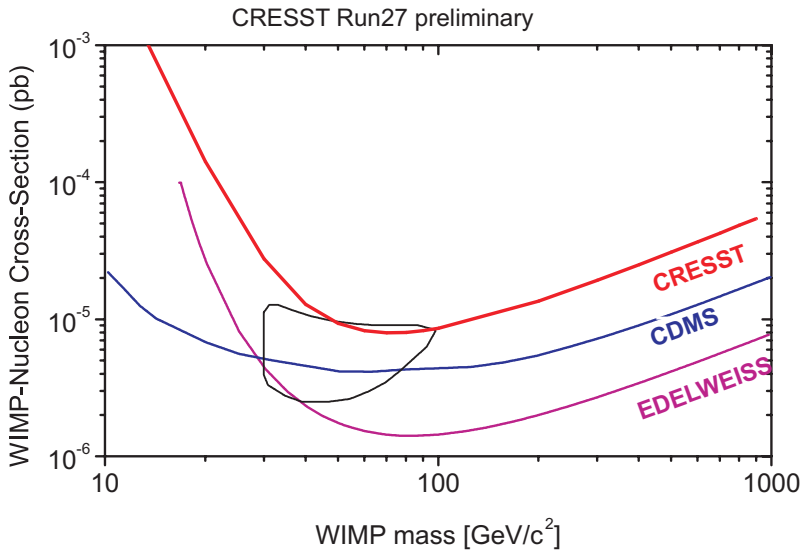

Figure 6: Preliminary exclusion plot for spin independent WIMP interaction, derived from 8.11 kg days of data from one 300 g CRESST-II detector module. The area above the curve is excluded at 90% c.l. For comparison, the DAMA positive evidence is shown and also the limits from other cryogenic experiments, CDMS and EDELWEISS.

readout system of CRESST-I, which at most allows to run two detectors in parallel. In the beginning of 2002 operation started again with testing and optimization of 300 g $CaWO_4$ prototype detector modules for CRESST-II. In 2002 and 2003 a series of runs was made to optimize the performande of the detector modules. The mounting systems of the crystals again tuned out to be a very critical issue, and it introduced spurious events. In the last run at the end of 2003 the problem was solved and daa were recorded for about two month with one detector. Form factor effects effectively limit the energy transfer to the heavy tungsten nuclei in elastic WIMP nucleus scattering to energies below 40 keV. We obtained 6 events in the nuclear recoil acceptance band in the relevant energy region between 20 keV and 40 keV in 8.11 kg days of data. The cryostat is still without neutron shield and this rate of 0.74 events per kg and day is consistent with the predicted neutron background. Moreover, five of this six recoil events have a clear light signal associated with the phonon signal as expected for neutron generated recoils. Neutron events in this energy range are dominantly oxyxgen recoils, whereas WIMPs with spin independent interaction almost exclusively ($\sigma \propto A^2$) recoil off tungsten nuclei. We have measured (still at room termperature) a very large quenching factor of $Q \approx 40$ for W-recoils, whereas the quenching factor for oxygen recoils is $Q = 7.3$ at mK temperatures and $Q \approx 10$ at room temperature. If a similar quenching factor applies for the tungsten recoils at low temperature, there should be no light emission observed in the 20 to 40 keV region within the detection limit. This argument confirmes that 5 out of the 6 recoil events are from neutrons. If we nevertheless conservatively assume that all recoil events are WIMP interactions, the exclusion plot shown in fig. 6 can be derived from the two month measuring period without neutron shield and just one detector.

The detector was calibrated with external ^{57}Co (122 keV γ's) and ^{60}Co (1.1 MeV and 1.3 MeV γ's) sources. With electric heater pulses the energy calibration is extended over the complete

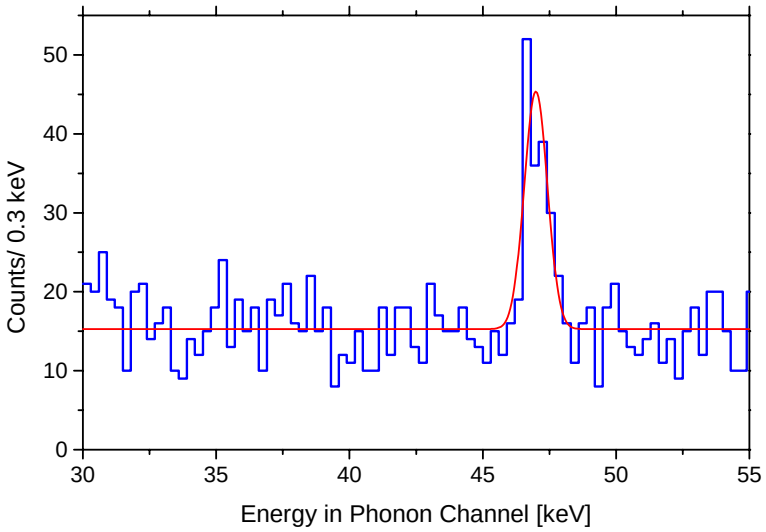

Figure 7: Energy spectrum of the phonon channel of a 300 g $CaWO_4$ detector. The peak at 46.53 keV, with a rate of 1.2 counts/day, is from an external ^{210}Pb contamination. The agreement with the nominal decay energy and the good resolution confirms the energy calibration and its stability.

energy range of interrest. Periodically injected heater pulses also serve to confirm the stability of the calibration and to measure the trigger efficiency close to threshold. The phonon channel had a detection threshold for reoils of 3 keV at 100% efficiency and the threshold of the light channel was 8 keV for γ andβ interactions. As shown in fig. 7, the phonon channel exhibited an energy resolution of 1 keV at a 46.53 keV peak from an external ^{210}Pb contamination during the whole measuring period.

5 Publications

"CaWO4 crystals as scintillators for cryogenic dark matter search" J. Ninkovic et al. to be published in NIM A Proceedings of the 7th International Conference on Inorganic Scintillators and their Use in Scientific and Industrial Applications, Valencia, Spain, September 7-12, 2003

"CRESST-II: dark matter search with scintillating absorbers" G. Angloher et al. Proceedings of the 10th International Workshop on Low Temperature Detectors, Genoa, Italy, 7-11 July 2003, to be published in NIM A

"Light detector development for CRESST-II" F. Petricca et al. Proceedings of the 10th International Workshop on Low Temperature Detectors, Genoa, Italy, 7-11 July 2003, to be published in NIM A

"A Textured Silicon Calorimetric Light Detector" P. C. F. Di Stefano et al. Submitted to Journal of Applied Physics

CUORICINO and CUORE. Neutrinoless Double Beta Decay Searches with Low Temperature Detectors

R. Ardito[1,2], C. Arnaboldi[1], D. R. Artusa[3], F. T. Avignone[3], M. Balata[4], I. Bandac[3], M. Barucci[5], J.W. Beeman[6], C. Brofferio[1], C. Bucci[4], S. Capelli[1], F. Capozzi[1], L. Carbone[1], S. Cebrian[7], O. Cremonesi[1], R. J. Creswick[3], A. de Waard[8], H. A. Farach[3], A. Fascilla[9], E. Fiorini[11], G. Frossati[8], A. Giuliani[9], P. Gorla[7], E. Guardincerri[10], E. E. Haller[6,11], I. G. Irastorza[7], R. J. McDonald[6], G. Maier[2], A. Morales[7], E. B. Norman[6], A. Nucciotti[1], E. Olivieri[5], P. Ottonello[10], M. Pallavicini[10], V. Palmieri[12], E. Pasca[5], M. Pavan[1], M. Pedretti[9], G. Pessina[1], S. Pirro[1], E. Previtali[1], M. Pyle[4], L. Risegari[5], C. Rosenfeld[3], M. Sisti[1], A. R. Smith[6], L. Torres[1], G. Ventura[5], and L. Zanotti[1]

1. Dipartimento di Fisica dell'Università di Milano-Bicocca e Sezione di Milano dell'INFN, Milano I-20126, Italy
2. Dipartimento di Ingegneria Strutturale del Politecnico di Milano, Milano I-20133, Italy
3. Dept.of Physics and Astronomy, University of South Carolina, Columbia, South Carolina, USA 29208
4. Laboratori Nazionali del Gran Sasso, I-67010, Assergi (L'Aquila), Italy
5. Dipartimento di Fisica dell'Università di Firenze e Sezione di Firenze dell'INFN, Firenze I-50125, Italy
6. Lawrence Berkeley National Laboratory, Berkeley, California, 94720, USA
7. Laboratorio de Fisica Nuclear y Altas Energias, Universidàd de Zaragoza, 50009 Zaragoza, Spain
8. Kamerling Onnes Laboratory, Leiden University, 2300 RAQ, Leiden, The Netherlands

[1]Spokeperson

9. Dipartimento di Scienze Chimiche, Fisiche e Matematiche dell'Università dell'Insubria e Sezione di Milano dell'INFN, Como I-22100, Italy

10. Dipartimento di Fisica dell'Università di Genova e Sezione di Genova dell'INFN, Genova I-16146, Italy

11. Dept. of Materials Science and Mineral Engineering, University of California, Berkeley, California 94720, USA

12. Laboratori Nazionali di Legnaro, I-35020 Legnaro (Padova), Italy

Abstract

CUORICINO is a bolometric experiment to search for $\beta\beta(0\nu)$ of ^{130}Te. It consists of 44 cubic TeO_2 crystals of $5\times5\times5$ cm^3 and 18 crystals of $3\times3\times6$ cm^3 arranged in a single 13 storey tower. With a mass of 40.7 kg it is the largest mass detector operating at low temperature ($\sim$ 10 mK). The progress achieved during 2003 is reported. In particular the early results concerning background analysis and neutrinoless double decay sensitivity are discussed. Based on the successful operation of CUORICINO, the construction of a larger detector (CUORE) aiming at reaching a sensitivity on $|\langle m_\nu \rangle|$ in the range 15–30 meV, was proposed in 2003. The CUORE detector will consist of an array of 1000 TeO_2 bolometers arranged in a square configuration of 25 towers of 40 $5\times5\times5$ cm^3 crystals each. CUORICINO is the first, slightly modified, operating CUORE tower.

1 Introduction

Strong interest has been recently revived in neutrinoless double beta decay (DBD) by the discovery of neutrino oscillations in solar [1, 2], atmospheric [3], and reactor [4] experiments. These experiments have in fact unequivocally demonstrated that neutrinos have mass and that the neutrino mass eigenstates mix, yielding valuable information on the mixing angles and on the mass differences of the three eigenstates. They cannot, however, determine the scale of the neutrino mass which can only be directly determined by beta decay end point spectral shape measurements, or in the case of Majorana neutrinos, by the observation and measurement of the neutrinoless double-beta decay half-life. By using the mixing angles and mass differences yielded by the oscillation experiments it is possible to predict with good accuracy a range of values of the effective mass of the Majorana electron neutrino which could be tested by the next generation $\beta\beta(0\nu)$ experiments. Consisting of an array of one thousand, 750 g, TeO_2 bolometers operating at $\sim$10 mK, the CUORE experiment is designed with a sensitivity capable of probing most of this range. The large natural abundance of ^{130}Te (33.87%) eliminates the requirement for the very expensive isotopic enrichment required in all of the other proposed next generation experiments. The proposed array has a cubic structure consisting of 25 towers of 40 detectors each. One such tower has been successfully constructed and is being operated in the Gran Sasso Laboratory as an independent experiment called CUORICINO. In 3 years of operation CUORICINO will reach a half-life sensitivity for neutrinoless double-beta decay of 6.1×10^{24} years (1σ), corresponding to an effective mass of the electron neutrino

of the order of 0.3 eV. This will be superior to the present upper bound on the effective electron-neutrino mass set by the ^{76}Ge experiments.

CUORICINO start in spring 2003 is therefore an important milestone in the field of $\beta\beta(0\nu)$ searches and definitely proves the effectiveness of the bolometric approach. Besides yielding improved limits on the ^{130}Te $\beta\beta(0\nu)$ half-life, the early CUORICINO data already give clear indications of what and where the sources of background are and how to reduce them. The required reduction in the background required for the full-scale experiment CUORE is therefore possible. This would allow the full CUORE array to achieve a 5-year sensitivity of 4.7×10^{26} years, corresponding to an effective mass of the order of 30 meV. Another order of magnitude reduction will present a real challenge, but is possible. In that case, a 5-year sensitivity in the effective mass would be around 15 meV.

2 Double Beta Decay and Low Temperature detectors

Double Beta Decay (DBD) consists of the direct emission of two electrons from a nucleus (A,Z) decaying to the corresponding isobar (A,Z+2). Various decay modes are possible. The *two neutrino DBD* is accompanied by the emission of two electron antineutrinos and conserves lepton number. It is allowed by the standard model of electroweak interactions, and it has been found in ten nuclei [5, 6, 7, 8]. On the contrary lepton number conservation is violated in the majoron decay mode, where the massless Goldstone boson accompanies the emission of the two electrons, and in the so called *neutrinoless* DBD, where only the two electrons are emitted. In the latter case the two electrons share the total transition energy and a peak would appear in their sum energy spectrum. Neutrinoless Double Beta Decay searches represent a unique tool to assess the Dirac/Majorana nature of neutrino. Moreover, the C-parity violation of weak interactions implies a dependence of the $\beta\beta(0\nu)$ rate on a combination of the neutrino mass eigenstates called *effective neutrino mass*: $|\langle m_\nu\rangle| \equiv ||U_{e1}^L|^2 m_1 + |U_{e2}^L|^2 m_2 e^{i\phi_2} + |U_{e3}^L|^2 m_3 e^{i\phi_3}|$ (U_{lk} are the neutrino mixing matrix elements, while ϕ_2 and ϕ_3 are the Majorana CP phases). In particular, the expected value for $|\langle m_\nu\rangle|$, or its upper limit is proportional to the square root of the rate, which makes $\beta\beta(0\nu)$ searches quite difficult. On the other hand this rate is proportional to the square of the nuclear matrix element, whose evaluation is at least presently, quite uncertain. Since the uncertainty in the value of the nuclear matrix element reflects itself directly in that of $|\langle m_\nu\rangle|$, searches for neutrinoless DBD should be carried out on several candidate nuclei.

No evidence was claimed so far for the neutrinoless channel in any nucleus, with the only exception of an alleged evidence for neutrinoless DBD of ^{76}Ge reported by a subset of the Heidelberg-Moscow collaboration [9, 10], but doubted by other authors [11, 12, 13], and even by a different subset of the same collaboration [14].

DBD can be searched for both indirectly, in radiochemical [15] or geochemical experiments [16, 17, 18, 19, 20] searching for the (A,Z+2) product nuclei, and directly, in real-time experiments looking for each single decay. A very effective approach is based on the use "calorimeters" [21] in which the detector itself is made of a material containing

the double beta active nucleus.
The use of cryogenic detectors to search for DBD was suggested in 1984 [22]. In a very naive approach they consist of a suitable (massive) absorber in good thermal contact with a proper phonon detector (temperature sensor). When made of diamagnetic and dielectric crystals, these bolometers are characterized by a heat capacity which, at low temperature, is proportional to the cube of the ratio between the operating and Debye temperatures [23, 24, 25]. As a consequence in a cryogenic set-up this capacity can become so small that even the small energy released by a single particle interaction in the form of heat generates a measurable increase of temperature. Cryogenic detectors offer therefore a wide choice of DBD candidates, the only requirement being that the candidate nucleus be part of a compound which can be grown in the form of a crystal with reasonable thermal and mechanical properties. The isotope ^{130}Te is an excellent candidate to search for DBD due to its high transition energy (2528.8 $\pm$ 1.3 keV) [26], and large isotopic abundance (33.8 %)[27] which allows a sensitive experiment to be performed with natural tellurium. In addition, the expected signal at 2528.8 keV happens to be in an energy region between the peak and the Compton edge of the ^{208}Tl γ-rays at 2615 keV, which generally dominates the γ background in this high energy region. Of the various compounds of this element, TeO_2 appears to be the most promising one due to its good mechanical and thermal properties.
Two cryogenic setups were installed in the eighties at LNGS by the Milano group. They consist of dilution refrigerators having powers of 1000 μW and 200 μW at 100 mK respectively and built with selected materials characterized by low activity levels. Both refrigerators are equipped with a dedicated Helium liquefier, providing a substantial recovery of the Helium and preventing Helium contamination of the tunnel atmosphere, and are housed inside Faraday cages to suppress electromagnetic interference. A series of experiments with various arrays of TeO_2 crystals of increasing mass have been therefore carried out at LNGS by a Milano-LNGS collaboration since the eighties [28]. A new massive set-up, CUORICINO, with a total mass of $\sim$40 kg of TeO_2 , and carried out by the CUORE international collaboration, has started operation this year.

3 CUORE

The CUORE project originates from the successful application of the bolometric approach to $\beta\beta(0\nu)$ searches, coupled with the possibility to build an array with a sensitivity in the $|\langle m_\nu \rangle|$ range foreseen by the results of the neutrino oscillation experiments. After the operation of a series of smaller (but constantly increasing) size experiments aiming at demonstrating the viability of the technique, the final project was finally proposed to the scientific community in 2003. The CUORE detector will consist of an array of 1000 TeO_2 bolometers arranged in a square configuration of 25 towers of 40 crystals each (Fig. 1). CUORE crystals will be grouped in modules of 4 bolometers, so that each tower will be a stack of 10 modules. The crystal temperature change will be recorded with Neutron Transmutation Doped (NTD) germanium thermistors, developed and produced at the Lawrence Berkeley National Laboratory (LBNL) and UC Berkeley Department of Material Science [29]. The TeO_2 crystals will be produced by the Shanghai Institute for

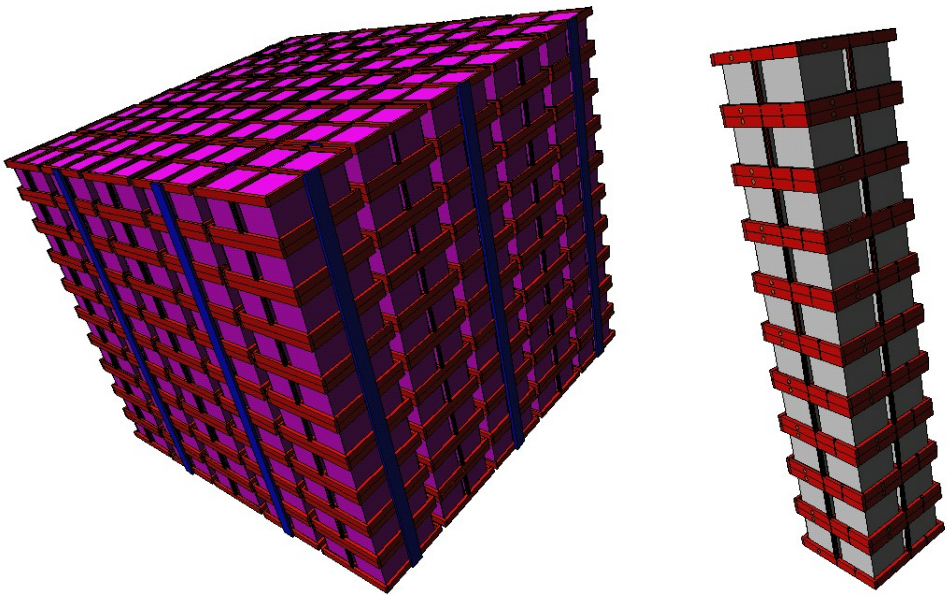

Figure 1: The CUORE detector (left), one of the 25 towers (right).

Ceramics (SICCAS), China. A single CUORE detector will consist of a $5\times5\times5$ cm^3 single crystal of TeO_2 acting both as a detector and source of the decay. The detectors will be supported in a copper frame in the 25 tower configuration shown in Fig. 1.

The copper frames and the dilution refrigerator mixing chamber to which they will be thermally connected, will form the heat sink, while the PTFE stand-offs will provide the thermal impedance which delays the re-cooling of the bolometers. The bolometers will operate at $\sim$ 10 mK. CUORE will be housed inside a dedicated dilution refrigerator built with selected, low activity materials. It will be shielded from environmental and material radioactivity by means of heavy shields held both at low and room temperature (Fig. 2).

The pertinent details of the CUORE detector as well as the background issues, electronics, DAQ and data-analysis can be found in the CUORE proposal [30]. We limit here to a brief discussion of the CUORE expected performance. According to the results of accurate Monte Carlo simulations based on the results of the background analysis of the *20 crystal array* (MiDBD) and CUORICINO [30], the background of these experiments in

Table 1: Expected CUORE $\beta\beta(0\nu)$ sensitivity (5 years). B is the background rate and Δ is the FWHM energy resolution. The $|\langle m_\nu\rangle|$ interval is evaluated according to different QRPA nuclear matrix element calculations.

B(counts/keV/kg/y)	Δ(keV)	$T_{1/2}$(y)	$\lvert\langle m_\nu\rangle\rvert$ (meV)
0.01	10	1.5×1026	23–118
0.01	5	2.1×1026	19–100
0.001	10	4.6×1026	13–67
0.001	5	6.5×1026	11-57

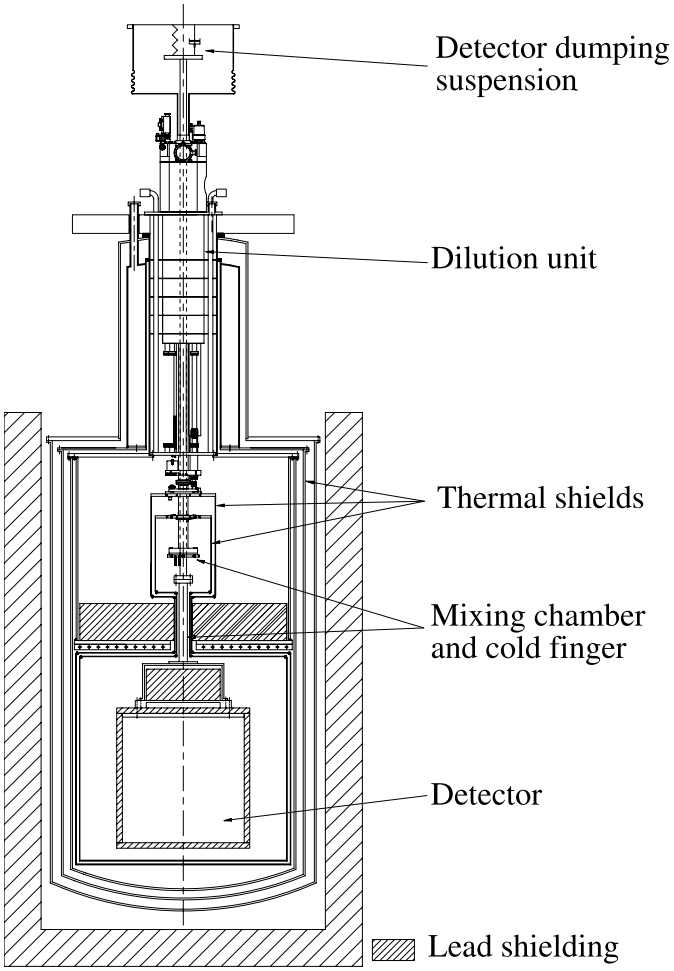

Figure 2: The CUORE setup.

the $\beta\beta(0\nu)$ region is still dominated by surface contaminations of the TeO_2 crystals and of the copper structures faced to them. A straighforward reduction of this background to a level of the order of 0.01 counts/keV/kg/y is expected as a result of the improvement of the adopted surface cleaning techniques, currently under investigation (a reduction by about an order of magnitude of the crystal and copper surface contamination is required). A further improvement by an order of magnitude could result from a more radical change of the surface treatment procedures but this will require a more extensive and long R&D. The expected sensitivity for different detector performance parameters is summarized in table 1.

The CUORE experiment was proposed to the LNGS Scientific Committee and to the INFN *Commissione Nazionale Scientifica II* in September and November 2003, repectively.

4 CUORICINO

Besides being a sensitive experiment on $\beta\beta(0\nu)$ of ^{130}Te on itself, CUORICINO is of course a crucial test of CUORE. In fact, its successful operation during 2003 is one of the main reasons for the actual CUORE proposal in fall 2003. Installed at LNGS during 2002 and cooled down for the first time in January 2003, CUORICINO has yield (in spite of the summer *misadventures* that led to a partial stop of its operation) important results concerning both the technical performance of the bolometric tower, the $\beta\beta(0\nu)$ background level and origin, and the $\beta\beta(0\nu)$ of ^{130}Te . Due to the importance of this early results we will discuss them in detail here.

4.1 The CUORICINO detector

The CUORICINO detector is a 13 storey CUORE-like tower (Fig. 3). Eleven planes are 4-crystal modules identical to those forseen for CUORE. Two additional planes are made of 9-crystal modules. In these two planes 18 of the 20 crystals used for the previous MiDBD experiment have been housed.

CUORICINO contains therefore 44 TeO_2 crystals of about $5\times5\times5$ cm^3 and mass 790 g, and 18 TeO_2 crystals of about $3\times3\times6$ cm^3 and average mass 330 g. The total mass of TeO_2 in CUORICINO is 40.7 kg. All the crystals are made of natural tellurium except for the 4 isotopically enriched crystals already used in MiDBD. Particular care was dedicated to the selection and treatment of the materials used for the construction of the CUORICINO array: the crystals where grown with low contamination materials in China and shipped to Italy where their surface was polished with specially selected low contamination powders. The mechanical structure of the array was made exclusively in radio-pure OFHC copper and Teflon All its components were separetely treated with acids to removes surface contamination. The array was finally assembled in an underground clean room in a N_2 atmosphere to minimize Rn contamination. Fig. 3 shows the CUORICINO tower just after assembly completion. Details of the two different used modules - the one with the large size crystals and that with the small size ones - are also shown.

Once closed inside its copper box, the array was mounted inside the same dilution refrigerator installed in the Hall A and used for the previous bolometric $\beta\beta(0\nu)$ experiments (e.g. MiDBD). Two of the cryostat thermal shields had to be replaced with larger ones in order to accomodate the CUORICINO tower.

The array is surrounded by a $\sim$1 cm thick roman lead shield (fig. 3, left). Two roman lead discs, 7.5 cm and 10 cm thick are positioned just below and above the tower respectively. As in the case of MiDBD, the refrigerator itself is shielded with a 20 cm thickness of low activity lead and a 10 cm thickness of borated PET. Nitrogen is flushed between the external lead shield and the cryostat to reduce Rn contribution to the detectors background.

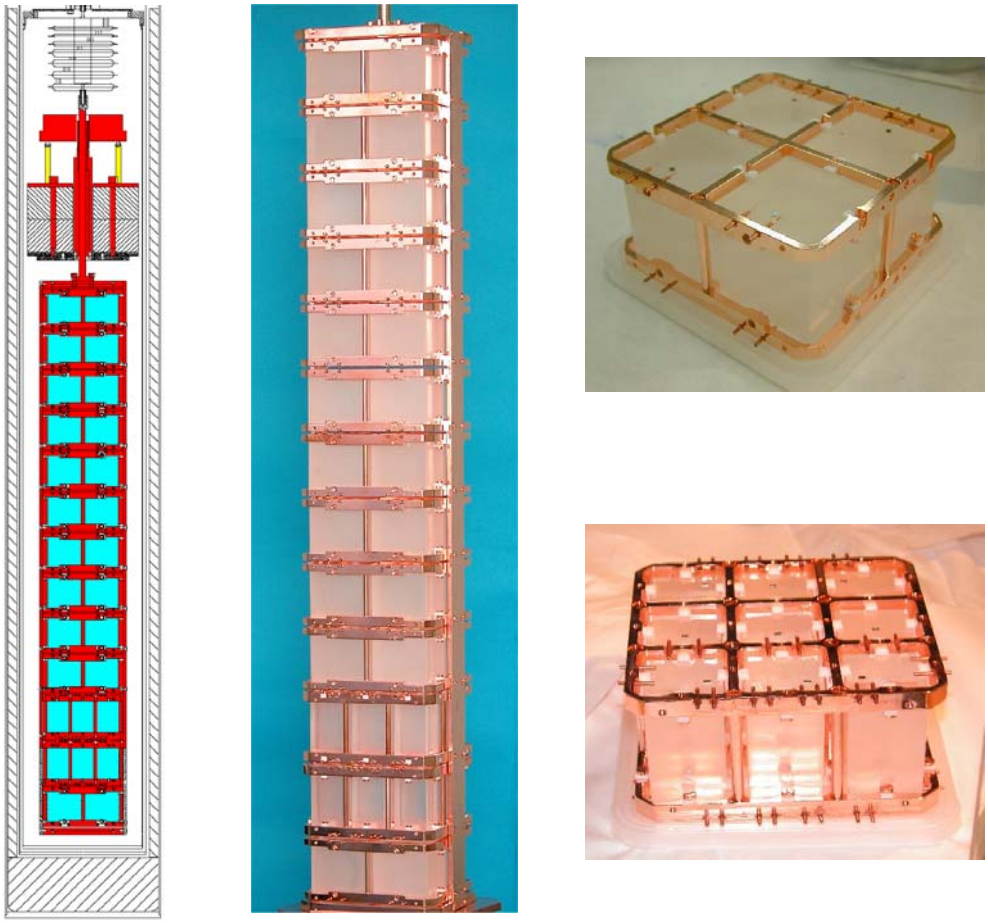

Figure 3: The CUORICINO detector: scheme of the tower and internal roman lead shields (left), the 13 planes tower (centre), the 4 crystal module (top right) and the 9 crystal module (bottom right).

4.2 CUORICINO operation and performance

CUORICINO was cooled at the beginning of 2003. Unfortunately during the cooling procedure some of the signal wires disconnected so that only 32 of the large crystals and 16 of the small ones could be read. The technical problem responsible for the disconnection of the wires was identified and in November 2003 the array was warmed to room temperature to repair the lost connections.
The performance of the electrically connected detectors was quite good: the average FWHM resolution measured during the calibration of the detectors with a ^{232}Th source is $\sim$7 keV for the 5×5×5 cm^3 crystals, and $\sim$9 keV for the 3×3×6 cm^3 crystals. Both these values were measured with the ^{208}Tl gamma line at 2615 keV. The sum calibration spectrum of all the operating large and small crystals is shown in Fig. 4. The distributions of the single detector energy responses and energy resolutions are shown in Fig. 5. In spite of the larger mass, they are comparable or even better than the corresponding ones in the previous MiDBD experiment.

On April 19th 2003 the first background measurement started and was over on July

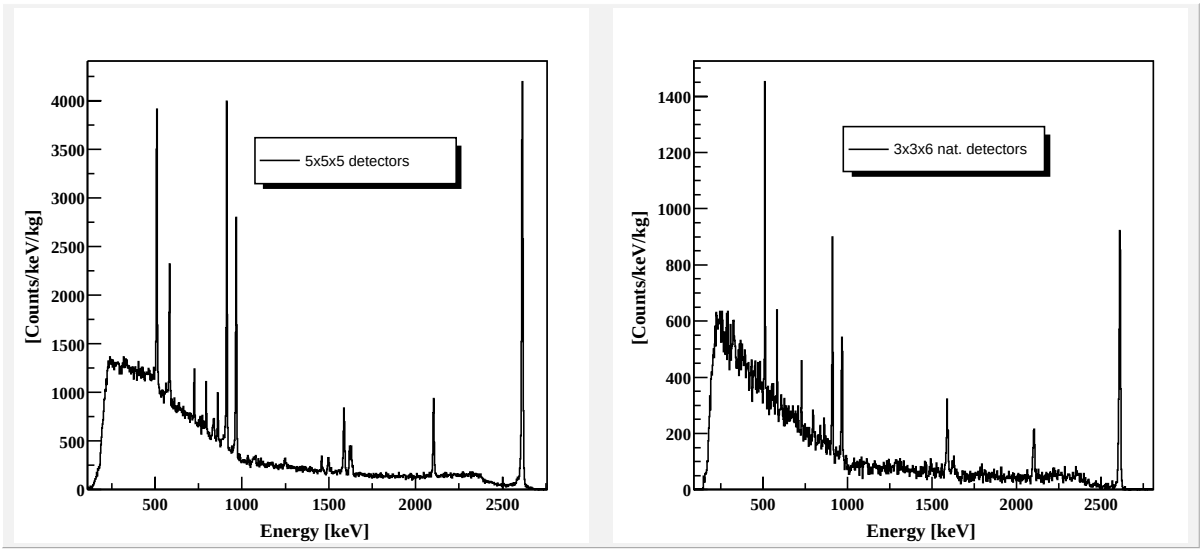

Figure 4: Summed calibration spectrum (^{232}Th source just outside the crysotat) from all the operating 5×5×5 cm^3 and 3×3×6 cm^3 crystals.

21th due to the interruption of the LNGS water supply. During this run, the live time was ∼72%, including the time required for the periodic calibration (usually every 15 days) of the detectors. The performance of the large size crystals during the entire run was quite good. We only had problems with 3 of the 32 detectors, once again due to faulty electrical connections. Indeed two detectors showed cross talk that prevented us from using them to compute the background while one of them had excessive spurious noise.

Therefore we used only 29 of the large crystals for background studies. In the case of the small crystals, one of the two central detectors had its Si heater disconnected, while another showed a variation in the reference pulse position after some weeks of running: once again there was a problem with the electrical connections. Therefore the number of well-working samll detectors was reduced to 11 natural crystals and 4 enriched ones.

CUORICINO operation was temporarily stopped on November 1st 2003 to repair the detector wiring system (restoration of the *lost* channels) and an extraordinary maintanance of the cryogenic setup (sorely-tried by the summer stop of the LNGS water cooling system).

4.2.1 CUORICINO background measurements

The total statistics collected in the above mentioned measurement period are of ∼25000 kg ×hours for 5×5×5 cm^3 crystals and ∼2300 kg ×hours for the 3×3×6 cm^3 ones. The corresponding background spectra are shown in Fig. 6. The gamma lines due to ^{60}Co, ^{40}K and of the ^{238}U and ^{232}Th chains are clearly visible.

These lines, originating from radioactive contamination of the apparatus materials, are not visible in the spectra of the single detectors: they appear only after summing the 29 detectors, and are a good check of the calibration and stability of the detectors during the background measurement. Also visible are the gamma lines due to Te activation (^{121}Te,

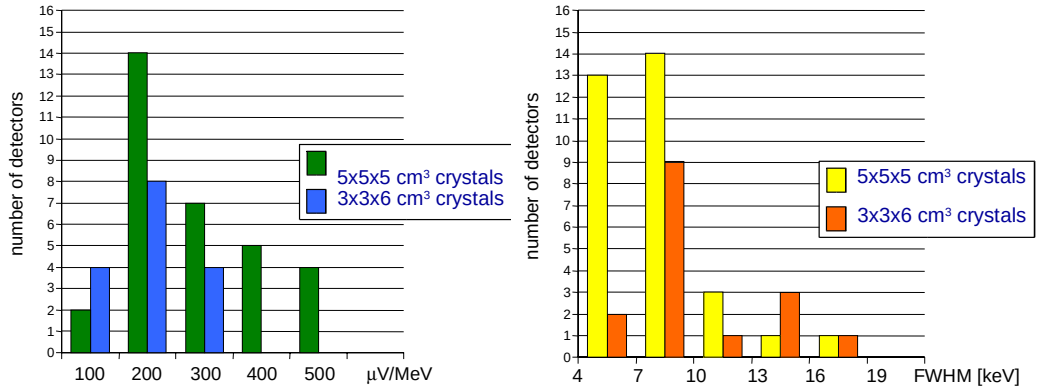

Figure 5: Distribution of the single CUORICINO detector energy responses normalized to 1 kg of TeO_2(left) and energy resolutions (FWHM) at the ^{208}Tl 2615 keV line (right).

^{121m}Te, ^{123m}Te, ^{125m}Te and ^{127m}Te) and those due to Cu activation (^{57}Co, ^{58}Co, ^{60}Co and ^{54}Mn) by cosmic ray neutrons while above ground.

The FWHM resolution of 5×5×5 cm^3 detectors at low energy, as evaluated on the 122 keV gamma line of ^{57}Co, is ∼2.8 keV. The ^{208}Tl gamma line at 2615 keV - clearly visible in the background sum spectrum - is used to evaluate the energy resolution in the region of double beta decay, the FWHM is 8.7 keV. The background in the double beta decay region (i.e. 2510-2580 keV) is 0.20 ± 0.03 counts/keV/kg/y.

The 3×3×6 cm^3 and 5×5×5 cm^3 crystal background spectra (sum of all the anticoincidence spectra of the detectors) are compared in Fig. 7 and Fig. 8.

Here the statistical accuracy is much less, nevertheless the gamma lines, not visible in the single detector spectra, are clearly visible in the background sum spectrum. The FWHM resolution at low energy, measured on the 122 keV gamma line of ^{57}Co, is ∼1.5 keV. The FWHM resolution on the ^{208}Tl gamma line at 2615 keV is evaluated to be of about 12 keV (this value has a large error due to the poor statistical significance of the peak). The background in the double beta decay region (i.e. 2510-2580 keV) is 0.2 ± 0.1 counts/keV/kg/y.

4.2.2 CUORICINO background analysis

Because of the low number of counts, any evaluation of the possible background sources necessarily has a large statistical uncertainty. Some preliminary considerations are however possible. They are based on the analysis of the sum spectra of the operating small and large crystals (the count rates of the single detector spectra are too low to consider them separately). In Fig. 7 and Fig. 8 a comparison between the background spectra of the large and small crystals is shown. General spectral shapes and counting rates (when normalized to the mass of the crystals) are quite similar. On the other hand the intensities of the gamma lines do not show a clear behaviour: the ^{214}Bi 1764 keV (the only clearly visible one of the U chain) and the ^{208}Tl 2615 keV lines (the only clearly visible one of the Th chain) seem to scale with the efficiency of the detectors (according to the results of a Monte Carlo analysis, the ratio of the detection efficiency of 5×5×5 cm^3 and 3×3×6 cm^3

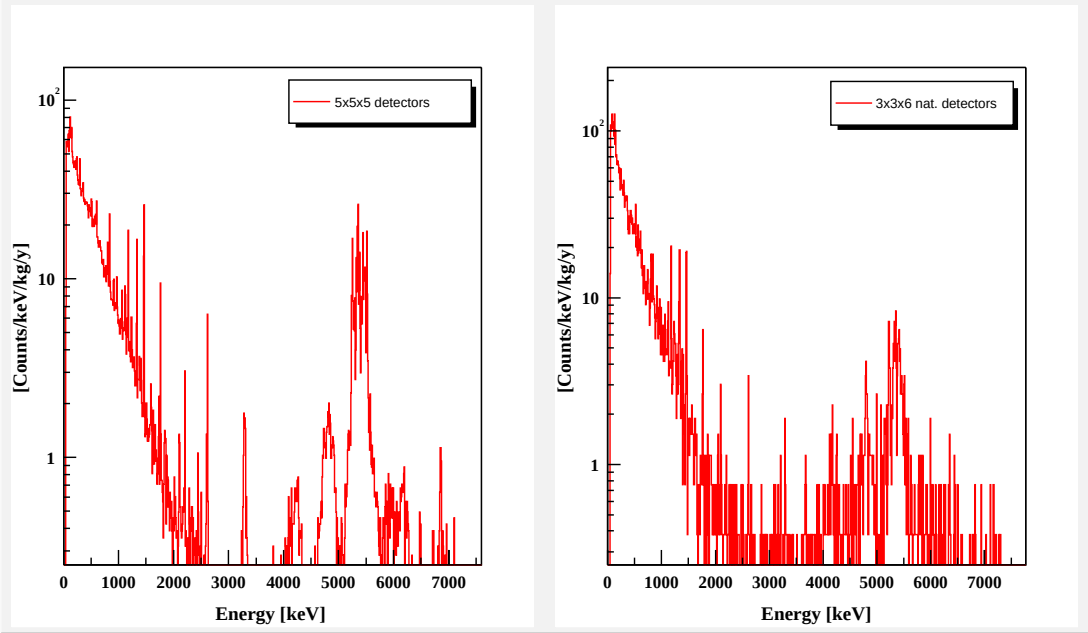

Figure 6: Summed background spectra from the operating 5×5×5 cm^3 and (natural abundance) 3×3×6 cm^3 crystals.

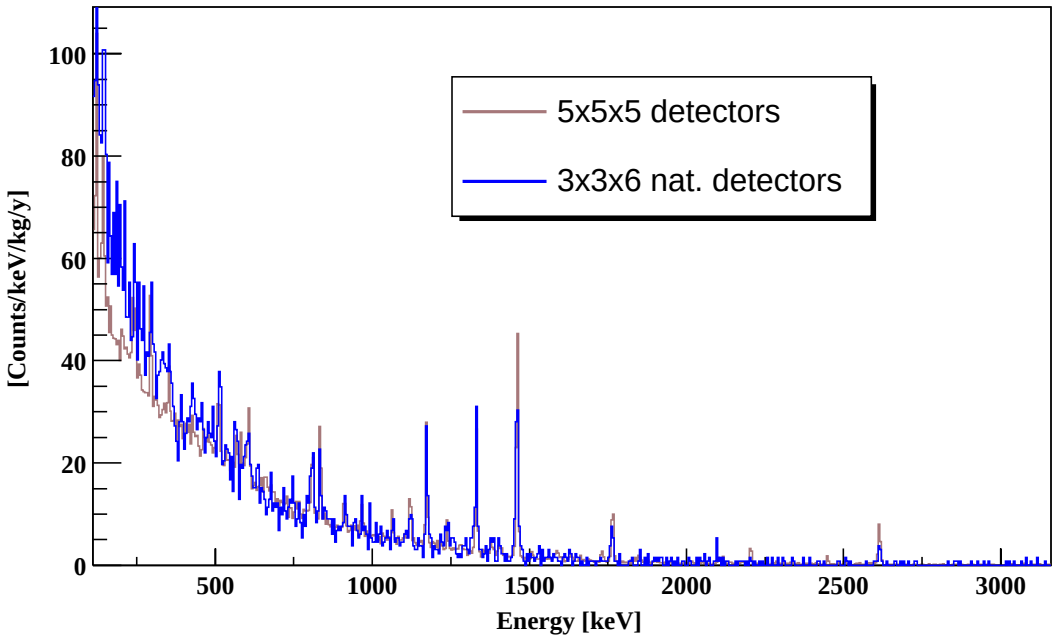

Figure 7: Comparison between the background of the 5×5×5 cm^3 crystals and that of the natural 3×3×6 cm^3 crystals in the gamma region.

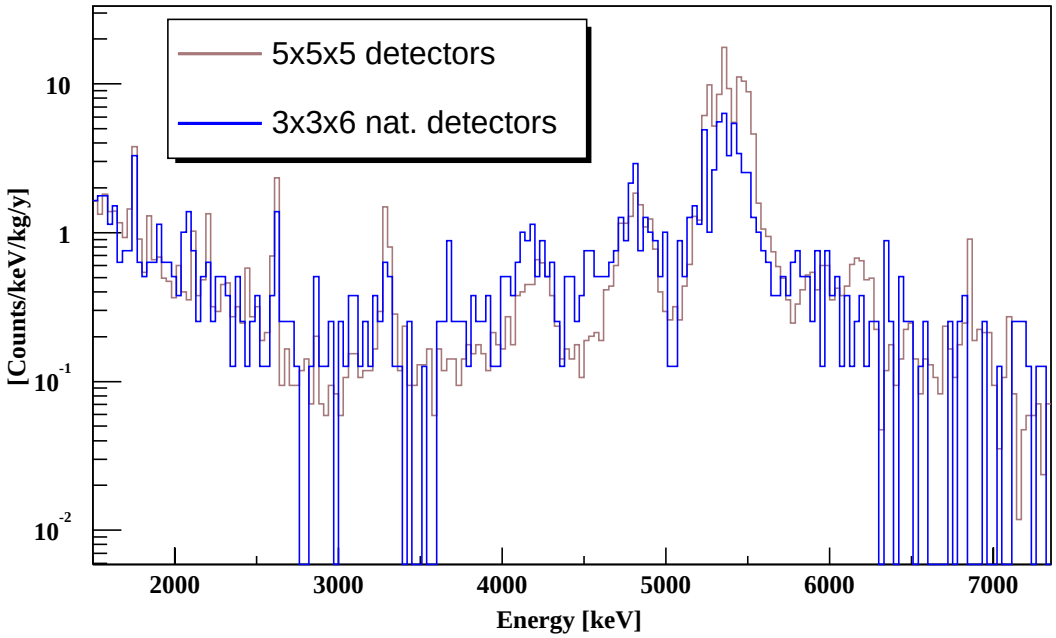

Figure 8: Comparison between the background of the 5×5×5 cm^3 crystals and that of the natural 3×3×6 cm^3 crystals in the alfa region.

crystals is ∼3). The ^{40}K line at 1460 keV has the same intensity per unit mass on the two kind of detectors. The ^{60}Co lines at 1173 and 1332 keV, on the contrary show a higher intensity per unit mass in small crystals. Moreover they undergo a larger reduction by the anticoincidence cuts with respect to other γ–lines.

In Fig. 9 a comparison between the background spectra of CUORICINO crystals and the background measured in MiDBD-II (20 crystal array second run) is shown.

In Table 2 the counting rates in different energy regions are reported. An evident improvement was obtained in the 2-3 MeV region (a reduction of ∼30% in the counting rates per unit mass either of the small and of the large crystals) despite the reduced internal lead shield used in CUORICINO (∼1.2 cm thickness of roman lead) with respect to MiDBD-II (∼3 cm thickness of roman lead). An even better reduction was obtained in the 3-4 MeV region where background is mainly dominated by surface contamination contributions. With better statistical accuracy it will be possible to analyze the reasons for this variation of the counting rates and also for the differences between small and large crystals.

To accomplish that, it is indeed necessary to disentangle the different sources of background by considering the counting rates in smaller (and significant) regions. This is the case, for example, of the energy interval between two gamma peaks at 2448 and 2615 keV (^{238}U and ^{232}Th chains respectively), where we expect contributions from both degraded α's from surface contaminations and ^{208}Tl γ's from bulk contaminations; another interesting region is the one just above the ^{208}Tl 2615 keV line, where background sources should be limited to surface contaminations). It should be stressed, moreover, that the

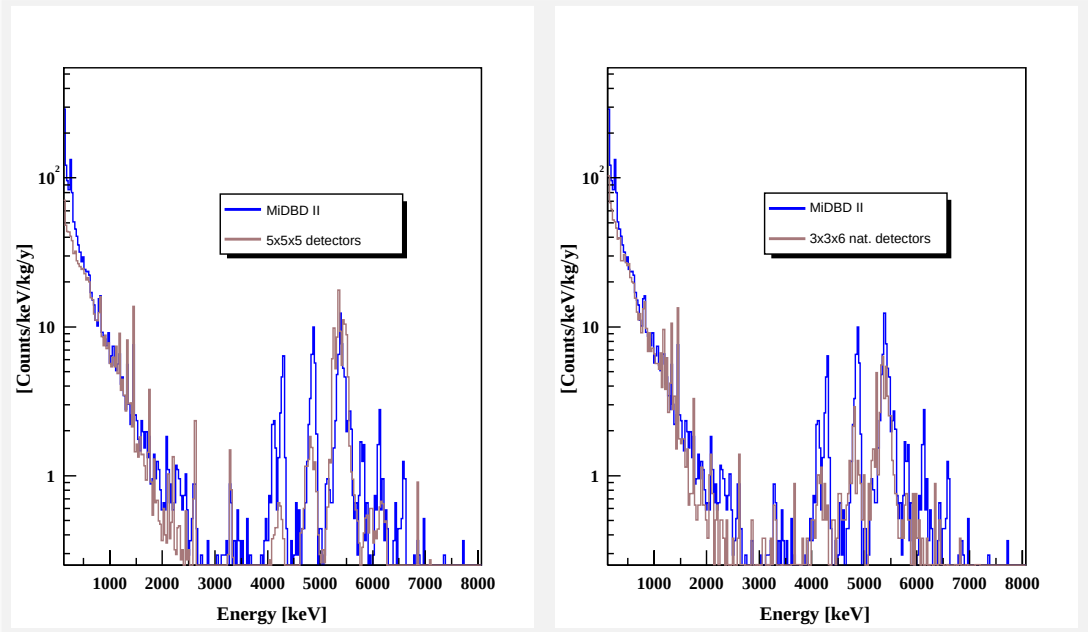

Figure 9: Comparison between the background spectra of CUORICINO crystals and the background measured in MiDBD-II experiment.

	1-2 MeV	2-3 MeV	3-4 MeV	4-5 MeV
MiDBD-II	3.21±0.08	0.61±0.04	0.29±0.02	1.88±0.06
3×3×6 natural	3.29±0.11	0.38±0.04	0.24±0.03	0.78±0.05
5×5×5	3.25±0.09	0.41±0.03	0.17±0.02	0.55±0.03

Table 2: Normalized counting rates (in counts/keV/kg/year units)in MiDBD-II and in CUORICINO.

effect of disconnected detectors in reducing the efficiency of the anticoincidence cut (a fundamental tool to study and localize background sources) is not negligible. A further improvement is therefore expected from the restoration of the lost connections.

By using the background model resulting from the experience gained in the previous bolometric $\beta\beta(0\nu)$ measurements (in particular MiDBD[30]) it is possible to estimate the dominant background contributions in the $\beta\beta(0\nu)$ region. The analysis was limited to the 5×5×5 cm^3 detectors for which the statistical accuracy is better. The result is summarized in table 3 in terms of relative percentage contribution from surface and bulk contaminations. A comparison with the $\beta\beta(0\nu)$ background contributions estimated for MiDBD (for which the total rate was 0.33 ± 0.11 counts/keV/kg/y) is also shown. The comparison is in good agreement with what expected when the changes adopted in CUORICINO are taken into account. It should be noticed that CUORICINO data seem to indicate a shallower depth for the crystal surface contaminations relative to MiDBD. A better determination of the actual depth and density profile of this contamination will be available when a fully operating CUORICINO and a better statistical accuracy will

allow a more significant analysis of the multiple events.

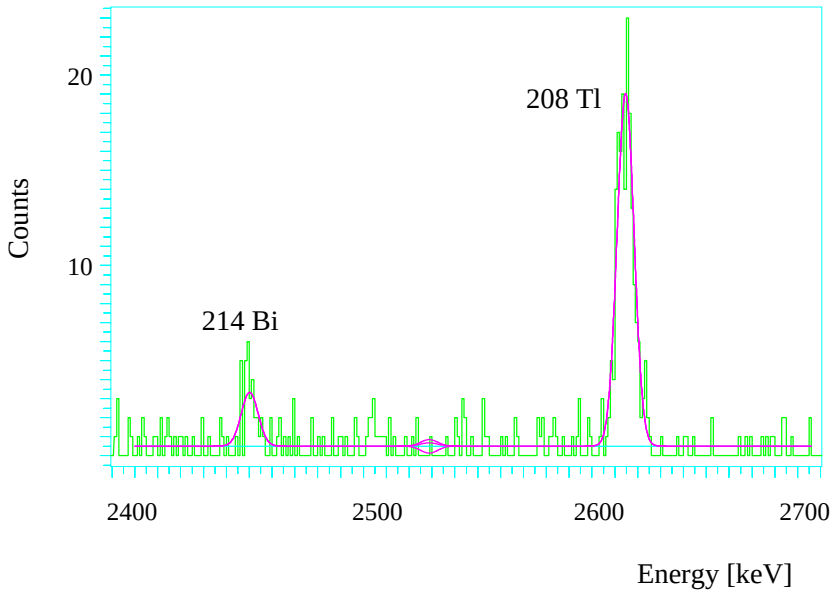

Figure 10: Summed background spectrum from all the operating crystals in the region of neutrinoless double beta decay of ^{130}Te (Q-value=2528.8 keV).

4.3 CUORICINO isotopically enriched crystals

The 4 enriched crystals show a considerable reduction (of the order of 20%) of their counting rates between 1 and 3 MeV with respect to the previous MiDBD measurements. The alpha peaks in the region 4-6 MeV have also undergone a similar reduction. The ^{40}K line now seems to have a similar counting rate in the four detectors while in MiDBD we had an excess in one of the ^{130}Te enriched crystals. A longer measurement is however required to improve the evaluation (reducing the statistical and systematic errors) obtained with the MiDBD data for the $\beta\beta(2\nu)$ half-life [33].

Table 3: Estimate of the relative contributions of the different sources responsible for the background measured in CUORICINO. A comparison with the $\beta\beta(0\nu)$ background contributions estimated for MiDBD is also shown.

Source	^{208}Tl	3-4 MeV	$\beta\beta(0\nu)$	$\beta\beta(0\nu)$ (MiDBD)
TeO_2 ^{238}U and ^{232}Th surface contamination	-	20± 10%	20± 15%	43± 13%
Cu ^{238}U and ^{232}Th surface contamination	∼15%	80± 10%	50± 20%	23± 11%
^{232}Th contamination of cryostat Cu shields	∼85%	-	30± 10%	20± 5%

4.4 Central crystals of the 9 crystal modules

The two central crystals of the 9 crystals modules were intended to disentangle the background contributions due to surface contaminations of the TeO_2 crystals from that of the copper mounting structure. Indeed the two central crystals face a copper surface that is $\sim$3 times smaller than the one faced by the crystals placed at the edges of the modules. This kind of analysis requires a good statistical accuracy in the 3-5 MeV region, with a good calibration of the detectors even in the alpha region. Presently we do not meet these requirements so this kind of analysis has to be postponed.

4.5 ^{130}Te Neutrinoless Double Beta

No peak appears in the anticoincidece background spectrum corresponding to the ^{130}Te double beta decay transition energy (see Fig. 10). A Maximum Likelihood procedure [31, 32] used to establish the maximum number of $\beta\beta(0\nu)$ events compatible with the measured background allows us to set a lower limit on the ^{130}Te $\beta\beta(0\nu)$ half-life of 5.5×10^{23} years at 90% C.L. The corresponding upper bound on the Majorana effective mass ranges from 0.38 to 2.2 eV depending on the QRPA nuclear model (these models seem the most suitable for heavy nuclei) used to interpret the data [30].

The early CUORICINO data already show that CUORICINO is a competitive experiment in the field of neutrinoless double beta decay[34, 35]. Once completely working CUORICINO will have a 5 year sensitivity (1σ) of about 10^{25} year for the $\beta\beta(0\nu)$ of ^{130}Te . This means that CUORICINO will be able to test the Majorana mass in the 100-500 meV range.

4.6 Conclusions

While being a self-consistent experiment, CUORICINO finds its place in the CUORE project as a test facility intended to verify the technical feasibility of CUORE. Indeed the good results obtained as far as the detector performances are concerned prove that the realization of CUORE could be more straightforward than expected. There is still some *R&D* that is required to improve detector reproducibility in order to reduce the spread in the main parameters that characterize detector performances (as the pulse height, the energy resolution and the detector signal rise and decay times). Nevertheless the good results obtained in CUORICINO prove that the increase in the number of bolometers and in the total mass of the array do not substiantially affect the quality of the experiment: the MiDBD experiment with 3 times fewer detectors, and a mass 6 times lower than CUORICINO, had a similar energy resolution in the background sum spectrum. For what concerns background evaluation, due to its completely different structure with respect to CUORE, CUORICINO cannot be a complete test of CUORE feasibility. Indeed CUORE will have a tightly packed structure where the operation of the detectors in anticoincidence should allow a strong reduction of background. Moreover the lead shield designed for CUORE will be optimized in order to practically cancel the background coming from outside. This optimization was not possible in CUORICINO housed in an old cryostat where the space is limited. Indeed to mount CUORICINO in the same cryostat that was used for MiDBD, the internal Roman lead shield thickness was necessarly

reduced. The CUORICINO background results, although preliminary, are however very promising. They demonstrate both the effectiveness of the procedures applied during its preparation and our knowledge of its main background contributions. The detailed study of CUORICINO background (i.e. with better statistical accuracy) will give more insight into background sources. Together with the other foreseen R&D activities (mainly surface cleaning and material selection) it will allow us to reach the required sensitivity for CUORE.

We would like to thank the Laboratori Nazionali del Gran Sasso for generous hospitality and support. We would like to acknowledge also the continuous and constructive help of C. Callegaro, M. Clemenza, G. Galotta, R. Gaigher, G. Nisi, P. Nuvolone, S. Parmeggiano, M. Perego, B. Romualdi and A. Rotilio in various stages of the CUORICINO experiment.
This experiment has been partly supported by the Commission of European Communities under contracts FMRX-CT98-03167 and HPRN-CT-2002-00322, by the U.S. Dept. of Energy under Contract number DE-AC03-76 SF000 98 and by the National Science Foundation.

5 List of 2003 Publications

1. C. Arnaboldi et al., *First Results on Neutrinoless Double Beta Decay of ^{130}Te with the Calorimetric Cuoricino Experiment*, accepted for publication on Phys. Lett. B.

2. C. Arnaboldi et al., *Physics potential and prospects for the CUORICINO and CUORE experiments*, Astroparticle Physics 20 (2003) 91-110.

3. C. Arnaboldi et al., *The CUORICINO ^{130}Te $\beta\beta$ -decay experiment and a new limit on $\beta\beta(0\nu)$* , Proc. of NANP2003, Dubna , June 24 2003, Russia.

4. M.Pavan et al., *First results of the CUORICINO experiment and CUORE prospects*, Proc. of the NDM03 Symposium, Nara 9-14 2003, Japan.

5. C. Bucci et al., *First results from the CUORICINO experiment*, Proc. of the X International Workshop on Low Temperature Detectors (LTD10), Ed. by F.Gatti Genoa 6-11 July 2003, to be published on Nucl. Instrum. and Meth. A.

6. A. Nucciotti et al., *Preliminary results on the search for neutrinoless double beta decay of ^{130}Te with the CUORICINO experiment*, Proc. of the International Europhysics Conference on High Energy Physics (HEP03), Aachen 17-23 July 2003, Germany.

7. O.Cremonesi et al., *First CUORICINO results and the CUORE project*, Proc. of MEDEX03, Praga 7-10 July 2003, Czech Republic.

8. S.Pirro et al., *First results of the CUORICINO experiment*, Proc. of TAUP 2003, Seattle 5-9 September, USA.

References

[1] Q.R.Ahmad et al , Phys.Rev.Lett.89 (2002) 001302 (and references therein); and Q.R.Ahmad et al., arXiv:nucl-ex/0309004

[2] S. Fukuda el al , Phys.Rev.Lett.86 (2001) 5656 (and references therein); and M.B.Smy et al., arXiv:hep-ex/0309011

[3] T.Kajita and Y.Totsuka, Rev.Mod.Phys. 73 (2001) 85 (and references therein); and Y.Hayato: Talk given at the International EPS Conference of High Energy Physics , July 17-23, 2003 , Aachen ,Germany

[4] K. Eguchi et al.,Phys.Rev.Lett.90 (2003) 021802

[5] S. Elliott and P. Vogel,Ann.Rev.Nucl.Part.Sci. 52 (2002) 115

[6] O. Cremonesi, Nucl.Phys. B (Proc.Suppl.)118 (2003) 287

[7] V.I. Tretyak and Yu.G. Zdesenko, Atomic Data and Nuclear Data Tables, 80 (2002) 83

[8] H. Ejiri , Prog. in Part. and Nucl. Phys. B 48 (2002) 185

[9] H.V. Klapdor-Kleingrothaus, A. Dietz, H.V. Harney and I.V. Krivosheina, Modern Physics Letters A 16 (2001) 2409 and hep-ph/0201231.

[10] L. Harney: Reply to the comment on "Evidence for neutrinoless double beta decay", arXiv:hep-ph/0205293.

[11] F.Feruglio, A. Strumia and F.Vissani, Nucl.Phys.B 637 (2002) 345, and addendum Nucl.Phys.B 659 (2003) 359.

[12] C.E Aalseth et al., Modern Phys. A 17 (2202) 1475 hep-ex/0202018.

[13] Yu.G.Zdesenko, F.A.Danevic, and V.I. Tretyak, Phys.Lett.546 (2002) 206.

[14] A.M. Bakaliarov et al : Results of the experiment on investigation of Germanium-76 double beta decay, presented to the NANP2003, Dubna , June 24, 2003.

[15] A.L. Turkevich, T.E. Economou, and G.A. Cowan, Phys. Rev. Lett. 67, 3211 (1992).

[16] O.K. Manuel, Proc. of the Int. Symp. on Nuclear Beta Decay and Neutrino, Osaka, Japan, World Scientific, Singapore,1986, p. 71; O.K. Manuel, J. Phys. G: Nucl. Part. Phys. 17, S221 (1991); J.T. Lee, O.K. Manuel and R.I. Thorpe, Nucl. Phys. A 529 (1991) 29 , and private communication by O.K. Manuel

[17] T. Kirsten, Proc.of the Int. Symp. on Nuclear Beta Decay and Neutrino, Osaka, Japan, World Scientific, Singapore (1986) p. 81, and private communication by T. Kirsten

[18] T. Bernatowicz et al., Phys. Rev.Lett. 69 (1992) 2341 and Phys. Rev. C47 (1993) 806.

[19] N. Takaoka, Y. Motomamura and K Nagao, Phys. Rev. C 53 (1996) 1557.

[20] A. Kawashima et al., Phys. Rev. C 47 (1993) 2452; this indication has been confirmed in a direct experiment by the NEMO II collaboration.

[21] G.F. Dell'Antonio and E. Fiorini, Suppl. Nuovo Cim. 17 (1960) 132.

[22] E. Fiorini and T. Niinikoski, Nucl. Instrum. and Meth. 224 (1984) 83.

[23] D. Twerenbold, Rep. Prog. Phys. 59 (1996) 349; N. Booth, B. Cabrera and E. Fiorini, Ann. Rev. of Nucl. Sci. 46 (1996) 471.

[24] Proc. of the IX International Workshop on Low Temperature Detectors, Ed. by F. Scott Porter, D. McCammon, M. Galeazzi and C.K. Stahle, Madison (Wisconsin) 22-27 July 2001. Amer. Inst. of Phys. Vol. 605 (2002)

[25] Proc. of the X International Workshop on Low Temperature Detectors, Ed. by F.Gatti Genoa 6-11 July 2003, to be published on Nucl. Instrum. and Meth.A

[26] G.R. Dyck et al., Phys. Lett. B 245 (1990) 343

[27] R.B. Firestone, C. Baglin and S.F. Chu: Tables of Isotopes (eight edition), 1998 CD-ROM update (1998)

[28] Previous LNGS Annual Reports.

[29] E.E. Haller et al., Proc. Fourth Int. Conf. on Neutron Transmutation Doping of Semiconductor Materials, Nat. Bureau of Standards, June 1,2 1982, Gaithersburg MD, R. D. Larrabee ed., (Plenum Press 1984) p 21.

[30] CUORE Collaboration, *CUORE (Cryogenic Underground Observatory for Rare Events): A proposal submitted to the INFN, the us doe and the us nsf by the international CUORE Collaboration*, 2003 (http://crio.mib.infn.it/wig).

[31] S. Baker and P.D. Cousins., Nucl. Instrum. and Meth. 221 (1984) 437.

[32] R.M. Barnett et al. (PDG), Phys. Rev. D54 (1996) 1.

[33] C. Arnaboldi et al., Phys. Lett. B 557 (2003) 167.

[34] C. Arnaboldi et al., Astroparticle Physics 20 (2003) 91-110

[35] C. Arnaboldi et al., accepted for publication on Phys. Lett. B. (2004)

DAMA. Dark Matter Search

DAMA collaboration:
P. Belli[a], R. Bernabei[a,@], A. Bussolotti[a,*], F. Cappella[a,b],
P. Delfini[a,*], F. Montecchia[a,c], F. Nozzoli[a], R. Cerulli[b],
A. d'Angelo[d,e], A. Incicchitti[d], A. Mattei[d,*], D. Prosperi[d],
C.J. Dai[f], H.H. Kuang[f], J.M. Ma[f], Z. P. Ye[f,g]

in neutron measurements: M.Angelone[h], P.Batistoni[h], M.Pillon[h]

in some by-product results: F.A. Danevich[i], V. Denisov[i], V.V. Kobychev[i], O.A. Ponkratenko[i], V.I. Tretyak[i], Yu.G. Zdesenko[i]

[a]Dip. di Fisica, Università di Roma "Tor Vergata" and INFN-Roma2, 00133 Roma, Italy;
[b]Laboratorio Nazionale del Gran Sasso, INFN, 67010 Assergi (Aq), Italy;
[c]Università "Campus Bio-Medico" di Roma, 00155 Roma, Italy;
[d]Dip. di Fisica, Università di Roma "La Sapienza" and INFN-Roma, 00185 Roma, Italy;
[e]Scuola di Specializzazione in FISICA SANITARIA, Università di Roma "Tor Vergata", 00133 Rome, Italy;
[f]IHEP, Chinese Academy, P.O. Box 918/3, Beijing 100039, China;
[g]University of Zhao Qing, Guang Dong, China;
[h]ENEA - C. R. Frascati, P.O. Box 65, 00044 Frascati, Italy;
[i]Institute for Nuclear Research, 252650 Kiev, Ukraine.

@ Spokesperson
* technical staff

Abstract

DAMA is investigating various rare processes by developing and using several kinds of radiopure scintillators. The main experimental set-ups are: i) the $\simeq$ 100 kg NaI(Tl) set-up (DAMA/NaI), which completed its data taking in July 2002; ii) the new $\simeq$ 250 kg NaI(Tl) LIBRA (Large sodium Iodide Bulk for RAre processes) set-up (DAMA/LIBRA), which has been preliminarily put in operation during year 2003; iii) the $\simeq$ 6.5 kg liquid Xenon pure scintillator (DAMA/LXe); iv) the R&D installation for measurements on prototype PMTs and detectors and for small scale experiments (DAMA/R&D). Moreover, in the framework of devoted R&D for higher

radiopure detectors and PMTs, sample measurements are carried out by means of the low background Ge detector of the DAMA experiment and in some cases at Ispra. In particular, during year 2003 the cumulative exposure collected by DAMA/NaI over its seven annual cycles of operation (107731 kg $\times$ day) has been released. The data of the last 3 annual cycles further confirm the previous model independent result and, in conclusion, the presence of Dark Matter particles in the galactic halo is now supported – in a model independent way – at 6.3 σ C.L.. No other experiment whose result can be directly compared with this one is available so far in the field of Dark Matter investigation.

1 Introduction

DAMA is an observatory for rare processes based on the development and use of various kinds of radiopure scintillators. Several low background set-ups have been realised and used; the main ones are: i) DAMA/NaI ($\simeq$ 100 kg of radiopure NaI(Tl)), which took data underground over seven annual cycles and was put out of operation in July 2002; ii) the new second generation DAMA/LIBRA ($\simeq$ 250 kg; more radiopure NaI(Tl)); iii) DAMA/LXe ($\simeq$ 6.5 kg liquid Xenon), whose performances have been improved several times; iv) DAMA/R&D, which is devoted to measurements on prototypes and to small–scale–experiments. Moreover, in the framework of devoted R&D for higher radiopure detectors and PMTs, sample measurements are carried out by means of the low background, low-Z window DAMA/Ge detector and, in some cases, by means of Ispra facilities.

The DAMA/NaI set-up and its performances have been described in details in ref. [2]. Since then some upgrading has been carried out; in particular, in summer 2000 the electronic chain and data acquisition system were completely renewed and improved [3]. As mentioned, DAMA/NaI took data over seven annual cycles up to July 2002 [3] having as main aim the investigation of the presence of a Dark Matter particle component in the galactic halo by means of the model independent annual modulation signature [4, 37, 38, 39, 40, 41, 42, 43, 44, 3]. The same experiment also achieved several other results on various approaches and rare processes [5, 6, 7, 8, 9, 10, 11, 12]. During year 2003, 107731 kg $\times$ day total exposure has been released [3]; the results are summarized in the following section.

An R&D activity to develop higher radiopure detectors is continuously carried out toward the creation of ultimate radiopure detectors and some studies on possible applications are also carried out (see ref. [13, 14] and 2003 publication list). In particular, as a result of a second generation R&D effort for NaI(Tl) radiopurification (by exploiting new material selections, new chemical/physical radiopurification of NaI and TlI powders and new protocols) the new DAMA/LIBRA set-up with exposed target-detector mass enlarged up to $\simeq$ 250 kg has been realized and put preliminarily in operation during year 2003.

At present a third generation R&D toward a possible ton NaI(Tl) set-up, we proposed in 1996, has been funded and is in progress of development.

Moreover, following the former Xelidon experiment on R&D developments of liquid Xenon detectors in latest 80's, DAMA considered many years ago (see e.g. ref. [15]) the

use of the liquid Xenon as target-detector material for particle dark matter search and realized several LXe prototype detectors using natural Xenon. Then, it preliminarily put in measurement the set-up employed in the data taking of ref. [16, 17] by using Kr-free Xenon enriched in ^{129}Xe at 99.5%. This set-up was significantly upgraded at fall 1995 and again – deeply – in summer 2000 when the handling of Kr-free Xenon enriched in ^{136}Xe at 68.8% and in ^{134}Xe at 17.1% was introduced. Main features of the set-up are described in ref. [18]. Investigations on several rare processes have been carried out with time passing in the various configurations [16, 17, 18, 19, 20, 21, 22, 23, 24, 25, 26, 27]. Further works have been carried out during year 2003 and some additional analyses have been presented (see 2003 publication list). Note that – on the contrary of the NaI(Tl) case – no plans for enlarging the exposed mass of a LXe set-up have been considered for the technical reasons we have pointed out several times in the past (see e.g. [76]).

Finally, as mentioned, the set-up named "R&D" is used for tests on prototype PMTs and/or detectors and for small scale experiments mainly devoted to the search for double beta decay processes in various isotopes, such as ^{136}Ce, ^{142}Ce, ^{40}Ca, ^{46}Ca, ^{106}Cd, ^{48}Ca [28, 29, 30, 31, 32]. Both the active and the passive source techniques have been exploited as well as – sometimes – the coincidence technique. The works and results in 2003 are also summarized in the following.

2 DAMA/NaI

The DAMA/NaI experiment has been built in order to have suitable mass, sensitivity and control of the running conditions to investigate the particle Dark Matter presence in the galactic halo by exploiting the annual modulation signature. We remind that the WIMP annual modulation signature is based on the annual modulation of the signal rate induced by the Earth revolution around the Sun; as a consequence, the Earth is crossed by a larger WIMP flux roughly in June (when its rotational velocity is summed to the one of the solar system with respect to the Galaxy) and by a smaller one roughly in December (when the two velocities are subtracted). The annual modulation signature is very distinctive since a WIMP-induced seasonal effect must simultaneously satisfy all the following requirements: the rate must contain a component modulated according to a cosine function (1) with one year period, T, (2) and a phase, t_0, that peaks around $\simeq 2^{nd}$ June (3); this modulation must only be found in a well-defined low energy range, where WIMP induced recoils can be present (4); it must apply to those events in which just one detector of many actually "fires" (*single-hit* events), since the WIMP multi-scattering probability is negligible (5); the modulation amplitude in the region of maximal sensitivity is expected to be $\lesssim$7% (6). For the sake of completeness, we mention that this latter rough limit would be larger either in case the WIMPs would match the scenario of ref. [33] (because of kinematic effects) or the scenario of ref. [34] (because of a possible external contribution to the dark halo from the Sagittarius Dwarf Tidal Stream). To mimic such a signature spurious effects or side reactions should not only be able to account for the whole observed modulation amplitude, but also to contemporaneously satisfy all the requirements; no one has been found or suggested by anyone over about a decade. We remark that no other rare process offers a so stringent signature.

As mentioned, to point out the modulation component of a signal, apparata with suitable mass, performances and control of the operating conditions are necessary, such as DAMA/NaI – which has been the only experiment able to effectively exploit such a WIMP signature over about a decade – and now the $\simeq$ 250 kg higher radiopure NaI(Tl) DAMA/LIBRA set-up. This approach – originally suggested by [35] – allows to investigate the presence of a Dark Matter particle component in the galactic halo independently on any astrophysical, nuclear and particle physics modeling. Corollary quests for the candidate particle require instead to choose a model; therefore, the results are not general and refer case by case to the considered model framework [1] as it is always the case for results given in form of exclusion plots (which, thus, have no generality) and for the values of mass and cross sections of a particle Dark Matter candidate derived from indirect searches (for some discussion see e.g. [3]).

The presence of a model independent positive evidence in the data of DAMA/NaI has been firstly reported by the DAMA collaboration at the TAUP conference in 1997 [36] and published also in [37], confirmed in [38, 39], further confirmed in [40, 41, 42, 43, 44] and conclusively confirmed, at end of experiment, in 2003 [3]. Corollary model dependent quests for a candidate particle have been carried out in some of the many possible model frameworks and have been improved with time. In particular, some scenarios either for mixed spin-independent (SI) and spin-dependent (SD) coupled WIMPs or for purely SI coupled WIMPs or for purely SD [2] coupled WIMPs have been considered in some of the many possible model frameworks as well as the case of WIMPs with *preferred inelastic* scattering.

For the sake of completeness we remind that the claims for contradiction by CDMS-I, Edelweiss-I and Zeplin-I are intrinsecally wrong and arbitrary. In fact, as it can be easily understood, no model independent comparison is possible among the exclusion plots they claim and the DAMA/NaI allowed regions, because of the different methodological approaches, of the different target nuclei, etc.. As regards possible model dependent comparisons – in addition to experimental considerations (see ref. [3]) – those experiments give result only in a single purely SI model framework with fixed/selected assumptions, neglecting experimental and theoretical uncertainties and generally quoting so far the DAMA/NaI result in an incorrect, unupdated and incomplete way; moreover, they also ignore the existence of other solutions to which they have no or poorer sensitivity. Some specific arguments have been addressed in ref. [3], where in addition some recent possible positive hints – not in contradiction with the DAMA/NaI result – from Dark Matter indirect searches[3] have also been summarised.

[1] We remark that a model framework is identified by the general astrophysical, nuclear and particle physics assumptions and by the set of values used for all the experimental and theoretical parameters needed in the calculations (for example WIMP nature, WIMP couplings, form factors, spin factors, scaling laws, quenching factors, halo model, WIMP local velocity, etc., which are either unknown or affected by relevant uncertainties, usually not accounted in results presented in the field; see for example discussions in ref. [3]).

[2] We remind that JHEP 0107 (2001) 044 is not at all in conflict with a purely SD solution since it considered only two particular purely SD couplings (of the many possible) in a strongly model dependent context and using modulation amplitudes valid instead only in a particular purely SI case. Moreover, the mixed SI & SD case was not involved at all in that discussion.

[3] For the sake of completeness we note that, as mentioned, the values of mass and cross section of

2.1 The final DAMA/NaI model independent result on the WIMP annual modulation signature over 7 annual cycles

A model independent investigation of the WIMP annual modulation signature has been realised by exploiting the time and energy behaviour of the experimental residual rates of the *single-hit* events in the lowest energy region over seven annual cycles (total exposure: 107731 kg × day) [3]. The experimental data are shown in Fig. 1 – *left*; they offer an immediate evidence of the presence of an annual modulation of the rate of the *single-hit* events in the lowest energy region.

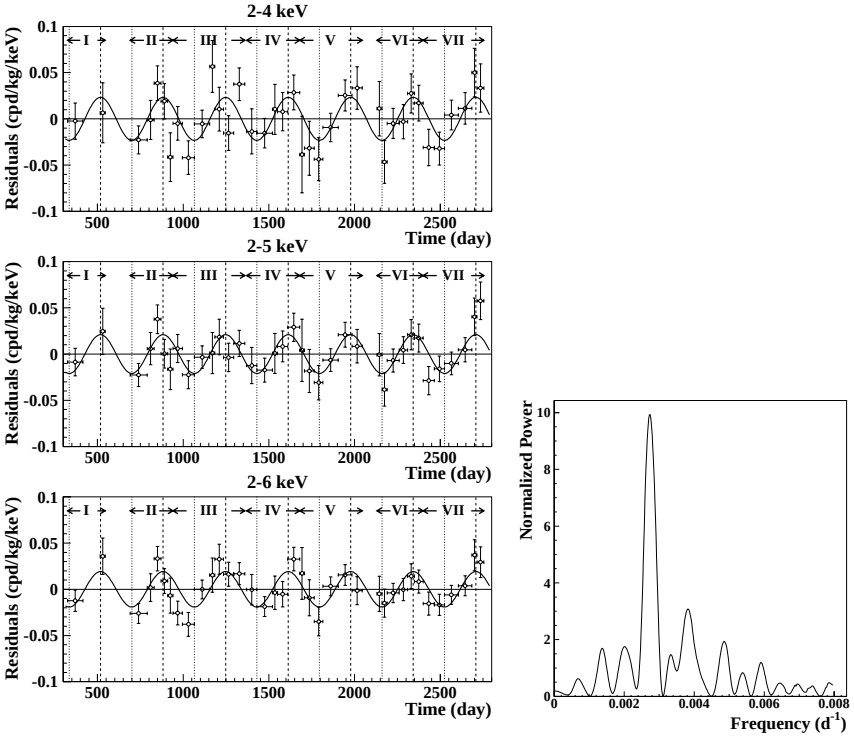

Figure 1: *On the left*: experimental residual rate for *single-hit* events in the (2–4), (2–5) and (2–6) keV energy intervals as a function of the time over 7 annual cycles (total exposure 107731 kg × day); end of data taking July 2002. The experimental points present the errors as vertical bars and the associated time bin width as horizontal bars. The superimposed curves represent the cosinusoidal functions behaviours expected for a WIMP signal with a period equal to 1 year and phase at 2^{nd} June; the modulation amplitudes have been obtained by best fit [3]. *On the right*: power spectrum of the measured (2–6) keV *single-hit* residuals calculated according to ref. [45], including also the treatment of the experimental errors and of the time binning. As it can be seen, the principal mode corresponds to a frequency of $2.737 \cdot 10^{-3}$ d^{-1}, that is to a period of $\simeq 1$ year. [3].

The data favour the presence of a modulated cosine-like behaviour ($A \cdot \cos\omega(t - t_0)$) at

particle Dark Matter candidates as derived from indirect searches (which can give only a model dependent result) have no univocal meaning since they depend on the assumed model framework and background component modeling.

6.3 σ C.L. and their fit for the (2–6) keV larger statistics energy interval offers modulation amplitude equal to (0.0200 ± 0.0032) cpd/kg/keV, $t_0 = (140 \pm 22)$ days and $T = \frac{2\pi}{\omega} = (1.00 \pm 0.01)$ year, all parameters kept free in the fit. The period and phase agree with those expected in the case of a WIMP induced effect ($T = 1$ year and t_0 roughly at $\simeq 152.5^{th}$ day of the year). The χ^2 test on the (2–6) keV residual rate in Fig. 1 – *left* disfavours the hypothesis of unmodulated behaviour giving a probability of $7 \cdot 10^{-4}$ ($\chi^2/d.o.f. = 71/37$). We note that, for simplicity, in Fig. 1 – *left* the same time binning already considered in ref. [40, 41] has been used; the result of this approach is similar by choosing other time binnings. The experimental residuals given in Fig. 1 – *left* have also been fitted, according to the previous procedure, fixing the period at 1 year and the phase at 2^{nd} June; the best fitted modulation amplitudes are: (0.0233 ± 0.0047) cpd/kg/keV for the (2–4) keV energy interval, (0.0210 ± 0.0038) cpd/kg/keV for the (2–5) keV energy interval, (0.0192 ± 0.0031) cpd/kg/keV for the (2–6) keV energy interval, respectively.

The same data have also been investigated by a Fourier analysis (performed according to ref. [45] including also the treatment of the experimental errors and of the time binning), obtaining the result shown in Fig. 1 – *right*, where a clear peak corresponding to a period of 1 year is evident.

In Fig. 2 the experimental *single-hit* residual rate from the total exposure of 107731 kg $\times$ day is presented, as in a single annual cycle, for two different energy intervals; as it can be seen the modulation is clearly present in the (2–6) keV energy region, while it is absent just above.

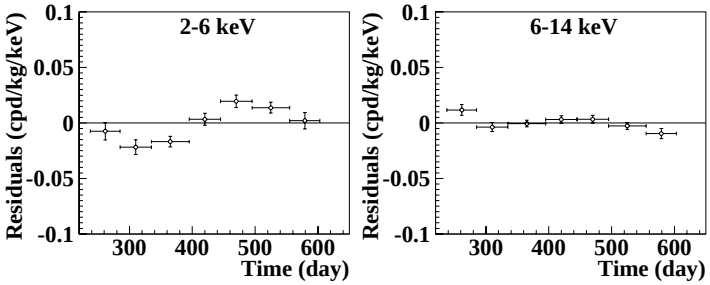

Figure 2: Experimental *single-hit* residual rate from the total exposure of 107731 kg $\times$ day as in a single annual cycle. The experimental points present the errors as vertical bars and the associated time bin width as horizontal bars. The initial time is taken at August 7^{th}. Fitting the data with a cosinusoidal function with period of 1 year and phase at 152.5 days, the following modulation amplitudes are obtained: (0.0195 ± 0.0031) cpd/kg/keV and $-(0.0009 \pm 0.0019)$ cpd/kg/keV, respectively. Thus, a clear modulation is present in the lowest energy region, while it is absent just above.

Finally, a suitable statistical analysis has shown that the modulation amplitudes are statistically well distributed in all the crystals, in all the data taking periods and considered energy bins [3].

On the investigation of possible systematic effects and side reactions. As previously mentioned, to mimic the annual modulation signature a systematic effect or side reaction should not only be able to account for the whole observed modulation amplitude, but also able to satisfy the requirements of a WIMP induced effect. A careful investigation of all the known possible sources of systematics and side reactions has been regularly

carried out and published at time of each data release. In particular, detailed quantitative discussions can be found in ref. [41, 3] and will not be repeated here [4]. As it can be seen there, no systematic effect or side reaction able to mimic a WIMP induced effect has been found.

As a further relevant investigation, the *multiple-hits* events also collected during the DAMA/NaI-6 and 7 running periods (when each detector was equipped with its own Transient Digitizer with a dedicated renewed electronics) have been studied and analysed by using the same identical hardware and the same identical software procedures as for the case of the *single-hit* events. The *multiple-hits* events class – on the contrary of the *single-hit* one – does not include events induced by WIMPs since the probability that a WIMP scatters off more than one detector is negligible.

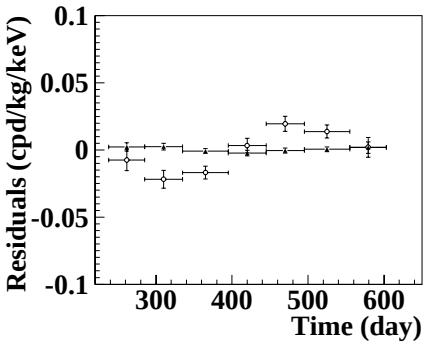

Figure 3: Experimental residual rates over seven annual cycles for *single-hit* events (open circles) – class of events to which WIMP events belong – and over the last two annual cycles for *multiple-hits* events (filled triangles) – class of events to which WIMP events do not belong – in the (2–6) keV cumulative energy interval. They have been obtained by considering for each class of events the data as collected in a single annual cycle and using in both cases the same identical hardware and the same identical software procedures. The initial time is taken on August 7^{th}.

Fig. 3 shows the behaviour of the residual rate of *multiple-hits* events in the (2–6) keV energy interval measured during the DAMA/NaI-6 and -7 running periods as a function of the time in a year. It is compared with the residual rate of the *single-hit* events measured in the same energy interval with the total exposure. Fitting these data with the function $A\cdot \cos\omega(t-t_0)$ with period of 1 year and phase at 152.5 days, the following modulation amplitudes are obtained: $A = (0.0195 \pm 0.0031)$ cpd/kg/keV and $A = -(3.9 \pm 7.9)\cdot 10^{-4}$ cpd/kg/keV for *single-hit* and *multiple-hits* residual rates, respectively. Thus, a 6.3 σ C.L. evidence of annual modulation is present in the *single-hit* residuals (events class to which the WIMP-induced recoils belong), while it is absent in the *multiple-hits* residual rate (event class to which only background events belong). Since the same identical hardware

[4]We take this opportunity only to comment that the sizeable discussions reported e.g. in [41, 3] already demonstrated that a possible modulation of neutron flux (possibly observed by the ICARUS coll. as reported in the ICARUS internal report TM03-01) cannot quantitatively contribute to the DAMA/NaI observed modulation amplitude, even if the neutron flux would be assumed to be 100 times larger than measured at LNGS by several authors with different techniques over more than 15 years; in addition, as widely known, it cannot satisfy all the peculiarities of the signature.

and the same identical software procedures have been used to analyse the two classes of events, the obtained result offers an additional strong support for the presence of Dark Matter particles in the galactic halo further excluding any side effect either from hardware or from software procedures or from background.

Conclusion. In conclusion, the presence of an annual modulation in the *single-hit* events residual rate in the lowest energy interval (2 – 6) keV satisfying all the features expected for a particle Dark Matter component in the galactic halo is supported by the data of the seven annual cycles at 6.3 σ C.L.. This is the experimental result of DAMA/NaI. It is model independent; no other experiment whose result can be directly compared with this one is available so far in the field of Dark Matter investigation.

2.2 A corollary result: quests for a candidate particle in some model frameworks with the data of the seven annual cycles

On the basis of the obtained model independent result, corollary investigations can also be pursued on the nature and coupling of the particle Dark Matter candidate. This latter investigation is instead model dependent and – considering the large uncertainties which exist on the astrophysical, nuclear and particle physics assumptions and on the parameters needed in the calculations – has no general meaning (as it is also the case – as mentioned above – of exclusion plots and of the WIMP parameters evaluated in indirect search experiments). Thus, it should be handled in the most general way as we have preliminarily pointed out with time in the past improving the related analyses [37, 38, 39, 40, 41, 42, 43, 44] and we have discussed in specific details in ref. [3]; other efforts on this topic are also in progress. Candidates, kinds of WIMP couplings with ordinary matter and implications, cross sections, nuclear form factors, spin factors, scaling laws, halo models, priors, etc. are discussed in details in ref. [3] and we invite the reader to this reference since these arguments are necessary to correctly understand the results obtained in corollary model dependent quests and the real validity of any claimed model dependent comparison in the field. The results presented in ref. [3] and briefly summarised here are, of course, not exhaustive of the many possible scenarios which at present level of knowledge cannot be disentangled. Some of the open questions are: i) which is the right nature for the WIMP particle [5]; ii) which is its right couplings with ordinary matter (mixed SI&SD, purely SI, purely SD or *preferred inelastic*) iii) which are the right form factors and related parameters for each target nucleus; iv) which is the right spin factor for

[5]Several candidates fulfil the cosmological and particle Physics requirements necessary in order to be considered as a Dark Matter candidate particle: not only the neutralino foreseen in the supersymmetric theories, but also a heavy neutrino of a 4^{th} family (there is still room for it as reported in literature), the sneutrino in the scenario described by [33] (providing – through the transition from lower to upper mass eigenstate – *preferred inelastic* scattering with target-nuclei), the "mirror" Dark Matter [46], etc.. Moreover, in principle whatever Weakly Interacting, neutral, (quasi-)stable and Massive (whose acronym is WIMP) particle, even not yet foreseen by a theory, can be a suitable candidate. As regards in particular the neutralino, we note that the theories have not stringent predictive capability for its cross sections and for its mass because of the large number of free parameters in the theory and of the several assumptions; thus, e.g. the expectations for its nuclear cross sections span over several orders of magnitude as it can also be seen in literature. In addition, we take this occasion to remind that the neutralino has both SI and SD couplings with the ordinary matter.

each target nucleus (some nuclei are disfavoured to some kinds of interactions; for example, in case of an interaction with SD component even a nucleus sensitive in principle to SD interaction could be blinded by the spin factor if unfavoured by the θ value[6]); v) which are the right scaling laws (let us consider as an example that even in a MSSM framework with purely SI interaction the scenario could be drastically modified as discussed recently in ref. [47]); vi) which is the right halo model and related parameters; vii) which are the right values of the experimental parameters within their uncertainties; etc. As an example, we remind that not only large differences in the measured rate can be expected when using target nuclei sensitive to the SD component of the interaction (such as e.g. ^{23}Na and ^{127}I) with respect to those largely insensitive to such a coupling (such as e.g. ^{nat}Ge and ^{nat}Si), but also when using different target nuclei although all – in principle – sensitive to such a coupling (compare e.g. the Xenon and Tellurium cases with the Sodium and Iodine cases) [3].

In the following some of the results discussed for some of the many possible model dependent quests for a particle Dark Matter candidate are briefly reminded [3]. In particular, they have been obtained from the data collected during all the seven annual cycles, considering the halo models summarized in [44, 3] for three of the possible values of the local velocity v_0: 170 km/s, 220 km/s and 270 km/s. The escape velocity has been maintained at the fixed value: 650 km/s, but it is worth to note that the present existing uncertainties on the knowledge of its value can play a relevant role in evaluating allowed regions (and corresponding best fit values for WIMP mass and cross section) e.g. in the cases of *preferred inelastic* WIMPs and of light mass WIMP candidates; its effect would be instead marginal at large WIMP masses. The possible scenarios have been exploited for those halo models in some discrete cases including some of the uncertainties which exist in the parameters of the used nuclear form factors and in the quenching factors; the prior from DAMA/NaI-0 has been considered as well. For the details see ref. [3]. The results summarised here are not exhaustive of the many scenarios possible at present level of knowledge: for some other recent ideas see e.g. the already quoted [34, 47].

For simplicity, here the results of these corollary quests for a candidate particle are presented in terms of allowed regions obtained as superposition of the configurations corresponding to likelihood function values *distant* more than 4σ from the null hypothesis (absence of modulation) in each of the several (but still a limited number) of the possible model frameworks considered here. Obviously, larger sensitivities than those reported in the following figures would be reached when including the effect of other existing uncertainties on the astrophysical, nuclear and particle Physics assumptions and related parameters; similarly, the set of the best fit values would also be enlarged as well.

As well known, DAMA/NaI is intrinsically sensitive both to low and high WIMP mass having both a light (the ^{23}Na) and a heavy (the ^{127}I) target-nucleus; in previous corollary quests WIMP masses above 30 GeV (25 GeV in ref. [37]) have been presented [38, 40, 42, 43, 44] for few (of the many possible) model frameworks. However, that bound holds only for the neutralino candidate when supersymmetric schemes based on GUT assumptions are adopted to analyse the LEP data [48]. Thus, since other candidates are possible and also other scenarios can be considered for the neutralino itself as recently

[6]We remind that $tg\theta = a_n/a_p$ is the ratio between the WIMP-neutron and the WIMP-proton effective SD coupling strengths, a_n and a_p, respectively [42, 3]; θ is defined in the $[0,\pi)$ interval.

pointed out [7], the present model dependent lower bound quoted by LEP for the neutralino in the supersymmetric schemes based on GUT assumptions (37 GeV [52]) is simply marked in the following figures. It is worth to note that when this mass limit is adopted, it selects the WIMP-Iodine elastic scattering as dominant because of the used scaling laws and of kinematical arguments.

WIMPs with mixed SI&SD interaction. The most general scenario of WIMP nucleus elastic interaction, to which the DAMA/NaI target nuclei are fully sensitive, is the one where both the SI and the SD components of the cross section are present. Thus, as first

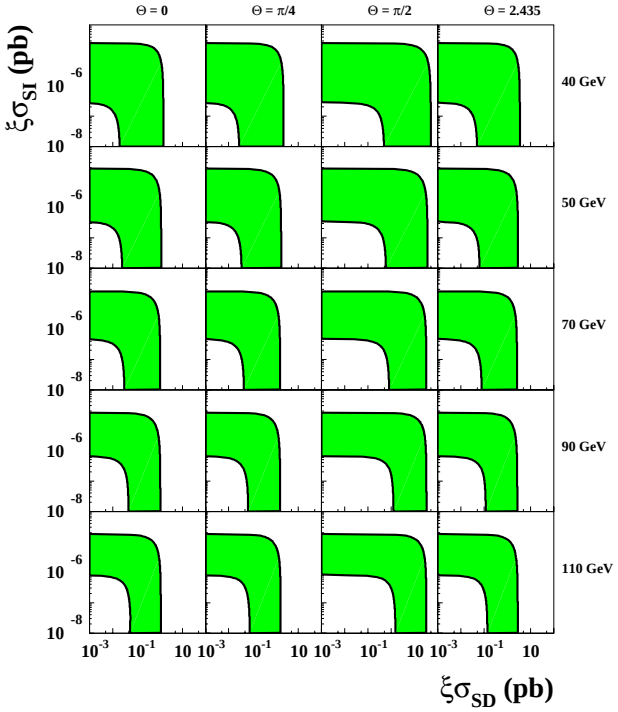

Figure 4: *Case of a WIMP with mixed SI&SD interaction in given model frameworks.* Coloured areas: example of slices (of the allowed 4-dimensional volume) in the plane $\xi\sigma_{SI}$ vs $\xi\sigma_{SD}$ for some of the possible m_W and θ values. Inclusion of other existing uncertainties on parameters and models would further extend the regions; for example, the use of more favourable form factors and/or of more favourable spin factors than the considered ones would move them towards lower cross sections. For details see [3].

the case for a candidate with both SI and SD couplings to ordinary matter (similarly as we did in the past also in ref. [42] on partial exposure) has been considered. In this general scenario the space of the free parameters is a 4-dimensional volume defined by m_W, $\xi\sigma_{SI}$ [8], $\xi\sigma_{SD}$ and θ (which varies from 0 to π). Thus, the general solution would be a four dimensional allowed volume for each considered model framework. Since the graphic representation of this allowed volume is quite difficult, we only show in Fig. 4 the obtained regions in the plane $\xi\sigma_{SI}$ vs $\xi\sigma_{SD}$ for some of the possible θ and m_W values in

[7] In fact, when the assumption on the gaugino-mass unification at GUT scale is released neutralino masses down to $\simeq$ 6 GeV are allowed [49, 50, 51].

[8] ξ ($\xi \leq 1$) is defined here as the fractional amount of local WIMP density.

the model frameworks considered here. In particular, we report just four couplings, which correspond to the following values of the mixing angle θ: i) $\theta = 0$ (a_n =0 and $a_p \neq 0$ or $|a_p| >> |a_n|$) corresponding to a particle with null SD coupling to neutron; ii) $\theta = \pi/4$ ($a_p = a_n$) corresponding to a particle with the same SD coupling to neutron and proton; iii) $\theta = \pi/2$ ($a_n \neq 0$ and $a_p = 0$ or $|a_n| >> |a_p|$) corresponding to a particle with null SD couplings to proton; iv) $\theta = 2.435$ rad ($\frac{a_n}{a_p}$ = -0.85) corresponding to a particle with SD coupling through Z_0 exchange. The case $a_p = -a_n$ is nearly similar to the case iv).

From the given figures it is clear that at present either a purely SI or a purely SD or a mixed SI&SD configurations are supported by the experimental data of the seven annual cycles. We remind that ^{nat}Ge detectors (as those of Cdms-I and Edelweiss-I) are intrinsically largely blinded to the SD component of the interaction; the same is for Xenon detectors (as those of Zeplin I) in the case of a particular choice of the θ value ($\theta \simeq 0$ or $\theta \simeq \pi$).

WIMPs with dominant SI interaction. Generally, the case of purely SI coupled WIMP is mainly considered in literature. In fact, often the spin-independent interaction with ordinary matter is assumed to be dominant since e.g. most of the used target-nuclei are practically not sensitive to SD interactions (as on the contrary ^{23}Na and ^{127}I are) and the theoretical calculations are even much more complex and uncertain. Thus, following an analogous procedure as for the previous case, we have exploited for the same model frameworks the purely SI scenario. In this case the free parameters are two: m_W and $\xi\sigma_{SI}$. In Fig. 5 – *left* the region allowed in the plane m_W and $\xi\sigma_{SI}$ for the considered model frameworks is reported. The configurations below the vertical line are of interest for neutralino when the assumption on the gaugino-mass unification at GUT scale is released and for every other kind of particle Dark Matter candidate. As shown in Fig. 5 – *left*, also WIMP masses above 200 GeV are allowed for some configurations; details can be found in ref. [3]. Of course, best fit values of cross section and WIMP mass span over a large range in the considered frameworks. In addition, configurations with $\xi\sigma_{SI}$ even much lower than those shown in Fig. 5 – *left* are accessible in case an even small SD contribution is present in the interaction. This possibility is clearly pointed out in Fig. 5 – *right* where an example of allowed regions in the plane (m_W, $\xi\sigma_{SI}$) corresponding to different SD contributions is reported for the case $\theta = 0$. As it can be seen, increasing the SD contribution the allowed regions involve SI cross sections much lower than 10^{-6} pb. It can be noted that for $\sigma_{SD} \geq 0.08$ pb the annual modulation effect observed is also compatible – for $m_W \simeq 40-75$ GeV – with a particle Dark Matter candidate with no SI interaction at all. Analogous situation is found for the other model frameworks. This also clearly shows that, in addition to other arguments, there is intrinsecally no meaning in bare comparisons between regions allowed in esperiments sensitive to SD coupling (such as DAMA/NaI) and exclusion plots achieved with target detectors which are not (such as CDMS/I and Edelweiss/I) as well as in bare comparisons between regions allowed in esperiments whose target nuclei have unpaired proton (such as DAMA/NaI) with exclusion plots quoted by experiments using target/nuclei with umpaired neutron (such as Zeplin/I).

Finally, the inclusion of other existing uncertainties on parameters and models would further extend the allowed region. For example The inclusion of other existing uncertainties on parameters and models would further extend the region; for example, the use

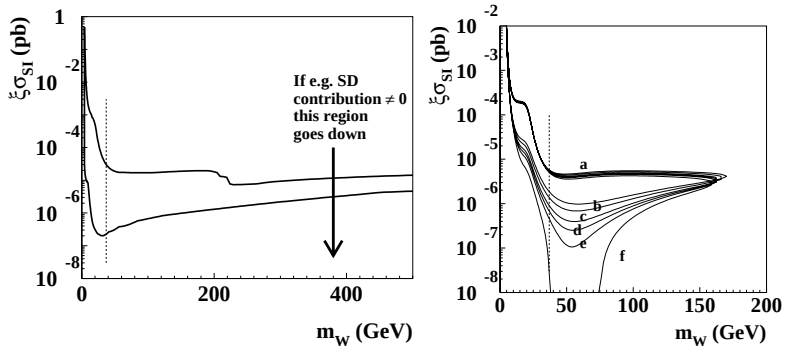

Figure 5: *On the left : Case of a WIMP with dominant SI interaction for given model frameworks.* Region allowed in the plane (m_W, $\xi\sigma_{SI}$). The vertical dotted line represents a bound in case of a neutralino candidate when supersymmetric schemes based on GUT assumptions are adopted to analyse the LEP data; the low mass region is allowed for neutralino when other schemes are considered and for every other particle Dark Matter candidate. While the area at WIMP masses above 200 GeV is allowed only for few configurations, the lower one is allowed by most configurations [3]. The inclusion of other existing uncertainties on parameters and models would further extend the region; for example, the use of more favourable SI form factor for Iodine alone would move it towards lower cross sections. *On the right : Example of the effect induced by the inclusion of a SD component different from zero on allowed regions given in the plane $\xi\sigma_{SI}$ vs m_W.* In this example the Evans' logarithmic axisymmetric $C2$ halo model with $v_0 = 170$ km/s, ρ_0 equal to the maximum value for this model and a given set of the parameters' values (see [3]) have been considered. The different regions refer to different SD contributions for the particular case of $\theta = 0$: $\sigma_{SD} = 0$ pb (a), 0.02 pb (b), 0.04 pb (c), 0.05 pb (d), 0.06 pb (e), 0.08 pb (f). Analogous situation is found for the other model frameworks.

of more favourable SI form factor for Iodine alone would move it towards lower cross sections.

WIMPs with dominant SD interaction. Let us now focus on the case of a candidate with purely SD coupling to which DAMA/NaI is – as mentioned – fully sensitive. When the SD component is different from zero, a very large number of possible configurations is available. In fact, in this scenario the space of free parameters is a 3-dimensional volume defined by m_W, $\xi\sigma_{SD}$ and θ (which can vary from 0 to π). Here, just as an example we show the results obtained only for a particular coupling, which correspond to a mixing angle $\theta = 2.435$ (Z_0 coupling); see Fig. 6; other configurations are possible in the considered frameworks when varying the θ value. The area at WIMP masses above 200 GeV is allowed for low local velocity and all considered sets of parameters by the Evans' logarithmic $C2$ co-rotating halo model [3]. Moreover, the accounting for the uncertainties e.g. on the form factors and/or on the spin factors as well as different possible formulations of the SD form factors would extend the allowed regions, e.g. towards lower $\xi\sigma_{SD}$ values. Moreover, $\xi\sigma_{SD}$ lower than those corresponding to the regions shown in Fig. 6 are possible also e.g. in case of an even small SI contribution (see ref. [3]). Finally, we again remind that ^{nat}Ge detectors are intrinsically largely blinded to the SD component of the interaction as well as for Xenon detectors in the case of either $\theta \simeq 0$ or $\theta \simeq \pi$.

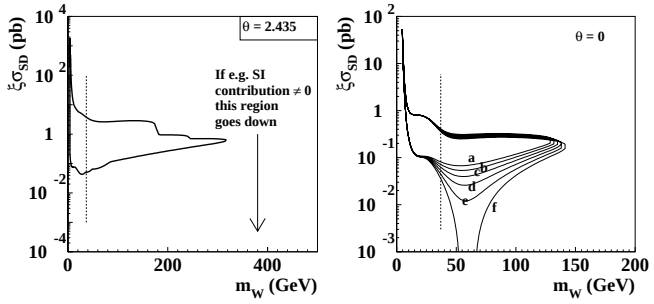

Figure 6: *Case of a WIMP with dominant SD interaction in given model frameworks.* An example of region allowed in the plane (m_W, $\xi\sigma_{SD}$) for $\theta = 2.435$ (Z_0 coupling); θ is defined in the $[0, \pi)$ range. For the definition of the vertical line see previous figure caption. Inclusion of other existing uncertainties on parameters and models (as discussed in ref. [3]) would further extend the SD allowed regions. For example, the use of more favourable SD form factors and/or more favourable spin factors would move them towards lower cross sections. Lower values of $\xi\sigma_{SD}$ are possible also e.g. in case of an even small SI contribution (see ref. [3]).

WIMPs with *preferred inelastic* interaction.

An analysis considering the same model frameworks has also been carried out for the case of WIMPs with *preferred inelastic* interaction [33] as we did also in the past in ref. [43] on partial exposure. In this inelastic Dark Matter scenario an allowed volume in

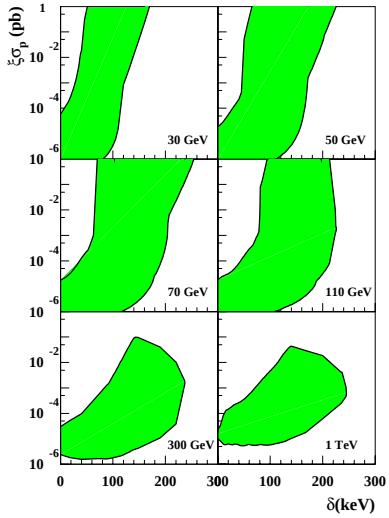

Figure 7: *Case of a WIMP with* preferred inelastic *interaction in given model frameworks.* Examples of slices (coloured areas) of the allowed volumes ($\xi\sigma_p$, δ, m_W) for some m_W values. Inclusion of other existing uncertainties on parameters and models would further extend the regions; for example, the use of a more favourable SI form factor for Iodine and of a different value for the escape velocity would move them towards lower cross sections [3].

the space ($\xi\sigma_p$, m_W, δ) is obtained; δ is the mass splitting of the WIMP particle which can be excited following an inelastic interaction [33, 43, 3]. For simplicity, as examples,

Fig. 7 shows slices of such an allowed volume at some given WIMP masses. There the superpositions of the allowed regions obtained, when varying the model framework within the considered set [3], are shown for each m_W shown as example. We remind that in these calculations v_{esc} has been assumed at fixed value (as in the previous cases), while its present uncertainties can play a significant role in this scenario of WIMP with *preferred inelastic* scattering.

Finally, it is worth to note that the allowed volume largely lies in the δ section where detection by experiments with light nuclei (such as e.g. Ge) is disfavoured.

Conclusion. In this section we have briefly summarized some quests for the candidate particle in some of the many possible scenarios. We further stress that, although several scenarios have been investigated, these corollary analyses are not exhaustive at all because of the present poor knowledge on many needed astrophysical, nuclear and particle Physics assumptions; moreover, additional scenarios can also be possible as shown e.g. by some recent papers appeared in literature. Therefore, bare comparisons among results from direct (and also indirect) search experiments have always only a marginal meaning.

2.3 Conclusion

DAMA/NaI has been a pioneer experiment running at LNGS for about a decade and investigating as first the WIMP annual modulation signature with suitable exposed mass, sensitivity and control of the running parameters. During seven independent experiments of one year each one, it has pointed out the presence of a modulation satisfying the many peculiarities of a particle Dark Matter induced effect, reaching an evidence at 6.3 σ C.L.. No other experiment has so far been in position to give a result directly comparable in a model independent way with that of DAMA/NaI. As a corollary, it has also pointed out the complexity of the quest for a particle Dark Matter candidate because of the present poor knowledge on the many astrophysical, nuclear and particle physics aspects.

3 DAMA/LIBRA

In the framework of the DAMA project, in 1996 a NaI(Tl) ton set-up [13] was proposed; a new R&D for NaI(Tl) radiopurification was carried out and the second generation set-up DAMA/LIBRA ($\simeq$250 kg NaI(Tl)) was funded as an intermediate step. This R&D with Crismatec-St.Gobain company exploited new chemical/physical radiopurification procedures in NaI and TlI powders. In this framework new materials were selected, prototypes were built and a devoted protocol was fixed. This has allowed - among others - to obtain NaI powders with ^{238}U residual contaminations about 30 times lower than those used in the past to build the highly radiopure DAMA/NaI detectors[2]. In addition, new selected materials and set-up components as well as new protocols have been employed for building, handling and installing all the parts of DAMA/LIBRA. In 2002 ended the production of detectors and of new parts of the installation and at fall 2002 the procedures needed to install the new set-up started.

The experimental site as well as many components of the installation itself have been implemented (environment, shield of PMTs, wiring, HP Nitrogen system, cooling water

of air conditioner, electronics and DAQ, etc...). Before the installation, all the Cu parts have been chemically etched (following a new devoted protocol) by subsequent baths with super-pure HCl solutions and super-pure water (for each brick the baths were changed). After each step the bath solution was analysed with ICP-MS technique. After cleaning, each brick was dried with HP N_2, sealed in a double envelope filled with HP N_2 atmosphere and then stored underground. In particular, all the procedures performed during the dismounting of DAMA/NaI and the installation of DAMA/LIBRA detectors have been carried out in HP Nitrogen atmosphere. This has been realised by using a Scuba system (a self-contained underwater breathing apparatus) modified in order to avoid that the entire breath is expelled into the surrounding air when the operator exhales; the air cylinders were kept five meters away and the output line was two meters long.

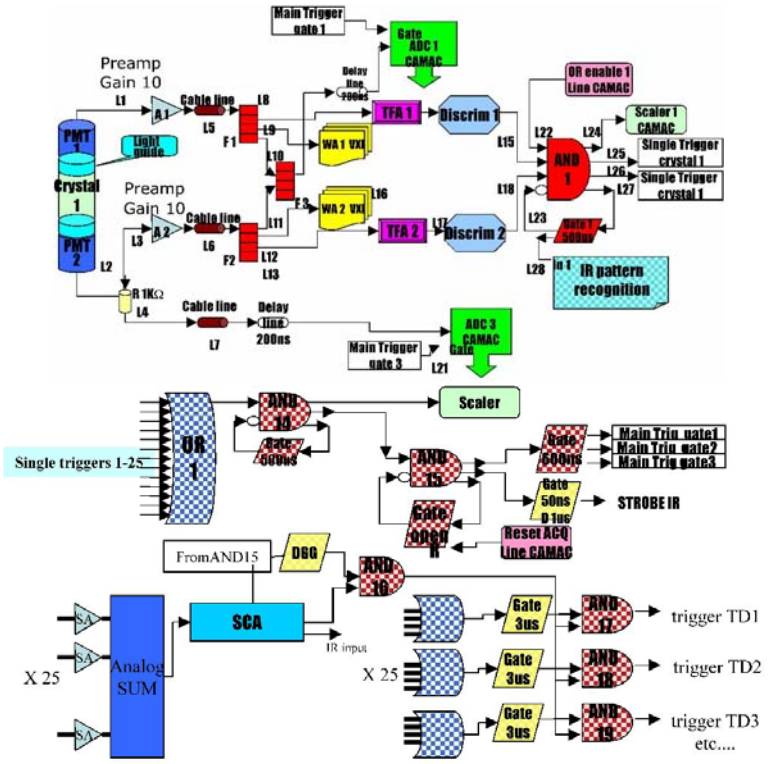

Figure 8: Top: Schema of the electronic chain referred to a single detector and its trigger; down: the schema of the main trigger of DAQ and of the trigger of Waveform Analysers.

In Fig. 8 the analogic schema of the electronic chain and the *single trigger* referred to a single detector, the main trigger of the acquisition system and the trigger system of the Waveform Analyzers (WA) are shown. The HV power supply for the PMTs has been given by a CAEN multichannel voltage supply with voltage stability of 0.1%. The signals from each PMT (there are two of them for each detector) are amplified by a preamplifier with 0-250 MHz bandwidth, with a factor 10 gain and with a voltage integral linearity $\pm 0.2\%$. In particular, the signal from one PMT is divided in two branches: 19/20 of the signal is sent to the input of the preamplifier, while the remaining 1/20 – suitably delayed – feeds a charge ADC channel. This last part processes the pulses with amplitude such

to saturate the remaining part of the electronics (they correspond to high energy events). The preamplified signals of each PMT – through linear Fan-in/Fan-out devices – are recorded through a channel of a Waveform Analyser (which processes the signal in a 2 μs time window). In particular, this is accomplished using fast VXI Tektronix four-channel TVS641A digitizers with a sampling frequency of 1 GSample/s and 250 MHz bandwidth. In addition, the sum pulses of the two PMTs are sent to the inputs for the charge ADCs.

The electronic devices, that provide the trigger of a single detector, are also shown in Fig. 8. In particular, the copies of the PMT signals are the inputs of Timing Filter Amplifiers which amplify and integrate the signal (integration time 50 ns); their outputs are discriminated with single photoelectron trigger level. The coincidence between the two logical NIM outputs provides the *single* trigger of the detector. A particular circuits allow: i) to reject afterglows and Bi-Po events in a 500μs time window after the occurrence of the event (introducing a systematic error on the measured rate of about 10^{-4}); ii) to enable the detector in the main trigger by a I/O Register during the calibrations. The outputs of the coincidence devices provide: i) the signal for a scaler to count the events for each detector; ii) the lines used in the main trigger (see later); iii) the line giving the start to a Gate Generator which - in addition to the veto of the coincidence – gives the signal issued to a 16-bit I/R Pattern Recognition which allows to identify the detector or the detectors which have generated the trigger.

The *main trigger* of the acquisition – see Fig. 8 – is provided by the logic OR of all the crystals. The main trigger pulses are counted by a Scaler, while devoted devices allow to manage the trigger only when the acquisition is ready. Therefore, the dead time of the acquisition is properly accounted in the estimate of the running time by using the information from the Scaler. When a general trigger occurs, the following logic signals are issued to: i) a Gate Generator generating the 600 ns gates the charge ADCs; ii) the Delay Gate Generator which gives the strobe signal to the I/R Pattern Recognition and generates the LAM (and, therefore, the interrupt to the CPU of the acquisition computer) in the CAMAC system; iii) the Delay Gate Generator which gives the signal to the trigger of the Waveform Analyzers. This last condition is verified only if the total energy deposited in the detectors is in an energy window suitably chosen (0.7 to 70 keV). For this purpose, each line feds a Spectroscopy Amplifier whose gain is equalized in order to have the same response for each detector. Therefore, a Single Channel Analyzer made by the two discriminators allows to select only events in the chosen energy window.

A devoted electronic circuit, shown in Fig. 8, allows to trigger only the Waveform Analysers which correspond to fired detectors; it gives a trigger to each Waveform Analysers when: i) at least one of its corresponding lines has a trigger; ii) the *main trigger* is present; iii) the total energy of the events is in the chosen energy window. Let us remind that for the events with energy outside this energy window (e.g. high energy events) the ADC values are acquired in any case.

The data acquisition system is made of a Workstation by Compaq with Linux SuSe operative system, which is interfaced with the hardware system through MXI-2 and GPIB buses. The GPIB bus allows to communicate with the CAMAC crate housing the ADCs, the scalers and the I/O registers, while the MXI-2 bus allows to communicate with the three VXI mainframes, where the Waveform Analysers are installed.

An hardware/software system to monitor the running conditions is also operative; in

particular, several probes are read out by the data acquisition system and stored with the production data. Moreover, self-controlled computer processes are operational to automatically control several parameters and to manage alarms.

The new DAMA/LIBRA, having an exposed mass of $\simeq$ 250 kg, an higher overall radiopurity and improved performances, offers an increased experimental sensitivity to further investigate the DAMA/NaI observed effect[3] and to improve investigations on the nature of the candidate particle trying to disentangle among different possible astrophysical, nuclear and particle physics models as well as more complete scenarios (as discussed in some details in [3]) and also new ideas, see just as an example the case of the *mirror* Dark Matter [46], the case of a contribution to the dark halo from the Sagittarius Dwarf Tidal Stream [34], the case of possible different nuclear scaling laws even for the neutralino candidate in MSSM [47], etc.. The low background DAMA/LIBRA is particularly suitable for this purpose since it is e.g. sensitive: i) both to low (through interaction on ^{23}Na) and to high (through interaction on ^{127}I) mass Dark Matter particles; ii) to mixed SI&SD, to purely SI, to purely SD couplings and to *preferred inelastic* scattering as well as to other possible kind of Dark Matter candidates. Moreover, DAMA/LIBRA can also effectively investigate with increased sensitivity several other rare processes, as previously done by DAMA/NaI.

DAMA/LIBRA has started the data taking on March 2003 and it has been planned to run for several years in order to collect an exposure significantly larger than that of DAMA/NaI.

4 R&D-III and beyond

As mentioned, a third generation R&D toward a possible ton NaI(Tl) set-up, we proposed in 1996, has been funded and is in progress of development. In particular, during year 2003 new powders have been selected and new purification processes have been considered. Purified powders have been produced and their residual trace radioactivity will be soon measured at high sensitivity mass spectrometer. Prototypes are planned to be built during year 2004.

Moreover, measurements and analysis to qualify new special low background PMTs are in progress.

5 DAMA/LXe

The year 2003 has been dedicated to a further improvement of the set-up; in particular, a new chiller for cooling of the recirculating water of the pumps and of the compressor of the cryogenerator has been installed as well as a new DAQ system based on Digital UNIX alpha server, a new control and alarm system and some other improvements e.g. in the shielding.

In addition, information on possible charge non-conserving (CNC) decay of ^{136}Xe into ^{136}Cs and on possible nucleon and di-nucleon decay into invisible channels in ^{136}Xe has been extracted from the data of ref. [27] and presented (see in 2003 publication list) as summarized in the following.

5.1 The search for charge-non-conserving decay of ^{136}Xe into ^{136}Cs

The conservation of the electric charge, which is related with a gauge invariance and masslessness of a photon in accordance with the Weinberg theorem, is considered as an absolute law in the standard quantum electrodynamics. Nevertheless, the possibility of charge non-conserving (CNC) phenomena has widely been discussed in the literature (see [53] and references therein) mainly in connection with future unified theories and with the possible existence of extra dimensions.

The approach, firstly considered in ref. [57], has been exploited here: if in a β decay $(A, Z) \rightarrow (A, Z+1) + e^- + \overline{\nu}_e$ some massless uncharged particle would be emitted instead of the electron (e.g., ν_e or γ or Majoron), an additional 511 keV energy is at disposal. Thus, usually forbidden decays to the ground state or to the excited levels of the daughter nuclei would become energetically possible. The presence of the $(A, Z+1)$ isotope or of its daughter products in a sample, initially free from them, would indicate the existence of the CNC decay searched for. In particular, large advantages arise when the so-called "active-source" technique (source = detector) is considered as in the present case.

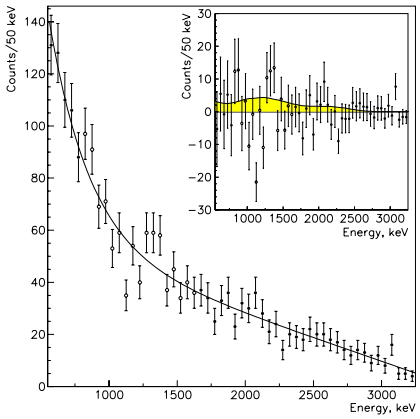

Figure 9: Experimental data collected by the LXe detector, shown as circles with error bars, together with fit by the background model (continuous line). Experimental points, excluded from the background fit, are shown as open circles. Inset: residuals between the experimental spectrum and the background fit (circles) and 90% C.L. excluded distribution of the CNC decay of ^{136}Xe into ^{136}Cs with $\tau_{CNC} = 1.3 \cdot 10^{23}$ y (shaded histogram).

In particular, after a possible ^{136}Xe CNC decay, a daughter nucleus ^{136}Cs will be created. It is β unstable ($T_{1/2}$ = 13.16 d) with quite high energy release (Q_β = 2.548 MeV) [58, 59]. The expected response function of the LXe detector for the β decay of ^{136}Cs has been simulated with the help of the EGS4 package [60]. The whole scheme of the decay [58, 59] with 6 levels of ^{136}Ba fed and 22 possible transitions in the following deexcitation process in ^{136}Ba was implemented in an event generator which described the initial kinematics of the events. The simulated response function of the ^{136}Cs β decay is shown in the inset of Fig. 9. Comparing the experimental energy distribution measured during 8823.54 h with the expected response function, no evidence for the effect searched for has been found. The fit of the experimental energy distribution with a background

model is shown in Fig. 9; the energy region 800–1650 keV — where a peak in the response function of the ^{136}Cs decay is expected — has been excluded from this fit. The experimental data are well described by the background model: χ^2/n.d.f = 0.74.

Thus, the life-time limit is: $\tau_{CNC}(^{136}\text{Xe}\rightarrow^{136}\text{Cs}) > 1.3 \cdot 10^{23}$ y at 90% C.L. The found $\tau_{CNC}(^{136}\text{Xe}\rightarrow^{136}\text{Cs})$ limit is one of the highest available limit for similar processes, but the bound on the charge non-conserving admixture in the weak interactions which can be derived, according to ref. [61], is modest: $\epsilon_\nu^2 < 1.1 \cdot 10^{-5}$ at 90% C.L., mainly due to the high degree of forbiddeness of the considered CNC transition.

5.2 The search for nucleon and di-nucleon decay into invisible channels in ^{136}Xe

The same data have been considered to investigate possible nucleon and di-nucleon decays into invisible channels for the ^{136}Xe isotope: disappearance or decay to neutrinos, Majorons, etc. The approach, exploited in [25] at the first time, consists in a real-time search for radioactive decay of unstable daughter nuclei created as result of the N or NN disappearance in parent nucleus. As mentioned if half-life of the daughter nucleus is of order of 1 s or greater, such a decay will be time-resolved from prompt products if they were emitted and observed in a detector. Here, in contrast with our previous experiment when the set-up was filled in ^{129}Xe at 99.5% [25], the set-up has been filled with the Xenon enriched in ^{136}Xe at 68.8% having in this way the possibility to investigate also the case of the np disappearance not studied previously.

After the disappearance of one or two nucleons in the parent ^{136}Xe nucleus, the following nuclei will be created inside the sensitive LXe volume: ^{135}Xe (n decay); ^{135}I (p decay); ^{134}Xe (nn decay); ^{134}I (np decay); ^{134}Te (pp decay). Since the ^{134}Xe nucleus is stable, it is not possible to search for the nn disappearance in the present case.

The expected response functions of the LXe detector for the β decays of ^{135}Xe, ^{135}I, ^{134}I and ^{134}Te were simulated with the help of the EGS4 package [60]. The whole schemes of the decays, using the information from ref. [62] for the $A = 134$ mass chain and ref. [63] for the $A = 135$ chain, were implemented in an event generator which described the initial kinematics of the events. For example, 23 levels of ^{135}Xe populated in ^{135}I β decay and 85 different transitions in the following dexcitation process were taken into account; possibility to emit conversion electron or e^+e^- pair instead of γ quantum in such transitions were also considered. The simulated response functions are shown in Fig. 10 – *left*.

Comparison of the experimental spectrum (see Fig. 10 – *right*) with the calculated response functions gives no indication for the β decays of the nuclides created in result of the N and NN disappearance in ^{136}Xe. Thus only the limits on the probability of these processes have been extracted: $\tau_n > 3.3 \cdot 10^{23}$ y, $\tau_p > 4.5 \cdot 10^{23}$ y, $\tau_{np} > 3.2 \cdot 10^{23}$ y and $\tau_{pp} > 1.9 \cdot 10^{24}$ y at 90% C.L. (Fig. 10 – *right* demonstrates the case of the pp decay). These restrictions are valid for any "invisible" channel in which nucleons or di-nucleons disappear (e.g. into extra dimensions) or decay emitting some weakly interacting particles which do not destroy the daughter nucleus (neutrinos of any flavours, Majorons, etc.). The values for τ_n and τ_p are lower than those given by other experiments, while the τ_{pp} limit is near 3 times higher than that obtained in our measurements with ^{129}Xe [25], but it

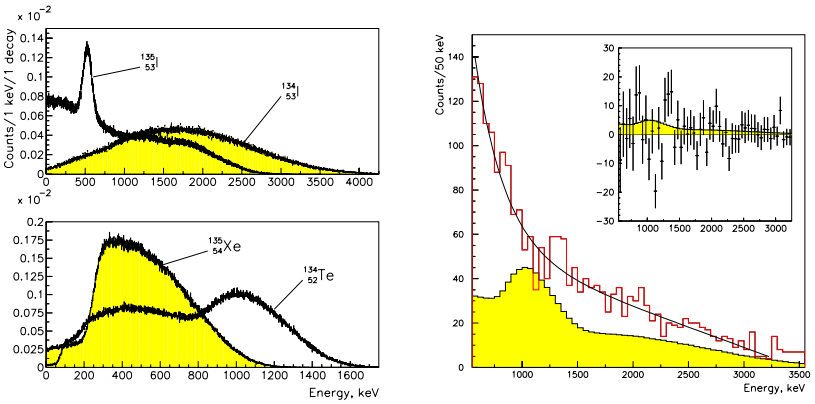

Figure 10: *On the left*: simulated response functions of the LXe detector for the decays of $^{135}_{54}$Xe (produced inside the detector in result of the n disappearance in $^{136}_{54}$Xe), $^{135}_{53}$I (p disappearance), $^{134}_{53}$I (np disappearance) and $^{134}_{52}$Te (pp disappearance). *On the right*: Experimental spectrum measured during 8823.54 h (thick histogram). The shaded histogram is the response function for the chain of β decays ^{134}Te + ^{134}I which corresponds to the pp disappearance with $\tau_{pp} = 2.1 \cdot 10^{23}$ y excluded at 90% C.L. in the most conservative approach. In the inset the residuals between the experimental spectrum and the background fit are shown (points with error bars) together with excluded ^{134}Te + ^{134}I distribution for $\tau_{pp} = 1.9 \cdot 10^{24}$ y (shaded histogram).

is lower than the value declared recently by the BOREXINO Collaboration [64]). Finally, the τ_{np} limit has been determined here for the first time.

5.3 Conclusions

The DAMA/LXe set-up has been improved with time passing and has allowed to achieve competitive results in the searches for various rare processes. In particular, during year 2003 some additional information have been derived on the basis of already published data and presented. Moreover, the experimental set-up has been further improved.

6 DAMA/R&D

During year 2003 measurements on new prototype PMTs without any glass and ceramics components have been started. In addition, new results have been published on the basis of the measurements carried out deep underground by using a CeF_3 crystal scintillator; they are summarized in the following.

6.1 Performances and results by a CeF_3 crystal scintillator

Measurements were carried out deep underground by using a CeF_3 crystal scintillator ($2\times2\times2$ cm^3, mass of 49.3 g) directly coupled to two low radioactive EMI9265FLB53 photomultipliers (3″ in diameter) working coincidence. The relative light output for α particles as compared with that for β particles (or γ rays), named α/β ratio has been measured for α particles in the range 2 – 8.8 MeV (for details see the paper quoted in the

2003 publication list); the derived energy dependence of the α/β ratio is shown in Fig. 11 – *left*.

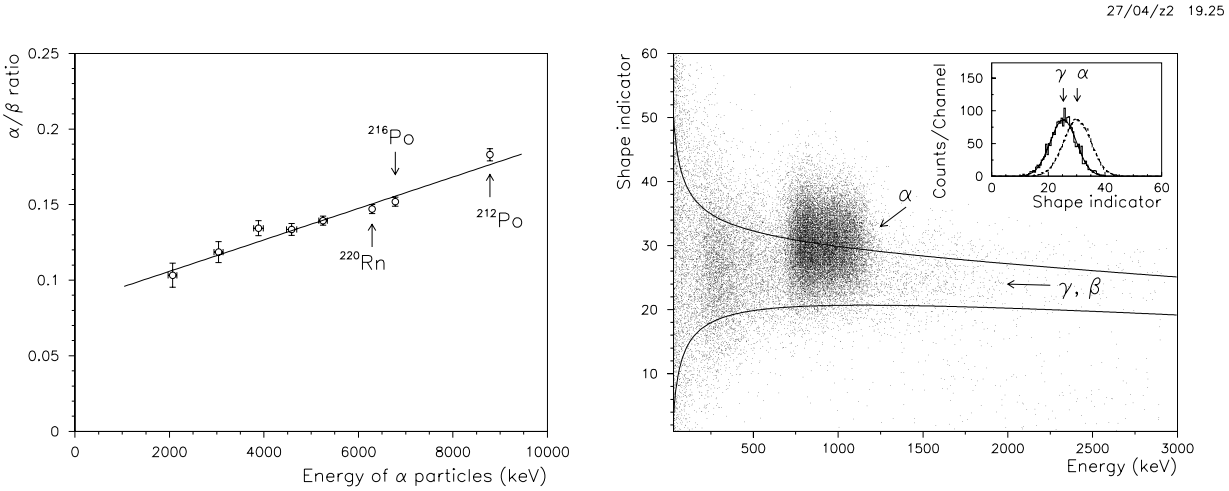

Figure 11: *On the left*: Energy dependence of the α/β ratio for the CeF_3 scintillator as measured with an ^{241}Am alpha source. The points corresponding to the α peaks of ^{220}Rn and ^{216}Po have been selected by the time-amplitude analysis (see text and Fig. 5); the peak of ^{212}Po has been obtained by the pulse-shape analysis of the background data (see text and Fig. 3). Solid line represents the fitting curve of the experimental points. *On the right*: Scatter plot of the shape indicator (see text) versus energy for 20.9 h of background exposition with the CeF_3 scintillation detector. One sigma interval for shape indicator values corresponding to γ quanta (β particles) is drawn. Points with lower SI values are due to events $^{212}\text{Bi} \rightarrow {}^{212}\text{Po} \rightarrow {}^{208}\text{Pb}$. In the inset: the distributions of the shape indicator measured for γ quanta and for α events selected from the background data.

Scintillation light pulses induced by α particles in the CeF_3 are modestly faster than those of γ quanta (β particles), allowing the discrimination between α and $\gamma(\beta)$ events with the help of a pulse-shape discrimination technique. The pulse shapes of the CeF_3 crystal scintillator were investigated for γ rays in the energy range of $0.06 - 1.33$ MeV (with ^{137}Cs and ^{60}Co sources) and for α particles in the energy range of $5.5 - 6.8$ MeV (using α active impurities inside the crystal). The measured shape indicators for γ quanta and for α particles are plotted in Fig. 11 – *right*.

Another technique of background rejection has also been applied to the fast sequence of decays from the ^{232}Th family: ^{212}Bi (Q_β = 2254 keV) $\rightarrow$ ^{212}Po (E_α = 8784 keV, $T_{1/2}$ = 0.299 μs) $\rightarrow$ ^{208}Pb. A typical example of such an analysis is presented in Fig. 12, where the β spectrum of ^{212}Bi, the α peak of ^{212}Po and the distribution of the time intervals between the first and the second pulse are depicted. The energy and time spectra are in a good agreement with those expected for the ^{212}Bi β decay and for the subsequent ^{212}Po α decay. All such double pulses (Fig. 12d) with delay time in the interval $\Delta t = (0.11 - 0.65)$ μs have been discarded from the raw data to reduce the background.

The background spectrum of the CeF_3 crystal measured during 2142 h in the low background set-up has also been analysed in order to estimate the background components; a detailed discussion can be found in the paper quoted in the 2003 publication list.

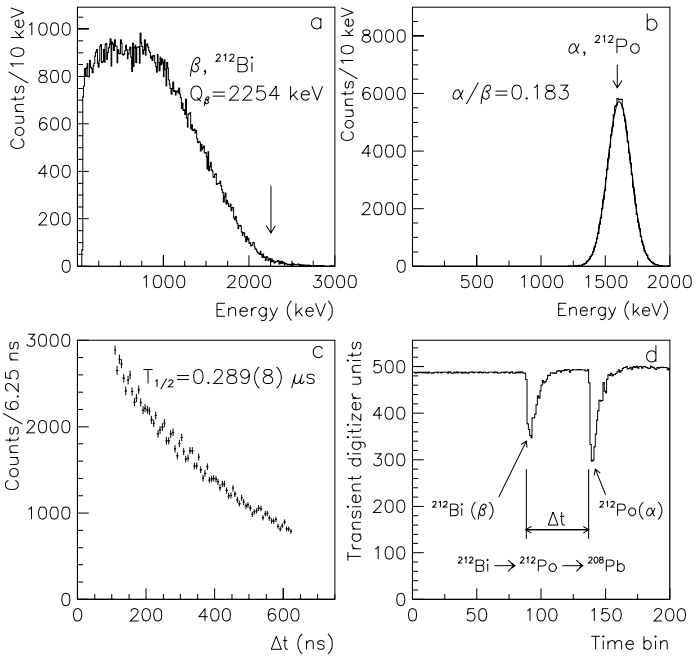

Figure 12: The energy (a,b) and time (c) distributions of the fast sequence of β (^{212}Bi, $Q_\beta = 2254$ keV) and α (^{212}Po, $E_\alpha = 8784$ keV, $T_{1/2} = 0.299(2)$ μs [58]) decays selected by pulse-shape analysis from the background data recorded over 2142 h. The fit of the time distribution gives an half-life: $T_{1/2} = 0.289(8)$ μs, which is in good agreement with the result from literature for ^{212}Po [58]. (d) Example of such an event in the CeF_3 scintillator.

The results on the performances of the CeF_3 crystal scintillator have been exploited to investigate its application capability to the search for rare decays of Ce isotopes. In particular, for two cerium isotopes the capture of two K electrons from the atomic shell with emission of two neutrinos is energetically allowed: i) $^{136}\mathrm{Ce} \to {}^{136}\mathrm{Ba}$ (mass difference $\Delta M = 2400(50)$ keV [68]; abundance $\delta = 0.185\%$ [69]; number of ^{136}Ce nuclei in the CeF_3 crystal $N = 2.79{\times}10^{20}$); ii) $^{138}\mathrm{Ce} \to {}^{138}\mathrm{Ba}$ (mass difference $\Delta M = 693(10)$ keV; abundance $\delta = 0.251\%$; number of ^{138}Ce nuclei $N = 3.78{\times}10^{20}$). In both such processes the full energy released in the CeF_3 detector is equal to $2E_K$ (where $E_K = 37.4$ keV is the binding energy of electrons on the K shell of Ba atoms), while neutrinos carry out the rest of the available energy ΔM.

The part of the measured energy distribution up to the energy of 250 keV after the discrimination of the PMT noise and of the double pulses does not show any peak in the vicinity of the $2E_K$ energy, thus limits for the probability of the $2\nu 2K$ capture in ^{136}Ce and ^{138}Ce have been set; they are:

$$T_{1/2}^{2\nu 2K}(^{136}\mathrm{Ce}) \geq 2.7(4.5){\times}10^{16} \text{ yr} \qquad \text{at } 90\%(68\%) \text{ C.L.},$$
$$T_{1/2}^{2\nu 2K}(^{138}\mathrm{Ce}) \geq 3.7(6.1){\times}10^{16} \text{ yr} \qquad \text{at } 90\%(68\%) \text{ C.L.}$$

These half-life bounds are well below the existing theoretical predictions for the $2\nu 2K$

capture of ^{136}Ce [70] and the same can be expected for $2\nu 2K$ capture of ^{138}Ce, for which calculations are not available; nevertheless they are more than two orders of magnitude higher than those established in previous experiment [71].

In addition, one of the cerium isotopes, ^{142}Ce, can decay to the ground state of ^{138}Ba with emission of an α particle; the corresponding energy release is equal to 1299.6±3.5 keV [68], thus expected energy of α particle is $E_\alpha = 1263$ keV. The previous experimental limit was: $T_{1/2} \geq 5 \times 10^{16}$ yr [72].

The number of ^{142}Ce nuclei (natural abundance δ=11.114% [69]) in our CeF_3 crystal is 1.67×10^{22}. Taking into account the α/β ratio, the α peak of ^{142}Ce could be expected at the energy (127 ± 7) keV (with FWHM = 53 keV), where the experimental α spectrum contains at least 99% of α events. By using the energy spectrum obtained by discarding the double pulses and following a standard procedure a new lower bound on the half-life of ^{142}Ce α decay has been obtained:

$$T^{\alpha}_{1/2}(^{142}\mathrm{Ce}) \geq 2.9(7.3)\times10^{18} \text{ yr} \qquad \text{at } 90\%(68\%) \text{ C.L.}$$

It is worth to note that this obtained experimental limit – although significantly higher than that previously available [72] – is still much lower than the existing theoretical estimates [73, 74, 75].

6.2 Conclusions

The DAMA/R&D set-up has allowed to achieve several competitive results in the searches for various rare processes and in the developments of low background scintillators and PMTs. In particular, during 2003 for the first time the response of a CeF_3 crystal scintillator to α particles has been investigated in the wide $(2 - 8.8)$ MeV energy region and the capability of a pulse-shape discrimination between α particles and γ quanta has also been demonstrated. The study of the residual radioactive contaminants in a similar detector has been carried out and the application capability of such a detector to the search for some rare processes in Ce isotopes has been investigated, obtaining some improved experimental limits.

Moreover, the analysis of data collected with a BaF_2 scintillator has also been carried out and the results are in progress to be released.

New data taking to qualify new low background PMTs and the materials for RD-III on further radiopurification of NaI(Tl) detectors toward a ton NaI(Tl) set-up are in progress. Other small scale experiments are in preparation.

Finally, a modification of the shield of this set-up has been designed and will be completely realized during year 2004.

7 DAMA/Ge

Various R&D developments to improve low background set-ups and scintillators as well as new developments for higher radiopure PMTs are regularly carried out. The related measurements on samples are usually performed by means of the DAMA low background Ge detector, specially realized with a low Z window. It is operative deep underground

in the low background facility of the Gran Sasso Laboratory. Selected materials such as highly purified NaI and TlI powders are in addition measured at ISPRA facility.

During year 2003 the project to further improve the DAMA/Ge insulation from environment has been carried out and the realization of the related parts will be completed during year 2004.

8 Conclusions

In conclusion, the main activities during year 2003 can be summarized as in the following:

I. the final model independent analysis of the data collected during seven annual cycles by DAMA/NaI has been released as well as some of the many possible corollary model dependent investigations on the nature of the particle Dark Matter candidate. In particular, the final result of DAMA/NaI is a 6.3 σ C.L. model independent evidence for the presence of a particle Dark Matter component in the galactic halo.

II. the new DAMA/LIBRA set-up has been completely installed and put in operation.

III. the LXe set-up has been upgraded and some further data analyses have been carried out.

IV. the R&D set-up has been employed for new measurements on PMT prototypes. Results obtained with CeF_3 detector have been released. Data analyses on data taken with a BaF_2 scintillator have also been carried out.

9 List of Publications during 2003

1. R. Bernabei, M. Amato, P. Belli, F. Cappella, R. Cerulli, C.J. Dai, G. Ignesti, A. Incicchitti, H.H. Kuang, J.M. Ma, F. Montecchia, F. Nozzoli, Z.P. Ye, D. Prosperi, *Searching for the Dark Universe by the DAMA experiment*, Nucl. Phys. A719 (2003) 257c.

2. P. Belli, R. Bernabei, R. Cerulli, C.J. Dai, F.A. Danevich, A. Incicchitti, V.V. Kobychev, O.A. Pronkratenko, D. Prosperi, V.I. Tretyak, Yu.G. Zdesenko, *Performances of a CeF_3 crystal scintillator and its application to the search for rare processes*, Nucl. Instr. & Meth. A498 (2003) 352.

3. R. Bernabei, P. Belli, F. Cappella, R. Cerulli, F. Montecchia, F. Nozzoli, A. Incicchitti, D. Prosperi, C.J. Dai, H.H. Kuang, J.M. Ma, Z.P. Ye, *DAMA results*, in the volume of the Proc. of the Int. Workshop on "Neutrino Telescopes", papergraf ed. (2003) 403 (*astro-ph 0305542*).

4. R. Bernabei, P. Belli, F. Cappella, F. Montecchia, F. Nozzoli, A. Incicchitti, D. Prosperi, R. Cerulli, C.J. Dai, H.H. Kuang, J.M. Ma, Z.P. Ye, *DAMA/NaI results and the new DAMA/LIBRA*, 1st Yamada Symposium on "Neutrinos and Dark Matter in Nuclear Physics" edited by H. Ejiri and I. Ogawa, (2003) XIII p.13.

5. R. Bernabei, P. Belli, F. Cappella, F. Nozzoli, F. Montecchia, A. Incicchitti, D. Prosperi, R. Cerulli, C.J. Dai, *Search for rare processes with DAMA/LXe at Gran Sasso*, 1st Yamada Symposium on "Neutrinos and Dark Matter in Nuclear Physics" edited by H. Ejiri and I. Ogawa, (2003) poster section p.3.

6. R. Bernabei, P. Belli, F. Cappella, F. Montecchia, F. Nozzoli, A. Incicchitti, D. Prosperi, R. Cerulli, C.J. Dai, H.H. Kuang, J.M. Ma, Z.P. Ye, *Results from DAMA*, in publication on the Proceed. of CIPANP03, New York, May 2003.

7. R. Bernabei, P. Belli, F. Nozzoli, A. Incicchitti, *Anisotropic scintillators for WIMP direct detection: revisited*, Eur. Phys. J. C28 (2003) 203.

8. R. Bernabei, M. Amato, P. Belli, F. Cappella, R. Cerulli, C.J. Dai, H.L. He, G. Ignesti, A. Incicchitti, H.H. Kuang, J.M. Ma, F. Montecchia, F. Nozzoli, D. Prosperi, *WIMP search by the DAMA experiment at Gran Sasso*, Nucl. Phys. B (Proc. Suppl.) 124 (2003) 181.

9. R. Bernabei, P. Belli, F. Cappella, F. Montecchia, F. Nozzoli, A. Incicchitti, D. Prosperi, R. Cerulli, C.J. Dai, H.H. Kuang, J.M. Ma, Z.P. Ye, *Results from DAMA/NaI and perspectives for DAMA/LIBRA*, astro-ph/0311046 and in publication on the Proceed. of the Conf. "Beyond the Desert 03", Rindberg Castle, June 2003.

10. R. Bernabei, P. Belli, F. Cappella, R. Cerulli, C.J. Dai, V. Denisov, A. Incicchitti, F. Montecchia, F. Nozzoli, D. Prosperi, V. Tretyak, *The search for rare processes with DAMA/LXe*, INFN/EXP-08/03 and in publication on the Proceed. of the Conf. "Beyond the Desert 03", Rindberg Castle, June 2003.

11. R. Bernabei, P. Belli, F. Cappella, F. Montecchia, F. Nozzoli, A. Incicchitti, D. Prosperi, R. Cerulli, C.J. Dai, H.H. Kuang, J.M. Ma, Z.P. Ye, *DAMA results and perspectives*, in publication on the Proceed. of the EPS 2003 Conf., Aachen, July 2003.

12. R. Bernabei, P. Belli, F. Cappella, R. Cerulli, F. Montecchia, F. Nozzoli, A. Incicchitti, D. Prosperi, C.J. Dai, H.H. Kuang, J.M. Ma, Z.P. Ye, *Dark Matter search*, La Rivista del Nuovo Cimento 26 n.1 (2003) 1-73 (*astro-ph/0307403*).

13. R. Bernabei, P. Belli, F. Cappella, R. Cerulli, F. Montecchia, F. Nozzoli, A. Incicchitti, D. Prosperi, C.J. Dai, H.H. Kuang, J.M. Ma, Z.P. Ye, *Dark Matter and double beta decay search by the DAMA experiment*, in publication on the Proceed. of MEDEX03, Praha, July 2003.

14. R. Bernabei, P. Belli, F. Cappella, F. Montecchia, F. Nozzoli, A. d'Angelo, A. Incicchitti, D. Prosperi, R. Cerulli, C.J. Dai, H.H. Kuang, J.M. Ma, Z.P. Ye, *Prospects for DAMA/LIBRA and beyond*, in publication on the Proceed. of the TAUP03, Seattle, September 2003.

15. R. Bernabei, P. Belli, F. Cappella, F. Montecchia, F. Nozzoli, A. Incicchitti, D. Prosperi, R. Cerulli, C.J. Dai, H.H. Kuang, J.M. Ma, Z.P. Ye, *Further results on the*

WIMP annual modulation signature by DAMA/NaI, in publication on the Proceed. of the TAUP03, Seattle, September 2003.

16. R. Bernabei, P. Belli, F. Cappella, F. Montecchia, F. Nozzoli, A. Incicchitti, D. Prosperi, R. Cerulli, C.J. Dai, H.H. Kuang, J.M. Ma, Z.P. Ye, *Direct search for WIMPS*, in publication on the Proceed. of the Conf. "Thinking, Observing and Mining the Universe", Sorrento, September 2003.

17. R. Bernabei, P. Belli, F. Cappella, F. Montecchia, F. Nozzoli, A. Incicchitti, D. Prosperi, R. Cerulli, C.J. Dai, H.H. Kuang, J.M. Ma, Z.P. Ye, *The DAMA/NaI results on WIMP annual modulation signature at Gran Sasso*, in publication on the Proceed. of the ICATPP03, Como, October 2003.

18. R. Bernabei, P. Belli, F. Cappella, F. Montecchia, F. Nozzoli, A. Incicchitti, D. Prosperi, R. Cerulli, C.J. Dai, H.H. Kuang, J.M. Ma, Z.P. Ye, *Further results on the WIMP annual modulation signature by DAMA/NaI*, in publication on the Proceed. of the AHEP03, Valencia, October 2003.

References

[1] P. Belli, R. Bernabei, C. Bacci, A. Incicchitti, R. Marcovaldi, D. Prosperi, DAMA proposal to INFN Scientific Committee II, April 24^{th} 1990.

[2] R. Bernabei et al., Il Nuovo Cimento A112 (1999) 545.

[3] R. Bernabei et al., La Rivista del Nuovo Cimento 26 n.1 (2003) 1-73 (*astro-ph/0307403*) and references therein.

[4] R. Bernabei, Prog. Part. Nucl. Phys. 48 (2002) 263.

[5] R. Bernabei et al., Phys. Lett. B389 (1996) 757.

[6] R. Bernabei et al., Il Nuovo Cimento A112 (1999) 1541.

[7] R. Bernabei et al., Phys. Rev. Lett. 83 (1999) 4918.

[8] F. Cappella et al., Eur. Phys. J.-direct C14 (2002) 1.

[9] R. Bernabei et al., Phys. Lett. B515 (2001) 6.

[10] R. Bernabei et al., Phys. Lett. B408 (1997) 439.

[11] P. Belli et al., Phys. Rev. C60 (1999) 065501.

[12] P. Belli et al., Phys. Lett. B460 (1999) 236.

[13] R. Bernabei et al., Astrop. Phys. 4 (1995) 45; R. Bernabei, "Competitiveness of a very low radioactive ton scintillator for particle Dark Matter search", in the volume *The identification of Dark Matter*, World Sc. pub. (1997) 574.

[14] I.R. Barabanov et al., Astrop. Phys. 8 (1997) 67; I.R. Barabanov et al., Nucl. Phys. B546 (1999) 19; I.R. Barabanov et al., New Journal of Physics 3 (2001) 5.1.

[15] P. Belli et al., Il Nuovo Cimento A103 (1990) 767.

[16] P. Belli et al., Il Nuovo Cimento C19 (1996) 537.

[17] P. Belli et al., Astrop. Phys. 5 (1996) 217.

[18] R. Bernabei et al., Nucl. Instr. & Meth. A482 (2002) 728.

[19] P. Belli et al., Phys. Lett. B387 (1996) 222 and Phys. Lett. B389 (1996) 783 (erratum).

[20] R. Bernabei et al., Phys. Lett. B436 (1998) 379.

[21] R. Bernabei et al., Eur. Phys. J.-direct C11 (2001) 1.

[22] R. Bernabei et al., New Journal of Physics 2 (2000) 15.1.

[23] P. Belli et al., Phys. Rev. D61 (2000) 117301.

[24] P. Belli et al., Phys. Lett. B465 (1999) 315.

[25] R. Bernabei et al., Phys. Lett. B493 (2000) 12.

[26] R. Bernabei et al., Phys. Lett. B527 (2002) 182.

[27] R. Bernabei et al., Phys. Lett. B546 (2002) 23.

[28] R. Bernabei et al., Il Nuovo Cimento A110 (1997) 189.

[29] R. Bernabei et al., Astrop. Phys. 7 (1997) 73.

[30] P. Belli et al., Nucl. Phys. B563 (1999) 97.

[31] P. Belli et al., Astrop. Phys. 10 (1999) 115.

[32] R. Bernabei et al., Nucl. Phys. A705 (2002) 29.

[33] D. Smith and N. Weiner, Phys. Rev. D64 (2001) 043502.

[34] K. Freese et al., *astro-ph/0309279*.

[35] K.A. Drukier et al., Phys. Rev. D33 (1986) 3495; K. Freese et al., Phys. Rev. D37 (1988) 3388.

[36] R. Bernabei et al., Nucl. Phys. B (Proc. Suppl.) 70 (1999) 79.

[37] R. Bernabei et al., Phys. Lett. B424 (1998) 195.

[38] R. Bernabei et al., Phys. Lett. B450 (1999) 448.

[39] P. Belli et al., Phys. Rev. D61 (1999) 023512.

[40] R. Bernabei et al., Phys. Lett. B480 (2000) 23.

[41] R. Bernabei et al., Eur. Phys. J. C18 (2000) 283.

[42] R. Bernabei et al., Phys. Lett. B509 (2001) 197.

[43] R. Bernabei el al., Eur. Phys. J. C23 (2002) 61.

[44] P. Belli et al., Phys. Rev. D66 (2002) 043503.

[45] W.H. Press and G. B. Rybicki, Astrophys. J. 338 (1989) 277; J.D. Scargle, Astrophys. J. 263 (1982) 835.

[46] R. Foot, *astro-ph/0309330*, *hep-ph/0308254*.

[47] G. Prezeau et al., *astro-ph/0309115*.

[48] D.E. Groom et al., Eur. Phys. J. C15 (2000) 1.

[49] A. Bottino et al., Phys. Rev. D67 (2003) 063519; A. Bottino et al, *hep-ph/0304080*.

[50] D. Hooper and T. Plehn, MADPH-02-1308, CERN-TH/2002-29, *hep-ph/0212226*.

[51] G. Bélanger, F. Boudjema, A. Pukhov and S. Rosier-Lees, *hep-ph/0212227*.

[52] K. Hagiwara et al., Phys. Rev. D66 (2002) 010001.

[53] S. Weinberg, Phys. Rev. B135 (1964) 1049; L.B. Okun, Sov. Phys. Usp. 32 (1989) 543; L.B. Okun, Comments Nucl. Part. Phys. 19 (1989) 99; Particle Data Group, K. Hikasa et al., Phys. Rev. D45 (1992) VI.10; F.J. Yndurain, Phys. Lett. B256 (1991) 15; N. Arkani-Hamed et al., Phys. Lett. B429 (1998) 263; S.L. Dubovsky et al., Phys. Rev. D62 (2000) 105011; S.L. Dubovsky et al., JHEP 08 (2000) 041; V.A. Rubakov, Phys. Uspekhi 44 (2001) 87.

[54] H.O. Back et al., Phys. Lett. B525 (2002) 29.

[55] Yu.G. Zdesenko, V.I. Tretyak, Phys. Lett. B553 (2003) 135.

[56] V.I. Tretyak, Yu.G. Zdesenko, Phys. Lett. B505 (2001) 59.

[57] G. Feinberg, M. Goldhaber, Proc. Nat. Acad. Sci. U.S.A. 45 (1959) 1301.

[58] *Table of Isotopes*, ed. by R.B. Firestone, V.S. Shirley, et al., (8-th ed., John Wiley & Sons, N.Y., 1996)

[59] A.A. Sonzogni, Nucl. Data Sheets 95 (2002) 837.

[60] W.R. Nelson et al., SLAC-Report-265, Stanford, 1985.

[61] J.N. Bahcall, Rev. Mod. Phys. 50 (1978) 881; J.N. Bahcall, *Neutrino Astrophysics*, Cambridge University Press (1989) 359.

[62] Yu.V. Sergeenkov, Nucl. Data Sheets 71 (1994) 557.

[63] Yu.V. Sergeenkov et al., Nucl. Data Sheets 84 (1998) 115.

[64] H.O. Back et al., Phys. Lett. B563 (2003) 23.

[65] J.B. Birks, *Theory and Practice of Scintillation Counting,* Pergamon, New York, 1967.

[66] F.A. Danevich et al., Phys. Rev. C62 (2000) 045501.

[67] E. Gatti, F. De Martini, Nuclear Electronics 2, IAEA, Vienna, (1962) 265.

[68] G. Audi, A.H. Wapstra, Nucl. Phys. A595 (1995) 409.

[69] I.L. Barnes et al., Pure and Appl. Chem. 63 (1991) 991.

[70] V.I. Tretyak, Yu.G. Zdesenko, At. Data Nucl. Data Tables 61 (1995) 43; 80 (2002) 83.

[71] F.A. Danevich et al., Nucl. Phys. A694 (2001) 375.

[72] R.D. Macfarlane, T.P. Kohman, Phys. Rev. 121 (1961) 1758.

[73] B. Al-Bataina, J. Janecke, Phys. Rev. C37 (1988) 1667.

[74] D.N. Poenaru, M. Ivascu, J. Physique 44 (1983) 791.

[75] B. Buck et al., J. Phys. G17 (1991) 1223.

[76] R. Bernabei et al., in the volume "Cosmology and particle Physics", AIP ed. (2001) 189.

GENIUS-TF. Test Facility fot the GENIUS Project

H.V. Klapdor-Kleingrothaus*[a], I.V. Krivosheina[a,b],
H. Strecker[a], C. Tomei[a,c], O. Chkvoretz[a]

[a] Max-Planck Institut für Kernphysik, Heidelberg, Germany
[b] Institute of Radiophysical Research, Nishnij Novgorod, Russia
[c] University of L'Aquila, Italy
* Spokesman of the Collaboration; E-mail: klapdor@gustav.mpi-hd.mpg,
Home-page: http://www.mpi-hd.mpg.de.non_acc/

Abstract

The first four naked high purity Germanium detectors (10 kg) were installed successfully in liquid nitrogen in the GENIUS-Test-Facility (GENIUS-TF) in the GRAN SASSO Underground Laboratory on May 5, 2003. This is the first time ever that this novel technique aiming at extreme background reduction in search for rare decays is going to be tested underground. First operational parameters are presented.
The GENIUS-TF experiment, aims to search for the annual modulation of the Dark Matter signal using 40 kg of naked-Ge detectors in liquid nitrogen. It should be able to confirm the DAMA result within two or three years of measuring time.

1 Introduction

The present status of further cold dark matter search, of investigation of neutrinoless double beta decay and of low-energy solar neutrinos all require new techniques of *drastic* reduction of background in the experiments. For this purpose we proposed the GENIUS (GErmanium in liquid NItrogen Underground Setup) project in 1997 [1, 2, 3, 4, 5, 6]. The idea is to operate 'naked' Ge detectors in liquid nitrogen, and thus, by removing all materials from the immediate vicinity of the Ge crystals, to reduce the background considerably with respect to conventionally operated detectors. The liquid nitrogen acts both as a cooling medium and as a shield against external radiactivity.

That the removal of material close to the detectors is the crucial point for improvement of the background, we know from our experience with the HEIDELBERG-MOSCOW double beta decay experiment [10, 16], which is the most sensitive double beta experiment for 10 years now. Monte Carlo simulations for the GENIUS project, and investigation of the new physics potential of the project have been performed in great detail, and have

been published elsewhere [5, 7]. Already in 1997 it has been shown experimentally in our Heidelberg low-level facility (shielding $\sim$ 10 mwe) that the techniques of operating 'naked' Ge detectors in liquid nitrogen is working and we were the first to show that such device can be used for spectroscopy [5].

A small scale version of GENIUS, the GENIUS-Test-Facility has been approved by the Gran Sasso Scientific Committee in March 2001. The idea of GENIUS-TF is to prove the feasibility of some key constructional features of GENIUS, such as detector holder systems, achievement of very low thresholds of specially designed Ge detectors, long term stability of the new detector concept, reduction of possible noise from bubbling nitrogen, etc.

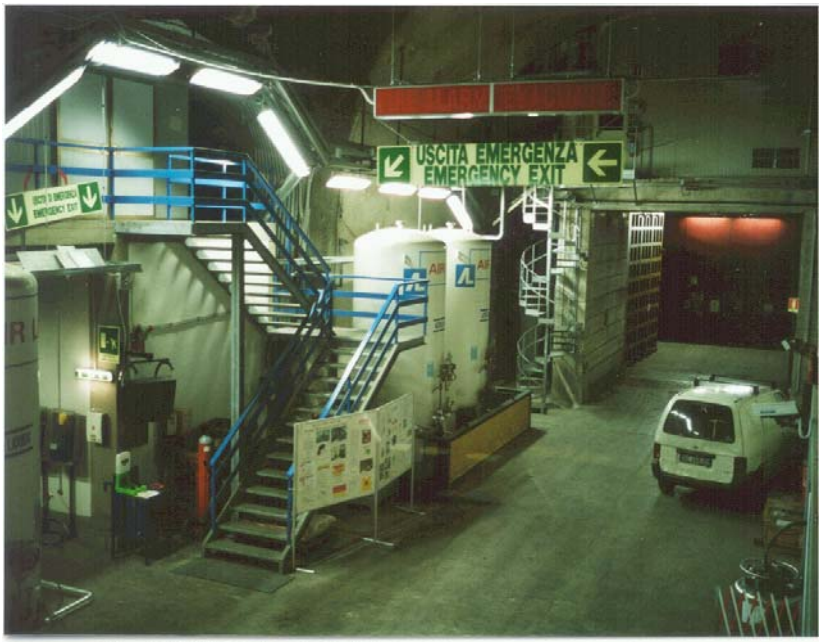

Figure 1: Location of GENIUS-TF is the building on the right (car in front), opposite to the HEIDELBERG-MOSCOW experiment building (left side) (see also Fig. 6).

Additionally the GENIUS-TF will improve the limits on WIMP-nucleon cross sections with respect to our results with the HEIDELBERG-MOSCOW and HDMS experiments [18, 19] thus allowing for a test of the claimed evidence for WIMP dark matter from the DAMA experiment [20, 23]. The relatively large mass of Ge in the full scale GENIUS-TF compared to existing experiments would permit to search directly for a WIMP signature in form of the predicted [21] seasonal modulation of the event rate [13]. Introducing the strongly 'cooled down' enriched detectors of the HEIDELBERG-MOSCOW $\beta\beta$-experiment into the GENIUS-TF setup, may allow, in a later stage, to improve the present accuracy of the effective Majorana neutrino mass determined recently [8, 9, 10, 16]. A detailed description of the GENIUS-TF project is given in [11].

After installation of the GENIUS-TF setup in 2002 between halls A and B in Gran Sasso, opposite to the buildings of the HEIDELBERG-MOSCOW double beta decay experiment and of the DAMA experiment (Figs. 1, 6), the first four detectors have been

installed in liquid nitrogen on May, 5 2003 and have started operation. This has been reported in [14] and [15].

This is the first time ever, that this novel technique for extreme background reduction in search for rare decays is tested under realistic background conditions in an underground laboratory.

In section 2 we will describe the actual setup, including the measures taken for producing high-purity nitrogen, the measurement system of the liquid nitrogen level, the new digital data acquisition system [12], and will present first measured spectra. In section 3 we briefly demonstrate the potential of GENIUS-TF to probe the DAMA signal for cold dark matter by looking for the expected modulation signal.

2 Description of Setup and of Present Performance

On May 5, 2003 the first four naked Ge detectors were installed under clean-room conditions into the GENIUS-TF setup [15]. Fig. 3 shows the contacted crystals after taking them out of the transport dewars, in the holder made from high-purity PA5 (a type a teflon), in which they then are put into liquid nitrogen. Each detector has a weight of 2.5 kg. The depth of the core of the detectors was reduced to guarantee a very low threshold, estimated by ORTEC to be around 0.5-0.7 keV, with only marginal deterioration of the energy resolution. Fig. 2 shows the sucessesful team after installation of the first four detectors on May 5, 2003.

Figure 2: The successful team after installation of the first four detectors on May 5, 2003. From left to right: Irina Krivosheina and Claudia Tomei, Hans Volker Klapdor-Kleingrothaus, Oleg Chkvoretz and Herbert Strecker.

The liquid nitrogen (in total $\sim$ 70 l) is kept in a thin-walled (1 mm) box of high-purity electrolytic copper of size 50x50x50 cm^3. Inside this copper box, i.e. also inside the liquid nitrogen, is installed another box with walls of 5 - 10 cm monocristalline Ge bricks ($\sim$300 kg) forming the first highly efficient shield of the Ge detectors (see Fig. 5).

The copper box is thermally shielded by 20 cm of special low-level styropor, followed by a shield of 10 cm of electrolytic copper (15 tons) and 20 cm of low-level (Boliden) lead

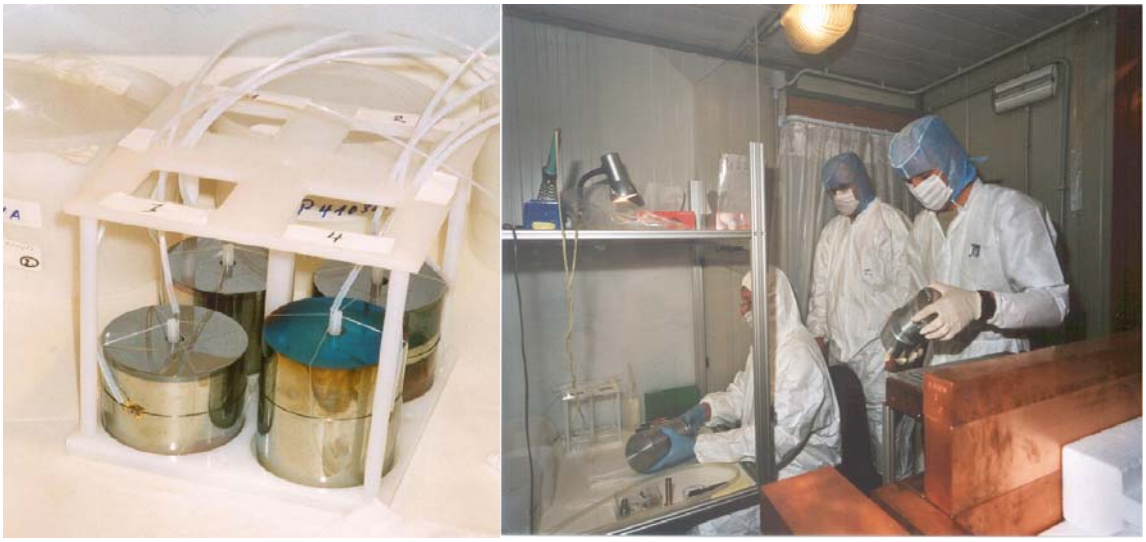

Figure 3: Right: Taking out the crystals from the transport dewars and fixing the electrical contacts in the clean room of the GENIUS-TF building - from left to right: Herbert Strecker, Hans Volker Klapdor-Kleingrothaus, Oleg Chkvorets. Left: The first four contacted naked Ge detectors before installation into the GENIUS-TF setup.

(35 tons). Fig. 5 shows the geometry of the setup. Fig. 4 shows the setup in the status of not yet fully closed copper and lead shields, and the fully closed setup (status December 2, 2003). The setup will finally by shielded against neutrons with 10 cm Boronpolyethylene plates.

The high-purity liquid nitrogen used, is produced by the BOREXINO nitrogen plant, which has been extended for increase of the production capacity to be able to provide enough nitrogen also for GENIUS-TF. Liquid nitrogen of standard quality (99.99% purity) is directly purified in the liquid phase by an adsorber column system, consisting of two independent columns (Low Temperature Adsorber - LTA) filled with about 2 kg of 'activated carbon' each. One of them we purchased to supplying GENIUS-TF. The system is designed to continuously produce about 150 l of liquid nitrogen per hour, respectively about 100 m^3/h gaseous nitrogen for both experiments. During the regeneration phase of one column the other one is in use. The plant is shown in Fig. 6. For the experimentally measured strong reduction of Rn by the cryogenic column adsorption see [17].

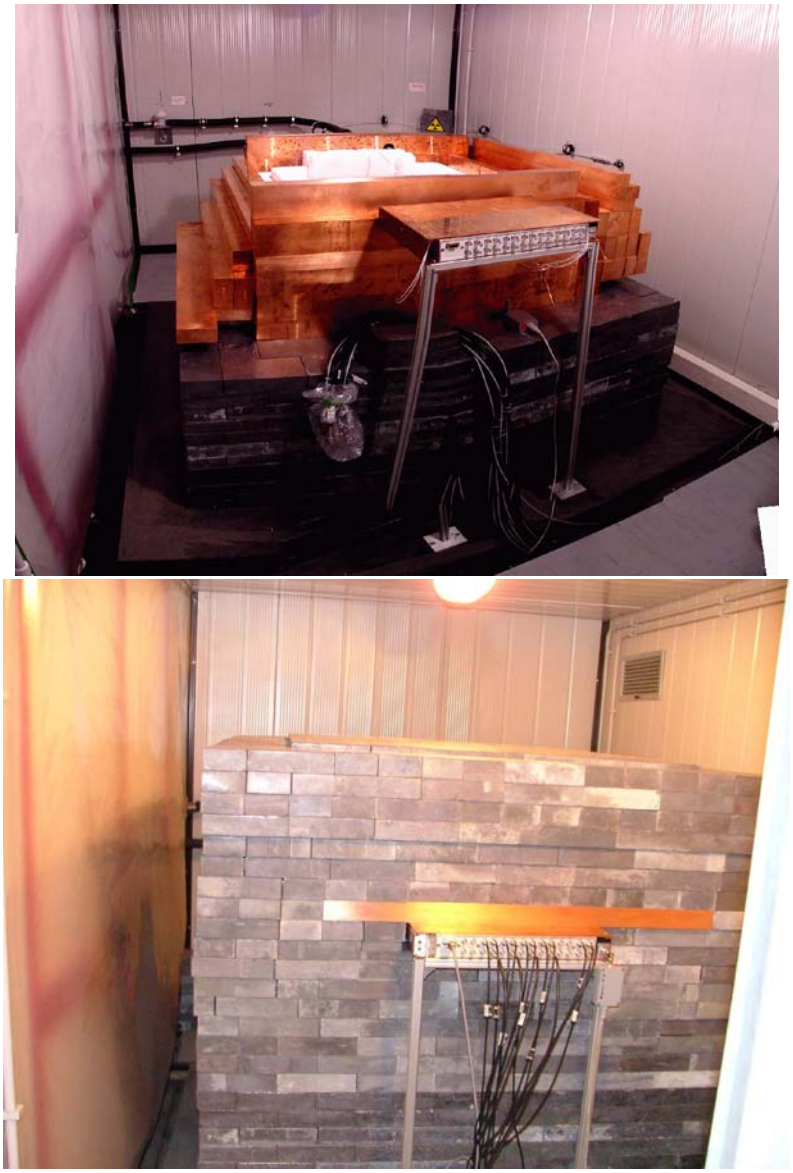

Figure 4: View of GENIUS-TF in the Gran Sasso Underground Laboratory in Italy. Left: The setup with detectors inside, but shielding only partly mounted. In front the preamplifier system. Status May 5, 2003. Right: The full shielding of GENIUS-TF, status December 2, 2003.

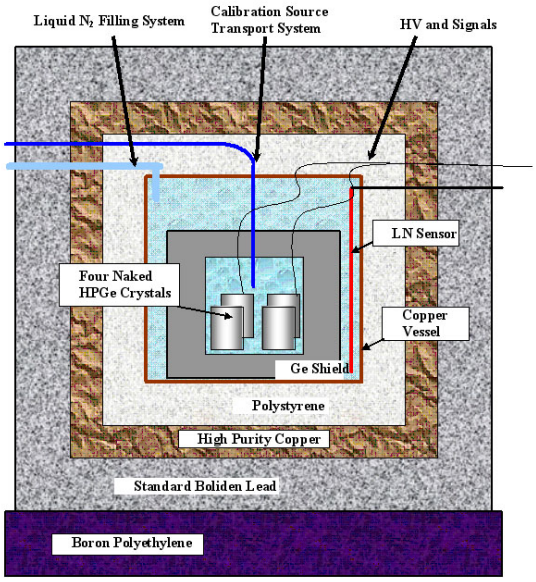

Figure 5: Cross section of the setup.

Figure 6: BOREXINO-GENIUS-TF nitrogen purification system in GRAN SASSO (left and upper right). The left part shows the absorber column (low temperature absorber - LTA) provided by the GENIUS-TF group. The nitrogen is transported by 200 l vessels to the GENIUS-TF building (lower right).

From the production plant the liquid nitrogen is transported by 200 l vessels to the building of the experiment. Filling of the copper container with liquid nitrogen is provided by connecting them to the filling system consisting of isolated teflon tubes as shown in Fig. 7. The nitrogen level in the detector chamber is measured by a capacitive sensor consisting of two 40 cm long isolated selected-material copper tubes, one inside the other. The change of the medium between the tubes by the entering liquid nitrogen leads to a change of the capacity, which is measured by subsequent electronics and indicated by LED's outside of the setup. We measure the nitrogen level in ten steps between 0 and 100%. GENIUS-TF has to be refilled every two days (with some reserve of one more day).

The data acquisition system we developped recently for GENIUS-TF and GENIUS is decribed in detail in [12]. It uses multichannel digital processing technology with FLASH ADC modules with high sampling rates of 100 MHz and resolution of 13 bits. It allows to capture the detailed shape of the preamplifier signal with high-speed ADC, and then perform digitally all essential data processing functions, including precise energy measurement over a range of 1 keV - 3 MeV, rise time analysis, ballistic deficit correction and pulse shape analysis. Thus we obtain both the energy and the pulse shape information from one detector using one channel of the Flash ADC module.

To allow for regular calibration of the detectors, a source of ^{133}Ba fixed on a wire can be introduced through a teflon tube into the center among the detectors. The source is transported via a magnetic system. The activity of the source is 401 kBq.

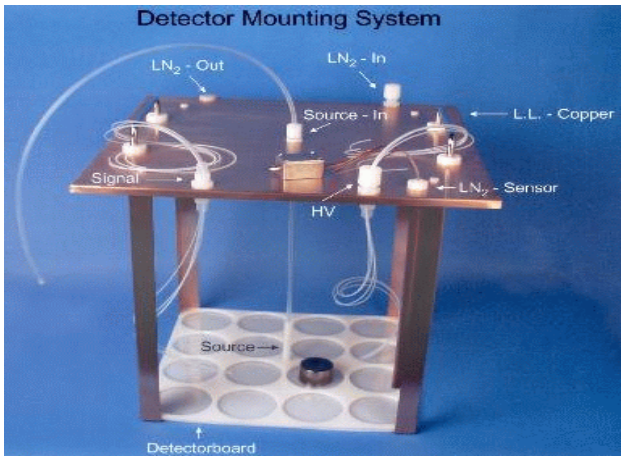

Figure 7: Connections of electronics, liquid nitrogen, source and LN_2 sensor to the inner part of GENIUS-TF.

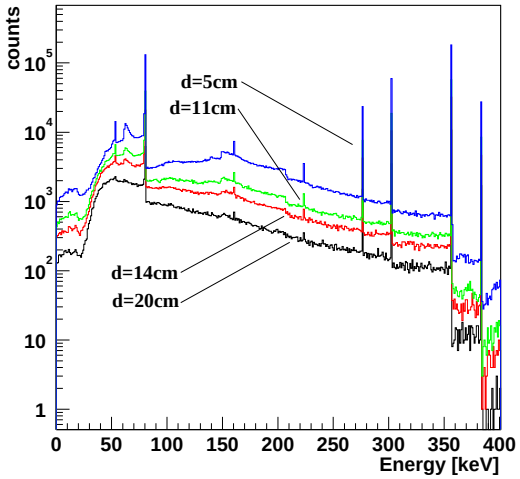

Figure 8: Monte Carlo simulation of GENIUS-TF calibration measurements with a movable ^{133}Ba source, for different source-detector distance, with GEANT4. **d** is the vertical distance of the source from the plane, on which the detectors are sitting (from [15]).

Fig. 8 shows the dependence of the expected spectrum seen by the four detectors as function of the position in the setup (d is the vertical distance of the source from the plane, on which the detectors are lying. For $d \sim$ 7-10 cm the source is approximately on top of the detectors).

Figs. 9, 10 show two spectra measured a few days after installation. A first spectrum measured with a ^{60}Co source *outside* the setup, and the ^{133}Ba source *inside*, is shown in Fig. 9. The resolution at this moment (two days after installation) is 3 keV in the 1330 keV region.

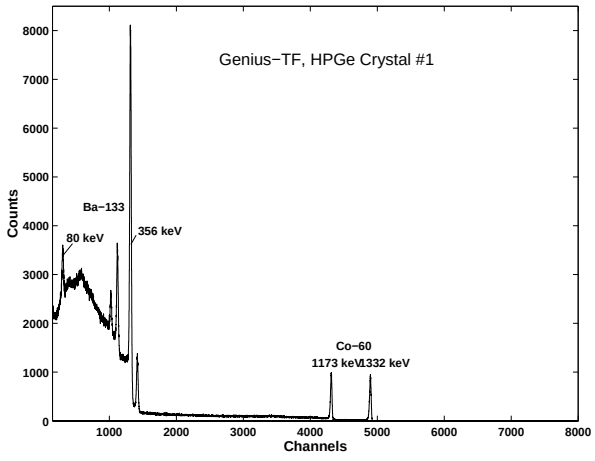

Figure 9: A first spectrum measured with detector 1 with a ^{60}Co source outside, and the ^{133}Ba source inside the setup (see [15]).

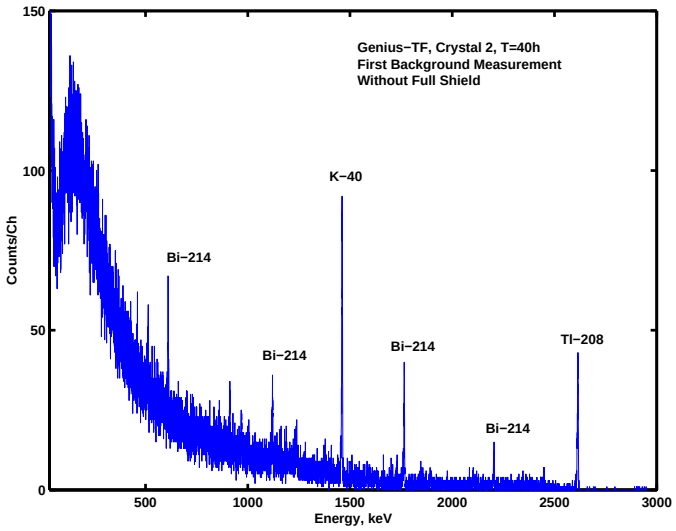

Figure 10: The first background spectrum measured with detector 2 over 40 hours without shield of the setup to the top (see [15]).

Fig. 10 shows the background, measured with the still *open* setup to the top. When the liquid nitrogen level *decreases*, the background slightly *increases*. This shows that the radioactive impurities seen (from ^{40}K, and the ^{232}Th and ^{238}U natural decay chains) are located *outside* the setup. No cosmologically produced impurities in the detectors are seen on the present level of sensitivity.

The effect of microphonics from bubbling in the liquid nitrogen is as far as it can be seen now, negligible for high energies, but has to be discriminated by pulse shape analysis for low energies. This can be done by the new digital data acquisition system [12].

3 Searching for the Annual Modulation of Dark Matter signal with the GENIUS-TF experiment.

It is generally assumed that our galaxy is embedded in a halo of dark matter particles (WIMPs) with energy density $\rho \simeq 0.3$ GeV/cm^3 and velocities distributed according to a Maxwellian distribution with parameter v_0 (defined as $\sqrt{(\frac{2}{3})}\ v_{\rm rms}$) and cut-off velocity equal to the escape velocity in the Galaxy ($v_{\rm esc} \simeq 650$ km/s).

The recoil spectrum produced by WIMP-nucleus scattering in a target detector is expected to show the so-called annual modulation effect, due to the Earth's motion around the sun [22].

We have investigated the potential of GENIUS-TF for searching for this modulation effect [13]. Fig. 11 shows the expected WIMP rate in Ge for different masses. Fig. 12 shows the result, which can be obtained after two years of measurement if a WIPM exists as claimed by DAMA [20].

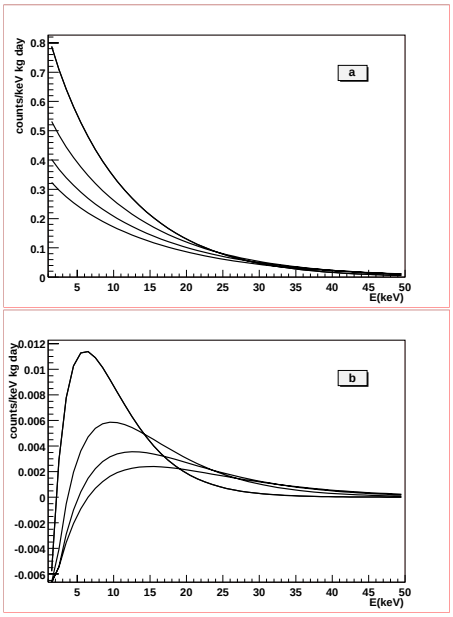

Figure 11: Expected WIMP rate in Ge for m_W= 40, 60, 80, 100 GeV (from top to bottom) and $\sigma_{Ge} = 10^{-34}$ cm^2: a) time-independent component of the signal (S_0) ; b) amplitude of the modulated component ($S_{\rm m}$) (from [13]).

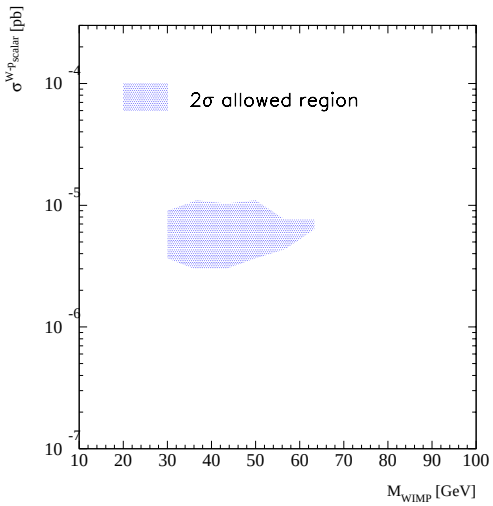

Figure 12: Allowed region at 2σ C.L. corresponding to the best-fit values of $m_W = (39.9 \pm 5.6)\, GeV$, and $\sigma_p = (7.0 \pm 1.6) \cdot 10^{-6}$ (see for details [13]). The region is calculated (see [13]) and has to be interpreted as the result that can be given by GENIUS-TF after two years of measurement if a WIMP exists with the properties assumed so far (from [13]).

4 Conclusions

The annual modulation, due to the motion of the earth with respect to the galactic halo, is the main signature of a possible WIMP signal. A positive indication of this modulation has been found over the past years by the DAMA experiment and it would be of great importance to look for the same effect with another experiment, expecially in the region of the WIMP parameter space indicated by the DAMA results.

The GENIUS-TF experiment [15, 11], a prototype for the GENIUS experiment with a mass of 40 kg and a projected background of 4 counts/(kg y keV), can be used to look for Dark Matter, not only through the direct detection of WIMP-induced nuclear recoils, but also through the annual modulation of the experimental rate. GENIUS-TF will be - in addition to DAMA [25] - the *only* experiment which will be able to probe the annual modulation signature in a foreseeable future (see Figs. 11, 12). The at present much discussed cryo detector experiments, such as CDMS [26], CRESST [27], EDELWEISS [28] have at present hardly a chance to do this (except perhaps EDELWEISS) because the mass used and projected in operation in these experiments is still by far too low (see also [24]).

The first four naked Ge detectors (10 kg) have been installed in liquid nitrogen into the GENIUS-Test-Facility in the GRAN SASSO Underground Laboratory on May 5, 2003. This is the first time that this novel technique is applied under realistic background conditions of an underground laboratory. With the successful start of GENIUS-TF a historical step has been achieved into a new domain of background reduction in underground physics in the search for rare events. Besides testing of constructional parameters for the GENIUS project one of the first goals of GENIUS-TF will be to test the signal of cold dark matter reported by the DAMA collaboration [20, 23].

5 Acknowledgement:

The authors would like to thank the technical staff of the Max-Planck Institut für Kernphysik and of the Gran Sasso Underground Laboratory. We acknowledge the invaluable support from BMBF and DFG, and LNGS of this project. We are grateful to the former State Committee of Atomic Energy of the USSR for providing the monocristalline Ge shielding material used in this experiment.

6 List of Edited Proceedings (2003)

1. H.V. Klapdor-Kleingrothaus (ed.) Physics Beyond the Standard Model: Beyond the Desert 02, Proc. of Intern. Conf. BEYOND'02, Oulu, Finland, 2-7 Jun 2002, IOP, Bristol, 2003, 734 pages.

2. H.V. Klapdor-Kleingrothaus (ed.) Physics Beyond the Standard Model: Beyond the Desert 03, Proc. of Intern. Conf. BEYOND'03, Tegernsee, Germany, 4-9 June 2003, Springer, Heidelberg, 2004 (in preparation).

7 List of Publications (2003)

1. H.V. Klapdor-Kleingrothaus, O. Chkvorez, I.V. Krivosheina, H. Strecker, C. Tomei, Nucl. Instrum. Meth. A 511 (2003) 341-346 and hep-ph/0309170,
"First 10 kg of Naked Germanium Detectors in Liquid Nitrogen installed in the GENIUS-Test-Facility".

2. H.V. Klapdor-Kleingrothaus, CERN Courier 43 N6 (2003) 9 and hep-ph/0307329,
"'Naked' Crystals go Underground".

3. H.V. Klapdor-Kleingrothaus and I.V. Krivosheina, Found. Phys. 33 (2003) 831-837,
"Search for cold dark matter and solar neutrinos with GENIUS and GENIUS-TF".

4. H.V. Klapdor-Kleingrothaus, C. Tomei, Nucl. Instrum. Meth. A 508 (2003) 337-342 and hep-ph/0306258, *"^{85}Kr and ^{39}Ar background in GENIUS".*

5. C. Tomei, A. Dietz, I. Krivosheina, H.V. Klapdor-Kleingrothaus, Nucl. Instrum. Meth. A 508 (2003) 343-352 and hep-ph/0306257, *"Searching for the Annual Modulation of Dark Matter signal with the GENIUS-TF experiment".*

6. T. Kihm, V.F. Bobrakov, H.V. Klapdor-Kleingrothaus, Nucl. Instrum. Meth. B 498 (2003) 334-339 and hep-ph/0302236, *"A digital multi-channel spectroscopy system with 100 MHz flash ADC module for the GENIUS-TF and GENIUS projects".*

8 List of Contributions to Conferences (2003)

1. H.V. Klapdor-Kleingrothaus and I.V. Krivosheina, in Proc. of Intern. Conf. IHEPP03, Valencia, September 2003, PRHEP-AHEP2003/060, *"GENIUS-Test-Facility Started Operation in GRAN SASSO - with First Ten kg of Naked Germanium Detectors in Liquid Nitrogen".*

2. H.V. Klapdor-Kleingrothaus, in Proc. of Intern. Conf. BEYOND'03, Physics Beyond the Standard Model: Beyond the Desert 03, Tegernsee, Germany, 4-9 June 2003, Springer, Heidelberg, 2004, H.V. Klapdor-Kleingrothaus (ed.),
"GENIUS-TF, Status of the Project".

3. H.V. Klapdor-Kleingrothaus, presented at Arbeitstreffen "Hadronen und Kerne", Meißen, St.-Afra-Klosterhof, Germany, 8.-11. September 2003, *"Aktueller Status des Neutrinolosen Doppel-Beta-Zerfalls".*

4. I.V. Krivosheina, in Proc. of Intern. Conf. BEYOND'03, Physics Beyond the Standard Model: Beyond the Desert 03, Tegernsee, Germany, 4-9 June 2003, Springer, Heidelberg, 2004, H.V. Klapdor-Kleingrothaus (ed.), *"SN87A - Historical View about Registration of the Neutrino Signal with KAMIOKANDE, BAKSAN and IMB Detectors".*

5. H.V. Klapdor-Kleingrothaus and I.V. Krivosheina*, in Proc. of Intern. Conf. BEYOND'02, Physics Beyond the Standard Model: Beyond the Desert 02, H.V. Klapdor-Kleingrothaus (ed.) Oulu, Finland, 2-7 Jun 2002, IOP, Bristol, 2003, 499 - 514, *"Search for cold dark matter and solar neutrinos with GENIUS and GENIUS-TF".*

6. H.V. Klapdor-Kleingrothaus and I.V. Krivosheina*, in Proc. of Zacatecas Forum in Physics 2002, Zacatecas, Mexico, 11-13 May 2002, Found. Phys. 33 (2003) 831-837, *"Search for cold dark matter and solar neutrinos with GENIUS and GENIUS-TF".*

7. H.V. Klapdor-Kleingrothaus*, A. Dietz, I.V. Krivosheina, Nucl. Phys. Proc. Suppl. 124: 209-213, 2003, D. Cline (ed.), for 5th International UCLA Symposium on Sources and Detection of Dark Matter and Dark Energy in the Universe (DM 2002), Marina del Rey, California, 20-22 Feb 2002, *"Search for Cold and Hot Dark Matter with the HEIDELBERG-MOSCOW Experiment, HDMS, GENIUS and GENIUS-TF".*

8. H.V. Klapdor-Kleingrothaus, in Proc. of International Europhysics Conference on High Energy Physics, European Physical Society (EPS), Aachen, Germany, 17 - 23 July 2003 *"The GENIUS Test Facility in GRAN SASSO".*

9. H.V. Klapdor-Kleingrothaus, Deutsche Physikalische Gesellschaft e. V. (DPG), Aachen, Germany, 24.-28. März, 2003, "Status of Evidence for Neutrinoless Double Beta Decay"

10. Ch. Dörr* and H.V. Klapdor-Kleingrothaus, Deutsche Physikalische Gesellschaft e. V. (DPG), Aachen, Germany, 24.-28. März, 2003, "Neue Ergebnisse für den neutrinobegleiteten Doppelbetazerfalls von ^{76}Ge im Rahmen des HEIDELBERG-MOSCOW Experiments"

11. H.V. Klapdor-Kleingrothaus, in Proc. of Intern. Conf. SUGRA2003, "20 years of SUGRA and the Search for SUSY and Unification", Boston, USA, March 17-20, 2003, *"Status of Evidence for Neutrinoless Double Beta Decay from the HEIDELBERG-MOSCOW Experiment - and Implications for Supersymmetry".*

12. H. V. Klapdor-Kleingrothaus, in Proc. of NOON 2003, Japan, Kanazawa, February 2003, World Scientific 2004, eds. Y Suzuki, hep-ph/0307330, *"Status of Evidence for Neutrinoless Double Beta Decay, and the Future: GENIUS and GENIUS-TF."*

9 List of Colloquia and Seminars Made During 2003

1. H.V. Klapdor-Kleingrothaus, Physikalisches Institut, Theorie Department, Bonn, 7. November 2003, *"Absolute Neutrino Mass After the First Evidence for Neutrinoless Double Beta Decay - and Implications of Double Beta Decay for Exotic Physics".*

2. H.V. Klapdor-Kleingrothaus, DESY, Zeuthen, Germany, 17 Juli (2003), *"First Evidence for Neutrinoless Double Beta Decay - and World Status of the absolute Neutrino Mass."*

3. H.V. Klapdor-Kleingrothaus, Fachbereich Physik, Bergische Universität Wuppertal, Germany 26 May 2003, *"The Absolute Neutrino Mass After the First Evidence for Neutrinoless Double Beta Decay".*

4. H.V. Klapdor-Kleingrothaus, Physikalisches Institut, Fakultät für Physik und Astronomie, Ruprecht-Karls-Universität, Heidelberg, Germany 28 April 2003, *"Status of Evidence for Neutrinoless Double Beta Decay".*

5. H.V. Klapdor-Kleingrothaus, Osaka University, Japan, 17 February 2003, *"First Evidence for Neutrinoless Double Beta Decay from the HEIDELBERG-MOSCOW Experiment and Implication for Particle Physics and Astrophysics".*

6. H.V. Klapdor-Kleingrothaus, Institut für Physik, Universität Mainz, Germany, 22 Januar 2003, *"First Evidence for Neutrinoless Double Beta Decay - and Future of the Field".*

References

[1] H.V. Klapdor-Kleingrothaus in Proceedings of BEYOND'97, First International Conference on Particle Physics Beyond the Standard Model, Castle Ringberg, Germany, 8-14 June 1997, edited by H.V. Klapdor-Kleingrothaus and H. Päs, *IOP Bristol* (1998) 485 - 531 and in *Int. J. Mod. Phys.* **A 13** (1998) 3953.

[2] H.V. Klapdor-Kleingrothaus, J.Hellmig and M.Hirsch, *GENIUS-Proposal*, 20 Nov. 1997.

[3] J. Hellmig and H.V. Klapdor-Kleingrothaus, *Z. Phys.* **A 359** (1997) 351 - 359, and nucl-ex/9801004.

[4] H.V. Klapdor-Kleingrothaus and M. Hirsch, *Z. Phys.* **A 359** (1997) 361 - 372.

[5] H.V. Klapdor-Kleingrothaus, J. Hellmig and M. Hirsch, *J. Phys.* **G 24** (1998) 483 - 516.

[6] H.V. Klapdor-Kleingrothaus, CERN Courier, Nov. 1997, 16 - 18.

[7] H.V. Klapdor-Kleingrothaus et al. **MPI-Report MPI-H-V26-1999**, and *Preprint: hep-ph/***9910205**, and in Proceedings of the 2nd Int. Conf. on Particle Physics Beyond the Standard Model BEYOND'99, Castle Ringberg, Germany, 6-12 June 1999, edited by H.V. Klapdor-Kleingrothaus and I.V. Krivosheina, *IOP Bristol* (2000) 915 - 1014.

[8] H.V. Klapdor-Kleingrothaus et al. hep-ph/0201231 and *Mod. Phys. Lett.* **A 16** (2001) 2409-2420.

[9] H.V. Klapdor-Kleingrothaus, A. Dietz and I.V. Krivosheina, *Part. and Nucl.* **110** (2002) 57-79.

[10] H.V. Klapdor-Kleingrothaus, A. Dietz and I.V. Krivosheina, *Foundations of Physics* **31** (2002) 1181-1223 and Corrigenda, 2003 home-page: http://www.mpi-hd.mpg.de/non_acc/main_results.html.

[11] H.V. Klapdor-Kleingrothaus et al., *Nucl. Instrum. Meth.* **A 481** (2002) 149-159.

[12] T. Kihm, V.F. Bobrakov and H.V. Klapdor-Kleingrothaus, *Nucl. Instrum. Meth.* **A 498** (2003) 334-339 and hep-ph/0302236.

[13] C. Tomei, A. Dietz, I. Krivosheina, H.V. Klapdor-Kleingrothaus, *Nucl. Instrum. Meth.* **A 508** (2003) 343-352, and hep-ph/0306257.

[14] H.V. Klapdor-Kleingrothaus, CERN Courier, 2003.

[15] H.V. Klapdor-Kleingrothaus, O. Chkvorez, I.V. Krivosheina, H. Strecker, C. Tomei, *Nuclear Instruments and Methods in Physics Research* **A 511** (2003) 341 - 346 and hep-ph/0309170, and H.V. Klapdor-Kleingrothaus and I.V. Krivosheina, in Proc. of Beyond the Desert 2002, BEYOND02, Oulu, Finland, June 2002, IOP 2003, ed. H.V. Klapdor-Kleingrothaus.

[16] H.V. Klapdor-Kleingrothaus, A. Dietz, I.V. Krivosheina, Ch. Dörr, C. Tomei, *Phys. Lett.* **B 578** (2204) 54-62 and hep-ph/0312171.

[17] G. Zuzel and G. Heusser, Verhandl. DPG (VI) 38/2 (2003) p. 61, Aachen 2003.

[18] HEIDELBERG-MOSCOW collaboration, Phys. Rev. D **59** (1998) 022001.

[19] H. V. Klapdor-Kleingrothaus, A. Dietz, G. Heusser, I.V. Krivosheina, D. Mazza, H. Strecker and C. Tomei, Astroparticle Physics, **18**, Issue 5 (2003) 525-530, and e-Print hep-ph/ 0206151.

[20] R. Bernabei et al., Phys. Lett. B **424** (1998) 195; Phys. Lett. B **450** (1999) 448; Phys. Lett. B **480** (2000) 23.

[21] K. Freese, J. Frieman and A. Gould, Phys. Rev. D **37** (1988) 3388.

[22] A.K. Drukier, K. Freese and D.N. Spergel, Phys. Rev. D 33 (1986) 3495.

[23] R. Bernabei et al., Riv. Nuovo Cim. 26 (2003) 1-73.

[24] H.V. Klapdor-Kleingrothaus, *Int. J. Mod. Phys.* **A17**, 3421-3431 (2002), in Proc. of *Internat. Conf. LP01*, Rome, Italy, July 2001.

[25] R. Bernabei et al., in *Proc. of Intern. Conf. on Physics Beyond the Standard Model: Beyond the Desert 02, BEYOND'02*, Oulu, Finland, 2-7 Jun 2002, *IOP, Bristol*, 2003, ed. H.V. Klapdor-Kleingrothaus.

[26] T. Saab et al., Nucl. Phys. Proc. Suppl. 110 (2002) 100-102.

[27] F. Probst et al., Nucl. Phys. Proc. Suppl. 110 (2002) 67-69.

[28] A. Benoit et al., Phys. Lett. B 545 (2002) 43-49.

G.N.O.
Gallium Neutrino Observatory

M. Altmann[a], M. Balata[b], P. Belli[c], E. Bellotti[d], R. Bernabei[c], E. Burkert[e], C. Cattadori[d], G. Cerichelli[f], R. Cerulli[c], M. Chiarini[e], M. Cribier[g], S. d'Angelo[c], G. Del Re[f], K. Ebert[h], F. von Feilitzsch[a], N. Ferrari[b], A. Germeroth[e], W. Hampel[e], F.X. Hartmann[e], E. Henrich[h], G. Heusser[e], L. Ioannucci[b], F.Kaether[e], J. Kiko[e], T. Kirsten[e], P. Mögel[e], D. Motta[d,e], T. Lachenmaier[a], J. Lanfranchi[a], M. Laubenstein[b], S. Nisi[b], J. Oehm[e], L. Pandola[b], W. Potzel[a], H. Richter[e], S. Schoenert[e], M. Weneser[a], L. Zanotti[d]

[a] Physik Department E15, Technische Universität München (TUM), James-Franck Straße, D-85748 Garching b. München, Germany

[b] INFN, Laboratori Nazionali del Gran Sasso (LNGS), S.S. 17/bis Km 18+910, I-67010 L'Aquila - Italy

[c] Dip. di Fisica, Università di Roma "Tor Vergata" and INFN, Sez. Roma II, Via della Ricerca Scientifica, I-00133 Roma - Italy

[d] Dip. di Fisica, Università di Milano "Bicocca", and INFN Sez. Milano, Via Emanueli, I-20126 Milano - Italy

[e] Max-Plank-Institut für Kernphysik (MPIK), P.O.B. 103980, D-69029 Heidelberg - Germany

[f] Dip. di Ingegneria Chimica e Materiali, Università dell'Aquila, Località Monteluco di Roio, L'Aquila - Italy

[g] DAPNIA/Service de Physique de Particules, CE Saclay, F-91191 Gif-sur-Yvette Cedex - France

[h] Institut für Technische Chemie, Forschungszentrum Karlsruhe (FZK), Postfach 3640, D-76021 Karlsruhe, Germany

Abstract

GNO (Gallium Neutrino Observatory) is monitoring the low energy solar neutrino flux with a 30 tons gallium detector at LNGS. During the year 2003, 4 solar runs and 1 blank run have been successfully performed; in total 58 solar runs (corresponding to $\approx$ 1713 days of live time) have been accumulated since spring 1998 when GNO started the data taking. The result of 58 solar runs is: $62.9^{+5.5}_{-5.3}$(stat)$\pm$2.5(syst) SNU. The combined result from both GNO and GALLEX together (123 solar runs) is 69.3$\pm$4.1(stat.)$\pm$3.6(syst) SNU. The data taking and the various activities performed during 2003 are also discussed in this report.

1 Introduction

GNO (Gallium Neutrino Observatory) is the experiment successor of GALLEX; it is devoted to the measurement of the interaction rate of solar neutrinos on gallium with a low energy threshold (233 keV), well below the maximum energy of the so-called *pp* neutrinos. The aims of GNO can be summarized as follow:

- to refine the measurement of the mean (i.e. mediated over the entire period of data taking) solar neutrino interaction rate on gallium, reducing the systematic and statistical errors to a level of 5% or less;
- to provide a monitor of the low energy neutrinos over a long period (one solar cycle);
- to investigate possible (unexpected) short and long term time variations of the signal.

The efforts of GNO are addressed to collect continously data on the interaction rate and to improve many details of the experimental procedure, in order to lower the systematic errors as much as possible. In this section we briefly recall the experimental aspects of the GNO detector, and we give an up to date overview of the solar neutrino physics, concentrating in particular on the scientific motivation of the GNO experiment. In section 3 we describe the GNO solar neutrino observations performed in 2003 and the results obtained from data analysis. In section 4 we discuss the experimental activities (besides data taking) performed in 2003. In section 5 we discuss the implication of the results in the context of solar neutrino physics and neutrino oscillations. In section 6 we describe the present status of the experiment.

2 The GNO detector

The gallium solar neutrino experiment at Laboratori Nazionali del Gran Sasso detects solar neutrinos via the reaction $^{71}Ga\,(\nu_e, e\,)^{71}Ge$, which has a threshold of 233 keV. The detector is sensitive mainly to pp-neutrinos (53% of the interaction rate according to the standard solar model [1]), with smaller contributions to the signal from ^{7}Be ν (27%), ^{8}B ν (12%), and CNO ν (8%). The target consists of 101 tons of a $GaCl_3$ solution in water

Table 1: Summary of GNO runs performed in 2003. For each extraction the following data are reported: extraction label; DAQ lable (SR=Solar Run, BL=BLank); extraction date, referred to the end of the extraction; exposure time in days; counter type and number used for ^{71}Ge counting (Fe=Iron cathode, Si=Silicon cathode, FC=Iron shaped cathode, SC=Silicon shaped cathode); counting time; chemical yield (tank to counter), measured by non-radioactive Ge carrier.

Extraction label	Type	Date	Exposure (days)	Counter	Counting time (days)	Chemical yield (%)
EX72	SR55	15-jan-03	28	FC-093	319.8	97.3
EX73	SR56	12-feb-03	28	FC-174	312.5	97.0
EX74	BL12	13-feb-03	1	FC-102	262.8	97.3
EX75	SR57	12-mar-03	27	Si-108	256.6	98.3
EX76	SR58	09-apr-03	28	SC-136	227.8	95.9

and HCl, containing 30.3 tons of natural gallium; this amount corresponds to $\sim 10^{29}$ ^{71}Ga nuclei. The ^{71}Ge atoms produced by solar neutrinos (at a rate of about 0.7 per day, one half of the amount predicted by solar models) are extracted from the gallium tank every 4 weeks [3] and introduced in low-background gas proportional counters [4] as germane gas (GeH_4). The decay of ^{71}Ge (EC, τ=16.5 days) produces a signal in the counters consisting of a point-like ionization at 10.4 keV, or 1.1 keV. The signal is recorded by fast digitizers to allow background reduction by pulse shape analysis. The solar neutrino interaction rate on ^{71}Ga is deduced from the number of ^{71}Ge atoms observed. For a complete description of the experimental procedure see [5]. The gallium detector was operated between 1991 and 1997 by the GALLEX Collaboration: 65 "solar runs" were performed. The solar neutrino capture rate on ^{71}Ga was measured with a global uncertainty of 10% as: 77.5 $\pm 6.2(\text{stat.})^{+4.3}_{-4.7}(\text{syst.})$ SNU[1] (1 σ) [5]. After maintenance of the chemical plants and renovation of the DAQ and electronics, a new series of measurements was started in April 1998, within the GNO (Gallium Neutrino Observatory) project [7], using the same 30-ton Gallium target.

3 Solar neutrino observations

3.1 Results

GNO started solar neutrino observations in May 1998: the list of the main parameters of the solar runs performed in 2003 is reported in Table 1: 4 solar runs and 1 blank run were successfully performed during the year. Data for runs performed before 2003 can be found in the LNGS Annual Reports of past years [8, 9, 10, 11, 12]. At the beginning of January

[1] 1 SNU (Solar Neutrino Unit) = 10^{-36} captures per second and per absorber nucleus

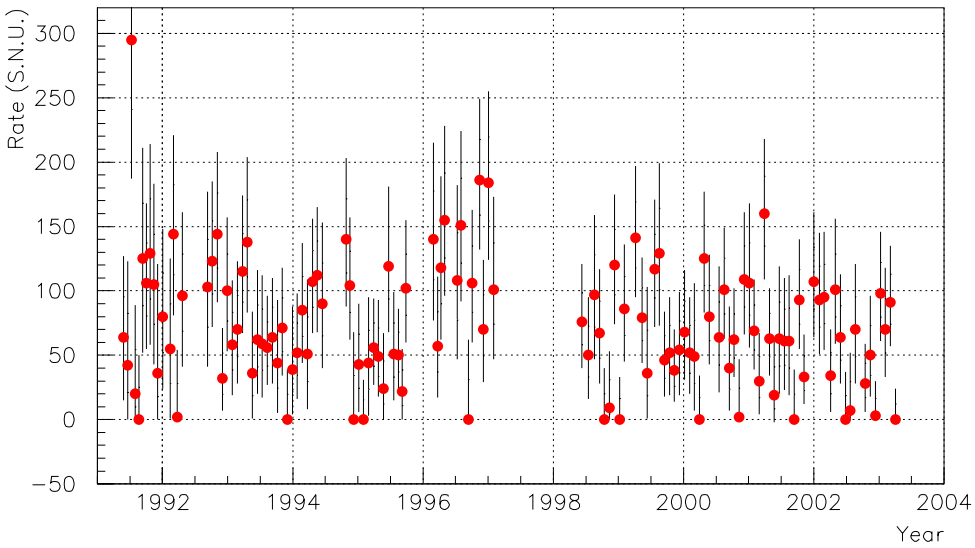

Figure 1: Measured solar neutrino capture rate (atoms/day) in the single 65 GALLEX solar runs and 58 GNO solar runs. A signal of 100 SNU corresponds to a production rate of 0.90 ^{71}Ge atoms per day inside the 30 tons gallium tank.

2004, the counting is completed for all the performed solar runs. Data from the latest 15 solar runs (GNO III), performed between January 2002 and April 2003, as well as from all the 58 GNO solar runs, have been evaluated and results have been presented at the TAUP 2003 conference [15]. The results of some runs belonging to the GNO I and GNO II data periods [13, 14] have been re-evaluated with respect to the previous publications because of the new measurements of absolute volume efficiencies of the counters (see Sect 4). A total of 239 decaying ^{71}Ge atoms were identified from the 1713 days of exposure in solar runs SR1-SR58, corresponding to 4.1 ^{71}Ge events/run. The ν interaction rate for GNO is

$$62.9^{+5.5}_{-5.3} \pm 2.6 \text{ SNU } (1\sigma) \quad [15]$$

The combined result for GALLEX and GNO (65+58=123 solar runs, corresponding to 1594+1713=3307 days of live time) is

$$69.3 \pm 4.1 \pm 3.6 \text{ SNU } (1\sigma) \quad [15].$$

The Davis-plot including the 65 single Gallex solar runs and the 58 GNO ones is shown in Fig. 1.

The results for the data periods GNO I-III, as well as for the full GNO, are summarized in Table 2, that also includes the separate analyses for the L- and the K- energy regions.

The main factors contributing to the systematic error in GNO are specified in Table 3. The 1σ systematic error amounts to $\sim$3.9% and is dominated by the uncertainties on the

Table 2: Measured solar neutrino capture rate (SNU) in the GNO and in the data periods GNO I - III. Separate contributions from L and K events are also shown. Statistical errors only.

	Solar runs	Date (dd.mm.yy)	L-peak (SNU)	K-peak (SNU)	L+K peaks (SNU)
GNO I	19	20.05.98-12.01.00	$73.4^{+16.4}_{-15.2}$	$60.1^{+13.0}_{-12.0}$	$65.6^{+10.2}_{-9.6}$
GNO II	24	12.01.00-08.01.02	$68.5^{+14.3}_{-13.3}$	$65.7^{+11.3}_{-10.4}$	$66.8^{+8.8}_{-8.3}$
GNO III	15	08.01.02-09.04.03	$61.7^{+16.8}_{-15.3}$	$49.7^{+12.4}_{-11.2}$	$54.3^{+10.0}_{-9.3}$
GNO	58	20.05.98-09.04.03	$68.2^{+8.9}_{-8.5}$	$59.5^{+6.9}_{-6.6}$	$\mathbf{62.9}^{+5.5}_{-5.3}$

Table 3: Summary of systematic error components in GNO (SR1-SR58). For comparison the same components are quoted for Gallex.

Item	GNO	Gallex	GNO + Gallex
Target size	0.8 %	0.8 %	
Chemical yield	2.0 %	2.0 %	
Energy cuts	2.2 %	4.0 %	
Pulse shape cuts	1.3 %	2.0 %	
Subtotal	3.4 %	5.0 %	4.2 %
Side reactions	1.2 SNU	1.2 SNU	
Rn cut ineff.	0.5 SNU	1.2 SNU	
^{68}Ge	0.0 SNU	$^{+0.7}_{-2.0}$ SNU	
Subtotal	1.3 SNU	$^{+1.8}_{-2.6}$ SNU	1.9 SNU
Total	2.5 SNU	4.5 SNU	3.6 SNU

counter efficiencies and on the chemical yield. The systematics have been substantially reduced with respect to Gallex and to the first GNO paper [13] (it was ∼5.8%). This improvement is mainly due to the absolute calibrations of the proportional counters with ^{69}Ge activity (the contribution of this item has been reduced from 4.0% to 2.2%) and, in a smaller but appreciable extent, to the new measurement of Rn-cut inefficiency and to the neural network-based pulse shape analysis (see section 4 and Refs. [11, 12]).

The scatter of single GNO runs (see Fig. 2) is fully compatible with the Monte Carlo generated distribution in the hypothesis of a constant neutrino rate of 62.9 SNU and the usual conditions (exposure time, counting efficiency, counting time, etc.) of normal single runs.

The energy spectrum of all the events observed in the 58 GNO solar runs (see Fig. 3) is well consistent with the expectation from ^{71}Ge decay: a clear excess of events in the L- and K-peak occurring in the first $\sim 3\tau$ of ^{71}Ge can be seen.

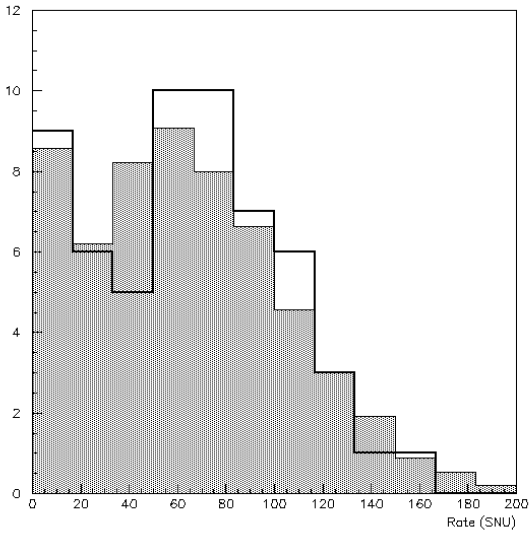

Figure 2: Monte Carlo distribution deduced from 5800 single run simulations using the actual conditions of the 58 runs in appropriate proportions (thin line). Superimposed is the histogram for the real 58 GNO single run results (thick line).

The time distribution of the candidate events in the GNO runs is also compatible with the expectation of a ^{71}Ge signal and a constant background (see Fig. 4). The experimental distribution (dots) has been superimposed with the best-fit curve obtained from the maximum likelihood analysis and the corresponding $\pm 1\sigma$ error band. The mean life of the decaying component that is deduced from all L+K data (798 candidate events surviving the pulse shape cuts) is 16.6$\pm$2.1 days, in excellent agreement with the known value for ^{71}Ge, 16.49 days.

A further test of consistency of the GNO data analysis can be performed taking into account the fraction of double-ionisation to total K candidate events: this is found to be 16.7% in the calibrations with ^{71}Ge activity and 19.2$\pm$2.3%) in the solar runs, according to the neural network algorithm [16]; the expected theoretical value is 20.9%[2].

The measured interaction rate (see Table 2) is lower than the value expected from *pp* neutrinos only, which, for a large class of solar models, is almost independent from the details of the models themselves. Therefore, as discussed in section 5, the gallium results strongly support by themselves that the solution of the solar neutrino problem must be found in the ν physics domain.

[2]This should actually be regarded as an upper limit, as the two components cannot be resolved if they are too close in time.

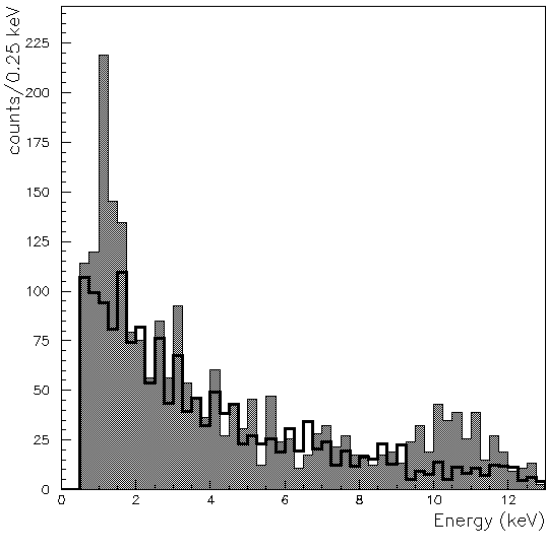

Figure 3: Energy distribution for all the events observed in the GNO solar runs SR1-SR58. The shaded histogram contains events occurred in the first 50 days ($\sim 3\tau$) of counting. The thick-line histogram includes events occurred after the first 50 days of counting (normalized).

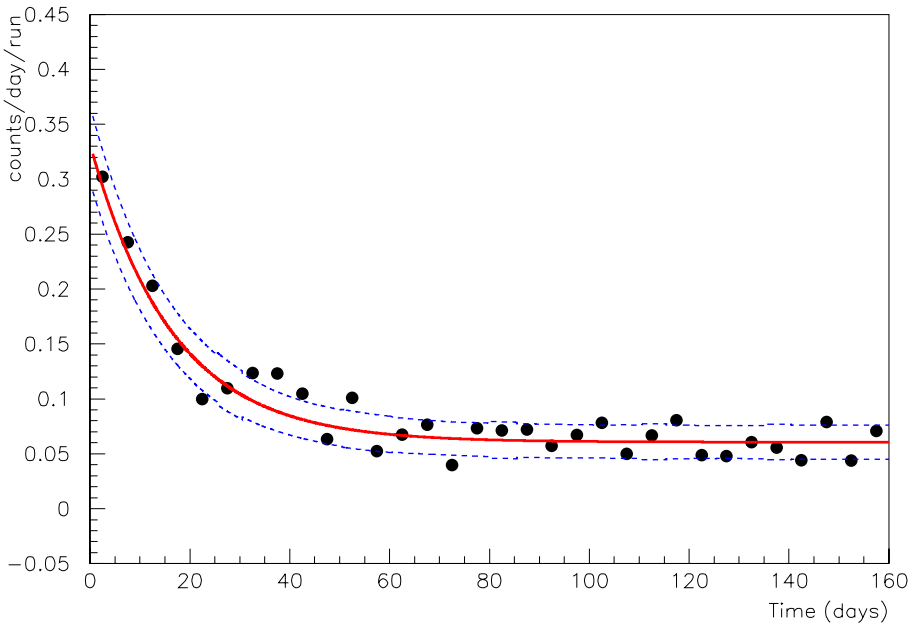

Figure 4: Counting rate of ^{71}Ge candidates vs. time.

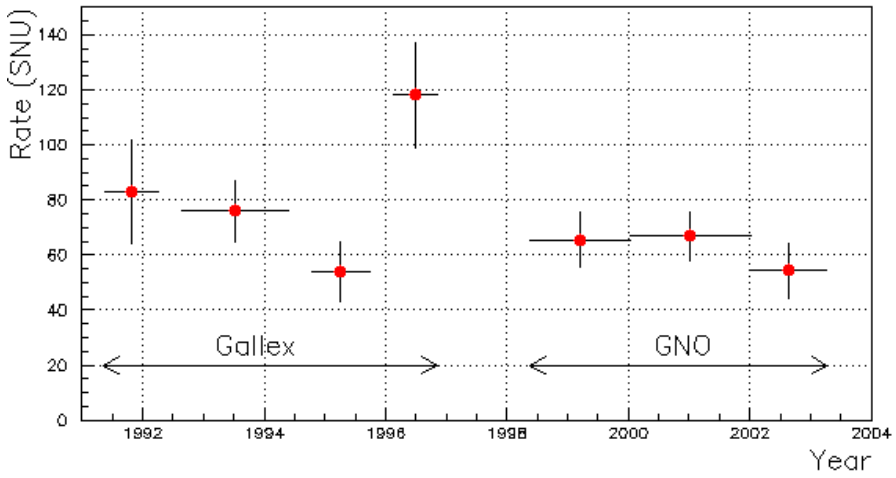

Figure 5: Gallium signal measured in the 4 data periods of Gallex and in the 3 data periods of GNO.

3.2 Time constancy and annual modulation

The consistency of GNO data with the hypothesis of a constant production rate has been verified by the application of the likelihood ratio test (see [5] for details). The resulting goodness-of-fit confidence level is 25.1%: the distribution of results of individual GNO runs hence agrees well with the hypothesis of quasi-normal fluctuations above a constant production rate. In order to verify also the consistency of joint Gallex and GNO data under the same hypothesis, we performed a χ^2 analysis taking into account the results and the errors from the 4 data periods of Gallex and the 3 data periods of GNO (see also Ref. [13]). In the assumption of a production rate that is constant over the entire data taking period (> 10 years), the χ^2 is 13.6 (6 d.o.f.), that corresponds to a goodness-of-fit p-value of 3.4% (see Fig. 5). Though the p-value is quite low, it is nevertheless higher than for Gallex alone [5] and statistically consistent with a normal distribution. The major contribution to the χ^2 ($\sim 60\%$) comes from the Gallex IV data point.
The Gallex+GNO data have been analyzed in terms of correlation with the seasonal Earth-Sun distance variation (the eccentricity of the Earth's orbit is 0.0167). The 123 solar runs have been divided in 6 about equally populated bins of similar Earth-Sun distance d. For each of them, a combined maximum likelihood analysis was performed, without applying the correction factor for the geometrical modulation $1/d^2$: results of SNU vs. $< d >$ are displayed in Fig. 6. No clear feature is apparent; the fit relative to the expectation of a solar neutrino rate constant in time (and affected only by the $1/d^2$ modulation due to the Earth-Sun distance) yields a confidence level of 69% (χ^2=3.0 with 5 d.o.f.).
The difference between winter and summer solar neutrino rate is $\Delta_{W-S} = -7.6 \pm 8.4$ SNU; the value expected from the $1/d^2$ geometrical modulation only is $\Delta_{W-S} = +2.5$ SNU.

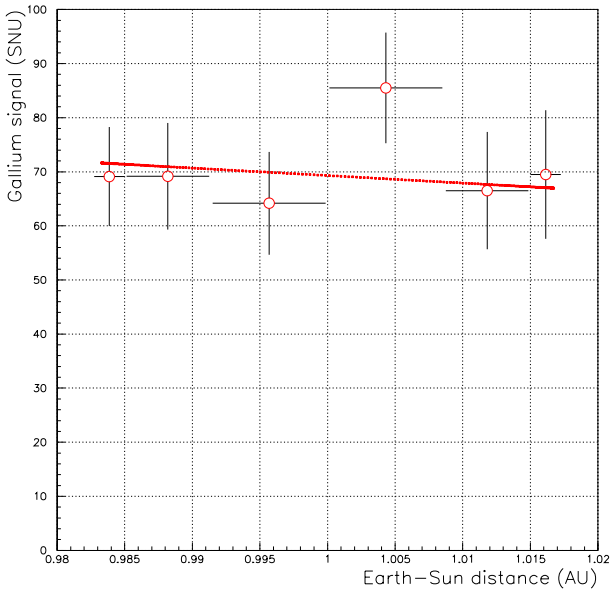

Figure 6: Gallium signal vs. heliocentric distance of the Earth. The line indicates expected flux variation for purely geometrical ($1/d^2$) reasons. The mean value for $d = 1$ is set equal to 69.3 SNU.

4 Experimental activity during 2003

4.1 Extraction system and synthesis line

During last year 2003 the following activities were performed:

- Maintenance of the GNO main building, including all the equipment and instruments used to carry out the operation for the germanium extraction.
- A new control board with a new computer and specific software for controlling and supervising the absorption plant was ordered, installed and tested. Unfortunately in April the last solar run was performed and the GNO activities were stopped, so that the new board was never used in a real run.
- Preparation and carrying out of 5 extraction runs from January 14^{th} 2003 (EX72) to April 8^{th} 2003 (EX76): 4 long exposure runs, 1 short exposure runs (no further runs were possible to carry out). Each extraction run involves a carrier addition (four different isotopes: ^{70}Ge, ^{72}Ge, ^{74}Ge and ^{76}Ge). The carrier is added to the gallium solution before each run is carried out.
- AAS analysis to determine the Ge contents in the different samples taken during each run and to control the extraction yield. A new determination of the carriers' concentration (^{70}Ge, ^{72}Ge, ^{74}Ge and ^{76}Ge) was performed using again the AAS analysis. These new values will help to correct the discrepancy among the yields calculated for each different Ge isotope. The results of these measurements were reported at the GNO meeting held in Rome last October.

- A new collaboration with the ITU (Institute for Transuranium Elements) of Karlsruhe for the isotopic measurement of the germanium mirrors was started. Extraction runs E24, E25, E26, E27 were successfully measured and the result were showed at the GNO meeting in Rome.

- A major test of the mechanical stability and tightness of the seven gallium emergency tanks was performed in October. The tanks were filled with water and inspected to check whether water came out through some possible cracks. The test showed that all the tanks were tight and this result was reported at the October GNO meeting in Rome.

4.2 Reduction of the systematic error

One of the most important goals for GNO is to substantially reduce the systematic error that affected the final Gallex result; in the last years we faced this problem starting several experimental activities to decrease the systematic error and to consequently improve the quality of the data.
The major component ($\sim$4%) of the systematic error in Gallex came from the actual knowledge of the absolute counting efficiency of counters, which slightly varies from one to another as they are piece of handcraft. We started in 2001 a program to absolute measure the counting efficiency of each counter with 1% accuracy by filling them with ^{69}Ge activity [12]. In former time the counting efficiency was determined for a few counters filled with a calibrated ^{71}Ge activity and then extrapolated to the other counters of the same type. At present, we have 13 absolute calibrated counters, that counted 50 of the 58 GNO solar runs. The measured efficiencies have been taken into account for the data analysis: the average shift between these values and the old determination (from extrapolation) is Δ=-1.7%. Thanks to these measurement, the component of the systematic error has been lowered from the former 4% to the present 2.3%.
A Radon test was performed (using a modified counter containing a Ra source) with the aim of improving the characterization of Radon events in the GNO proportional counters. The measurement was carried on from May 1999 to March 2001 (1.8 years counting time). After this long measurement, the emanation valve was closed and the intrinsic background of the counter was measured for 2.0 years. Using these data, we re-evaluated in 2003 the inefficiency of the Rn cut, that is (0.0$\pm$4.4)%, in agreement with the previous Gallex estimate (9$\pm$5)%.
In Table 3 the components of the systematic error both for Gallex and GNO are summarized and compared: as a result, the overall systematic error decreased from 4.5 to 2.5 SNU.

4.3 The z-scanning system

During 2003 it has been realized a small set-up devoted to the systematic measurements of the detection efficiencies of the miniaturized proportional counters used in the GNO experiment as a function of the coordinate along the anode wire. This can assure a better

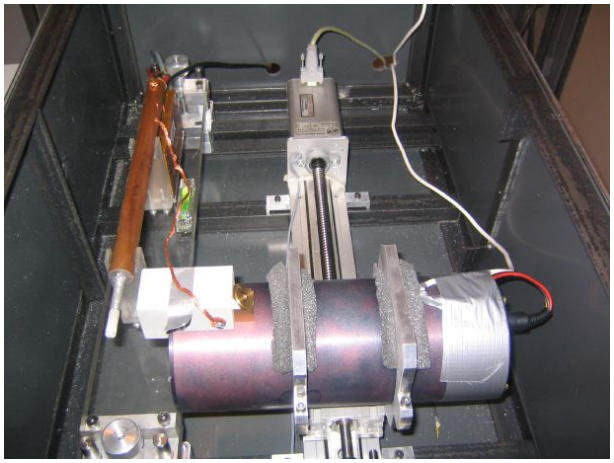

Figure 7: Photo of the z-scanning set-up. All the devices of the set-up are shown: the miniaturized proportional counter, the X-ray tube and the motor step.

knowledge of these quantities, previously extrapolated for all the counters from a few determinations. In particular, an automatic system allows to measure the response of the counter longitudinally at given steps with a collimated X-ray source of fixed intensity and to collect at each position the pulses profiles and the energy distribution measured by the exposed counter. The pulses profiles are recorded by a TEKTRONIX VXI TVS645A waveform analyzer, with 5 Gsample/s and band-width 1 GHz, interfaced with a Digital Alpha Workstation by a PCI-GPIB card. The energy spectrum is simultaneously collected by a devoted multi-channel analyser. In the Fig. 7 a picture of the z-scanning system is shown. In particular, it can be seen the X-ray tube mounted on a motor step – that allows to move the source in the z direction with a precision of few microns – and the proportional counter settled in a plexiglas support. All these devices are placed inside an iron box. The first measurements started on January 2004. An example of the collected energy spectrum obtained positioning the collimated X-ray beam in the middle and at one end of the counter are reported in Fig. 8. The variation of the detection efficiency can be estimated by considering the different position of the 5 keV peak. In fig. 9 an example of pulse profile recorded with the Waveform Analyzer is depicted. Systematic measurements with various miniaturized proportional counters will be carried out in the first part of 2004.

4.4 Common data analysis with the SAGE Collaboration

In the past years, two different radiochemical experiments could detect low-energy solar neutrinos via the β-inverse reaction ^{71}Ga (ν_e,e$^-$)^{71}Ge on ^{71}Ga : GNO and SAGE. The SAGE expreriment is run by a Russian-American Collaboration at the Baksan Neutrino Observatory, in Russia. The ^{71}Ga target used in SAGE is consituted by $\sim$50 tons of metallic gallium. The extraction procedure is different than for GNO, because of the different chemical form of the gallium target, but all the successive phases (concentration, synthesis and counting) are qualitatively similar to the corresponding GNO ones. The

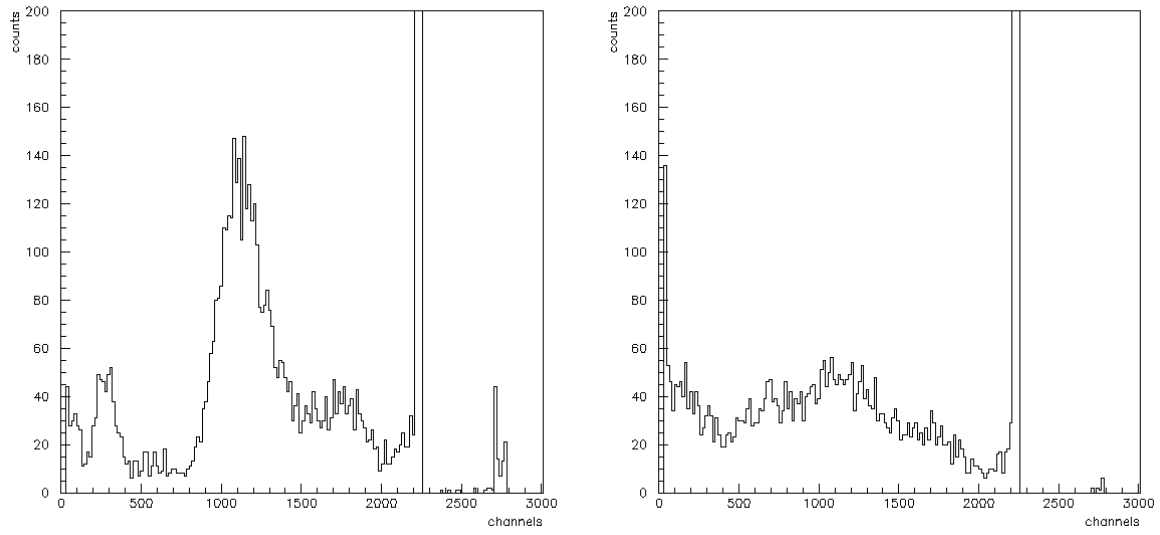

Figure 8: Energy spectra collected by irradiating a proportional counter with the collimated X-ray beam placed in the middle of the counter (left) and at one end of it (right).

SAGE measurements started in January 1990 and the solar neutrino rate is $69.1^{+5.7}_{-5.4}$ SNU (1 σ) [18], very close to the value measured by Gallex/GNO, 69.3±4.1±3.6 SNU [15].
In 2003 we had intensive contacts with the SAGE Collaboration ongoing in order to join the efforts, with the intention to produce data superior to those obtained in the two separate experiments.
The present stage of the collaboration is an extensive comparison of the procedures and of the analysis methods used in the two experiments, in order to study the feasibility of a combined maximum likelihood analysis of all SAGE and Gallex/GNO data. Though this analysis would not add much information to the measurement of the solar neutrino interaction rate (with respect to the weighted mean of the two data), it could be very significant in the investigation for possible time modulations of the signal in gallium. In 2003 a delegation of the SAGE Collaboration spent one week at Gran Sasso in order to perform a joint work to study the feasibility of this kind of common analysis.

5 The role of GALLEX and GNO in the solar neutrino research

The results from GALLEX followed by GNO have played a central role both for neutrino physics and astrophysics. GALLEX was able to demonstrate for the first time that the solar neutrino deficit observed by the Chlorine and Superkamiokande experiments for ^{8}B solar neutrinos, is effective also for the low energy *pp* and ^{7}Be neutrinos [5]. The combined results of the Chlorine experiment, the water Cerenkov experiment Kamiokande and the two Gallium experiments (GALLEX and SAGE) were strongly suggesting neutrino

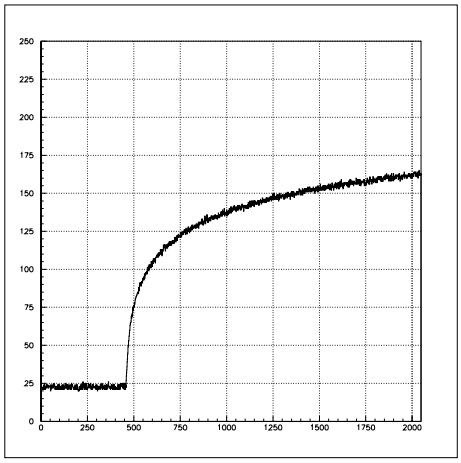

Figure 9: Example of a pulse profile recorded with the TEKTRONIX waveform analyzer.

flavour oscillations already in the middle nineties. The oscillation scenario as a solution of the solar neutrino deficit has been further supported by Superkamiokande [21], and by the increasing precision and the calibrations of the Gallium experiments. Recently the results of SNO [22] and Kamland [23] have directly proven that neutrino oscillation is the dominant effect which explains the observed solar neutrino energy spectrum:

- SNO demonstrated that the missing ^{8}B ν with electronic component not observed by Kamiokande and Homestake is actually converted into a non-electron active component: the sum of the electron and non-elecxtron flavour components is perfectly in agreement with the predictions of the SSM.
- Kamland was able to detect for the first time neutrino oscillations with reactors antineutrinos.

The best fit oscillation parameters, able to explain both the Kamland result and all solar neutrino experimental results are:

$$\theta = 32.5 \pm 2.3, \Delta m^2 = 7.1^{+1.2}_{-0.6} \cdot 10^5 \mathrm{eV}^2. \quad (1)$$

It is important to notice that the oscillation parameters are quite well determined by SNO+Kamland alone, almost independently from any solar model constraint. In this context experimental results on detection sub-MeV neutrinos are a unique tools to probe solar physics. In particular the radiochemical Gallium detectors are the only experiments presently sensitive to the basic *pp* component of the solar neutrino flux. The Ga radiochemical technique will remain for the next years probably the only sensitive to the *pp* neutrino component, while we will probably have new real time information on the ^{7}Be neutrinos from experiments such as Borexino and Kamland.
The solar neutrino interaction rate R^{Ga} on ^{71}Ga can be expressed as follows:

$$R^{Ga} = \sum_i \int \frac{d\phi_i}{dE}(E) \cdot \sigma(E) \cdot P^{ee}(E) dE \quad (2)$$

where the sum i is extended over the different neutrino sources (*pp*, *pep*, ^{7}Be, CNO, ^{8}B), $\frac{d\phi_i}{dE}$(E) is the differential solar neutrino flux in energy at the Earth surface, $\sigma(E)$ is the electron neutrino capture cross section on ^{71}Ga, and $P^{ee}(E)$ is the electron neutrino survival probability, taking into account that electron neutrinos are partly converted into other flavours before reaching the Earth. The probablity $P^{ee}(E)$ depends on the mixing paramenters Δm^2 and $\tan^2(2\theta)$.
We can rewrite (2) as:

$$R^{Ga} = \sum_i \Phi_i \cdot \overline{\sigma}_i \cdot \overline{P}_i. \tag{3}$$

Here Φ_i is the integral flux of the neutrinos of type i, $\overline{\sigma}_i$ is the capture cross section averaged over the neutrino energy spectrum:

$$\overline{\sigma}_i = \frac{1}{\Phi_i} \int \frac{d\phi_i}{dE}(E) \cdot \sigma_i(E) dE \tag{4}$$

and P_i is the average probability that a neutrino of type i is captured by gallium taking into account its oscillation probability:

$$\overline{P}_i = \frac{\int \frac{d\phi_i}{dE}(E) \cdot \sigma(E) \cdot P_{ee}(E) dE}{\int \frac{d\phi_i}{dE}(E) \cdot \sigma(E) dE} \tag{5}$$

In Table 4 we give the result of the numerical calculation of the coefficients $\overline{P}_i$ for the LMA best fit oscillation parameters $\theta = 32.5 \pm 2.3, \Delta m^2 = 7.1^{+1.2}_{-0.6} \cdot 10^5 \mathrm{eV}^2$ together with the terms Φ_i and $\overline{\sigma}_i$ for the different neutrino types, assuming the solar ν fluxes from the recently updated calculations in [2]. The Ga rate is in perfect agreement with the present SSM+oscillation scenario.
Solar neutrino fluxes are constrained by the so called "Luminosity constraint"

$$L_{sun} = \sum_i \Phi_i \cdot \alpha_i, \tag{6}$$

where $L_{sun} = 8.53 \cdot 10^{11}$ MeV cm^{-2}s^{-1} is the solar luminosity, and α_i are the energy releases in photons per emitted neutrino. The luminosity constraint links the electromagnetic solar luminosity with the solar neutrino fluxes, assuming that nuclear fusion reactions are the only energy production mechanism inside the Sun. Apart from this assumption, the luminosity constraint is solar model independent. A very important quantity for the energy production mechanism inside the sun is the luminosity fraction of the CNO cycle:

$$\frac{L_{CNO}}{L_{sun}} = \frac{\Phi_O \cdot \alpha_O + \Phi_N \cdot \alpha_N}{\sum_i \Phi_i \cdot \alpha_i}. \tag{7}$$

Taking into account Eqs. (2) and (6) it is evident that we can estimate at the same time Φ_{pp} and Φ_{CNO} once we know the ^{8}B, ^{7}Be, and *pep* fluxes, the neutrino capture cross section on ^{71}Ga , and the electron neutrino survival probability as a function of energy. In particular:

- the ^{8}B electron neutrino flux has been measured with a precision of the order of 10% by SNO [22];

- the ^{7}Be neutrino flux is not directly measured up to now. We assume here the SSM value [2] with an uncertainty of 10%: this flux will hopefully be replaced in the next years a by measured number, provided Borexino or Kamland will come into operation;

- the neutrino capture cross section on ^{71}Ga is theoretically calculated. Ground state to ground state transitions are calculated from the halflife of the inverse reaction ^{71}Ge(e,ν_e)^{71}Ga with a rather small uncertainty. Transitions to excited states are very poorly known, and have to be computed indirectly from evaluation of nuclear matrix elements in (p, n) reactions of ^{71}Ga . Uncertainties can be very large, of the order of 50 %, but fortunately their contribution to the total neutrino capture rate is rather small. For details on calculation of the ν-Ga cross section see [20]. We notice that the overall cross section at the ^{7}Be ν energy was experimentally measured with the ^{51}Cr source experiments with a precision of about 8% [19];

- the electron neutrino survival probability as a function of energy can be calculated from the oscillation parameters presently determined by SNO and Kamland [23].

With the assumpion above and taking into account the uncertainties summarized in table 5 we can extract from the Gallium capture rate measured by GALLEX/GNO the following constraints:

$$\Phi_{pp} = 59.9(1 \pm 0.02) \cdot 10^9 \text{ cm}^{-2}\text{s}^{-1}$$

$$\Phi_{CNO} \leq 9 \cdot 10^9 \text{ cm}^{-2}\text{s}^{-1} \ (3\sigma)$$

or, in terms of CNO fractional luminosity:

$$\frac{L_{CNO}}{L_{sun}} \leq 7\% \ (3\sigma),$$

in agreement with the results obtained in [24] with a multi-parameter global fit. The result for the CNO luminosity taking into account the gallium rate measured by GALLEX and GNO is graphically shown in Fig. 10.
It has to be stressed again that in order to obtain the results above we assumed that the ^{7}Be neutrino flux is known with a 10% uncertainty. Presently this flux is not experimentally measured but calculated by SSM, and the limits above can be considered as an important self-consistency test of the SSM, the oscillation scenario, and the gallium data. If in the future, when a direct determination of the ^{7}Be neutrino flux will become available, the Ga rate will become a direct experimental determination of the *pp* (and CNO) luminosity in neutrinos.

6 Status of the experiment

In August 2002 an accident occurred in the hall C, resulting in the dispersion in the ambient of a limited quantity of pseudocumene. This accident started a series of events

Table 4: Solar neutrino fluxes, average cross sections on ^{71}Ga, electron neutrino average survival probabilities for best fit oscillation parameters, and corresponding induced gallium rate. We consider here the solar standard model in [2] including the recent results on the p,^{14}N from LUNA [25].

ν type	Flux Φ_i (10^9 cm^{-2} s^{-1})	Av. Cross sect. $\overline{\sigma}_i$ (10^{-46}cm^2)	Surv.prob. $\overline{P}_i$	Rate r_i (SNU)	α_i (MeV)
pp	60.33	11.7	0.578	40.8	13.10
^{7}Be	4.53	71.7	0.557	18.1	12.60
^{15}O	0.226	115	0.541	1.4	21.57
^{13}N	0.305	60.2	0.557	1.0	3.46
^{8}B	0.00521	24500	0.324	4.1	6.63
pep	0.143	15.7	0.531	1.5	11.92
Tot				67.0	

Table 5: Uncertainties of the parameters used for the evaluation of the *pp* and CNO fluxes from Eqs. (2) and (6).

Parameter	Input	Parameter Uncertainty	Uncertainty on Ga rate (SNU)
Mixing angle θ	SNO+Kamland	2.5 deg	2.9
^{7}Be flux	SSM (Borexino)	10 %	1.9
Cross section GS-GS	Calculation	2.3 %	1.5
Cross section GS-ES	Calculation	50 %	1.6
^{8}B flux	SNO	9 %	0.4
pep flux	SSM	1.5%	0.1

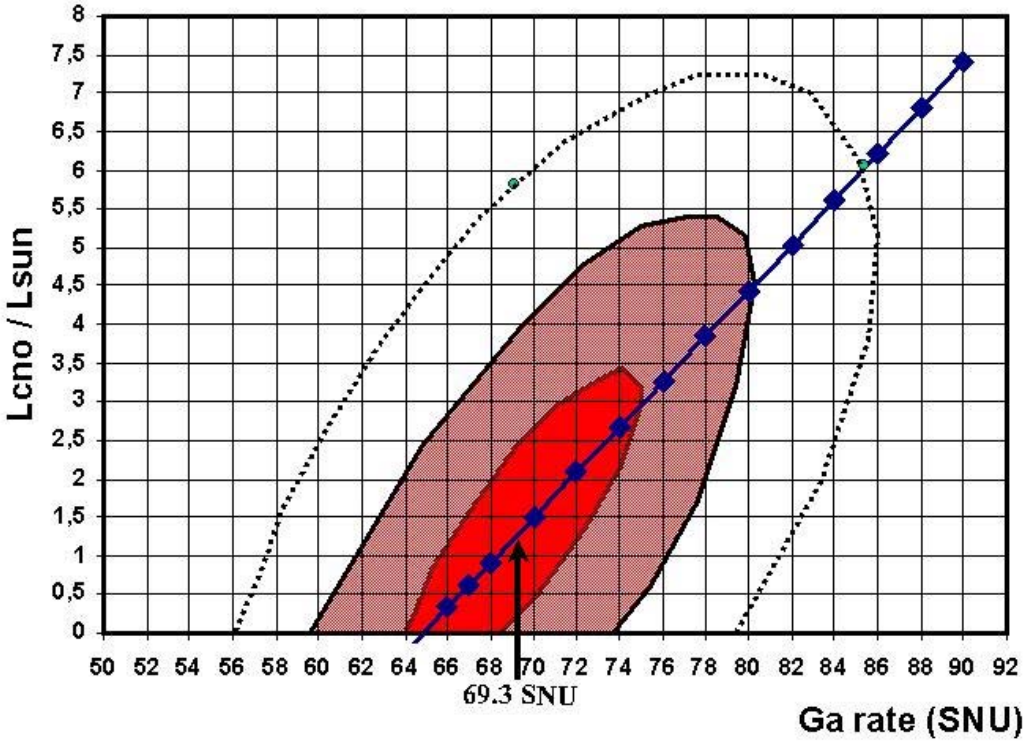

Figure 10: Scatter plot of the fraction CNO solar luminosity (in percent) versus gallium rate. The CNO luminosity can be extracted from the Ga rate using Eqs. (2) and (6) with the assumptions discussed in the text for the ^{7}Be, ^{8}B, and *pep* fluxes, the oscillation parameters and the ν-Ga cross section. The contours represent respectively the 1σ, 2σ, and 3σ limits allowed by the GALLEX/GNO experimental result on the gallium rate and the uncertainties quoted in Table 5 for the other parameters. The luminosity constraint as expressed in (6) is represented graphycally by the blue line.

that affected in a negative way the life of the Laboratory. In May 2003, the INFN decided to suspend all the activities dealing with the manipulation of any kind of liquid; as a consequence extractions and synthesis of GNO were stopped. Slightly later, the Government declared the "state of emergency" for the entire Gran Sasso system (laboratory, highway, pubblic water supply system); a Commissioner was appointed to define a program of improvements on the laboratory structure. In conclusion, taking also into account the excellent results achieved by GALLEX first and GNO later with more than 10 years of solar neutrino observations, the GNO collaboration was invited to conclude the experiment. The future activities in the field (cooperation with SAGE, use of the counting facility, fate of the gallium) are presently under discussion among the members of the Collaboration. A defined program will be formulated in the first months of the incoming year.

7 List of Publications (2003)

1. GNO collaboration, "GNO progress report for 2002", LNGS annual Report 2002, LNGS/EXP-07/03 (2003);

2. L. Pandola *et al.*, *Neural network analysis for proportional counters events*, accepted by NIM A for publication; preprint LNGS/EXP-06/03;

3. L. Pandola, *The GNO experiment*, to appear in the Proceedings of the XII International School "Particle and Cosmology", April 2003, Baksan Valley, Russian Federation;

4. N. Ferrari, *Experiments for the detection of solar neutrinos*, to appear in the Proceedings of the Workshop "XV Incontri di Fisica delle Alte Energie", April 2003, Lecce, Italy;

5. J.-C. Lanfranchi, T. Lachenmaier, W. Potzel and F. von Feilitzsch, *Development of a cryogenic detection concept for GNO*, in the Proceedings of the XX International Workshop on Low Temperature Detectors, accepted by NIM A for publication;

6. E. Bellotti, *The Gallium Neutrino Observatory (GNO)*, to appear in the Proceedings of the VIII International Workshop on Topics in Astroparticle and Underground Physics (TAUP 2003), September 2003, Seattle, United States

7. E. Bellotti, *The Gallium Observatory*, to appear in the Proceedings of the II International Workshop on Neutrino Oscillation in Venice (NO-VE), December 2003, Venice, Italy.

8 List of Conference Presentations (2003)

1. F. Kaether, W. Hampel, F.X. Hartmann, D. Motta for the GNO Collaboration, *Absolute calibration of proportional counters for the GNO solar neutrino experi-*

ment, Spring Meeting of the German Physical Society (DPG), March 2003, Aachen, Germany;

2. E. Bellotti, *GNO, Gallium Neutrino Observatory*, IV International Workshop on Low Energy Solar Neutrinos (LowNu03), June 2003, Paris, France;

3. L. Pandola, *The GNO experiment*, XII International School "Particle and Cosmology", April 2003, Baksan Valley, Russian Federation;

4. N. Ferrari, *Experiments for the detection of solar neutrinos*, Workshop "XV Incontri di Fisica delle Alte Energie", April 2003, Lecce, Italy

5. E. Bellotti, *The Gallium Neutrino Observatory (GNO)*, VIII International Workshop on Topics in Astroparticle and Underground Physics (TAUP 2003), September 2003, Seattle, United States

6. R. Bernabei, *GALLEX-GNO experiments: status and reports*, II International Summer Student School on Neutrino Physics in memory of Bruno Pontecorvo, September 2003, Alushta, Ucraina

7. E. Bellotti, *The Gallium Observatory*, II International Workshop on Neutrino Oscillation in Venice (NO-VE), December 2003, Venice, Italy

9 Theses (2003)

1. F. Kaether, *Eichung der absoluten Nachweiswahrscheinlichkeiten von Zaehlrohren des Sonnenneutrino-Experiments GNO*, Diploma Thesis, University of Heidelberg, February 2003.

References

[1] J.N. Bahcall, Phys. Rept. 333 (2000) 47-62; S. Turck-Chiéze et al, Nucl. Phys. (Proc. Suppl.) 87 (2000) 162-171; V. Castellani et al., Nucl. Phys. (Proc. Suppl.) 70 (1999) 301-314.

[2] S. Degl'Innocenti et al., astro-ph/0312559 (2003).

[3] E.Henrich, K.H.Ebert, Angew. Chemie Int. Ed. (Engl.) 31 (1992) 1283; E.Henrich et al., "GALLEX, a challenge for chemistry", Proc. IV Int'l. Solar Neutrino Conf., ed. W.Hampel, MPI Kernph., Heidelberg (1997) 151-162.

[4] R. Wink et al. Nucl. Inst. and Meth. A329 (1993) 541.

[5] GALLEX collaboration, Phys.Lett. B285 (1992) 376; Phys.Lett. B314 (1993) 445; Phys.Lett. B327 (1994) 377; Phys.Lett. B342 (1995) 440; Phys.Lett. B357 (1995) 237; Phys.Lett. B388 (1996) 384, Phys.Lett. B447 (1999) 127.

[6] T.Kirsten, Rev.Mod.Phys., 71 (1999) 1213-1232.

[7] E.Bellotti et al., GNO collaboration, LNGS report INFN/AE-96-27.

[8] GNO collaboration, LNGS annual report 1998, pag. 55-69.

[9] GNO collaboration, LNGS annual report 1999, pag. 57-68.

[10] GNO collaboration, LNGS annual report 2000, pag. 57-68.

[11] GNO collaboration, LNGS annual report 2001, pag. 79-94.

[12] GNO collaboration, LNGS annual report 2002, pag. 57-76.

[13] GNO collaboration, M. Altmann *et al.*, "GNO solar neutrino observations: results for GNO I", Phys.Lett.B 490(2000), 16;

[14] T. Kirsten for the GNO collaboration, "Progress in GNO", Talk at XXth International Conference on Neutrino Physics and Astrophysics, Munich (2002), Nucl.Phys.B (Proc. Suppl.) 118 (2003), 33;

[15] E. Bellotti, "The Gallium Neutrino Observatory (GNO)", Talk at VIII International Workshop on Topics in Astroparticle and Underground Physics (TAUP 2003), Seattle (2003), to appear in the Proceedings;

[16] L. Pandola *at al.*, "Neural network analysis for proportional counters events", accepted by NIM A; preprint LNGS/EXP-06/03;

[17] INTAS 06-0145 Feasibility of re-activation of the GALLEX Cr source at Russian reactors for the use in the BOREXINO and GNO Solar neutrino experiments at Gran Sasso - Final Report - Proj. coordinator T. Kirsten.

[18] V.N. Gavrin for the SAGE Collaboration, "SAGE and SAGE-Gallex-GNO", Talk at IV International Workshop on Low Energy Solar Neutrinos (LowNu 03), Paris (2003) and V.N. Gavrin for the SAGE Collaboration, "Results from the Russian American Gallium Experiment (SAGE)", Talk at VIII International Workshop on Topics in Astroparticle and Underground Physics (TAUP 2003), Seattle (2003), to appear in the Proceedings;

[19] W.Hampel et al., GALLEX coll., Phys. Lett. B420 (1998) 114.

[20] J.N.Bahcall, Phys.Rev.C56 (1997) 3391.

[21] SuperKamiokande Collaboration, Phys.Rev.Lett. 86 (2001) 4651.

[22] SNO collaboration, Phys.Rev.Lett. 87 (2001) 071301; Phys.Rev.Lett. 89 (2002) 011302; nucl-ex/0309404 v1 submitted to PRL (2003)

[23] KamLAND Collaboration, K.Eguchi et al., submitted to PRL (2002)

[24] J.N. Bahcall, C. Pena-Garay, JHEP 0311 (2003) 004

[25] LUNA collaboration, nucl-ex/0312015.

HDMS. Dark Matter Search

H.V. Klapdor-Kleingrothaus*[a], C. Tomei[a,c], I.V. Krivosheina[a,b], O. Chkvoretz[a], H. Strecker[a]

[a] Max-Planck Institut für Kernphysik, Heidelberg, Germany
[b] Institute of Radiophysical Research, Nishnij Novgorod, Russia
[c] University of L'Aquila, Italy
* Spokesman of the Collaboration; E-mail: klapdor@gustav.mpi-hd.mpg, Home-page: http://www.mpi-hd.mpg.de.non_acc/

Abstract

We present the latest results from the HDMS (Heidelberg Dark Matter Search) detector at LNGS, obtained analysing data collected from February 2001 to July 2003 (423.18 d, corresponding to 85.5 kg d) and a smaller set of data collected using, for the same detector, a different electronics and acquisition system which allowed us to obtain a threshold of 2.7 keV. We present our limits for WIMP-nucleon coupling both for the spin-independent and for the spin-dependent case, improving the present best limits on the WIMP-neutron spin-dependent cross section for low WIMP masses.

Introduction

There is strong observational and theoretical evidence for the existence of nonbaryonic dark matter. Many candidates for this kind of Dark Matter have been proposed: among the most favoured ones there are slow thermal relics born in an early phase of the Universe, stable or very long lived. These weakly interacting, massive (1 GeV - 1 TeV) particles (WIMPs) arise independently from cosmological considerations in supersymmetric models as neutralinos - the lightest supersymmetric particles. Direct detection of neutralinos can occur in very low background experiments, where the elastic

neutralino scattering off target nuclei is observed. First evidence for cold dark matter has been observed by DAMA [8].

The HDMS (Heidelberg Dark Matter Search) project operates two ionization HPGe detectors at the Gran Sasso National Laboratory (LNGS). The unique configuration of the two crystals is shown in Fig. 1: a small p-type enriched ^{73}Ge crystal (the measured level of enrichment is 86%) is surrounded by a well-type natural Ge crystal. Both the detectors are mounted in the same copper cryostat. The coaxial configuration of the two detectors was especially designed to reduce the background of the inner detector by means of two effects:

- the shielding provided by the outer crystal (germanium is one of the radio-purest known materials)
- the anti-coincidence between the two detectors. Since WIMP interactions will take place in only one of the two detectors, events occurring in both inner and outer crystals (like multiple scattered photons) can be rejected.

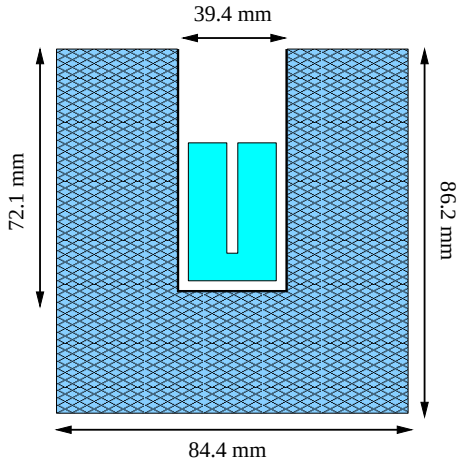

Figure 1: Schematic view of the HDMS detector configuration. The inner detector is made from ^{73}Ge, the outer from natural germanium.

The final setup of HDMS was installed at the LNGS during August 2000, after a first prototype phase [1, 2] which took data over a period of about

Property	Inner Detector	Outer Detector
Crystal Type	p–type	n–type
Mass [g]	200	2111
Active Volume [cc]	37	383
Crystal diameter [mm]	35.2	84.4
Crystal length [mm]	40.3	86.2
Operation Bias	+2500	-1500
Optimum pulse shaping [μs]	4	2–3
FWHM (1332 keV) [keV] (ORTEC)	1.92	4.41
FWHM (1332 keV) [keV] (Heidelberg)	1.87	4.45
FWHM (351 keV) [keV] (LNGS)(*)	1.4 $\pm$ 0.1	3.6 $\pm$ 0.01
Zero-energy resolution [keV] (**)	0.90 $\pm$ 0.01	3.91 $\pm$ 0.04
Threshold (Heidelberg) [keV]	2.5	7.5
Threshold (LNGS) [keV]	4.0	10
Cross-talk parameters ($^+$)	0.104 (6)	0.0059 (1)

Table 1: Detector properties for the small inner Ge-detector and the active veto-shield, the outer well-type Ge-detector. (*) Calculated from the 351.9 keV ^{214}Bi line of the background spectrum. (**) Calculated after the cross-talk correction (see [1]). ($^+$) From a ^{228}Th measurement.

15 months with a inner detector made of natural germanium. The inner detector was then replaced with an enriched ^{73}Ge crystal of the same mass and dimensions.
Some technical properties of the HDMS detectors are listed in Table 1; further details on the setup and previous performances of HDMS have been published in [3].

In Fig. 2 (right) is shown the anti-coincidence spectrum of the HDMS detector corresponding to the full set of data from February 2001 to July 2003 (lifetime = 85.5 kg d). This spectrum has been obtained applying a off-line anti-coincidence between the two HDMS detectors, that is all events having an energy deposition in both detectors are rejected. An example of the off-line anti-coincidence and its reduction power is given in the same Fig. 2 (left).

We also show, as a comparison, the recoil spectrum measured during the first phase of the HDMS experiment [1] (see Fig. 3, left), with the inner detector made of natural germanium and a new spectrum of the HDMS detector corresponding to a measuring time of 14.8 kg d (right). This new

measurement has been performed with a different electronics and acquisition system, which allows to apply an on-line rejection of coincidence events.

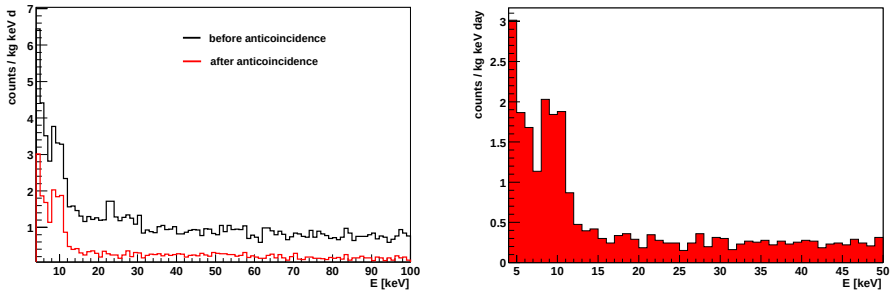

Figure 2: Left: Background spectrum of the HDMS detector corresponding to the measuring period from February 2001 to July 2003 (lifetime = 85.5 kg d) before and after the anti-coincidence cut is applied. Right: anticoincidence spectrum of the HDMS detector corresponding to the full set of data (lifetime = 85.5 kg d).

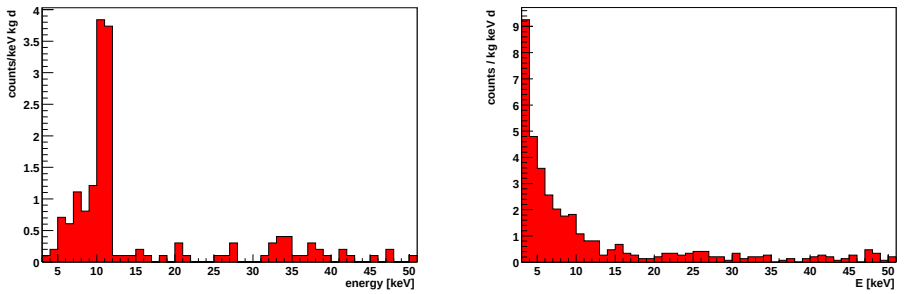

Figure 3: Left: Spectrum of the HDMS detector in the test-phase setup (inner detector made of natural germanium) corresponding to an exposure of 9.9 kg d. Right: spectrum of the final HDMS detector (with enriched ^{73}Ge) corresponding to a measuring time of 14.8 kg d, with a different electronics and acquisition system (see text).

1 Dark Matter Limits

The HDMS detector can provide constraints on WIMP-nucleon coupling in the usual form of exclusion plots in the plane (σ_p, m_W). Moreover, thanks to the enrichment in ^{73}Ge, which is the only naturally occurring germanium isotope with spin different from zero, these constraints can be calculated for both spin-independent and spin-dependent WIMP-nucleon coupling. The procedure to calculate the WIMP parameters (mass and cross section) is the same for the two cases but they are treated separately, that is we consider either SI-coupling only, or SD-coupling only.

The starting point for the program is the anti-coincidence spectrum, a list of detector parameters and a list of astrophysical parameters concerning the WIMP velocity distribution and the WIMP density in the Galaxy (see Table 2). The program performs a maximum-likelihood comparison of the experimental spectrum with the theoretical spectrum. Extracting those limits requires also some assumptions on the model framework and on several astrophysical quantities. We assumed, as usual, an isothermal WIMP-halo model with a truncated Maxwelllian WIMP-velocity distribution. The values of the astrophysical parameters used in this work are listed in Table 2.

Parameter	Value
rms velocity	270 km/s
escape velocity	600 km/s
earth velocity	232 km/s
WIMP local halo density	0.3 GeV/cm^3

Table 2: Values of the astrophysical quantities used to extract limits on WIMP-nucleon coupling.

We have analysed 3 different data-sets:

- data collected in the HDMS prototype phase (200 g natural Ge crystal, see spectrum in Fig. 3, left) evaluated in the framework of SI coupling only (HDMS natGe-SI),
- complete HDMS data-set (200 g enriched ^{73}Ge crystal, see spectrum in Fig. 2, right) evaluated considering first only SI coupling (HDMS ^{73}Ge-SI) and then only SD coupling (HDMS ^{73}Ge-SD),

- data from the latest HDMS run with the new electronics (see spectrum in Fig. 3, right), evaluated again considering first only SI coupling (HDMS new ^{73}Ge-SI) and then only SD coupling (HDMS new ^{73}Ge-SD).

The resulting exclusion plots for the spin-independent WIMP-proton cross-section are shown in Fig. 4.

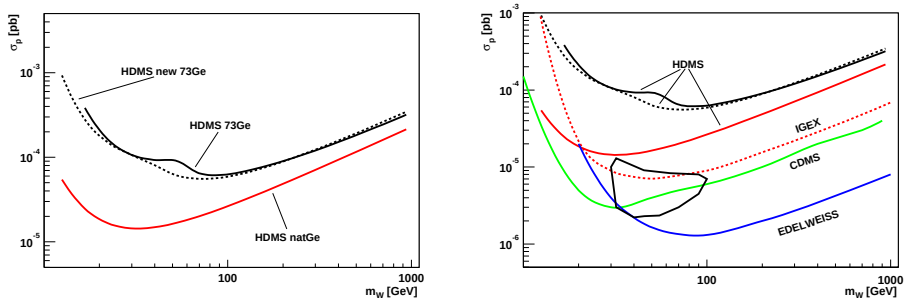

Figure 4: Limits on SI WIMP-proton cross section from the HDMS experiment. Left: limits from the HDMS experiment for two different sets of data (see text). Right: comparison with the results from other experiments. The closed contour corresponds to the allowed region at $3\,\sigma$ from the DAMA1-4 annual modulation data [7] analysed in the framework of SI WIMP-proton coupling.

The limit set by the first phase of the HDMS setup (natural Ge) is the most stringent. This is because in this first phase a lower threshold has been reached (2 keV instead of the 4 keV of the second phase) and moreover the background index in the low-energy region is lower (despite the presence of the X-ray peaks from ^{68}Ge). As a comparison, we show our results together with the results on spin-independent WIMP-nucleon coupling from IGEX [6], CDMS [5], EDELWEISS [4] and DAMA [7].

While in the spin-independent case the conversion from σ_{Ge} to σ_p is straightforward, in the spin-dependent case we have to deal with the problem of the WIMP-type dependence of the cross-section (see [9, 10]). However, with the simplifying assumption that the nuclear spin is carried mostly by protons (neutrons), the WIMP-dependence cancels out and we can obtain WIMP-independent SD limits for the WIMP-proton (WIMP-neutron) coupling. Since ^{73}Ge is a odd-N nucleus (J=9/2) we can obtain WIMP-type

independent limits for the WIMP-neutron SD cross section in the following way (see [9]):

$$\sigma_n = \frac{3}{4}\,\sigma_A\,\frac{\mu_n^2}{\mu_A^2}\,\frac{1}{\langle S_n\rangle^2}\,\frac{J}{J+1} \tag{1}$$

The values of $\langle S_n\rangle$ and $\langle S_p\rangle$ are provided by nuclear model calculations. In Fig. 5 we plot the exclusion curve for $\sigma_n^{\rm lim}$ obtained from the HDMS data, the two limits corresponding to the original setup and the new electronic setup described in this work. To draw the exclusion plots we assumed the most recent values of $\langle S_n\rangle = 0.378$ and $\langle S_p\rangle = 0.030$, as in ref. [11]. We plot as comparison the current best limit on SD WIMP-nucleon cross section coming from an odd-neutron nucleus (^{129}Xe), provided by the DAMA Xenon experiment [12]. Our results are already competitive with the DAMA results, improving the limit in the region of low WIMP masses.

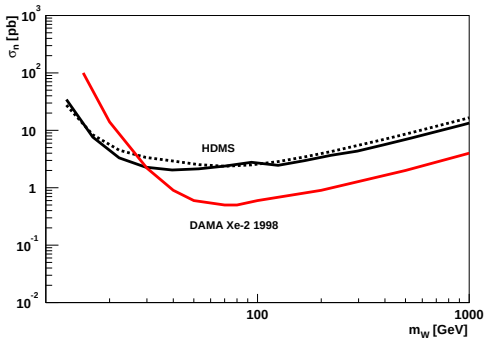

Figure 5: Experimental limits on WIMP-neutron SD coupling from the HDMS experiment. The two HDMS exclusion plots correspond to the original setup (solid) and the new electronic setup (dashed) described in this work. The result of the DAMA Xenon experiment [12] is shown as comparison.

2 Conclusions

The HDMS (Heidelberg Dark Matter Search) experiment is operating at the LNGS since August 2000, with 200 g of enriched ^{73}Ge as a WIMP detector. ^{73}Ge is the only naturally occurring germanium isotope with non-zero

spin and this allows us to be sensitive to both spin-independent and spin-dependent WIMP-nucleus interactions.

In this work we presented the latest HDMS results, arising from the analysis of the data collected from February 2001 to July 2003 (423.18 d, corresponding to 85.5 kg d). Moreover we analysed a smaller set of data (exposure = 14.8 kg d) collected using a different electronics and acquisition system, that we mounted in parallel with the usual set up. This allowed us to obtain an on-line rejection of background through anti-coincidence (while previously this rejection was performed off-line) and a low energy threshold of 2.7 keV, with respect to the previous value of 4 keV. At present both the electronics are taking data.

We presented our limits directly in terms of WIMP-proton SI cross section and WIMP-neutron SD cross section, in order to compare our results with other experiments.

For SD interactions we improve the best present limits on the WIMP-neutron SD cross section for low WIMP masses.

Publications

[1] H.V. Klapdor-Kleingrothaus, A. Dietz, G. Heusser, I.V. Krivosheina, D. Mazza, H. Strecker, C. Tomei, *First Results from the HDMS experiment in the Final Setup*, hep-ph/ 0206151 and Astrop. Phys. **18**, Issue 5 (2003) 525-530.

References

[1] HDMS coll., Phys. Rev. **D 63** (2000) 022001.

[2] HDMS coll., Nucl. Phys. **B** (Proc. Suppl.) 70 (1999) 106.

[3] H.V Klapdor Kleingrothaus et al., Astrop. Phys., **18**, Issue 5 (2003) 525-530, and hep-ph/ 0206151.

[4] A. Benoit et al., Phys. Lett. **B 545** (2002) 43-49.

[5] D. Abrams, Phys. Rev. **D 66** (2002) 122003.

[6] A. Morales et al., Phys. Lett. **B 532** (2002) 8.

[7] R. Bernabei et al., Phys. Lett. **B 480** (2000) 23.

[8] R. Bernabei et al., Riv. Nuovo Cim. **26** (2003) 1-73.

[9] D.R. Tovey et al., Phys. Lett. B**488** (2000) 17-26.

[10] J.D. Lewin, P.F. Smith, Astropart. Phys. **6** (1996) 87.

[11] V. Dimitrov, J. Engel and S. Pittel, Phys. Rev. **D 51** (1995) 291-295.

[12] R. Bernabei et al., Phys. Lett. **B 480** (2000) 23.

Heidelberg - Moscow Experiment on Neutrinoless Double Beta Decay

H.V. Klapdor-Kleingrothaus*[a], I.V. Krivosheina[a,b], A. Dietz[a], C. Tomei[a,c], O. Chkvoretz[a], H. Strecker[a]

[a] Max-Planck Institut für Kernphysik, Heidelberg, Germany
[b] Institute of Radiophysical Research, Nishnij Novgorod, Russia
[c] University of L'Aquila, Italy
* Spokesman of the Collaboration; E-mail: klapdor@gustav.mpi-hd.mpg,
Home-page: http://www.mpi-hd.mpg.de.non_acc/

Abstract

The HEIDELBERG-MOSCOW experiment, which is the most sensitive double beta decay experiment since ten years has been regularly continued until end of November 2003. An analysis of the data has been performed already until May 20, 2003. The experiment yields now, on a 4σ level, evidence for lepton number violation and proves that the neutrino is a Majorana particle. It further shows that neutrino masses are degenerate. In addition it puts several stringent constraints on other physics beyond the Standard Model. Among others it opens the door to test various supersymmetric theory scenarios, for example it gives the sharpest limit on the parameter λ'_{111} in the R-parity violating part of the superpotential, and gives information on the splitting of the sneutrino-antisneutrino system. The result from the HEIDELBERG-MOSCOW experiment is consistent with recent results from CMB investigations, with high energy cosmic rays, with the result from the g-2 experiment and with recent theoretical work. It is indirectly supported by the analysis of other Ge double beta experiments. Recent criticism of various kind has been shown to be wrong, among others by measurements performed in 2003 with a ^{214}Bi source (^{226}Ra), by simulation of the background in the range of $Q_{\beta\beta}$ by GEANT4, and by deeper investigation of statistical features such as sensitivity of peak search, and relevance of width of window of analysis.

1 Introduction

Double beta decay is the most sensitive probe to test lepton number conservation. Further it seems to be the only way to decide about the Dirac or Majorana nature of the neutrino.

Double beta decay can contribute decisively to the field of neutrino physics also by setting an absolute scale to neutrino masses, which cannot be observed from neutrino oscillation experiments.

The observable of double beta decay is the effective neutrino mass

$$\langle m \rangle = |\sum U_{ei}^2 m_i| = |m_{ee}^{(1)}| + e^{i\phi_2}|m_{ee}^{(2)}| + e^{i\phi_3}|m_{ee}^{(3)}|,$$

with U_{ei} denoting elements of the neutrino mixing matrix, m_i neutrino mass eigenstates, and ϕ_i relative Majorana CP phases. It can be written in terms of oscillation parameters [14]

$$|m_{ee}^{(1)}| = |U_{e1}|^2 m_1, \quad (1)$$

$$|m_{ee}^{(2)}| = |U_{e2}|^2 \sqrt{\Delta m_{21}^2 + m_1^2}, \quad (2)$$

$$|m_{ee}^{(3)}| = |U_{e3}|^2 \sqrt{\Delta m_{32}^2 + \Delta m_{21}^2 + m_1^2}. \quad (3)$$

The effective mass $\langle m \rangle$ is related with the half-life for $0\nu\beta\beta$ decay via $\left(T_{1/2}^{0\nu}\right)^{-1} \sim \langle m_\nu \rangle^2$, and for the limit on $T_{1/2}^{0\nu}$ deducible in an experiment we have

$$T_{1/2}^{0\nu} \sim \epsilon \times a \sqrt{\frac{Mt}{\Delta E B}}, \quad (4)$$

Here a is the isotopical abundance of the $\beta\beta$ emitter; M is the active detector mass; t is the measuring time; ΔE is the energy resolution; B is the background count rate and ϵ is the efficiency for detecting a $\beta\beta$ signal. Determination of the effective mass fixes the absolute scale of the neutrino mass spectrum [14, 19].

The HEIDELBERG-MOSCOW experiment has been regularly continued in 2003. It had to be stopped, on November 30, 2003, according to contract. Unfortunately the Kurchatov institute did not agree to prolong the contract. The experiment is already since 2001 operated only by the Heidelberg group, which also performed the analysis of the experiment from its very beginning.

The experiment is *since ten years now* the most sensitive double beta experiment worldwide. In this report we will describe in section II the evidence for neutrinoless double beta decay $(0\nu\beta\beta)$, found by an analysis of the HEIDELBERG-MOSCOW experiment including the three more years of data taking.

The result derived from the full data taken until May 20, 2003 is

$$\mathrm{T}_{1/2}^{0\nu} = (0.69 - 4.18) \times 10^{25}\mathrm{y} \quad (99.73\% c.l.) \quad (5)$$

with best value of $\mathrm{T}_{1/2}^{0\nu} = 1.19 \times 10^{25}\ y$. Thus double beta decay is the slowest nuclear decay process observed until now in nature. Assuming the neutrino mass mechanism to dominate the decay amplitude, we deduce

$$\langle m_\nu \rangle = (0.24 - 0.58)\, eV \quad (99.73\% c.l.), \quad (6)$$

with best value of 0.44 eV. This value we obtained using the nuclear matrix element of [25]. Allowing for an uncertainty of $\pm 50\%$ of the matrix elements (see [5, 19]), this range widens to

$$\langle m_\nu \rangle = (0.1 - 0.9)\, eV \quad (7)$$

The result (2) and (3) determines the neutrino mass scenario to be degenerate [15, 20]. The common mass eigenvalue follows then to be $m_{com} = (0.14 - 3.6)\, eV$ (99.73%).

The new results with three more years of statistics confirm our earlier results [1, 2, 3, 4, 5, 7] on a higher confidence level. The signal is now seen on a 4.2σ level (see section 2).

If we allow for other mechanisms (see [17, 18, 19, 16]), the value given in eq. (6),(7) has to be considered as an upper limit. In that case very stringent limits arise for some other fields of beyond standard model physics. To give an example, it gives the sharpest limit on the Yukawa coupling λ'_{111} in the R-parity violating part of the superpotential [23]. It also gives information on R-parity conserving supersymmetry. New R-parity conserving SUSY contributions to $0\nu\beta\beta$ decay occur at the level of box diagrams [22]. Double beta decay then yields information on the mass splitting in the sneutrino-antisneutrino system [22]. These constraints leave room for accelerator searches for certain manifestations of the second and third generation (B-L)-violating sneutrino mass term, but are most probably too tight for first generation (B-L)-violating sneutrino masses to be searched for directly. It has been discussed recently [67] that $0\nu\beta\beta$ decay by R-parity violating SUSY experimentally may not be excluded, although this would require making R-parity violating couplings generation dependent.

We show, in section III that indirect support for the observed evidence for neutrinoless double beta decay evidence comes from analysis of other Ge double beta experiments (though they are by far less sensitive, they yield independent information on the background in the region of the expected signal).

Table 1: Recent support of the neutrino mass deduced from $0\nu\beta\beta$ decay [1, 2, 5, 12, 11] by other experiments, and by theoretical work.

Experiment	References	m_ν (degenerate ν's)(eV)
$0\nu\beta\beta$	[1, 2, 5, 12, 11]	0.05 - 3.2
WMAP	[75, 77]	< 0.23, or 0.33, or 0.50
CMB	[74]	< 0.7
CMB+LSS+X-ray gal. Clust.	[79]	~ 0.2 eV
SDSS + WMAP	[84]	< 0.57 eV
Z - burst	[65, 73]	0.08 - 1.3
g-2	[66]	> 0.2
Tritium	[54]	< 2.2 - 2.8
ν oscillation	[69, 70]	> 0.04
Theory:		
A_4-symmetry	[71]	> 0.2
identical quark and ν mixing at GUT scale	[72]	> 0.1
Alternative cosmological 'concordance model'	[80]	order of eV

The discussion in section IV, V, VI, may now just still be of historical interest. Here we disprove some criticism of our *earlier* given results. We show by measurements with a ^{226}Ra source, performed in 2003 [12], and by various statistical calculations, that the criticism by Aalseth et al., (see Mod. Phys. Lett. A17 (2002) 1475-1478), Zdesenko et

al., (see Phys. Lett. B 546 (2002) 206-215), Ianni (in NIM 2004), Feruglio et al., (see Nucl. Phys. B 637 (2002) 345) of our earlier results [1, 2, 5] just was *wrong*.

In section VII we give a short discussion, stressing that the evidence for neutrinoless double beta decay has been supported by various recent experimental results from other fields of research (see Table 1). It is consistent [20] with recent results from cosmic microwave background experiments [74, 75, 77]. The precision of WMAP even allows to rule out some old-fashioned nuclear double beta decay matrix elements (see [76]).

It has been shown to be consistent with the neutrino masses required for the Z-burst scenarios of high-energy cosmic rays [73, 65]. It is consistent with a (g-2) deviating from the standard model expectation [66]. It is consistent also with the limit from the tritium decay experiments [45] but the allowed confidence range still extends down to a range which cannot be covered by future tritium experiments (apart from some principle theoretical problems, which tritium decay may have to see neutrino masses [81]. It is further supported by recent theoretical work [71, 72, 83].

Cosmological experiments like WMAP are now on the level that they can seriously contribute to terrestrial research. The fact that WMAP and less strictly also the tritium experiments cut away the upper part of the allowed range for the degenerate neutrino mass ($m_{com} = (0.14 - 3.6)\, eV$) could indicate that the neutrino mass eigenvalues have the same CP parity [21].

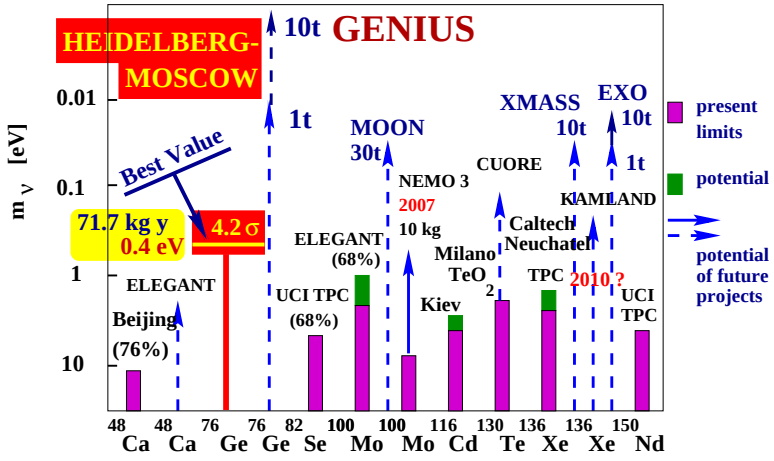

Figure 1: Present sensitivity, and expectation for the future, of the most promising $\beta\beta$ experiments. Given are limits for $\langle m \rangle$, except for the HEIDELBERG-MOSCOW experiment where the measured *value* is given (3σ c.l. range and best value). Framed parts of the bars: present status; not framed parts: future expectation for running experiments; solid and dashed lines: experiments under construction or proposed, respectively. For references see [19, 2, 5, 61, 59].

Finally we briefly comment in section VIII about the possible future of the field of double beta decay. First results from GENIUS-TF which has come into operation on May 5, 2003 in Gran Sasso with first in world 10 kg of naked Germanium detectors in liquid nitrogen [50, 52, 51], are discussed in another contribution to this report [48].

2 Results Obtained in the Period August 2, 1990 Until May 20, 2003.

The status of present double beta experiments is shown in Fig. 1 and is extensively discussed in [19]. The HEIDELBERG-MOSCOW experiment using the largest source strength of 11 kg of enriched ^{76}Ge (enrichment 86%) in form of five HP Ge-detectors is running since August 1990 in the Gran-Sasso underground laboratory [19, 5, 8, 2, 46, 43, 7]. We present here in Figs. 2,3 the results obtained with three more years data, until May 20, 2003. Fig. 2 shows the full spectrum, Fig. 3 the range around the $Q_{\beta\beta}$ value. They correspond to a total measuring time of 71.7 kg y.

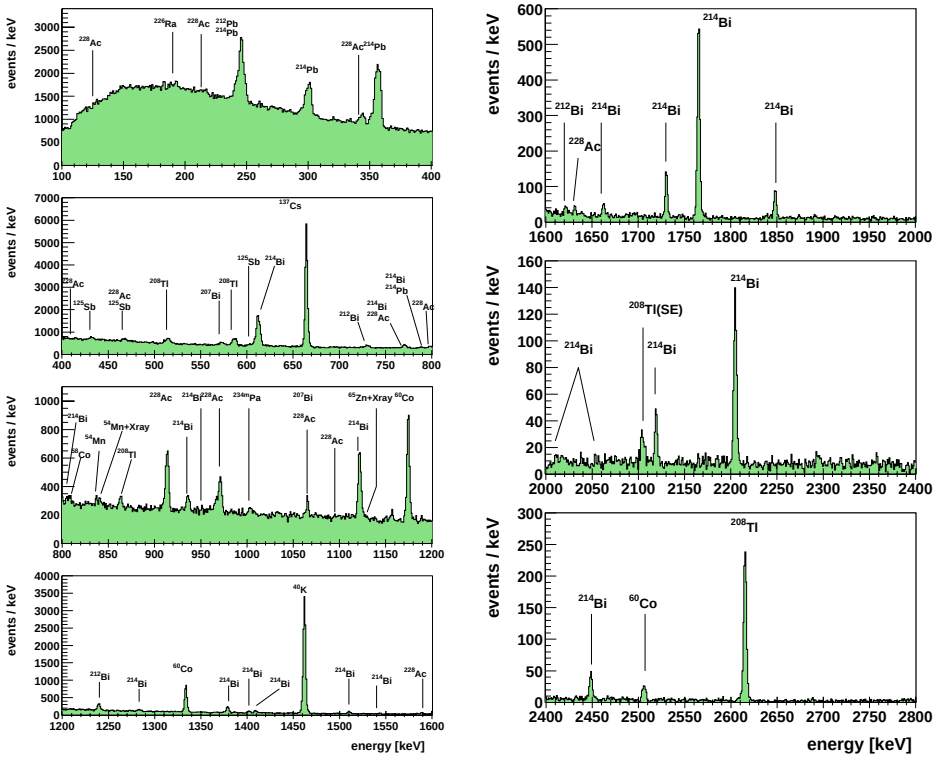

Figure 2: The total sum spectrum measured over the full energy range (low-energy part (left), and higher energy part (right)) of all five detectors (in total 10.96 kg enriched in ^{76}Ge to 86%) - for the period 2 August 1990 to 20 May 2003.

Fig. 3 shows that the line at $Q_{\beta\beta}$ is now - as the Bi lines at 2010.7, 2016.7, 2021.8, 2052.9 keV - directly clearly seen, while in our first results they had to be projected out from the background by a peak search procedure [1, 2, 5, 7].

Earlier measurements of $Q_{\beta\beta}$ by [29, 30, 31] yielded 2040.71±0.52 keV, 2038.56 ± 0.32 keV and 2038.668±2.142 keV. The precision measurement of [28] yields 2039.006 (50) keV.

The data have been analysed with various statistical methods. We always process background-plus-signal data since the difference between two Poissonian variables does *not* produce a Poissonian distribution [33]. This is important, but sometimes overlooked

(see section 6). Analysis of the spectra by nonlinear least squares method, using the Levenberg-Marquardt algorithm yields the fits, shown in Fig. 3.

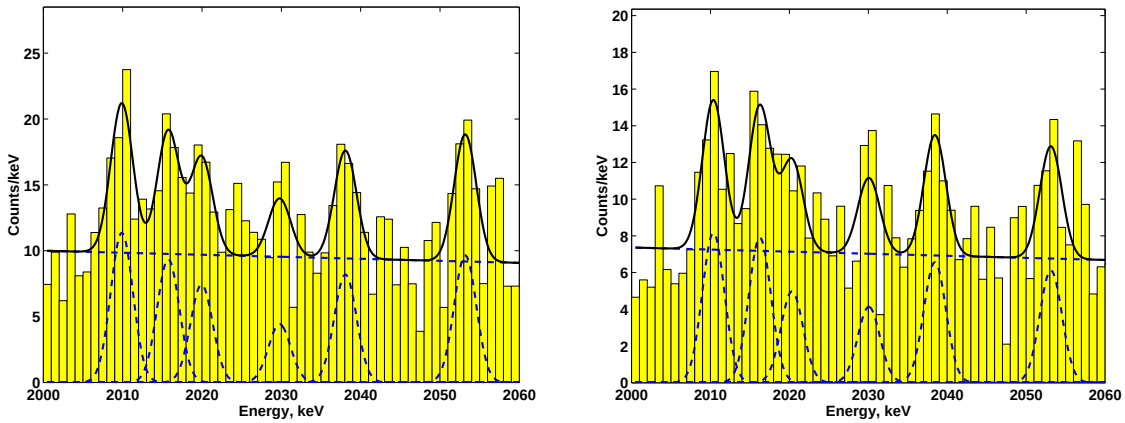

Figure 3: The total sum spectrum of all five detectors (in total 10.96 kg enriched in ^{76}Ge), for the period August 1990 to May 2003 (71.7 kg y) left, and for the period November 1995-2003 (56.66 kg y) in the range 2000 - 2060 keV and its fit (see section 3.2).

In these fits the peak positions, widths and intensities of all lines are determined simultaneously, and also the absolute level of the background. The shape of the latter was chosen to be slightly decreasing with energy, corresponding to the complete simulation of the background performed in [13] by GEANT4. E.g. in Fig. 3, right, the *fitted* background corresponds to (55.94±3.92) kg y if extrapolated from the background *simulated* in [13] for the measurement with 49.59 kg y of statistics (see Fig. 15). This is almost *exactly* the statistical significance of the present experiment (56.66 kg y) and thus a very nice proof of consistency. Assuming a *constant* background in the range 2000 - 2060 keV or keeping also the *slope* of a linearly varying background as a free parameter, yields very similar results. Analysis with the Maximum Likelihood Method gives results consistent with the above method.

The signal at $Q_{\beta\beta}$ in the full spectrum (the fit of Fig. 3, right, yields 2038.44±0.45 keV), reaches a 4.2σ confidence level for the period 1990-2003, and of 4.1σ for the period 1995-2003 (for details we refer to [6]. A detailed description of the analysis of the full data 1990-2003 will be given in the next Annual Report.

3 Measurements With a ^{214}Bi Source, Comparison With Other Ge-Experiments

By the peak search procedure developped [2, 5] on basis of the Bayes and Maximum Likelihood Methods, exploiting as important input parameters the experimental knowledge on the shape and width of lines in the spectrum, weak lines of ^{214}Bi had been identified at the energies of 2010.7, 2016.7, 2021.6 and 2052.9 keV already in [1, 2, 5, 10]. Though the lines with our improved statistics and analysis are now clearly seen directly in the spectrum (Fig. 3), we show for comparison the result of the peak search procedure for the spectrum taken 1995-2003, in Fig. 4. As usual, shown is the probability that there is

a line of correct width and of Gaussian shape at a given energy, assuming all the rest of the spectrum as flat background (which is a highly conservative assumption).

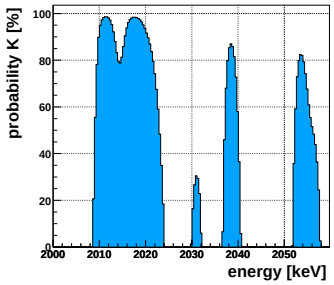

Figure 4: Scan for lines in the full spectrum taken from 1995 - 2003 with detectors Nr. 1,2,3,4,5, with the MLM method (see text). The Bi lines at 2010.7, 2016.7, 2021.8 and 2052.9 keV are clearly seen, and in addition a signal at $\sim$ 2039 keV.

Concerning the intensities of these ^{214}Bi lines, one has to note that the 2016 keV line, as an E0 transition, can be seen only by coincident summing of the two successive lines $E = 1407.98$ keV and $E = 609.316$ keV. Its observation proves that the ^{238}U impurity from which it is originating, is located in the Cu cap of the detectors.

We performed, in the first half of 2003, a *measurement* of a ^{226}Ra source with a high-purity germanium detector [12]. The aim of this work was to investigate the difference in the Bi spectra when changing the position of the source with respect to the detector, and to verify the effect of TCS (true coincidence summing) for the weak ^{214}Bi lines seen in the HEIDELBERG-MOSCOW experiment .

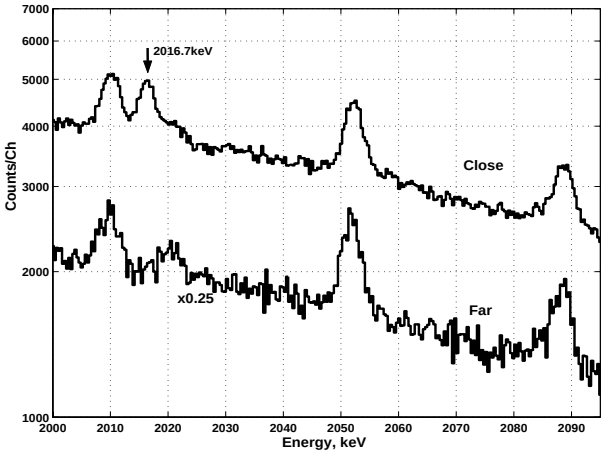

Figure 5: Measured ^{226}Ra spectrum in the energy range from 2000 to 2100 keV. The upper spectrum corresponds to the close geometry, the bottom spectrum to the far geometry. The weak lines from ^{214}Bi are nicely visible, together with the effect of the true coincidence summing at 2016.7 keV (from [12]).

The activity of the ^{226}Ra source was 95.2 kBq. The isotope ^{226}Ra appears in the ^{238}U natural decay chain and from its decays also ^{214}Bi is produced. The γ-spectrum of

^{214}Bi is clearly visible in the ^{226}Ra measured spectrum (see Fig. 5). We also performed a simulation of our measurement with the GEANT4 simulation tool and we find good agreement between the simulation and the measurement [12]. The premature estimates of the Bi intensities given in *Aalseth et al.*, hep-ex/0202018 and Feruglio et al., Nucl. Phys. B 637 (2002), 345, *are incorrect*, because this long-known spectroscopic effect of true coincident summing [27] has not been taken into account, and also no simulation of the setup has been performed (for details see [5, 3, 9, 12, 7]).

These Bi lines occur also in other investigations of double beta decay. There are three other Ge experiments which have looked for double beta decay of ^{76}Ge. First there is the experiment by Caldwell et al. [34], using natural Germanium detectors (7.8% abundance of ^{76}Ge, compared to 86% in the HEIDELBERG-MOSCOW experiment). This was the most sensitive *natural* Ge experiment. With their background a factor of 9 higher than in the HEIDELBERG-MOSCOW experiment and their measuring time of 22.6 kg years, they had a statistics of the background by a factor of almost four l a r g e r than in the HEIDELBERG-MOSCOW experiment. This gives useful information on the composition of the background.

Applying the same method of peak search as used in Fig. 4, yields (see also [7, 11]) indications for peaks essentially at the same energies as in Fig. 4 (see Fig. 6). This shows that these peaks are not fluctuations. In particular it sees the 2010.78, 2016.7, 2021.6 and 2052.94 keV ^{214}Bi lines, but a l s o the unattributed lines at higher energies. It finds, however, n o line at 2039 keV. This is consistent with the expectation from the rate found in the HEIDELBERG-MOSCOW experiment. About 29 identified events observed during 1990-2003 in the latter correspond to 0.7 expected events in the Caldwell experiment, because of the use of non-enriched material and the shorter measuring time. Fit of the Caldwell spectrum allowing for the ^{214}Bi lines and a 2039 keV line yields 0.4 events for the latter (see [5] and Fig. 9).

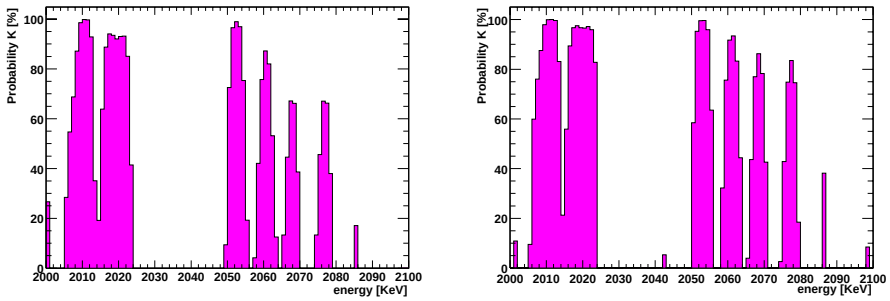

Figure 6: Result of the peak-search procedure performed for the UCBS/LBL spectrum [34] (left: Maximum Likelihood method, right: Bayes method). On the y axis the probability of having a line at the corresponding energy in the spectrum is shown (from [7, 11]).

The first experiment using enriched (but not high-purity) Germanium 76 detectors was that of Kirpichnikov and coworkers [35]. These authors show only the energy range between 2020 and 2064 keV of their measured spectrum. The peak search procedure finds also here indications of lines around 2028 keV and 2052 keV (see Fig. 7), but n o t any indication of a line at 2039 keV. This is consistent with the expectation, because for

their low statistics of 2.95 kg y they would expect here (according to HEIDELBERG-MOSCOW) 1.1 counts.

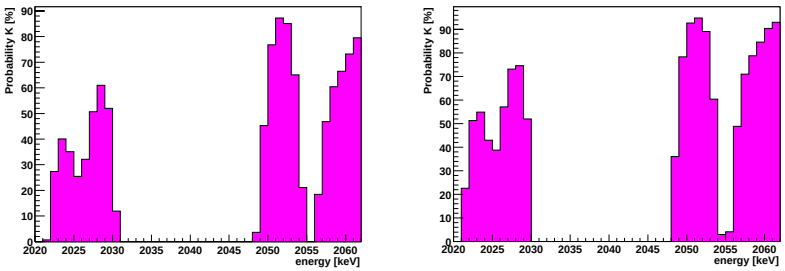

Figure 7: Result of the peak-search procedure performed for the ITEP/YePI spectrum [35] (from [7, 11]).

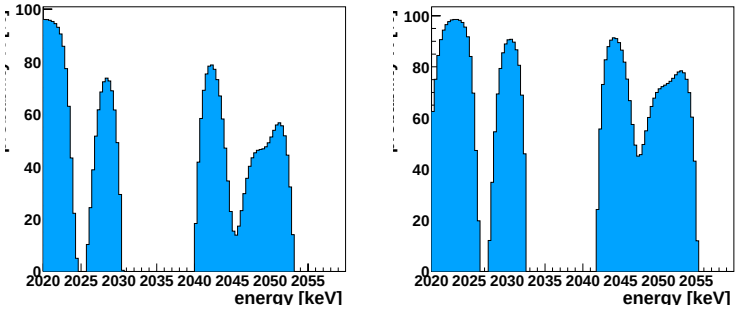

Figure 8: Result of the peak-search procedure performed for the IGEX spectrum [57]. Left: Maximum Likelihood method, right: Bayes method. On the y axis the probability of having a line at the corresponding energy in the specrtum is shown (from [7, 11]).

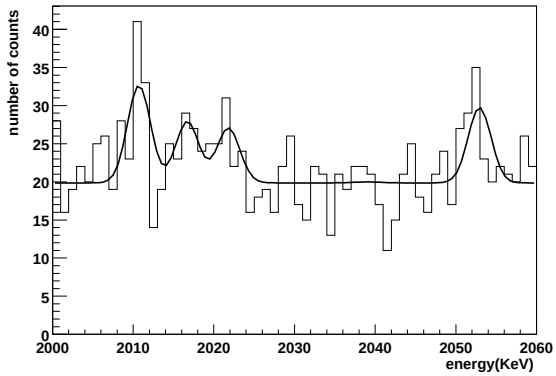

Figure 9: Analysis of the spectrum measured by D. Caldwell et al. [34], with the Maximum Likelihood Method, in the energy range 2000-2060 keV assuming lines at 2010.7, 2016.7, 2021.6, 2052.9, 2039.0 keV. No indication for a signal at 2039 keV is observed in this case (see [7]).

Another experiment (IGEX) used between 6 and 8.8 kg of enriched ^{76}Ge, but collected since beginning of the experiment in the early nineties till shutdown in 1999 only 8.8 kg years of statistics [57]. The authors of [57] unfortunately show only the range 2020 to 2060 keV of their measured spectrum in detail. Fig. 8 shows the result of our peak scanning of this range. Clear indications are seen for the lines at 2021 and 2052 keV, but also of the unidentified structure around 2030 keV. Because of the conservative assumption on the background treatment in the scanning procedure (see above) there is no chance to see a signal at 2039 keV because of the 'hole' in the background of that spectrum (see Fig. 1 in [57]). With some good will one might see, however, an indication of ∼3 events here, consistent with the expectation of the HEIDELBERG-MOSCOW experiment of ∼ 2.6 counts.

4 Statistical Features: Sensitivity of Peak Search, Analysis Window

For historical reasons, at this point it may be useful to demonstrate the potential of the peak search procedure used in [1, 2, 5]. Fig. 10 shows a spectrum with Poisson-generated background of 4 events per channel and a Gaussian line with width (standard deviation) of 4 channels centered at channel 50, with intensity of 10 (left) and 100 (right) events, respectively. Fig. 12, shows the result of the analysis of spectra of different line intensity with the Bayes method (here Bayes 1-4 correspond to different choice of the prior distribution: (1) $\mu(\eta) = 1$ (flat), (2) $\mu(\eta) = 1/\eta$, (3) $\mu(\eta) = 1/\sqrt{\eta}$, (4) Jeffrey's prior) and the Maximum Likelihood Method. For each prior 1000 spectra have been generated with equal background and equal line intensity using random number generators available at CERN [24]. The average values of the best values agree (see Fig. 12) very well with the known intensities also for very low count rates (as in Fig. 10, left).

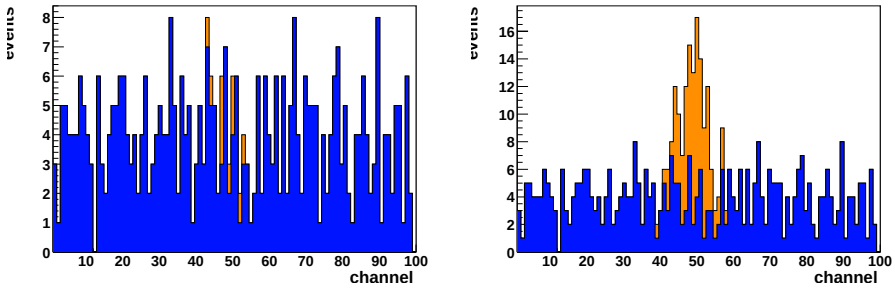

Figure 10: Example of a random-generated spectrum with a Poisson distributed background with 4.0 events per channel and a Gaussian line centered in channel 50 (line-width corresponds to a standard-deviation of $\sigma = 4.0$ channels). The left picture shows a spectrum with a line-intensity of 10 events, the right spectrum a spectrum with a line-intensity of 100 events. The background is shown dark, the events of the line bright (see [11]).

In Fig. 13 we show two simulations of a Gaussian line of 15 events, centered at channel 50, again with width (standard deviation) of 4 channels, on a Poisson-distributed background with 0.5 events/channel. The figure gives an indication of the possible degree of deviation of the energy of the peak maximum from the transition energy, on the level of

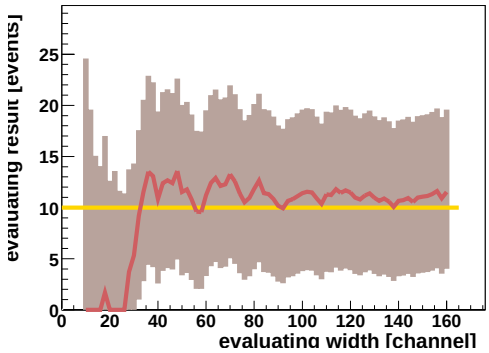

Figure 11: Result of an analysis as function of the evaluation width. The used spectrum consists of a Poisson distributed background with 4 events per channel, and a line of 10 events (see Fig. 10, left part). The dark area corresponds to a 68.3% confidence area with the dark line being the best value. Below an evaluation width of 35 channels the result becomes unreliable, above 35 channels the result is stable (see also [7, 11]).

statistics collected in experiments like the HEIDELBERG-MOSCOW experiment (here one channel corresponds to 0.36 keV). This should be kept in mind.

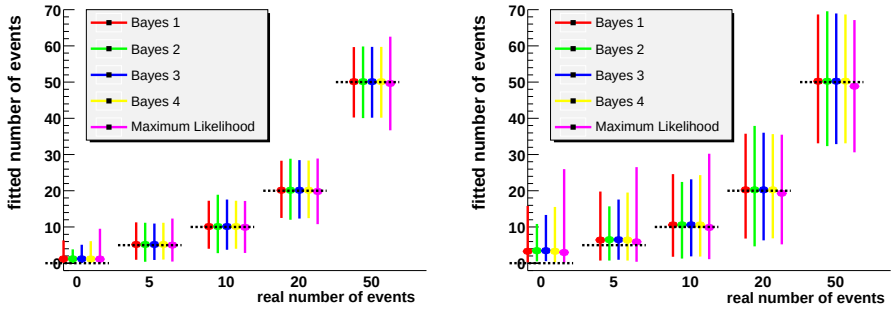

Figure 12: Results of analysis of random-number generated spectra, using Bayes and Maximum Likelihood method (the first one with different prior distributions). For each number of events in the simulated line, shown on the x-axis, 1000 random generated spectra were evaluated with the five given methods. The analysis on the left side was performed with an Poisson distributed background of 0.5 events per channel, the background for the spectra on the right side was 4.0 events per channel. Each vertical line shows the mean value of the calculated best values (thick points) with the 1σ error area. The mean values are in good agreement with the expected values (horizontal black dashed lines) (see [7, 11]).

The influence of the choice of the energy range of the analysis around $Q_{\beta\beta}$ has been thoroughly discussed in [2, 5]. Since erroneous ideas about this point are still around, let us remind of the analysis given in [2, 5, 11, 7] which showed that a reliable result is obtained for a range of analysis of not smaller than 35 channels (i.e. $\pm$18 channels) - one channel corresponding to 0.36 keV in the HEIDELBERG-MOSCOW experiment (see Fig. 11). This is an important result, since it is, in case of a weak signal, *of course* important to keep the range of analysis as s m a l l as possible, to avoid to include lines in the vicinity of the weak signal into the background (see, e.g. Fig. 9 in [82]). This unavoidably occurs

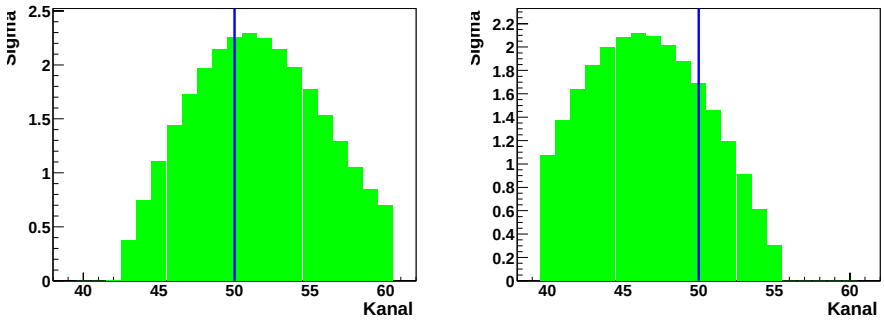

Figure 13: Two spectra with a Poisson-distributed background and a Gaussian line with 15 events centered in channel 50 (with a width (standard-deviation) of 4.0 channels) created with different random numbers. Shown is the result of the peak-scanning of the spectra. In the left picture the maximum of the probability corresponds well with the expected value (black line) whereas in the right picture a larger deviation is found. When a channel corresponds to 0.36 keV the deviation in the right picture is ~ 1.44 keV (see [7, 11]).

when e.g. proceeding as suggested in F. Feruglio et al., hep-ph/0201291 and Nucl. Phys. B 637 (2002) 345-377, Aalseth et. al., hep-ex/0202018 and Mod. Phys. Lett. A 17 (2002) 1475, Yu.G. Zdesenko et. al., Phys. Lett. B 546 (2002) 206, A. Ianni, in Press NIM 2004. The arguments given in those papers are therefore *incorrect*. Also Kirpichnikov, who states [35] that his analysis finds a 2039 keV signal in the HEIDELBERG-MOSCOW spectrum on a 4 sigma confidence level (as we also see it) makes this mistake, when analysing the pulse shape spectrum.

The above discussion is now in this context only of historical interest, since with the better statistics we have now, we can analyze simultaneously a large energy range (as shown in Fig. 3).

5 Simulation with GEANT4

Finally the background around $Q_{\beta\beta}$ will be discussed from the side of simulation. A very careful new simulation of the different components of radioactive background in the HEIDELBERG-MOSCOW experiment has been performed by a new Monte Carlo program based on GEANT4 [13]. This simulation uses a new event generator for simulation of radioactive decays basing on ENSDF-data and describes the decay of arbitrary radioactive isotopes including alpha, beta and gamma emission as well as conversion electrons and X-ray emission. Also included in the simulation is the influence of neutrons in the energy range from thermal to high energies up to 100 MeV on the measured spectrum. Elastic and inelastic reactions, and capture have been taken into account, and the corresponding production of radioactive isotopes in the setup. The neutron fluxes and energy distributions were taken from published measurements performed in the Gran Sasso. Also simulated was the cosmic muon flux measured in the Gran Sasso, on the measured spectrum. To give a feeling for the quality of the simulation, Fig. 14 shows the simulated and the measured spectra for a ^{228}Th source spectrum for as example one of our five detectors. The agreement is excellent.

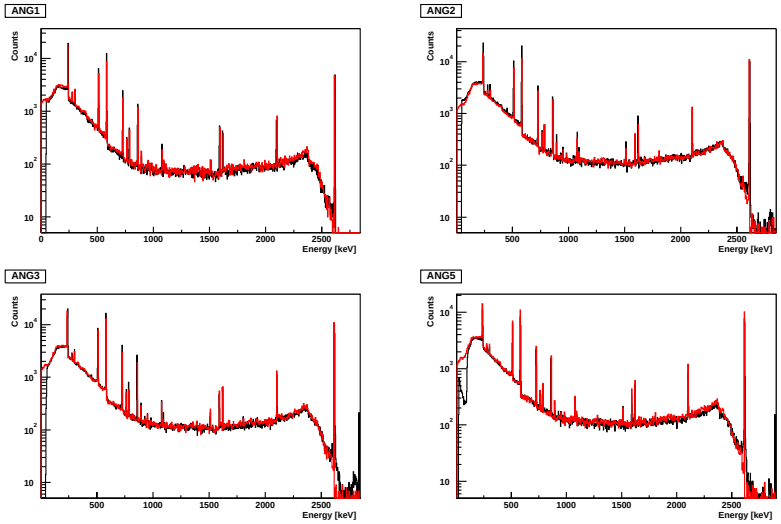

Figure 14: Comparison of the measured data (black line, November 1995 to April 2002) and simulated spectrum (red line) for the detectors Nrs. 1,2,3 and 5 for a ^{232}Th source spectrum. The agreement of simulation and measurement is excellent (from [13]).

The simulation of the background of the experiment reproduces all lines observed in the sum spectrum of the five detectors, in the energy range between threshold (around 100 keV) and 2020 keV [13].

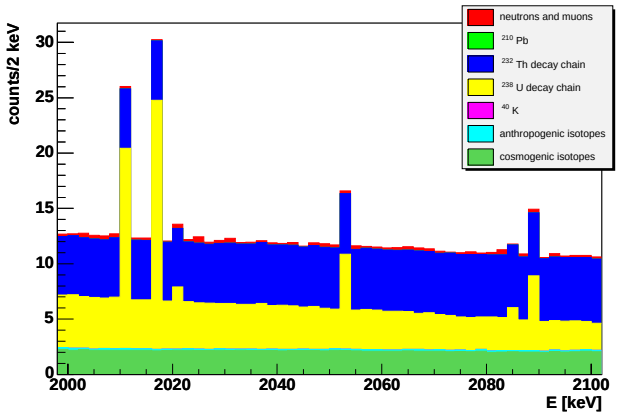

Figure 15: Simulated background of the HEIDELBERG-MOSCOW experiment in the energy range from 2000 to 2100 keV with all known background components, for the period 20 November 1995 to 16 April 2002 (from [13]).

Fig. 15 shows the simulated background in the range 2000-2100 keV with all known background components.

The background around $Q_{\beta\beta}$ is according to the simulations flat, the only expected lines come from ^{214}Bi (from the ^{238}U natural decay chain) at 2010.89, 2016.7, 2021.6, 2052.94, 2085.1 and 2089.7 keV. Lines from cosmogenically produced ^{56}Co (at 2034.76 keV and 2041.16 keV), half-life 77.3 days, are not expected since the first 200 days of measurement of each detector are not used in the data analysis. Also the potential contribution

from decays of ^{77}Ge, ^{66}Ga, or ^{228}Ac, should not lead to signals visible in our measured spectrum near the signal at $Q_{\beta\beta}$. For details we refer to [13].

6 Proofs and disproofs

Our earlier result published in [1, 2, 5], which now is confirmed on a 4σ level, had been questioned in some papers [Aalseth et al, hep-ex/0202018, and in Mod. Phys. Lett. A 17 1475-1478; Feruglio et al., Nucl. Phys. B 637 (2002) 345; Zdesenko et al., Phys. Lett. B 546 (2002) 206], and Kirpichnikov, talk at Meeting of Physical Section of Russian Academy of Sciences, Moscow, December 2, 2002, (and priv. communication, Dec. 3, 2002) and A. Ianni, Nucl. Instruments A (2004) (available online 28 September 2003). We think that we have shown in a convincing way during 2002 and 2003 that these claims against our results were incorrect in various ways, and have published our arguments in [12, 11, 7, 10]. In particular the estimates of the intensities of the ^{214}Bi lines in the first two papers do not take into account the effect of true coincidence summing, which can lead to drastic underestimation of the intensities. A correct estimate would also require a Monte Carlo simulation of our setup, which has not been performed in the above papers.

The paper by Zdesenko et al. starts from an arbitrary assumption, namely that there are lines in the spectrum *at best* only at 2010 and 2053 keV. This contradicts to the experimental result, according to which there are further lines in the spectrum (see Fig. 3 in this report). For example they could have easily deduced from the intensity of the 2204 keV Bi line in the measured spectrum (Fig. 2) that lines at 2053 keV etc. are expected [32]. In this way and also by some subtraction procedure, ignoring that the result of subtracting a Poisson-distributed spectrum from a Poisson-distributed spectrum does *not* give a Poisson distributed spectrum (see, e.g. [33]) they come to wrong conclusions.

Kirpichnikov states [36] that from his analysis he clearly sees the 2039 keV line in the full (not pulse-shape discriminated) spectrum on a 4σ level. He claims that he does not see the signal in the pulse shape spectrum. The simple reason to see less intensity is that in this case he averages for determination of the background over the full energy range without allowing for any lines.

All of these papers, when discussing our earlier choice of the width of the search window (in the analysis of the data taken until May 2000), ignore the results of the statistical simulations - we present here, and have published in [2, 3, 4, 5, 7, 10, 11].

The strange effects found recently by the Kurchatov people [55] in their rough analysis of part of the data, have been traced back to including corrupt data into the analysis. The artefacts seen in their Figs. 4,5,7,8 do not exist in our data, which lead to the results shown in Figs. 2,3 (for details see [6, 56]).

7 Discussion of results

We emphasize that we find in all analyses of our spectra a line at the value of $Q_{\beta\beta}$. The results confirm our earlier result with higher statistics. For details we refer to the next Annual Report and to [6].

The result obtained is consistent with all other double beta experiments - which reach in general by far less sensitivity. The most sensitive experiments following the

HEIDELBERG-MOSCOW experiment are the geochemical ^{128}Te experiment with $T^{0\nu}_{1/2} > 2(7.7) \times 10^{24}$ y (68% c.l.), [37] the ^{136}Xe experiment by the DAMA group with $T^{0\nu}_{1/2} > 1.2 \times 10^{24}$ y (90% c.l.), a second enriched ^{76}Ge experiment with $T^{0\nu}_{1/2} > 1.2 \times 10^{24}$ y [35] and a ^{nat}Ge experiment with $T^{0\nu}_{1/2} > 1 \times 10^{24}$ y [34]. Other experiments are already about a factor of 100 less sensitive concerning the $0\nu\beta\beta$ half-life: the Gotthard TPC experiment with ^{136}Xe yields [38] $T^{0\nu}_{1/2} > 4.4 \times 10^{23}$ y (90% c.l.) and the Milano Mibeta cryodetector experiment $T^{0\nu}_{1/2} > 1.44 \times 10^{23}$ y (90% c.l.).

Another experiment [57] with enriched ^{76}Ge, which has stopped operation in 1999 after reaching a significance of 8.8 kg y, yields (if one believes their method of 'visual inspection' in their data analysis), in an analysis correcting for on arithmetic error which has been made in [57] (for discussion see [58]) a limit of about $T^{0\nu}_{1/2} > 5 \times 10^{24}$ y (90% c.l.). The ^{128}Te geochemical experiment yields $\langle m_\nu \rangle < 1.1$ eV (68 % c.l.) [37], the DAMA ^{136}Xe experiment $\langle m_\nu \rangle < (1.1{-}2.9)$ eV and the ^{130}Te cryogenic experiment yields $\langle m_\nu \rangle < 1.8$ eV.

Concluding we obtain, with $> 4\sigma$ probability, evidence for a neutrinoless double beta decay signal. Following this interpretation, at this confidence level, lepton number is not conserved. Further the neutrino is a Majorana particle. If the $0\nu\beta\beta$ amplitude is dominated by exchange of a massive neutrino the effective mass $\langle m \rangle$ is deduced from the full spectrum (using the matrix elements of [25]) to be $\langle m \rangle = (0.1$ - $0.9)$ eV (3σ confidence range), allowing already for a $\pm$ 50% uncertainty of the matrix element. The best value is 0.4 eV.

Assuming other mechanisms to dominate the $0\nu\beta\beta$ decay amplitude, the result allows to set stringent limits on parameters of SUSY models, leptoquarks, compositeness, masses of heavy neutrinos, the right-handed W boson and possible violation of Lorentz invariance and equivalence principle in the neutrino sector. For a discussion and for references we refer to [19, 39, 42, 18, 59, 16].

With the value deduced for the effective neutrino mass, the HEIDELBERG-MOSCOW experiment excludes several of the neutrino mass scenarios allowed from present neutrino oscillation experiments (see Fig. 16) - allowing only for a degenerate mass scenario [15, 20, 6]. Fig. 16 shows also the limits obtained from WMAP, which at the present level of sensitivity is not able to rule out any neutrino mass scheme.

The evidence for neutrinoless double beta decay has been supported by various recent experimental and theoretical results (see Table 1). Assuming the degenerate scenarios to be realized in nature we fix - according to the formulae derived in [14] - the common mass eigenvalue of the degenerate neutrinos to m = $(0.1$ - $3.6)$ eV. Part of the upper range is excluded by tritium experiments, which give a limit of m < $(2.2$ - $2.8)$ eV (95% c.l.) [45]. The full range can only partly (down to $\sim$ 0.5 eV) be checked by future tritium decay experiments, but might be checked by some future $\beta\beta$ experiments (see next section). Recent theoretical work [81] even doubts, that tritium experiments are in *principle* capable to check a $0\nu\beta\beta$ result. The deduced best value for the mass is consistent with expectations from experimental $\mu \rightarrow e\gamma$ branching limits in models assuming the generating mechanism for the neutrino mass to be also responsible for the recent indication for as anomalous magnetic moment of the muon [66]. It lies in a range of interest also for Z-burst models recently discussed as explanation for super-high energy cosmic ray events beyond the GKZ-cutoff [65, 73] and requiring neutrino masses in the range (0.08 - 1.3)

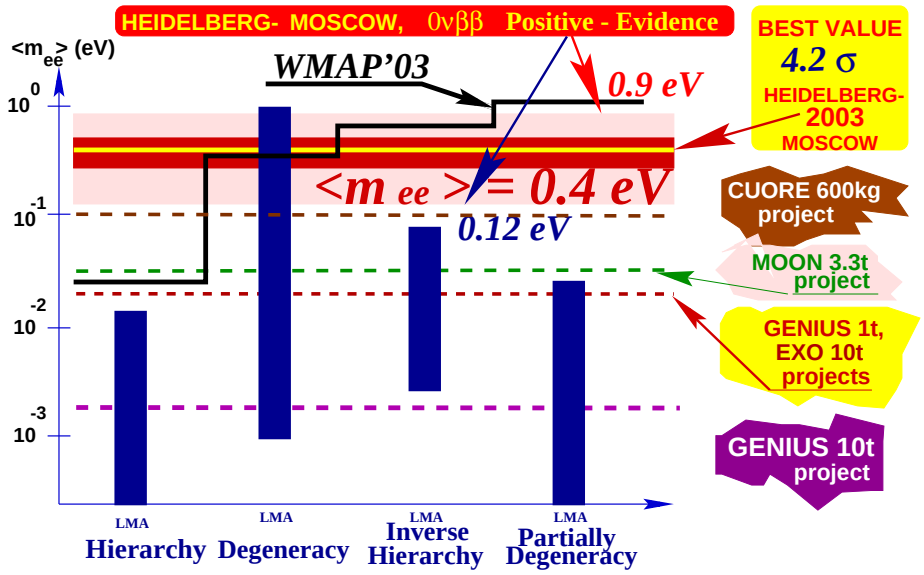

Figure 16: The impact of the evidence obtained at (4.2σ c.l.) for neutrinoless double beta decay (best value of the effective neutrino mass $\langle m \rangle = 0.4\,\mathrm{eV}$, 3σ confidence range (0.1 - 0.9) eV - allowing already for an uncertainty of the nuclear matrix element of a factor of $\pm$ 50%) on possible neutrino mass schemes. The bars denote allowed ranges of $\langle m \rangle$ in different neutrino mass scenarios, still allowed by neutrino oscillation experiments (see [15, 20]). All models except the degenerate one are excluded by the new $0\nu\beta\beta$ decay result. Also shown is the exclusion line from WMAP, plotted for $\sum m_\nu < 1.0\,eV$ [77]. WMAP does not rule out any of the neutrino mass schemes. Further shown are the expected sensitivities for the future potential double beta experiments CUORE, MOON, EXO and the 1 ton and 10 ton project of GENIUS [19, 18, 60, 41] (from [20]).

eV. A recent model with underlying A_4 symmetry for the neutrino mixing matrix also leads to degenerate Majorana neutrino masses > 0.2 eV, consistent with the present result from $0\nu\beta\beta$ decay [68, 71]. The result is further consistent with the theoretical paper of [72]. Starting with the hypothesis that quark and lepton mixing are identical at or near the GUT scale, Mohapatra et al. [72] show that the large solar and atmospheric neutrino mixing angles can be understood purely as result of renormalization group evolution, if neutrino masses are quasi-degenerate (with same CP parity). The common Majorana neutrino mass then must be, in this model, larger than 0.1 eV. An completely independent theoretical proof, that neutrinos should have Majorana nature, has been given recently by [83].

For WMAP a limit for the sum of the neutrino masses of $m_s = \sum m_i < 0.69$ eV at 95% c.l., was given by the analysis of ref. [75]. More realistically this limit on the total mass should be [77] $m_s = \sum m_i < 1.0$ eV at 95%c.l. The latter analysis also shows, that four generations of neutrinos are still allowed and in the case of four generations the limit on the total mass is increased to 1.38 eV. If there is a fourth neutrino with very small mass, then the limit on the total mass of the three neutrinos is even further weakened and there is essentially no constraint on the neutrino masses. In our Fig. 16 we show the contour

line for WMAP assuming $\sum m_i < 1.0$ eV.

A recent analysis of the Sloan Digital Sky Survey, together with WMAP yields [84]

$$m_s = \sum m_i < 1.7 \text{ eV} \qquad \text{at } 2\sigma. \tag{8}$$

Comparison of the WMAP results with the effective mass from double beta decay rules out completely (see [76]) a 15 years old old-fashioned nuclear matrix element of double beta decay, used in a recent analysis of WMAP [78]. In that calculation of the nuclear matrix element there was not included a realistic nucleon-nucleon interaction, which has been included by all other calculations of the nuclear matrix elements over the last 15 years.

The range of $\langle m \rangle$ fixed in this work is, in the range to be explored by the satellite experiments MAP and PLANCK [14, 75, 77]. The limitations of the information from WMAP are seen in Fig. 16, thus results of PLANCK are eagerly awaited.

The neutrino mass deduced leads to $0.002 \geq \Omega_\nu h^2 \leq 0.1$ and thus may allow neutrinos to still play an important role as hot dark matter in the Universe [47].

8 Future of $\beta\beta$ experiments

With the HEIDELBERG-MOSCOW experiment, the era of the small smart experiments is over. New approaches and considerably *enlarged experiments* (as discussed, e.g. in [17, 39, 19, 42, 60, 41, 44, 47]) will be required in future to fix the $0\nu\beta\beta$ half life of ^{76}Ge with higher accuracy. This will, however, because of the uncertainties in the nuclear matrix elements, which probably hardly *can* be reduced to less than 50%, *only marginally reduce* the precision *of the deduced neutrino mass.*

Since it was realized in the HEIDELBERG-MOSCOW experiment, that the remaining small background is coming from the material close to the detector (holder, copper cap, ...), elimination of *any* material close to the detector will be decisive. Experiments which do not take this into account, will allow at best only rather limited steps in sensitivity. Furthermore there is the problem in cryodetectors that they *cannot* differentiate between a β and a γ signal, as this is possible in Ge experiments.

Another crucial point is the energy resolution, which can be optimized *only* in experiments using Germanium detectors, or, to some less extent, with bolometers. It will be difficult to probe evidence for this rare decay mode in experiments, which have to work - as result of their limited resolution - with energy windows around $Q_{\beta\beta}$ of several hundreds of keV.

Another important point is the efficiency of a detector for detection of a $\beta\beta$ signal. For example, with 14% efficiency a potential future 100 kg ^{82}Se experiment would be, because of its low efficiency, equivalent only to a 10 kg experiment (not talking about the energy resolution).

In the first proposal for a third generation double beta experiment, our GENIUS proposal [39, 17, 40, 42, 60, 41], the idea is to use 'naked' Germanium detectors in a huge tank of liquid nitrogen. It seems to be at present the *only* proposal, which can fulfill *both* requirements mentioned above - to increase the detector mass and simultaneously reduce the background drastically. At the *present* status of results of the HEIDELBERG-MOSCOW experiment, however - with a confidence level of $\sim 4\sigma$, it is *questionable*, whether GENIUS would be needed for $\beta\beta$ decay. Probably it would be preferable to

perform an experiment with another isotope *but fulfilling* all requirements mentioned above. The GENIUS-Test-Facility, originally planned to prove the feasibility of some key constructional parameters of GENIUS, and put into operation on May 5, 2003 in GRAN SASSO, could however, play an important role in testing the evidence seen [63] for cold dark matter by DAMA (see [50, 52], and another Report to this volume). Only a GENIUS with some ten tons of enriched ^{76}Ge might possibly be of interest, to investigate whether another exotic mechanism such as exchange of SUSY particles, (see, e.g. [19]) might contribute to the $0\nu\beta\beta$ decay amplitude. This may be, however, a very far dream.

9 Summary

The HEIDELBERG-MOSCOW experiment has been continued regularly in 2003. Unfortunately, it had to stop operation according to non-prolongation of our contract with Kurchatov institute, at 30 November 2003. Since then still various calibration measurements with radioactive sources are going on.

The first analysis of the full data taken with the HEIDELBERG-MOSCOW experiment in the period 2 August 1990 until 20 May 2003 is presented. The improved statistics and data analysis leads to a $\sim 4\sigma$ evidence for a signal at the Q-value for neutrinoless double beta decay. This confirms our earlier claim [1, 2, 5, 6]. Additional support for this evidence has been presented by showing consistency of the result - for the signal, a n d for the background - with other double beta decay experiments using non-enriched or enriched Germanium detectors (see also [7, 11]). In particular it has been shown that the lines seen in the vicinity of the signal are seen also in the other experiments. This is important for the correct treatment of the background. Furthermore, the sensitivity of the peak identification procedures has been demonstrated by extensive statistical simulations. It has been further shown by new extensive simulations of the expected background by GEANT4, that the background around $Q_{\beta\beta}$ should be flat, and that no known gamma line is expected at the energy of $Q_{\beta\beta}$ (see [13]). The 2039 keV signal is seen o n l y in the HEIDELBERG-MOSCOW experiment, which has a *by far larger* statistics than all other double beta experiments.

The importance of first evidence for violation of lepton number and of the Majorana nature of neutrinos is obvious. It requires beyond Standard Model Physics on one side, and may open a new era in space-time structure [62]. It has been discussed that the Majorana nature of the neutrino tells us that spacetime does realize a construct that is central to construction of supersymmetric theories.

One of the consequences of the result of the HEIDELBERG-MOSCOW experiment on the present confidence level, may be, that to obtain *deeper* information on the process of neutrinoless double beta decay, *new experimental approaches, different from all, what is at present persued*, may be required. The unique importance of double beta decay to investigate the neutrino mass, is stressed by the recent observation, that tritium experiments might suffer from principle problems to see a neutrino mass at all [81].

With the successful start of operation of GENIUS-TF with the first four naked Ge detectors in liquid nitrogen on May 5, 2003 in GRAN SASSO, which is described in [49, 50] (see our second contribution to this Report) a historical step has been achieved of a novel technique and into a new domain of background reduction in underground physics in the

search for rare events. In the light of the above comments, natural task of GENIUS-TF will be to look for cold dark matter by the modulation signal.

Acknowledgement:

The authors would like to thank all colleagues, who have contributed to the experiment. Our thanks extend also to the technical staff of the Max-Planck Institut für Kernphysik and of the Gran Sasso Underground Laboratory. We acknowledge the invaluable support from BMBF and DFG, and LNGS of this project. We are grateful to the former State Committee of Atomic Energy of the USSR for providing the monocristalline Ge shielding material used in this experiment.

List of Edited Proceedings (2003)

1. H.V. Klapdor-Kleingrothaus (ed.) Physics Beyond the Standard Model: Beyond the Desert 02, Proc. of Intern. Conf. BEYOND'02, Oulu, Finland, 2-7 Jun 2002, IOP, Bristol, 2003, 734 pages.

2. H.V. Klapdor-Kleingrothaus (ed.) Physics Beyond the Standard Model: Beyond the Desert 03, Proc. of Intern. Conf. BEYOND'03, Tegernsee, Germany, 4-9 June 2003, Springer, Heidelberg, 2004 (in preparation).

List of Publications (2003)

1. H.V. Klapdor-Kleingrothaus, A. Dietz, I.V. Krivosheina, Ch. Dörr and C. Tomei, Phys. Lett. B 578 (2004) 54-62 and hep-ph/0312171, *"Support of Evidence for Neutrinoless Double Beta Decay".*

2. A. Dörr and H.V. Klapdor-Kleingrothaus, Nucl. Instrum. Meth. A 513 (2003) 596-621, *"New Monte-Carlo simulation of the HEIDELBERG-MOSCOW double beta decay experiment".*

3. H.V. Klapdor-Kleingrothaus, O. Chkvorez, I.V. Krivosheina, C. Tomei , Nucl. Instrum. Meth. A 511 (2003) 335-340 and hep-ph/0309157, *"Measurement of the ^{214}Bi spectrum in the energy region around the Q-value of ^{76}Ge neutrinoless double-beta decay".*

4. H.V. Klapdor-Kleingrothaus, A. Dietz, I.V. Krivosheina, C. Dörr, C. Tomei, Nucl. Instrum. Meth. A 510 (2003) 281-289 and hep-ph/0308275, *"Background Analysis around $Q_{\beta\beta}$ for ^{76}Ge Double Beta Decay experiments, and Statistics at Low Count Rates".*

5. H.V. Klapdor-Kleingrothaus and V. Bednyakov, CERN Courier 43 N2 (2003) 29-30, *"Neutrinos Lead Beyond the Desert".*

6. H.V. Klapdor-Kleingrothaus and U. Sarkar, Mod. Phys. Lett. A 18 (2003) 2243 & hep-ph/0304032, *"Consequences of neutrinoless double beta decay and WMAP".*

7. H.V. Klapdor-Kleingrothaus, Int. J. Mod. Phys. A 18 (2003) 4113 & hep-ph/0303217, *"To be or not to Be? - First Evidence for Neutrinoless Double Beta Decay".*

8. G. Bhattacharyya, H.V. Klapdor-Kleingrothaus, H. Päs, A. Pilaftsis, Phys. Rev. D 67 (2003) 113001 and hep-ph/0212169, *"Neutrinoless Double Beta Decay from Singlet Neutrinos in Extra Dimensions".*

9. H.V. Klapdor-Kleingrothaus, Utpal Sarkar, Phys. Lett. B 554 (2003) 45-50 and hep-ph/0211274, *"Neutrinoless double beta decay with scalar bilinears".*

10. H.V. Klapdor-Kleingrothaus, A. Dietz, G. Heusser, I.V. Krivosheina, D. Mazza, H. Strecker, C. Tomei, Astropart.Phys. 18 (2003) 525-530 and hep-ph/0206151, *"First Results from the HDMS experiment in the Final Setup".*

11. H.V. Klapdor-Kleingrothaus, hep-ph/0302237 and in Indian National Science Academy (INSA) - Special issue: Neutrinos, (2003) eds. D. Indumathi, G. Rajasekaran and M.V.N. Murthy; *"One Year of Evidence for Neutrinoless Double Beta Decay".*

12. H.V. Klapdor-Kleingrothaus, Zacatecas Forum in Physics 2002, Zacatecas, Mexico, 11-13 May 2002, Found. Phys. 33 (2003) 813-829, and hep-ph/0302234, *"First Evidence for Neutrinoless Double Beta Decay".*

List of Contributions to Conferences (2003)

1. H.V. Klapdor-Kleingrothaus and I.V. Krivosheina, in Proc. of Intern. Conf. IHEPP03, Valencia, September 2003, PRHEP-AHEP2003/060, *"Status of Absolute Neutrino Mass and Double Beta Decay".*

2. G. Bhattacharyya, H.V. Klapdor-Kleingrothaus, H. Päs*, A. Pilaftsis, in Proc. of Intern. Conf. IHEPP03, Valencia, September 2003, *"Double beta decay and the extra-dimensionsinal seesaw mechanism".*

3. H.V. Klapdor-Kleingrothaus, in Proc. of Intern. Conf. BEYOND'03, Physics Beyond the Standard Model: Beyond the Desert 03, Tegernsee, Germany, 4-9 June 2003, Springer, Heidelberg, 2004, H.V. Klapdor-Kleingrothaus (ed.), *"First Evidence for Neutrinoless Double Beta Decay - and World Status of the Absolute Neutrino Mass".*

4. H.V. Klapdor-Kleingrothaus, in Proc. of Arbeitstreffen "Hadronen und Kerne", Meißen, St.-Afra-Klosterhof, Germany, 8.-11. September 2003, *"Aktueller Status des Neutrinolosen Doppel-Beta-Zerfalls".*

5. H.V. Klapdor-Kleingrothaus in Proc. of Intern. Conf. BEYOND'02, Physics Beyond the Standard Model: Beyond the Desert 02, H.V. Klapdor-Kleingrothaus (ed.), Oulu, Finland, 2-7 Jun 2002, IOP, Bristol, 2003, 215 - 240, *"Further support of evidence for neutrinoless double beta decay".*

6. H.V. Klapdor-Kleingrothaus and U. Sarkar, in Proc. of Intern. Conf. BEYOND'02, Physics Beyond the Standard Model: Beyond the Desert 02, H.V. Klapdor-Kleingrothaus (ed.), Oulu, Finland, 2-7 Jun 2002, IOP, Bristol, 2003, 253 - 269, *"Consequences of neutrinoless double beta decay".*

7. H.V. Klapdor-Kleingrothaus*, A. Dietz, I.V. Krivosheina, Nucl. Phys. Proc. Suppl. 124: 209-213, 2003, D. Cline (ed.), for 5th Intern. UCLA Symposium on Sources and Detection of Dark Matter and Dark Energy in the Universe (DM 2002), Marina del Rey, California, 20-22 Feb 2002, *"Search for Cold and Hot Dark Matter with the HEIDELBERG-MOSCOW Experiment, HDMS, GENIUS and GENIUS-TF".*

8. H.V. Klapdor-Kleingrothaus, in Proc. of International Europhysics Conference on High Energy Physics, European Physical Society (EPS), Aachen, Germany, 17 - 23 July 2003 *"The GENIUS Test Facility in GRAN SASSO".*

9. H.V. Klapdor-Kleingrothaus, Deutsche Physikalische Gesellschaft e. V. (DPG), Aachen, Germany, 24.-28. März, 2003, *"Status of Evidence for Neutrinoless Double Beta Decay".*

10. Ch. Dörr* and H.V. Klapdor-Kleingrothaus, Deutsche Physikalische Gesellschaft e. V. (DPG), Aachen, Germany, 24.-28. März, 2003, *"Neue Ergebnisse für den neutrinobegleiteten Doppelbetazerfall von ^{76}Ge im Rahmen des HEIDELBERG-MOSCOW Experiments".*

11. H.V. Klapdor-Kleingrothaus, in Proc. of Intern. Conf. SUGRA2003, "20 years of SUGRA and the Search for SUSY and Unification", Boston, USA, March 17-20, 2003, *"Status of Evidence for Neutrinoless Double Beta Decay from the HEIDELBERG-MOSCOW Experiment - and Implications for Supersymmetry".*

12. H.V. Klapdor-Kleingrothaus, in Proc. of Neutrinos and implications for physics beyond the standard model, Stony Brook, USA, 11-13 October, 2002, 4113-4128, Int. J. Mod. Phys. A 18 (2003) 4113-4128 and hep-ph/0303217, *"To be or not to Be? - First Evidence for Neutrinoless Double Beta Decay".*

13. H. V. Klapdor-Kleingrothaus, in Proc. of NOON 2003, Japan, Kanazawa, February 2003, World Scientific 2004, eds. Y. Suzuki, hep-ph/0307330, *"Status of Evidence for Neutrinoless Double Beta Decay, and the Future: GENIUS and GENIUS-TF."*

List of Colloquia and Seminars Made During 2003

1. H.V. Klapdor-Kleingrothaus, Physikalisches Institut, Theorie Department, Bonn, 7. November 2003, *"Absolute Neutrino Mass After the First Evidence for Neutrinoless Double Beta Decay - and Implications of Double Beta Decay for Exotic Physics".*

2. H.V. Klapdor-Kleingrothaus, DESY, Zeuthen, Germany, 17 Juli (2003), *"First Evidence for Neutrinoless Double Beta Decay - and World Status of the absolute Neutrino Mass."*

3. H.V. Klapdor-Kleingrothaus, Fachbereich Physik, Bergische Universität Wuppertal, Germany 26 May 2003, *"The Absolute Neutrino Mass After the First Evidence for Neutrinoless Double Beta Decay".*

4. H.V. Klapdor-Kleingrothaus, Physikalisches Institut, Fakultät für Physik und Astronomie, Ruprecht-Karls-Universität, Heidelberg, Germany 28 April 2003, *"Status of Evidence for Neutrinoless Double Beta Decay"*.

5. H.V. Klapdor-Kleingrothaus, Osaka University, Japan, 17 February 2003, *"First Evidence for Neutrinoless Double Beta Decay from the HEIDELBERG-MOSCOW Experiment and Implication for Particle Physics and Astrophysics"*.

6. H.V. Klapdor-Kleingrothaus, Institut für Physik, Universität Mainz, Germany, 22 Januar 2003, *"First Evidence for Neutrinoless Double Beta Decay - and Future of the Field"*.

References

[1] H.V. Klapdor-Kleingrothaus et al. *Mod. Phys. Lett.* **A 16** (2001) 2409 - 2420.

[2] H.V. Klapdor-Kleingrothaus, A. Dietz, I.V. Krivosheina, Part. & Nucl. 110(2002)57.

[3] H.V. Klapdor-Kleingrothaus, hep-ph/0205228, in Proc. of DARK2002, Cape Town, South Africa, February 4 - 9, 2002, eds. by H.V. Klapdor-Kleingrothaus and R.D. Viollier, Springer (2002) 404 - 411.

[4] H.V. Klapdor-Kleingrothaus, hep-ph/0302248, Proc.DARK2002, Cape Town, South Africa, February 4 - 9, 2002, eds. by H.V. Klapdor-Kleingrothaus and R.D. Viollier, Springer (2002) 367 – 403.

[5] H.V. Klapdor-Kleingrothaus, A. Dietz and I.V. Krivosheina, *Foundations of Physics* **31** (2002) 1181-1223 and Corr., 2003: http://www.mpi-hd.mpg.de/non_acc/main_results.html.

[6] H.V. Klapdor-Kleingrothaus, et al., to be publ. 2004.

[7] H.V. Klapdor-Kleingrothaus, A. Dietz, I.V. Krivosheina, Ch. Dörr, C. Tomei, *Phys. Lett.* **B 578** (2004) 54-62 and hep-ph/0312171.

[8] H.V. Klapdor-Kleingrothaus et al., (HEIDELBERG-MOSCOW Col.), *Eur. Phys. J.* **A 12** (2001) 147, Proc. of "Third Intern. Conf. on Dark Matter in Astro- and Particle Physics", DARK2000, ed. H.V. Klapdor-Kleingrothaus, Springer (2001) 520 - 533.

[9] H.V. Klapdor-Kleingrothaus, hep-ph/0205228, and in Proc. of DARK2002, Cape Town, South Africa, February 4 - 9, 2002, eds. by H.V. Klapdor-Kleingrothaus and R.D. Viollier, Springer, Heidelberg (2002) 404 - 411.

[10] H.V. Klapdor-Kleingrothaus, hep-ph/0303217 and in Proc. of "Neutrinos and Implications for Phys. Beyond the SM", Stony Brook, 11-13 Oct. 2002, World Scientific (2003) pp. 367-382.

[11] H.V. Klapdor-Kleingrothaus, A. Dietz, I.V. Krivosheina, Ch. Dörr, C. Tomei, *Nucl. Instr. Meth.* **510 A** (2003) 281-289 and hep-ph/0308275.

[12] H.V. Klapdor-Kleingrothaus, O. Chkvorez, I. V. Krivosheina, C. Tomei, *Nucl. Instr. Meth.* **511 A** (2003) 335-340 and hep-ph/0309157.

[13] Ch. Dörr and H.V. Klapdor-Kleingrothaus, *Nucl. Instr. Meth.* **513 A** (2003) 596-621.

[14] H.V. Klapdor-Kleingrothaus, H. Päs and A.Yu. Smirnov, *Phys. Rev.* **D 63** (2001) 073005 and *hep-ph/***0003219**.

[15] H.V. Klapdor-Kleingrothaus and U. Sarkar, *Mod. Phys. Lett.* **A 16** (2001) 2469.

[16] H V Klapdor-Kleingrothaus, Special issue: Neutrinos, 2003, Proc. Indian Natl. Sci. Acad., hep-ph/0302237.

[17] H.V. Klapdor-Kleingrothaus, *Int. J. Mod. Phys.* **A 13** (1998) 3953.

[18] H.V. Klapdor-Kleingrothaus, *Springer Tracts in Modern Physics*, **163** (2000) 69 - 104, *Springer-Verlag, Heidelberg, Germany* (2000).

[19] H.V. Klapdor-Kleingrothaus, "60 Years of Double Beta Decay - From Nuclear Physics to Beyond the Standard Model", *World Scientific, Singapore* (2001) 1281 p.

[20] H.V. Klapdor-Kleingrothaus and U. Sarkar, hep-ph/0304032, and *Mod. Phys. Lett.* **A 18** (2003) 2243-2254.

[21] H.V. Klapdor-Kleingrothaus, to be publ. 2004, and in Proc. of Third Intern. Conf. on Particle Physics Beyond the Standard Model, BEYOND02, Oulu, Finland, 2-7 June 2002, ed. by H.V. Klapdor-Kleingrothaus, IOP, Bristol 2003, 215 - 240.

[22] M. Hirsch, H.V. Klapdor-Kleingrothaus and S.G. Kovalenko, *Phys. Lett.* **B 398** (1997) 311, *Phys. Lett.* **B 403** (1997) 291, and *Phys. Rev.* **D 57** (1998) 1947.

[23] M. Hirsch, H.V. Klapdor-Kleingrothaus and S.G. Kovalenko, *Phys. Rev. Lett.* **75** (1995) 17, and *Phys. Rev.* **D 53** (1996) 1329, and *Phys. Lett.* **B 372** (1996) 181; and G. Bhattacharya, H.V. Klapdor-Kleingrothaus, H. Päs *Phys. Lett.* **B 463** (1997) 77.

[24] CERN number generators (see e.g. http://root.cern.ch/root/html/TRandom.html)

[25] A. Staudt, K. Muto and H.V. Klapdor-Kleingrothaus, *Eur. Lett.* **13** (1990) 31.

[26] R.B. Firestone and V.S. Shirley, Table of Isotopes, 8th Ed., *John W.%S*, N.Y. (1998).

[27] G. Gilmore et al."Practical Gamma-Ray Spectr.", Wiley and Sons (1995).

[28] G. Douysset et al., *Phys. Rev. Lett.* **86** (2001) 4259 - 4262.

[29] J.G. Hykawy et al., *Phys. Rev. Lett.* **67** (1991) 1708.

[30] G. Audi, A.H. Wapstra, Nucl. Phys. A 595 (1995) 409-480.

[31] R.J. Ellis et al., Nucl. Phys. A 435 (1985) 34-42.

[32] K. Ya. Gromov, priv. communication, 2003.

[33] M.D. Hannam, W.J. Thompson, Nucl. Instr. Meth. A 431 (1999) 239-251.

[34] D. Caldwell, *J. Phys. G* **17**, S137-S144 (1991).

[35] I.V. Kirpichnikov et al. Mod. Phys. Lett. A 5 (1990) 1299 Preprint ITEP, 1991.

[36] I.V. Kirpichnikov, priv. communication, Dec. 3, 2002.

[37] O. Manuel et al., in Proc. Intern. Conf. Nuclear Beta Decays and the Neutrino, eds. T. Kotani et al., World Scientific (1986) 71, *J. Phys. G: Nucl. Part. Phys.* **17** (1991) S221-S229; T. Bernatovicz et al. *Phys. Rev. Lett.* **69** (1992) 2341 - 2344.

[38] R. Lüscher et al., *Phys. Lett.* (1998) 407.

[39] H.V. Klapdor-Kleingrothaus in Proc. of BEYOND'97, First Intern. Conf. on Particle Physics Beyond the Standard Model, Castle Ringberg, Germany, 8-14 June 1997, ed. by H.V. Klapdor-Kleingrothaus and H. Päs, *IOP Bristol* (1998) 485-531.

[40] H.V. Klapdor-Kleingrothaus, J. Hellmig & M. Hirsch, *J. Phys.* **G 24** (1998) 483.

[41] H.V. Klapdor-Kleingrothaus et al. MPI-Report MPI-H-V26-1999, hep-ph/9910205, in Proc. of the 2nd Int. Conf. on Particle Physics Beyond the Standard Model BEYOND'99, Castle Ringberg, Germany, 6-12 June 1999, eds. H.V. Klapdor-Kleingrothaus and I.V. Krivosheina, *IOP Bristol* (2000) 915-1014.

[42] H.V. Klapdor-Kleingrothaus, in Proc. of NEUTRINO 98, Takayama, Japan, 4-9 Jun 1998, (eds) Y. Suzuki et al. *Nucl. Phys. Proc. Suppl.* **77** (1999) 357 - 368.

[43] HEIDELBERG-MOSCOW Coll. (M. Günther et al.), *Phys. Rev.* **D 55** (1997) 54.

[44] H.V. Klapdor-Kleingrothaus, *Nucl. Phys.* **B 100** (2001) 309 - 313.

[45] J. Bonn et al., *Nucl. Phys.* **B 91** (2001) 273 - 279.

[46] H.V. Klapdor-Kleingrothaus, in Proc. of the Int. Symposium on Advances in Nuclear Physics, eds.: D. Poenaru and S. Stoica, *World Scientific, Singapore* (2000) 123-129.

[47] H.V. Klapdor-Kleingrothaus, *Int. J. Mod. Phys.* **A 17** (2002) 3421 -3431, and in Proc. of Intern Conf. LP01, WS 2002, Rome, Italy, July 2001.

[48] H.V. Klapdor-Kleingrothaus and I.V. Krivosheina, in Proc. of International Workshop on Astroparticle and High Energy Physics, Valencia, Spain, September 2003.

[49] H.V. Klapdor-Kleingrothaus, CERN Courier, 2003.

[50] H.V. Klapdor-Kleingrothaus, O. Chkvorez, I.V. Krivosheina, H. Strecker, C. Tomei, *Nucl. Instr. Meth.* **A 511** (2003) 341 - 346 and hep-ph/0309170, and H.V. Klapdor-Kleingrothaus and I.V. Krivosheina, in Proc. of Beyond the Desert 2002, BEYOND02, Oulu, Finland, June 2002, IOP 2003, ed. H.V. Klapdor-Kleingrothaus.

[51] C. Tomei, A. Dietz, I. Krivosheina, H.V. Klapdor-Kleingrothaus, *Nucl. Instr. Meth.* **A 508** (2003) 343-352, and hep-ph/0306257.

[52] H.V. Klapdor-Kleingrothaus et al., *hep-ph/*0103082, *NIM* **A 481** (2002) 149-159.

[53] H.V. Klapdor-Kleingrothaus and I.V. Krivosheina, in Proc. of "Forum of Physics", Zacatecas, Mexico, 11-13 May, 2002, eds. D.V. Ahluwalia and M. Kirchbach, *Found. Phys.* **33** (2003) 831-837.

[54] C. Weinheimer, in Appec meeting, Karlsrhue, 16-18 September 2003, http://www-ik.fzk.de/%7ekatrin/atw/talks.html, and J. Bonn et al., Nucl. Phys. Proc. Suppl. 110 (2002) 395-397.

[55] A.M. Bakalyarov et al. (Moscow grop of HEIDELBERG-MOSCOW experiment), hep-ex/0309016.

[56] H.V. Klapdor-Kleingrothaus et al., in preparation.

[57] C.E. Aalseth et al. (IGEX Collaboration), *Yad. Fiz.* **63, No 7** (2000) 1299 - 1302; *Phys. Rev.* **D 65** (2002) 092007.

[58] H.V. Klapdor-Kleingrothaus, A. Dietz and I.V. Krivosheina, *Phys. Rev.* **D** (2004).

[59] H.V. Klapdor-Kleingrothaus, Part. & Nucl., Lett. 104 (2001) 20 & hep-ph/0102319.

[60] H.V. Klapdor-Kleingrothaus, hep-ph/0103074 and in Proc. NOON 2000, World Scientific, Singapore (2001) 219-234.

[61] H.V. Klapdor-Kleingrothaus, Proc. LowNu2, World Scientific, Singapore (2001) 116-131 and hep-ph/0104028.

[62] D.V. Ahluwalia in Proc. of Beyond the Desert 2002, BEYOND02, Oulu, Finland, June 2002, IOP 2003, ed. H.V. Klapdor-Kleingrothaus, 143-160; D.V. Ahluwalia, M. Kirchbach, *Phys. Lett.* **B 529** (2002) 124.

[63] R. Bernabei et al., Riv. Nuovo Cim. 26 (2003) 1-73.

[64] H.V. Klapdor-Kleingrothaus, in GRAN SASSO Annual Report, 2004.

[65] D. Fargion et al., in Proc. of DARK2000, Heidelberg, Germany, July 10-15, 2000, Ed. H.V. Klapdor-Kleingrothaus, *Springer*, (2001) 455 -468 and in Proc. of Beyond the Desert 2002, BEYOND02, Oulu, Finland, June 2002, IOP 2003, ed. H.V. Klapdor-Kleingrothaus.

[66] E. Ma and M. Raidal, *Phys. Rev. Lett.* 87 (2001) 011802; Erratum-ibid. 87 (2001) 159901.

[67] Y. Uehara, *Phys. Lett.* **B 537** (2002) 256-260 and hep-ph/0201277.

[68] E. Ma in Proc. of Intern. Conf. on Physics Beyond the Standard Model: Beyond the Desert 02, BEYOND'02, Oulu, Finland, 2-7 Jun. 2002, IOP, Bristol (2003) 95 - 106, ed. H.V. Klapdor-Kleingrothaus.

[69] KamLAND Coll., *Phys. Rev. Lett.* **90** (2003) 021802 and hep-ex/0212021.

[70] G. L. Fogli et al., *Phys. Rev.* **D 67** (2003) 073002 and hep-ph/0212127.

[71] K. S. Babu, E. Ma and J.W.F. Valle (2002) hep-ph/0206292.

[72] R. N. Mohapatra, M. K. Parida and G. Rajasekaran, (2003) hep-ph/0301234.

[73] Z. Fodor, S. D. Katz and A. Ringwald, *Phys. Rev. Lett.* **88** (2002) 171101; Z. Fodor et al., *JHEP* (2002) 0206:046, or hep-ph/0203198, and in Proc. of Intern. Conf. on Physics Beyond the Standard Model: Beyond the Desert 02, BEYOND'02, Oulu, Finland, 2-7 Jun 2002, IOP, Bristol, 2003, ed. H V Klapdor-Kleingrothaus and hep-ph/0210123.

[74] J.E. Ruhl et al., astro-ph/0212229.

[75] D.N. Spergel et al., Astrophys. J. Suppl. **148** (2003) 175 and astro-ph/0302209.

[76] A. Pierce and H. Murayama, hep-ph/0302131.

[77] S. Hannestad, *JCAP* **0305** (2003) 004 and astro-ph/0303076.

[78] P. Vogel in PDG (ed. K Hagiwara et al.) *Phys. Rev.* (2002) **D 66** 010001.

[79] S.W. Allen, R.W. Schmidt, S.L. Bridle, *Astron. Astrophys.* **412** (2003) 35-44 and astro-ph/0306386.

[80] A. Blanchard, M. Douspis, M. Rowan-Robinson, S. Sarkar, astro-ph/0304237.

[81] M. Kirchbach, C. Compean and L. Noriega, hep-ph/0310297, and M. Kirchbach in Proc. of BEYOND03, 4th Int. Conf. on Particle Physics Beyond the Standard Model, Castle Ringberg, Germany, 9-14 June 2003, *Springer* (2004), ed. H V Klapdor-Kleingrothaus.

[82] S. Moriyama (for XMASS collaboration), in Proc. of BEYOND'03, 4th Int. Conf. on Particle Physics Beyond the Standard Model, Castle Ringberg, Germany, 9-14 June 2003, *Springer* (2004), ed. H V Klapdor-Kleingrothaus.

[83] R. Hofmann, hep-ph/0401017 v.1.

[84] M. Tegmark et al., astro-ph/0310723.

ICARUS T600: test run and results

S. Amerio[a], S. Amoruso[b], M. Antonello[c], P. Aprili[d], M. Armenante[b], F. Arneodo[d], A. Badertscher[e], B. Baiboussinov[a], M. Baldo Ceolin[a], G. Battistoni[f], B. Bekman[g], P. Benetti[h], E. Bernardini[d], M. Bischofberger[e], A. Borio di Tigliole[h], R. Brunetti[h], R. Bruzzese[b], A. Bueno[e,i], E. Calligarich[h], M. Campanelli[e], F. Carbonara[b], C. Carpanese[e], D. Cavalli[f], F. Cavanna[c], P. Cennini[j], S. Centro[a], A. Cesana[k,f], C. Chen[l], D. Chen[l], D.B. Chen[a], Y. Chen[l], R. Cid[i], D.B. Cline[m], K. Cieślik[n], A.G. Cocco[b], D. Corti[a], Z. Dai[e], C. De Vecchi[h], A. Dąbrowska[n], A. Di Cicco[b], R. Dolfini[h], A. Ereditato[b], M. Felcini[e], A. Ferella[c], A. Ferrari[j,f], F. Ferri[c], G. Fiorillo[b], S. Galli[c], D. Garcia Gamez[i], Y. Ge[e], D. Gibin[a], A. Gigli Berzolari[h], I. Gil-Botella[e], K. Graczyk[o], L. Grandi[h], A. Guglielmi[a], K. He[l], J. Holeczek[g], X. Huang[l], C. Juszczak[o], D. Kiełczewska[p,q], J. Kisiel[g], T. Kozłowski[p], H. Kuna-Ciskał[r], M. Laffranchi[e], J. Łagoda[q], Z. Li[l], B. Lisowski[m], F. Lu[l], J. Ma[l], G. Mangano[b], G. Mannocchi[s,t], M. Markiewicz[n], A. Martinez de la Ossa[i], C. Matthey[m], F. Mauri[h], D. Mazza[c], A.J. Melgarejo[i], A. Menegolli[h], G. Meng[a], M. Messina[e], J.W. Mietelski[n], C. Montanari[h], S. Muraro[f], S. Navas-Concha[e,i], M. Nicoletto[a], J. Nowak[o], G. Nurzia[c], C. Osuna[i], S. Otwinowski[m], Q. Ouyang[l], O. Palamara[d], D. Pascoli[a], L. Periale[s,t], G. Piano Mortari[c], A. Piazzoli[h], P. Picchi[u,t,s], F. Pietropaolo[a], W. Półchłopek[v], M. Prata[h], T. Rancati[f], A. Rappoldi[h], G.L. Raselli[h], J. Rico[e], E. Rondio[p], M. Rossella[h], A. Rubbia[e], C. Rubbia[h], P. Sala[f,e], R. Santorelli[b], D. Scannicchio[h], E. Segreto[c], Y. Seo[m], F. Sergiampietri[m,w], J. Sobczyk[o], N. Spinelli[b], J. Stepaniak[p], R. Sulej[x], M. Szeptycka[p], M. Szarska[n], M. Terrani[k,f], G. Trinchero[s,t], R. Velotta[b], S. Ventura[a], C. Vignoli[h], H. Wang[m], X. Wang[b], J. Woo[m], G. Xu[l], Z. Xu[l], X. Yang[m], A. Zalewska[n], J. Zalipska[p], C. Zhang[l], Q. Zhang[l], S. Zhen[l], W. Zipper[g]

[a] Università di Padova e INFN, Padova, Italy
[b] Università Federico II di Napoli e INFN, Napoli, Italy
[c] Università dell'Aquila e INFN, L'Aquila, Italy
[d] INFN - Laboratori Nazionali del Gran Sasso, Assergi, Italy
[e] Institute for Particle Physics, ETH Hönggerberg, Zürich, Switzerland
[f] Università di Milano e INFN, Milano, Italy
[g] Institute of Physics, University of Silesia, Katowice, Poland
[h] Università di Pavia e INFN, Pavia, Italy
[i] Dpto de Física Teórica y del Cosmos & C.A.F.P.E., Universidad de Granada, Granada, Spain
[j] CERN, Geneva, Switzerland
[k] Politecnico di Milano (CESNEF), Milano, Italy
[l] IHEP - Academia Sinica, Beijing, People's Republic of China
[m] Department of Physics, UCLA, Los Angeles, USA
[n] H.Niewodniczański Institute of Nuclear Physics, Kraków, Poland
[o] Institute of Theoretical Physics, Wroclaw University, Wroclaw, Poland
[p] A.Soltan Institute for Nuclear Studies, Warszawa, Poland
[q] Institute of Experimental Physics, Warsaw University, Warszawa, Poland
[r] Institute of Mechanics and Machine Design, Cracow University of Technology, Kraków, Poland
[s] IFSI, Torino, Italy
[t] INFN Laboratori Nazionali di Frascati, Frascati, Italy
[u] Università di Torino, Torino, Italy
[v] University of Mining and Metallurgy, Kraków, Poland
[w] INFN, Pisa, Italy
[x] Warsaw University of Technology, Warszawa, Poland

Abstract

The ICARUS T600 detector is the largest liquid Argon TPC ever built, with a size of about 500 tons of fully imaging mass. The design and assembly of the detector relied on industrial support and represents the applications of concepts matured in laboratory tests to the kton scale.

The detector was developed as the first element of a modular design. Thanks to the concept of modularity, it will be possible to realize a detector with several ktons active mass, to act as an observatory for astroparticle and neutrino physics at the Gran Sasso Underground Laboratory and a second generation nucleon decay experiment.

The ICARUS T600 was commissioned in 2001 for a technical run performed at surface in the Pavia INFN site. The run lasted about three months. During this period all the detector features were extensively tested with an exposure to cosmic–rays with a resulting data collection of about 30000 events.

Extensive off-line data analysis has been performed in since the run stop and led to important physical and technological results. Most of these have been published in 2003 or are being submitted for publication.

In this report a description of the ICARUS T600 is first given, followed by short summaries of the main outcome of some dedicated studies based on the test run data.

1 Introduction

The technology of the Liquid Argon Time Projection Chamber (LAr TPC), first proposed by C. Rubbia in 1977 [1], was conceived as a tool for a completely uniform imaging with high accuracy of massive volumes. The operational principle of the LAr TPC is based on the fact that in highly purified LAr ionization tracks can be transported practically undistorted by a uniform electric field over macroscopic distances. Imaging is provided by a suitable set of electrodes (wires) placed at the end of the drift path continuously sensing and recording the signals induced by the drifting electrons.

Non–destructive read–out of ionization electrons by charge induction allows to detect the signal of electrons crossing subsequent wire planes with different orientation. This provides several projective views of the same event, hence allowing space point reconstruction and precise calorimetric measurement.

The LAr TPC was developed in the context of the ICARUS programme and currently finds its application in studies concerning some of the major issues of particle and astroparticle physics:

- the study of solar and atmospheric neutrino interactions;
- the study of nucleon decay for some channels predicted by GUTs;
- the detection of neutrinos following a Supernova explosion;
- the study of neutrino oscillations with beams from particle accelerators.

After the original proposal, the feasibility of the technology has been first demonstrated by an extensive R&D programme, which included ten years of studies on small LAr volumes and five years of studies with several prototypes of increasing mass[2, 3, 4, 5, 6, 7, 8, 9, 10, 11, 12, 13, 14, 15, 16].

The second step was represented by the construction of the T600 module[17]: a detector employing about 600 tons of liquid Argon to be operated at LNGS. This step–wise strategy allowed to progressively develop the necessary know–how to build a multi–kton liquid Argon detector.

The realization of the T600 detector (from design to construction) lasted about four years and culminated with the full test of the experimental set–up, carried out at surface during 2001. This test demonstrated the maturity of the project. All technical aspects of the system, namely cryogenics, LAr purification, read–out chambers, detection of LAr scintillation light, electronics and DAQ had been tested and performed as expected. Statistically significant samples of cosmic–ray events (long muon tracks, spectacular high–multiplicity muon bundles, electromagnetic and hadronic showers, low energy events) were recorded. The subsequent analysis of these events, carried out in 2002-03, has allowed the development and fine tuning of the off–line tools for the event reconstruction and the extraction of physical quantities. It has also demonstrated the performance of the detector in a quantitative way, issuing in a number of papers recently published or accepted for publication.

Beyond the T600, the ICARUS Collaboration has proposed an extension of the sensitive mass to about 3000 tons, also in view of the realization of experiments in the CNGS

neutrino beam from CERN to Gran Sasso, by cloning the present T600 module [18]. This scientific programme has been approved by both CERN and INFN.

The first part of this report is dedicated to a brief description of the T600 detector and of its technical performance as obtained from acceptance tests. This description complements the experimental results obtained from the data collected during the test run and reported in the subsequent sections:

- Analysis of the liquid Argon purity in the T600 detector [19];
- Observation of very long ionizing tracks [20];
- Measurement of the muon decay spectrum [21];
- Study of ionization quenching in liquid Argon [22];

2 Detector overview

Extracted from "Design, construction and tests of the ICARUS T600 detector", ICARUS Collaboration, accepted for publication on NIM A (Dec. 2003).

ICARUS T600 (Fig. 1) is composed of a large cryostat split into two identical, adjacent half–modules, each one with internal dimensions of 3.6 m (width) $\times$ 3.9 m (height) $\times$ 19.6 m (length). Each half–module houses an inner detector made of two Time Projection Chambers, the field shaping system, monitors and probes, and of a system for the LAr scintillation light detection. The half–modules are externally surrounded by thermal insulation layers. In the following, we shall refer to each half–module as "T300". The full scale test reported was carried on after the commissioning of one T300.

Dimensions and shape of the cryostat were defined by the requirement that the LAr containers (cold vessels) had to be transported through the Italian highways into the underground Gran Sasso Laboratory and installed there. In order to collect significant samples of solar and atmospheric neutrino events, the ICARUS Collaboration adopted a solution with two coupled containers with dimensions corresponding to a total LAr volume of about 550 m^3.

Outside the detector are located the read–out electronics, on the top side of the cryostat, and the cryogenic plant composed of a liquid Nitrogen (LN_2) cooling circuit and of a system of purifiers needed to achieve the required LAr purity.

The inner detector structure of each T300 consists of two TPCs (called *left* and *right* chambers) separated by a common cathode. Each TPC is made of three parallel wire–planes, 3 mm apart, oriented at 60 degrees with respect to each other, with a wire pitch of 3 mm, as shown in Fig. 2. The three wire planes of each TPC are held by a sustaining frame (see Fig. 3) positioned onto the longest walls of the half–module. The total number of wires in the T600 detector is 53248. The read–out of the signals induced on the TPC wires by the electron drift allows a full three–dimensional (3D) image reconstruction of the event topology.

A uniform electric field perpendicular to the wires is established in the LAr volume of each half–module by means of a high voltage (HV) system, as required to allow and guide

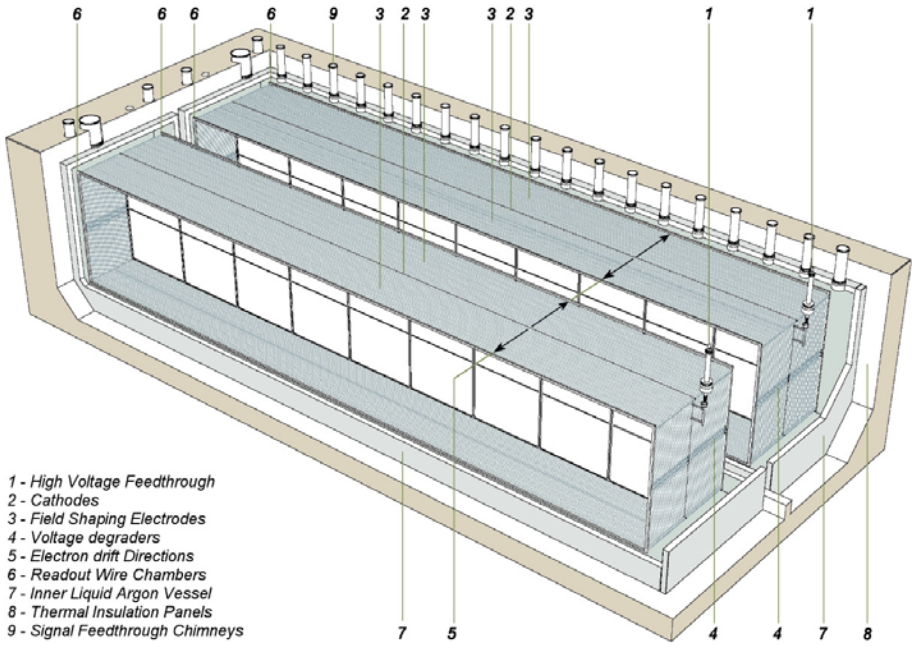

Figure 1: Artist cutaway view of the ICARUS T600 detector.

the drift of the ionization electrons. The system is composed of a cathode plane, parallel to the wire planes, placed in the center of the LAr volume of each half–module at a distance of about 1.5 m from the wires of each side. This distance defines the maximum drift path (see Fig. 3). The HV system is completed by field shaping electrodes to guarantee the uniformity of the field along the drift direction, and by a HV feedthrough to set the required voltage on the cathode. At the nominal voltage of 75 kV, corresponding to an electric field of 500 V/cm, the maximum drift time in LAr is about 1 ms.

The top side of the cryostat hosts the exit flanges equipped with cryogenic feedthroughs for the electrical connection of the wires with the read–out electronics, and for all the internal instrumentation (PMTs, LAr purity monitors, level and temperature probes, etc.).

The electronic chain is designed to allow for continuous read–out, digitization (with a sampling time of 0.4 μs) and wave–form recording of the signals from each wire of the TPC. It is composed of three basic units, see Fig. 4, serving 32 channels:

1. the decoupling board receives analog signals from the TPC wires via vacuum tight feedthrough flanges and passes them to the analog board. It also provides biasing of the wires and distribution of calibration signals;

2. the analog board houses the signal amplifiers, performs 16:1 multiplexing and the data conversion (10 bit) at a 40 MHz rate;

3. the digital board uses custom programmable chips (two per board) specially developed for ICARUS, called DAEDALUS, that implement a hit finding algorithm. Each board receives the multiplexed digital data via an external serial–link cable.

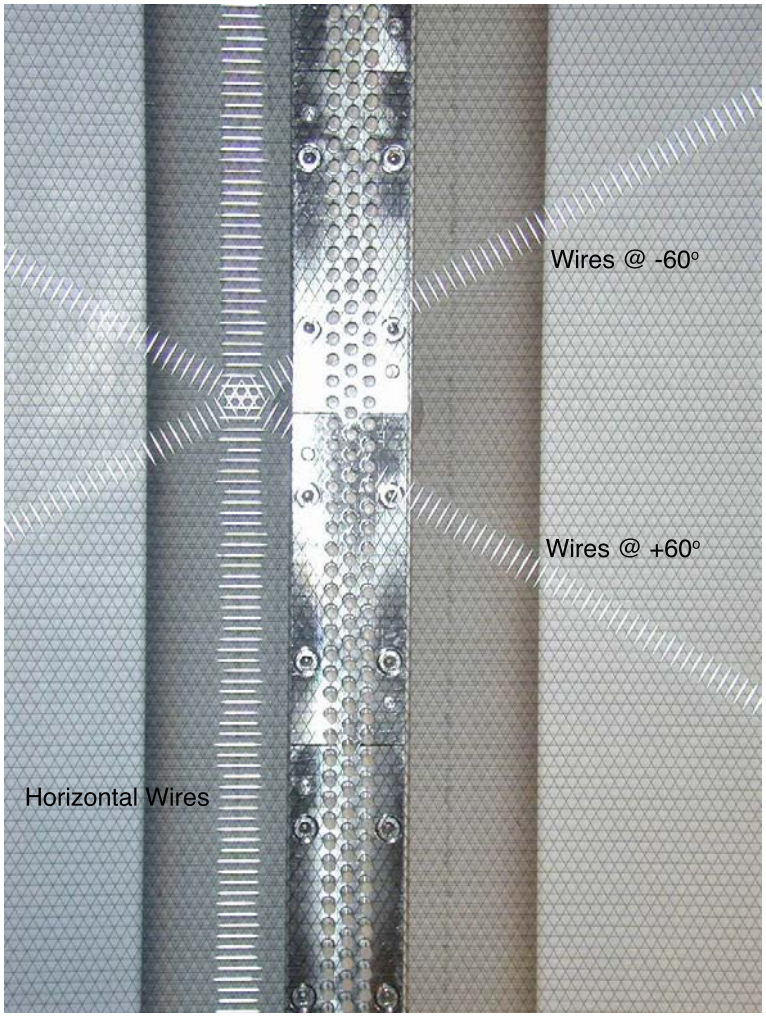

Figure 2: Picture of the three wire planes of a TPC installed in the T600 detector.

Ionization in LAr is accompanied by scintillation light emission. Detection of this light can provide an effective method for absolute time measurement of the event, as well as an internal trigger signal. A system to detect this LAr scintillation light has been implemented based on large–surface (8") PMTs directly immersed in the LAr, see Fig. 5.

The spatial reconstruction of ionizing tracks inside the LAr volume is performed by the simultaneous exploitation of the charge and of the light release following the energy loss processes of charged particles which cross the detector:

1. electrons from ionization induce detectable signals on the TPC wires during their drift motion towards and across the wire planes (wire coordinate);

2. UV photons from scintillation provide a prompt signal on the PMTs that allows the measurement of the absolute drift time and, hence, of the distance traveled by the drifting electrons (drift coordinate).

In this way, each of the planes of the TPC provides a two–dimensional projection of

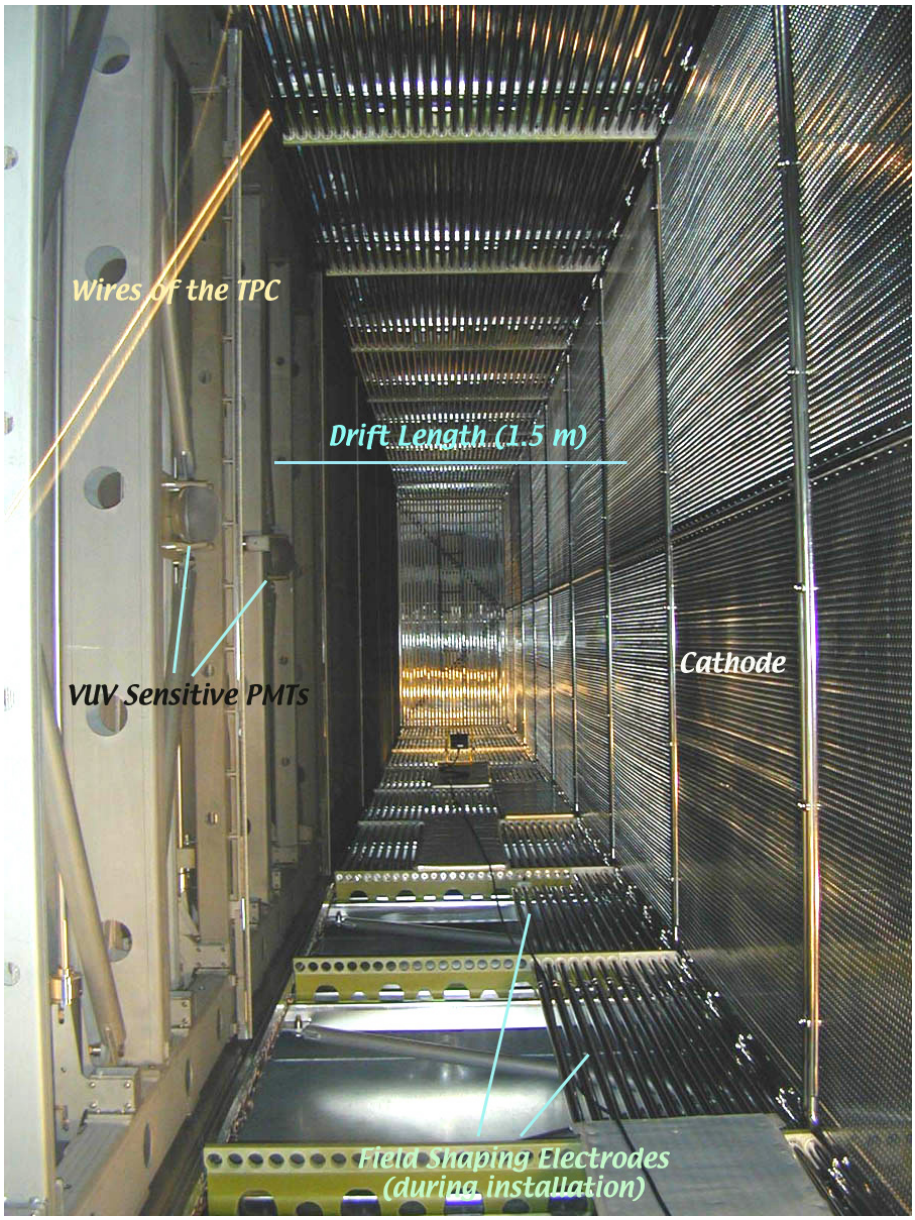

Figure 3: Picture of the inner detector layout inside the first half–module: the cathode (vertical plane on the right) divides the volume in two symmetric sectors (*chambers*). The picture refers to the left sector where wires and mechanical structure of the TPC and some photo–multipliers (PMTs) are visible.

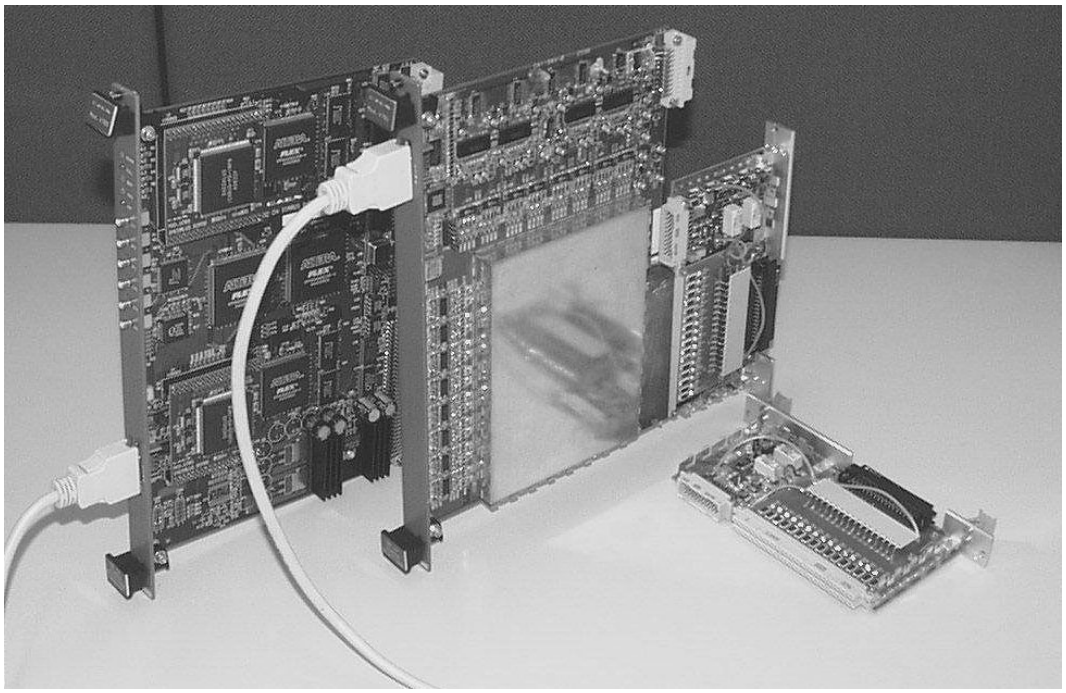

Figure 4: The three basic electronics modules: the small decoupling board (DB) that receives 32 analog signals from the chamber via the feedthrough and passes them to the analog board; the analog board (V791 by CAEN) that houses the amplifiers for 32 channels; the digital board (V789 by CAEN) Arianna that has the two DAEDALUS VLSI, mounted on small piggy back PCBs.

the event image, with one coordinate given by the wire position and the other by the drift distance. The Collection view of a spectacular cosmic–ray event composed of many parallel tracks is displayed in Fig. 6. The event extends up to the full length (about 18 m) and drift (1.5 m) of the detector, as shown in the upper image. The zoomed regions show several electromagnetic and hadronic showers, muon tracks and low energy electrons from γ-conversion.

The various projections have a common coordinate (the drift distance). A full 3D reconstruction of the event is obtained by correlating the signals from two different planes at the same drift distance (e.g. see Sec. 5).

The calorimetric measurement of the energy deposited by the ionizing particle in the LAr volume is obtained by collecting information from the last of the three wire planes, working in charge collection mode (e.g. see Sec. 4).

3 Measurements of LAr purity

Extracted from "Analysis of the Liquid Argon Purity in the ICARUS T600 TPC", ICARUS Collaboration, Nucl. Inst. Meth., A **516** (2004), 68.

Liquid Argon must be ultra–pure, even in the presence of a large number of feedthroughs for the signals and the high voltage supplies, and with wire chambers, cables, etc. in the

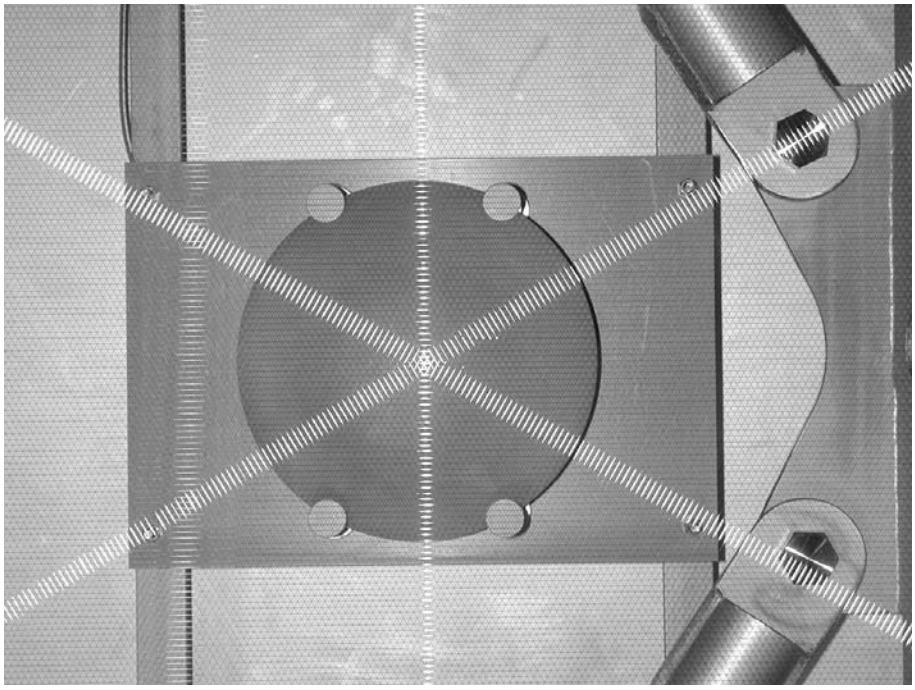

Figure 5: Picture one of the PMTs visible behind the three wire planes.

clean volume. The contamination of electronegative molecules must be as low as 0.1 ppb to allow drifts over long distances (meters) without capture of the ionization electrons. Argon purification is performed by means of a liquid and a gas recirculation systems. On top of the detector, the recirculation of the gas phase is implemented by flowing the gas through commercial purification cartridges. The recirculation in liquid phase is performed by a pump which forces liquid Argon into similar commercial cartridges.

During the drift path in LAr, attachment to impurities may take place reducing the amount of electron charge collected by the anode, compared to the charge initially released. The ratio of these charges is a function of the electron lifetime in LAr (τ_e) that can therefore be estimated. The lifetime is directly connected to the impurity concentration by an inverse linear relationship. The lifetime estimate thus provides a direct measurement of the LAr impurity content.

Two methods are used to measure the drift electron lifetime. The first one is based on the use of dedicated devices, the "purity monitors", that provide an on-line and local estimate of the drift electron lifetime. The second method is based on the off-line analysis of the collected events, by studying the attenuation of the signal amplitude as a function of the electron drift distance.

With the first method, the purity monitor geometry and the applied electric field are such that the device is sensitive up to several milliseconds lifetime with errors at the level of $<10\%$. The purity monitors were positioned at different heights in order to follow the drift electron lifetime level during the filling of the cryostat, to provide redundant readings during the steady-running phase, as well as indications on any possible lifetime gradient in the volume.

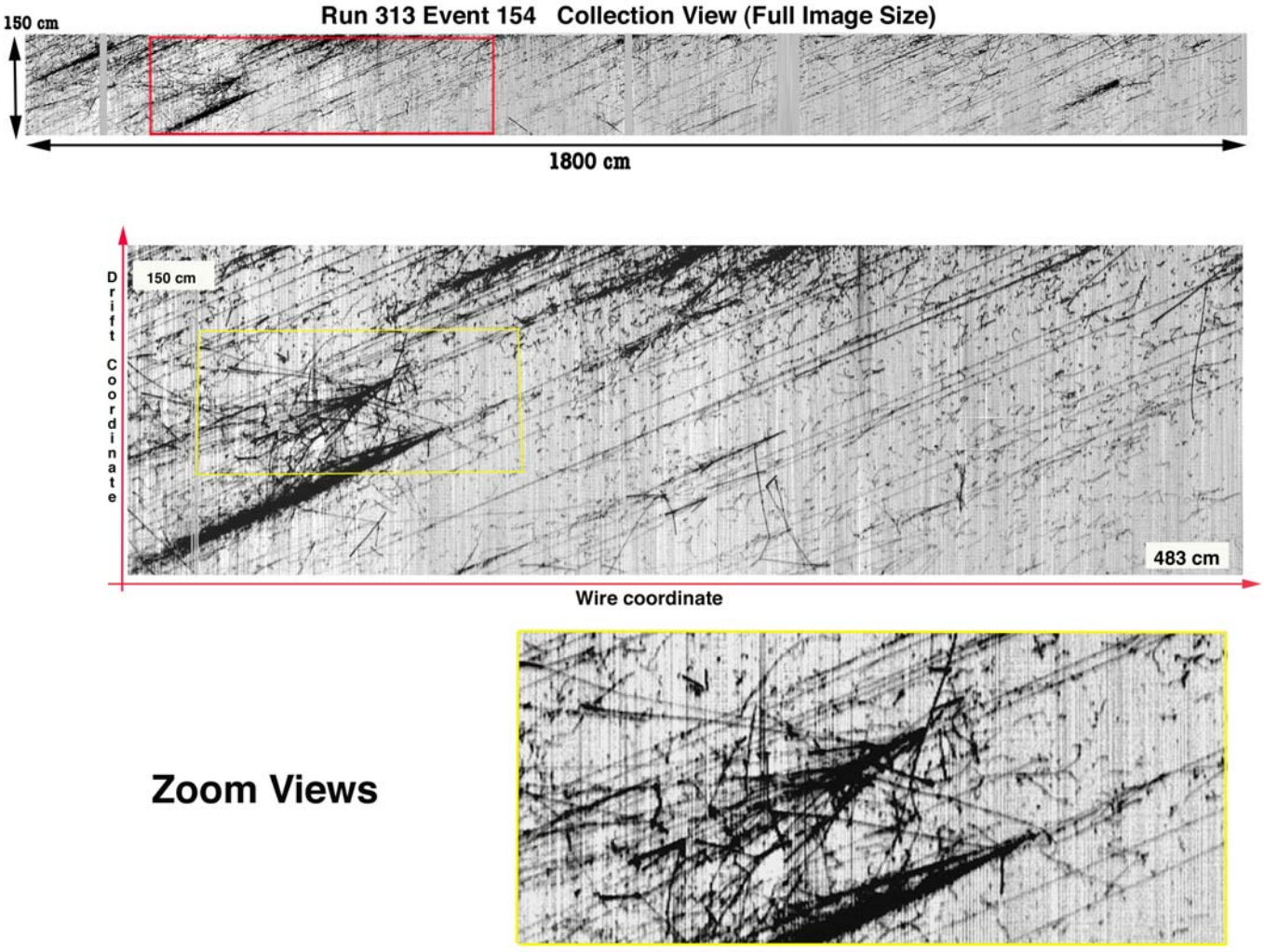

Figure 6: Run 313, Event 154, Collection view. Extensive air shower.

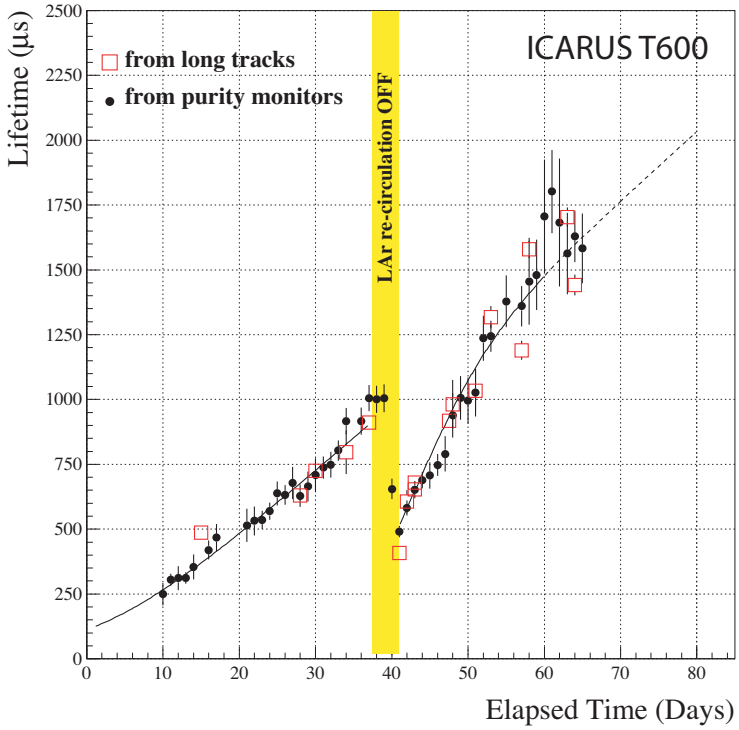

Figure 7: Evolution of the free electron lifetime during the T600 test run from purity monitor (*dots*) and from ionizing tracks analysis (*squares*). The period when the liquid re-circulation was switched off is indicated.

The drift electron lifetime evolution measured by the purity monitor located close to the extraction point of the LAr recirculation system (in one corner of the volume, at about 3.6 m height from the bottom of the cryostat) is reported in Fig. 7 (*dots*). The first data points, recorded just after filling, indicated a value in the range of 250 μs. The electron lifetime increased steadily when the recirculation systems were operated. At the run stop, the lifetime reached a maximum value of about 1.8 ms ($\pm 8\%$ error) and was still growing. The trend in Fig. 7 clearly shows how the steady increase of the drift electron lifetime was interrupted during the period when the liquid recirculation was turned off.

The working principle of the second method can be summarized as follows: after the spatial reconstruction of the tracks crossing the detector active volume and produced by cosmic m.i.p. events, the distributions of the charge (ΔQ) measured on the collection wires for 15 slices of the drift coordinate (10 cm wide each) are obtaned. For each slice, the value of the most probable charge released by the track (ΔQ_{mp}) is extracted by fitting the distribution to a Landau function, convoluted with a Gaussian function that describes the effect of the electronic noise of the read-out system. ΔQ_{mp} corresponds to the most probable value of the fitted distribution. Once this procedure is applied to all slices, the electron lifetime is given by an exponential fit of ΔQ_{mp} as a function of the drift coordinate (see also Sec. 4).

As an example, Fig. 8 shows the result of such a fit obtained for the tracks of a single multi-muon event. The inverse of the slope gives a drift electron mean free path of 220 cm corresponding to a drift electron lifetime of 1.43 ± 0.07 ms (error from the fit). This value can be considered as the *average* electron lifetime within the chamber, since the chosen tracks span the full liquid Argon volume in a rather uniform way.

The measured value of the electron lifetime τ_e can be used to account for the charge attenuation occurring during the drift process and to reconstruct the "corrected charge" ΔQ_{cor} released by the track:

$$\Delta Q_{cor} \; = \; e^{\,t_d/\tau_e} \; \cdot \Delta Q \tag{1}$$

where ΔQ is the charge measured on the wire and t_d is the drift time associated to the hit, obtained from the peak time of the hit and the T_0 of the event.

The same procedure was used to extract the electron lifetime at different data periods. The summary of the obtained values of τ_e as function of time is reported in Fig. 7 (squares).

Both methods show consistent results over the whole data taking period. Since the selected tracks were randomly distributed over the volume, the compatibility between the purity monitor and the tracks is consistent with a uniform purity within the whole volume.

4 Observation of very long ionizing tracks

Extracted from "Observation of Long Ionizing Tracks with the ICARUS T600 First Half–Module", ICARUS Collaboration, Nucl. Inst. Meth., A **508** (2003), 287.

During the test run, the coincidence of two scintillator vertical planes suitablypositioned onto the opposite end-caps of the T300 module providedtrigger signals for the

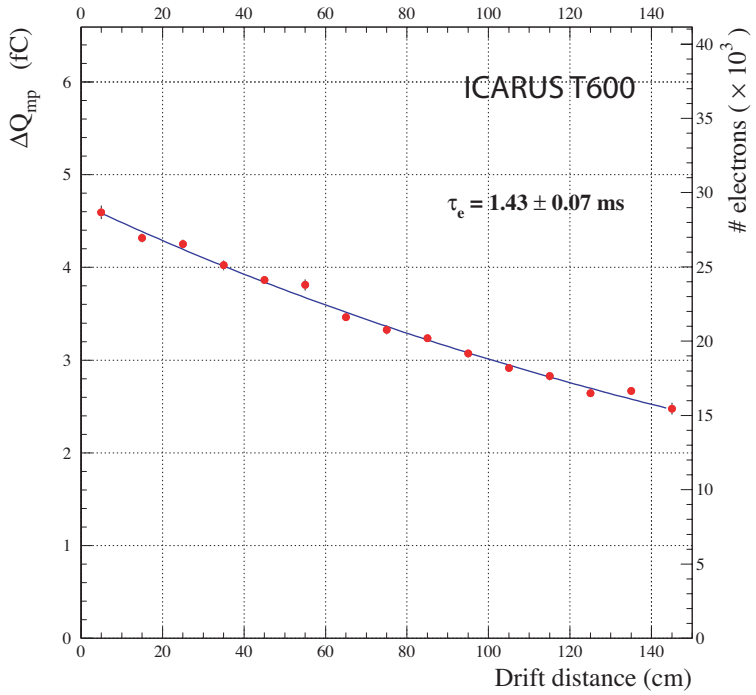

Figure 8: Determination of the drift electron lifetime from minimum ionizing tracks crossing the detector: exponential fit of the most probable value of the measured charge as a function of the drift distance (15 slices). The number of equivalent electrons is indicated on the right vertical axis.

long-awaited, almost horizontal muon tracks crossing up to the entire length of the detector.

Thanks to the unique features ofthe LAr-TPC, fine resolution and high granularity extended over verylarge active detector mass, the amount of information collected for these long tracks is such that accurate event analysis can beperformed at single event level.

Each single muon track from the external scintillator trigger is sampled by a very large number of wires onthe *collection*-plane of the two TPC's. The portion of the muon track length exposed to each wire (we refer to as the *track pitch length* Δx [cm]) depends on the relative orientationin space of the track with respect to the wire plane and to the orientationof the wires in the plane itself. The *track pitch length* foreach track can be calculated from the 3D reconstruction of the track. Using suitable algorithms applied

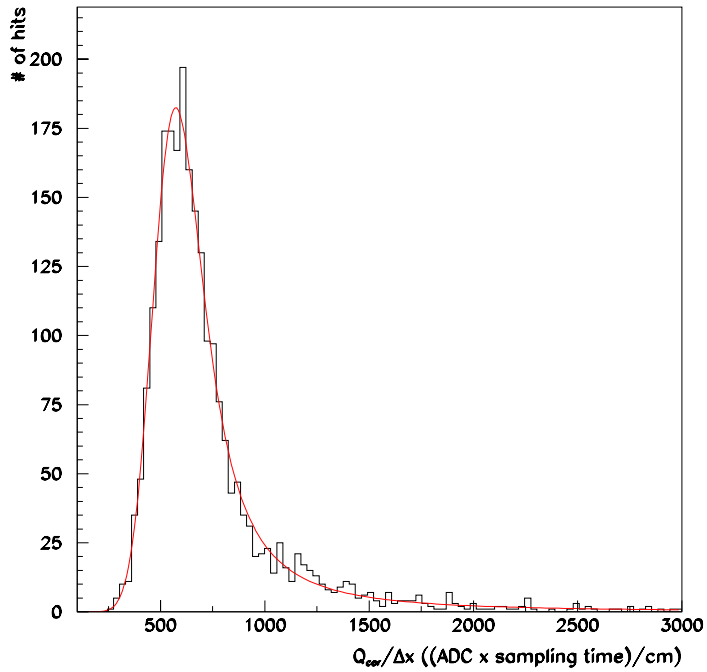

Figure 9: Distribution of the hit amplitude (lifetime corrected)per unit of track pitch length (0.4 μs of sampling time) for a single long muon track triggeredby the external scintillator system.The continuous line corresponds to the result of a fit with a convolution of a Landau function and a Gaussian function.

on the waveform recorded fromeach wire we extract the physical parameters (time and amplitude ΔQ) of the individual signal (the hit) corresponding to the track pitch seen by the current wire.

Attenuation during the drift motion by attachment to electro-negative impurities diluted in LAr is off-line corrected, ΔQ_{cor}, by knowing the level of purity of the liquid, routinely measured by dedicated devices during the run, according to Eq. (1).

This charge is in turn proportional to the energy released by the muonalong the pitch length. Therefore, the distribution of values $\Delta Q_{cor}/\Delta x$from a single muon track reconstruction on the *collection*-plane can be directly related tothe Landau distribution dE/dx [MeV/cm] of the energyreleased per unit track length along the muon track inside the detector active volume.The distribution of $\Delta Q_{cor}/\Delta x$ for a single track (e.g. *Run.* 893, *Evt.* 14) is shown in Fig. 9. On the same plot we report the result of a fit with a convolution of a Landau function and a Gaussian function(the Gaussian function describes fluctuations in the measured hit amplitude due to various sources, the main one being electronic noise). The fit gives the most probable value of the Landau distribution, determined with high precision. From comparison with Monte Carlo simulation, this allows exploitation of a self-calibration method for the calorimetric measurement of the energydeposited by long muon tracks (with accuracy at the level of $\mathcal{O}(\leq 3\%)$). This result entirely relies on the unique featuresof the ICARUS technology.

5 Measurement of the μ decay spectrum

Extracted from "Measurement of the Muon Decay Spectrum with the ICARUS T600 Liquid Argon TPC", ICARUS Collaboration, accepted for publication on EPJ (Nov. 2003).

The sample of events in which a muon enters, stops and eventually decays in the detector's sensitive volume – the *stopping muon* sample – constitutes an important benchmark to evaluate the physics performance of ICARUS. Because of their simple topology, stopping muon events are relatively easy to reconstruct in space, allowing the computation of the different calibration factors needed in the full calorimetric reconstruction. Thus, we can study the muon decay spectrum and measure the Michel ρ parameter, which constitutes the first physics measurement performed with the novel ICARUS detector technology, and proves that the technique is mature enough to produce physics results. Our new result is not competitive with those obtained from dedicated μ decay experiments, and barely with those obtained from τ decay experiments. However, it must be remarked that this result has been obtained using a limited statistics (1858 muon decay events) with a non optimized experiment (the first T600 test run). Our result stresses the capabilities of the ICARUS technology to produce robust physics results.

Data selection was carried out by visual scanning using topological criteria. Stopping muons can be recognized as minimum ionizing tracks entering the detector, with increasing energy deposition and multiple scattering angle when approaching the stopping point. For muon-decay events, a minimum ionizing electron track (length shorter than $\sim$23 cm) follows the muon. A full 3D reconstruction of the selected muon events is first performed. Figure 10 shows a 3D reconstructed stopping muon event. The muon decay topology is visible, with three reconstructed tracks corresponding to the muon, the decay electron and a $\gamma - e$ conversion, respectively.

The ionization charge released by the electron track is precisely measured at the Collection wire plane. The energy associated to a given hit is then related to the collected charge by means of suitable calibration factors (see Sec. 4). A total of 2690 stopping

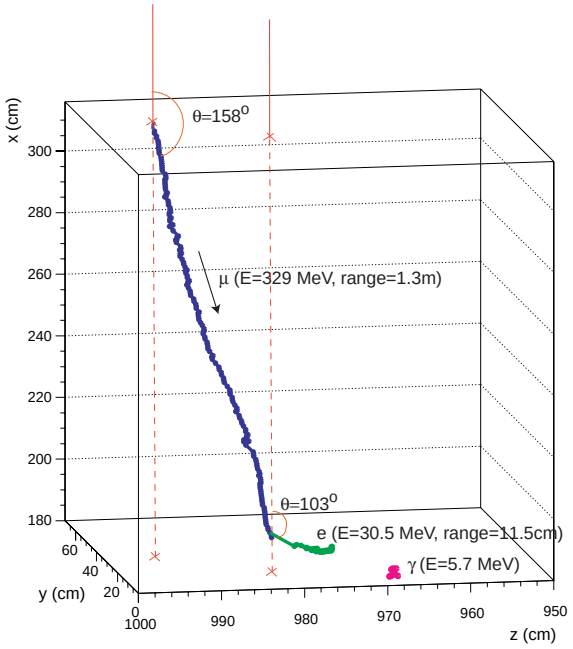

Figure 10: Run 966 Event 8 Right chamber: fully reconstructed muon decay event.

muon events were selected, with 1858 events containing electrons available for the determination of the Michel ρ. The measured electron energy does not correspond directly to the μ decay spectrum since no attempt to recover the energy loss by Bremsstrahlung radiation has been carried out. The spectrum corresponds in fact to the fraction of the electron energy lost only by ionization in LAr. Therefore, in order to measure the Michel ρ parameter we have chosen an approach based on the comparison with a Monte Carlo (MC) simulated event sample. The measured and simulated energy spectra are compared in Figure 11, and they are found to be in good agreement ($\chi^2/ndf = 14.0/20$). We extract the value of ρ as that for which the best fit between the simulated and measured energy spectra is obtained, which yields $\rho = 0.72 \pm 0.06$ in agreement with the SM value $\rho = 0.75$. This measurement involves the exploitation of both spatial and calorimetric reconstruction capabilities of the detector. Therefore, the obtained result constitutes a proof of the maturity of the detection technique to produce high quality physics results.

6 Analysis of Electron recombination

Extracted from "Study of the Electron Recombination in Liquid Argon with the ICARUS TPC", ICARUS Collaboration, accepted for publication on NIM (Oct. 2003).

The stopping muon sample in the T600 data has also been used to studythe behavior of electron recombination in Liquid Argon as a function ofstopping power. Due to electron-ion recombination inside the track, the collected charge Q is less than the produced charge Q_0 : $Q = \mathcal{R}Q_0$,where the recombination factor $\mathcal{R}$ depends on the drift electric field and

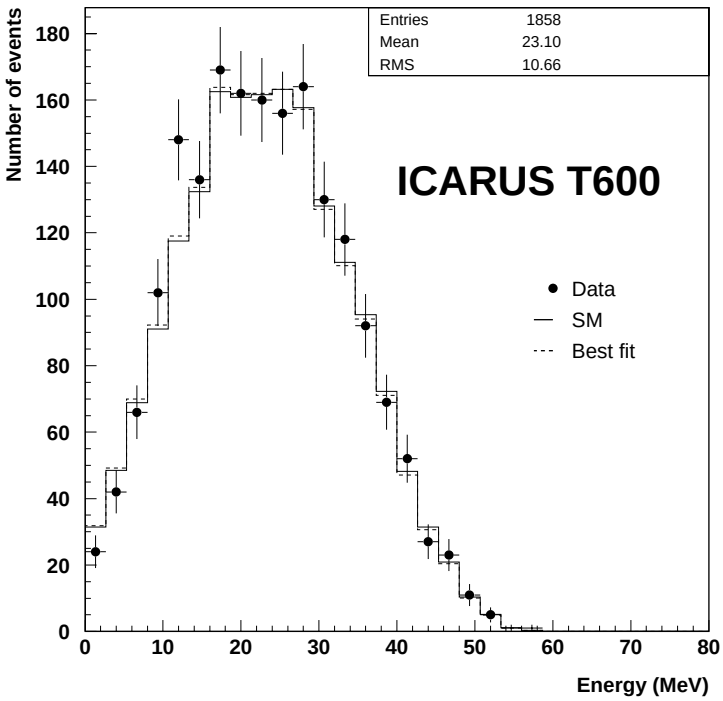

Figure 11: Energy spectrum of electrons from muon decays in the ICARUS T600 detector (electron energy lost by ionization in LAr). The plot shows the measured distribution (dots) compared both to the SM expectation (solid line) and the best fit with ρ as free parameter (dashed line).

onthe density of ionization. A precise knowledge of electron recombination is essential to understand the detector linearityand resolution.The muon tracks were reconstructed with the automatic procedure and the energy at each position evaluatedfrom the range to the decay point. In order to measure the recombination at different stoppingpowers, we exploited the variation of dE/dx with the muon energy along thetrack. The T600 data is

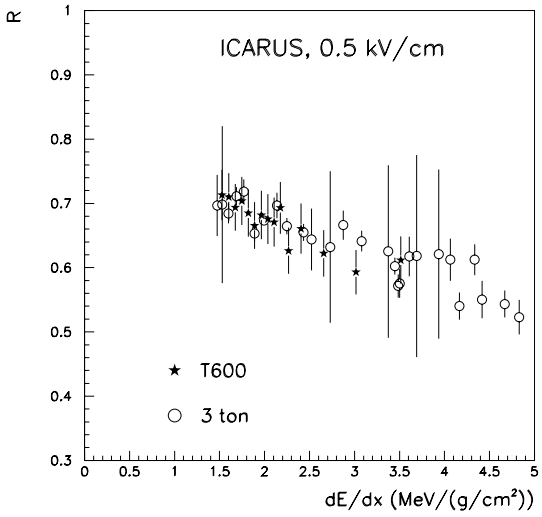

Figure 12: Recombination factors measured with the ICARUS T600 and 3 ton detectors at 500 V/cm.

fully compatible with results obtained with previousICARUS prototypes (fig. 12). Available theoretical models ofrecombination have been reviewed at the light of the ICARUS results and ofthe data available in the literature, arriving to the conclusion that allof them contain approximations that limit their range of validity, and thatthe experimentally determined recombination factor is always an"effective" quantity, that includes the contribution of trackssub-segment and of δ-rays. A phenomenological way to model this process and to reproduce it inthe ICARUS Monte Carlo simulations has been devised (see Fig .13).

7 Conclusions

We have presented a brief description of the ICARUS T600 detector, a large–mass Liquid Argon TPC meant as the basic unit for a 3000 ton astroparticle observatory and neutrino detector to be installed in the underground Gran Sasso Laboratory.

The design, the description of the basic components, assembly, start–up and run procedures of the detector have been recently published, as well as the demonstration of the off–line event reconstruction capabilities.

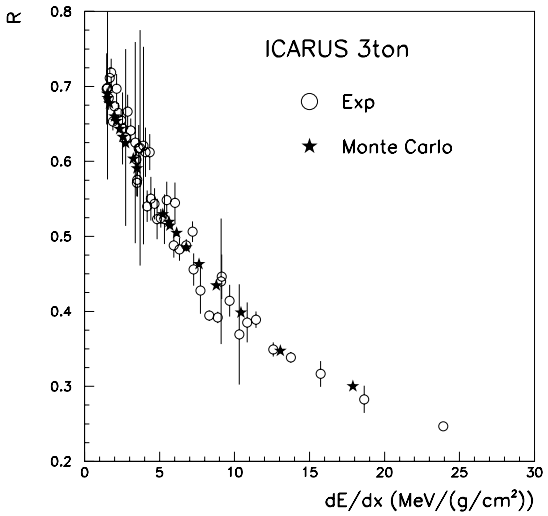

Figure 13: Experimental and Monte Carlo recombination factors at 500 V/cm.

The main conclusion is that the measurements and the experimental results demonstrate that it is feasible to master all technical issues related to the construction and operation of a large size LAr TPC, within and sometimes beyond the design specifications.

The collection of events gives only a flavor of the detector imaging capability and of its calorimetric performance. The detector space and energy resolution, particle identification and full events reconstruction have been the subjects of several analyses carried out with the events collected during the test run. at surface in the Pavia experimental hall.

The T600 is going to be transported to the INFN Gran Sasso Underground Laboratory where it will start to take data with atmospheric and solar neutrino interactions.

References

[1] C. Rubbia, *The Liquid-Argon Time Projection Chamber: A New Concept For Neutrino Detector*, CERN–EP/77–08, (1977).

[2] P. Benetti *et al.* [ICARUS Collaboration], *A 3 Ton Liquid Argon Time Projection Chamber*, Nucl. Instrum. Meth. A **332**, (1993) 395.

[3] P. Cennini *et al.* [ICARUS Collaboration], *Performance Of A 3 Ton Liquid Argon Time Projection Chamber*, Nucl. Instrum. Meth. A **345**, (1994) 230.

[4] F. Arneodo *et al.* [ICARUS Collaboration], *The ICARUS 50 l LAr TPC in the CERN neutrino beam*, arXiv:hep-ex/9812006.

[5] F. Arneodo *et al.* [ICARUS Collaboration], *First Observation Of 140-Cm Drift Ionizing Tracks In The Icarus Liquid-Argon Tpc*, Nucl. Instrum. Meth. A **449**, (2000) 36.

[6] F. Arneodo *et al.* [ICARUS Collaboration], *Determination Of Through-Going Tracks' Direction By Means Of Delta-Rays In The Icarus Liquid Argon Time Projection Chamber*, Nucl. Instrum. Meth. A **449**, (2000) 42.

[7] P. Cennini *et al.* [ICARUS Collaboration], *Detection Of Scintillation Light In Coincidence With Ionizing Tracks In A Liquid Argon Time Projection Chamber*, Nucl. Instrum. Meth. A **432**, (1999) 240.

[8] F. Arneodo *et al.* [ICARUS Collaboration], *Performance Evaluation Of A Hit Finding Algorithm For The Icarus Detector*, Nucl. Instrum. Meth. A **412**, (1998) 440.

[9] P. Cennini *et al.* [ICARUS Collaboration], *A Neural Network Approach For The Tpc Signal Processing*, Nucl. Instrum. Meth. A **356**, (1995) 507.

[10] P. Cennini *et al.* [ICARUS Collaboration], *Improving The Performance Of The Liquid Argon Tpc By Doping With Tetramethyl Germanium*, Nucl. Instrum. Meth. A **355**, (1995) 660.

[11] P. Benetti *et al.* [ICARUS Collaboration], *A 3D Image Chamber For The Lar Tpc On Multilayer Printed Circuit Board*, Nucl. Instrum. Meth. A **346**, (1994) 550.

[12] P. Benetti *et al.* [ICARUS Collaboration], *Argon Purification In The Liquid Phase*, Nucl. Instrum. Meth. A **333**, (1993) 567.

[13] A. Bettini *et al.* [ICARUS Collaboration], *A Study Of The Factors Affecting The Electron Lifetime In Ultrapure Liquid Argon*, Nucl. Instrum. Meth. A **305**, (1991) 177.

[14] S. Bonetti *et al.* [ICARUS Collaboration], *A Study Of The Electron Image Due To Ionizing Events In A Two-Dimensional Liquid Argon Tpc With A 24-Cm Drift Gap*, Nucl. Instrum. Meth. A **286**, (1990) 135.

[15] F. Arneodo *et al.* [ICARUS Collaboration], *Performance Of The 10 m^3 Icarus Liquid Argon Prototype*, Nucl. Instrum. Meth. A **498**, (2003) 293.

[16] F. Arneodo *et al.* [ICARUS Collaboration], *Detection Of Cerenkov Light Emission In Liquid Argon*, Nucl. Instrum. Meth. A **516** (2004), 348.

[17] ICARUS Collaboration, *A First 600 Ton ICARUS Detector Installed At The Gran Sasso Laboratory*, Addendum to Proposal by the ICARUS Collaboration, LNGS–95/10, (1995).

[18] P. Aprili *et al.* [ICARUS Collaboration], *The ICARUS experiment: A second-generation proton decay experiment and neutrino observatory at The Gran Sasso*

Laboratory. Cloning Of T600 Modules To Reach The Design Sensitive Mass. (Addendum), CERN-SPSC-2002-027;
ICARUS Collaboration, *A second-Generation Proton Decay Experiment And Neutrino Observatory At The Gran Sasso Laboratory*, LNGS–P28/2001;

[19] S. Amoruso *et al.* [ICARUS Collaboration], *Analysis Of The Liquid Argon Purity In The ICARUS T600 TPC*, Nucl. Inst. Meth., A **516**, (2004) 68.

[20] F. Arneodo *et al.* [ICARUS Collaboration], *Observation Of Long Ionizing Tracks With The ICARUS T600 First Half–Module*, Nucl. Inst. Meth., A **508**, (2003) 287.

[21] S. Amoruso *et al.* [ICARUS Collaboration], *Measurement Of The Muon Decay Spectrum With The ICARUS T600 Liquid Argon TPC*, accepted for publication on EPJ.

[22] S. Amoruso *et al.* [ICARUS Collaboration], *Study Of The Electron Recombination In Liquid Argon With The ICARUS TPC*, accepted for publication on Nucl. Instr. Meth. A.

LUNA. Laboratory for Underground Nuclear Astrophysics

D.Bemmerer[1], R.Bonetti[2], C.Broggini[3*], F.Confortola[4], P.Corvisiero[4], H.Costantini[4], J.Cruz[5], A.Formicola[7], Z.Fülöp[8], G.Gervino[9], A.Guglielmetti[2], C.Gustavino[11], G.Gyürky[8], G.Imbriani[10], A.P.Jesus[5], M.Junker[11], A.Lemut[4], R.Menegazzo[3], A.Ordine[10], P.Prati[4], V.Roca[10], D.Rogalla[6], C.Rolfs[7], M.Romano[10], C.Rossi Alvarez[3], F.Schümann[7], E.Somorjai[8], O.Straniero[12], F.Strieder[7], F.Terrasi[6], H.P.Trautvetter[7], S.Zavatarelli[4]

[1] Inst. für Atomare Physik und Fachdidaktik, Technische Univ. Berlin, Germany
[2] Università di Milano, Dipartimento Di Fisica and INFN, Milano, Italy
[3] INFN, Padova, Italy
[4] Università di Genova, Dipartimento di Fisica and INFN, Genova, Italy
[5] Centro de Fisica Nuclear, Universidade de Lisboa, Portugal
[6] Dipartimento di Scienze Ambientali, Seconda Univerità di Napoli, Caserta, Italy
[7] Institut für Experimentalphysik III, Ruhr-Univerität Bochum, Germany
[8] ATOMKI, Debrecen, Hungary
[9] Politecnico di Torino, Dipartimento di Fisica and INFN, Torino, Italy
[10] Università di Napoli, Dipartimento di Fisica and INFN, Napoli, Italy
[11] Laboratori Nazionali del Gran Sasso, Assergi, Italy
[12] Osservatorio Astronomico di Collurania, Teramo, Italy

Abstract

LUNA is measuring fusion cross sections down to the energy of the stellar nucleosynthesis. The activity during this year has been focused on the study of $^{14}N(p,\gamma)^{15}O$, both on the analysis of the last year data and on the running of the new high efficiency set-up. $^{14}N(p,\gamma)^{15}O$ is the slowest reaction of the CNO cycle, the key one for deciding its efficiency. In particular, the analysis of the data has halved the cross section value with respect to the one used in the Standard Solar Model. As a consequence, the predicted CNO solar neutrino flux has been decreased by about a factor 2 and the age of the oldest Globular Clusters has been increased by 0.7-1 Gyr with respect to the current estimates.

*Spokesperson

Introduction

Nuclear reactions that generate energy and synthesize elements take place inside the stars in a relatively narrow energy window: the Gamow peak. In this region, which is in most cases below 100 keV, far below the Coulomb energy, the reaction cross-section σ(E) drops almost exponentially with decreasing energy E:

$$\sigma(E) = \frac{S(E)}{E}\, exp(-2\,\pi\,\eta), \tag{1}$$

where $S(E)$ is the astrophysical factor and η is the Sommerfeld parameter, given by $2\,\pi\,\eta = 31.29\,Z_1\,Z_2(\mu/E)^{1/2}$. Z_1 and Z_2 are the nuclear charges of the interacting particles in the entrance channel, μ is the reduced mass (in units of amu), and E is the center of mass energy (in units of keV).

The extremely low value of the cross-section, from pico to femto-barn and even below, has always prevented its measurement in a laboratory at the Earth's surface, where the signal to background ratio would be too small because of cosmic ray interactions. Instead, the observed energy dependence of the cross-section at high energies is extrapolated to the low energy region, leading to substantial uncertainties. In particular, there might be a change of the reaction mechanism or of the centrifugal barrier, or there might be the contribution of narrow or sub-threshold resonances, not accounted for by the extrapolation, but which could completely dominate the reaction rate at the Gamow peak.

In addition, another effect can be studied at low energies: the electron screening. The electron cloud surrounding the interacting nuclei acts as a screening potential, thus reducing the height of the Coulomb barrier and leading to a higher cross-section. The screening effect has to be measured and taken into account in order to derive the bare nuclei cross-section, which is the input data to the models of stellar nucleosynthesis.

In order to explore this new domain of nuclear astrophysics we have installed two electrostatic accelerators underground in LNGS: a 50 kV accelerator and a 400 kV one. The qualifying features of both the accelerators are a very small beam energy spread and a very high beam current even at low energy.

Outstanding results obtained up to now are the only existing cross-section measurements within the Gamow peak of the sun: $^3He(^3He, 2p)^4He$ [1] and $d(p,\gamma)^3He$ [2]. The former plays a big role in the proton-proton chain, largely affecting the calculated solar neutrino luminosity, whereas the latter is the reaction that rules the proto-star life during the pre-main sequence phase.

With these measurements LUNA has shown that, by going underground and by using the typical techniques of low background physics, it is possible to measure nuclear cross sections down to the energy of the nucleosynthesis inside stars.

In the following we report on the activity during the year 2003, which has been dedicated to the study of $^{14}N(p,\gamma)^{15}O$. First, we show the final results from the analysis of the data taken with solid targets and germanium detectors. Then, we briefly describe the high efficiency set-up to measure the $^{14}N(p,\gamma)^{15}O$ cross section down to the lowest energies and we discuss the first results.

1 The $^{14}N(p,\gamma)^{15}O$ reaction

$^{14}N(p,\gamma)^{15}O$ (Q=7.297 MeV) is the slowest reaction of the CNO cycle, the key one to know the CNO solar neutrino flux, as well as to determine the age of the globular clusters, the oldest systems in the Galaxy. As a matter of fact, the CNO solar neutrino flux depends almost linearly on this cross section. The luminosity of the turn off point in the Hertzsprung-Russell diagram of a globular cluster (i.e. the bluest point on the main sequence) is also determined by the value of the $^{14}N(p,\gamma)^{15}O$ cross section and it gives the age of the cluster. The higher the cross section is, the younger is the age, for a given turn off luminosity.

The energy region studied so far in nuclear physics laboratories is well above the region of interest for the CNO burning in astrophysical conditions (20-80 keV). Below 2 MeV, several ^{15}O states contribute to the ^{14}N(p,γ)^{15}O cross section: a $J^\pi = 3/2^+$ sub-threshold state at $E_R = -507$ keV ($E_x = 6.79$ MeV), and 3 resonant states: $J^\pi = 1/2^+$ at $E_R = 259$ keV, $3/2^+$ at $E_R = 989$ keV and $E_R = 2187$ keV. The reaction was previously studied over a wide range of energies, i.e. $E_{cm} = E = 240$ to 3300 keV ([3] and references therein). According to Schröder et al. [3], who used the Breit-Wigner formalism, the main contribution to the total S-factor at zero energy, S(0),comes from the transitions to the ground state of ^{15}O and to its excited state at $E_x = 6.79$ MeV. In particular, they give $S(0) = 3.20 \pm 0.54\ keV \cdot b$. On the other hand, Angulo et al. [4] re-analyzed Schröder's experimental data using an R-matrix approach and they obtained the much smaller value of $S(0) = 1.77 \pm 0.20\ keV \cdot b$. The difference mainly comes from the different contribution of the direct capture to the ^{15}O ground state: Angulo et al. have a value lower by a factor 19 than the one of Schröder et al.. We underline that at the lowest energies Schröder et al. give only upper limits to the cross section, due to the presence of a strong cosmic ray background in the spectrum.

In summary, new measurements of the $^{14}N(p,\gamma)^{15}O$ cross section at energies E $\leq$ 240 keV are strongly demanded. In particular it is necessary to well measure the contribution of the direct capture to the ground state of ^{15}O. The peculiarities of the 400 kV LUNA facility [5] are particularly well suited for this study, where γ-rays with energy up to $\simeq$ 7.5 MeV have to be detected at very low count-rate. As a matter of fact, in such a measurement the cosmic ray background has to be strongly suppressed and ultra-low background detectors have to be employed. In addition, high beam intensities have to be coupled to targets of high stability and purity, in order to minimize the beam-induced background.

Due to the strong energy dependence of the cross section, we carefully determined the uncertainties of our accelerator: $\pm 300\ eV$ on the absolute energy from $E_p = 130$ to 400 keV, proton energy spread of better than 100 eV and long term energy stability of 5 eV per hour [5].

1.1 The results from the solid target data

The reported data has been obtained with the beam passing through an electrically insulated collimator with a negative voltage of 300 V (to suppress the effects of secondary electrons) and focused to a spot of about 1.5 cm diameter on the target. A liquid nitro-

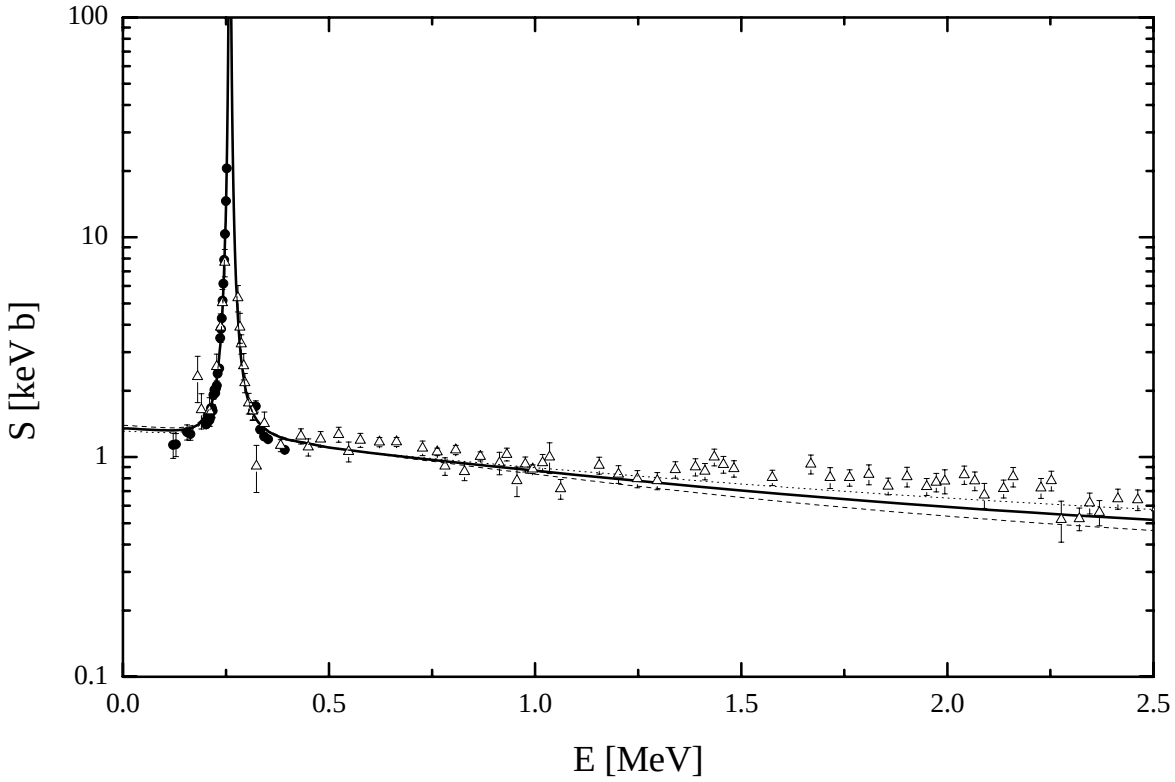

Figure 1: Transition to the 6.79 MeV state in ^{15}O. The S-factor data from our work are represented by solid points, those of [3] by open triangles. The R-matrix fit (solid line) was obtained for $a = 5.5$ fm, the dashed line for $a = 6$ fm and the dotted line for $a = 5$ fm (where a is the R-matrix radius). The data point in the 259 keV resonance is off scale.

gen cooled Cu shroud has been placed between the collimator and the target in order to minimize carbon deposition on the target itself.

The targets were manufactured in the INFN Laboratories of Legnaro and they consisted of a TiN layer (with a typical thickness of 80 keV) reactively sputtered on a 0.2 mm thick Ta backing. The stoichiometry of the TiN layer was verified via Rutherford Backscattering Spectrometry using a 2.0 MeV $^4He^+$ beam, resulting in $Ti/N = 1/(1.08 \pm 0.05)$. The target quality was checked frequently at the $E_R = 259$ keV resonance: no significant deterioration was observed after a bombarding time of several days. Typically, a new TiN target was used after a running time of 1 week.

For the measurement of excitation functions the capture γ-rays were observed with one Ge detector (126% efficiency) placed at 55° in close geometry to the target. The detector efficiency was determined using calibrated radioactive sources and the cascade condition for the transitions to the first three excited states at the $E_R = 259$ keV resonance. This procedure was performed with the Ge detector placed at 1.53, 5.5, 10.5, and 20.5 cm distances from the target in order to determine the summing-in contribution to the ground state transition and the summing-out for the transitions to the excited states. It turned out that the summing-in yield was about 3.5 times higher than the actual ground state

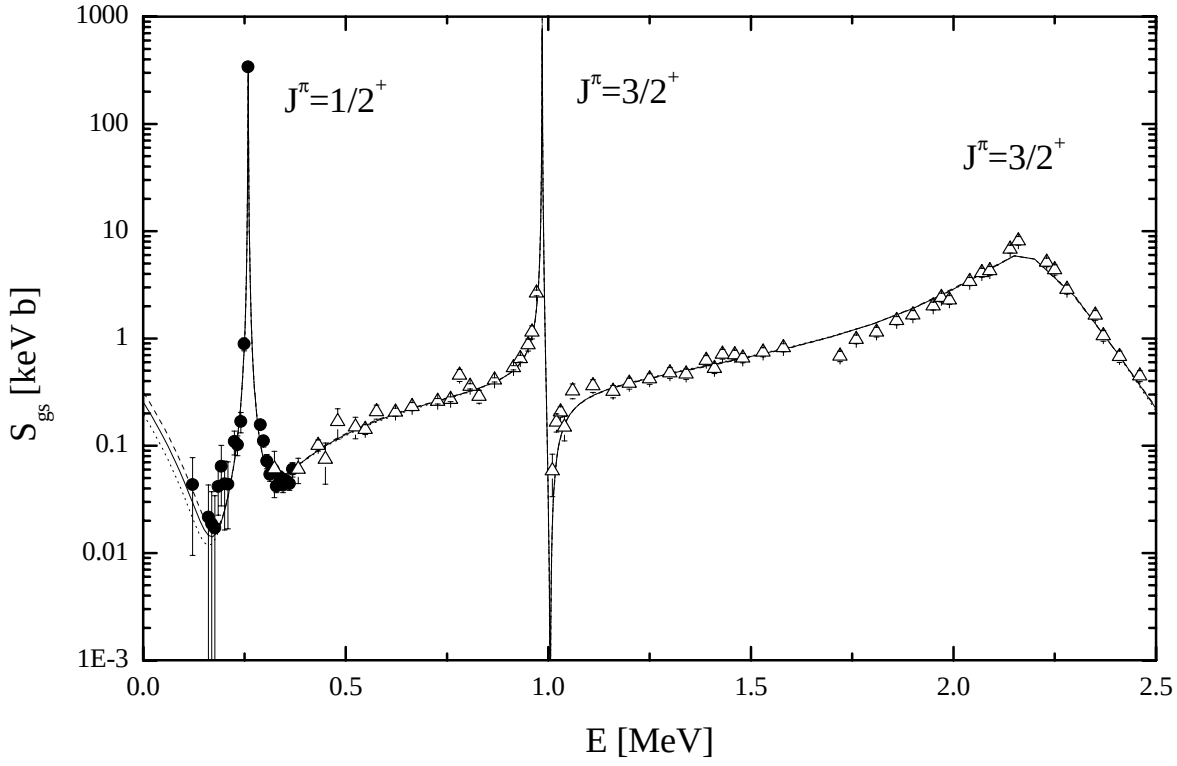

Figure 2: Astrophysical S(E)-factor for the ground state transition in ^{14}N(p, γ)^{15}O. Filled-in data points are the results from LUNA, while the open data points are from previous work [3] corrected for summing effects. The solid line corresponds to the R-matrix fit for $a = 5.5$ fm, the dashed line for $a = 6$ fm and the dotted line for $a = 5$ fm (where a is the R-matrix radius).

intensity at the 1.53 cm position. This 1.53 cm position was used for the entire cross section measurements. The efficiency curve was also calculated using the GEANT code and found to be in excellent agreement with observation. Branching and strength values of the $E_R = 259$ keV resonance were determined with low beam current to avoid dead time effects and at far distance (20.5 cm) to minimize summing effects from cascade transitions.

In another measurement, three Ge detectors were placed at 0° (126 %), 90° (120 %), and 125° (108 %), relative to the beam axis ($d = 7$ cm) for the measurement of the Doppler shift effect, excitation energies, and angular distributions.

In order to extract the absolute cross section from the observed γ-ray spectra, we studied in detail the expected gamma line shape [5][6]. This shape is determined by the cross section behavior $\sigma(E_p)$ in the proton energy interval spanned by the incident beam during the slowing-down process in the target (once the transformation from the energy E_p at which the reaction takes place to the corresponding γ-ray energy $E_\gamma = E_p^{cm} + Q$ is made).

Details for the procedure of the R-matrix fit can be found in [4], whereas details on the analysis of our data, which start at E=135 keV, are given in [7]. In short, the fit was

performed in two steps.

First, the transition to the 6.79 MeV state was fitted including the data set given by [3], which is in excellent agreement with the present results in the region of overlap. The R-matrix fit for the transition to the 6.79 MeV state is shown in Fig. 1. When extrapolated to zero energy it gives $S_{6.79}(0) = 1.35 \pm 0.05$ (statistical) ± 0.08 (systematic) $keV \cdot b$. This value is about 20 % lower than the R-matrix fit [4] of the data from [3] alone.

As the next step, we analyzed the LUNA data together with the data from [3] for the ground state transition. The S-factor values of [3] near the $E_R = 259$ keV resonance have been excluded since they represent integrated values over the target thickness, whereas the remaining data points had to be corrected to take into account the summing effect (such correction factor is at most 10% above E=500 keV). The data, together with the R-matrix fit, is shown in Fig. 2. When extrapolated to zero energy the fit gives $S_{gs}(0) = 0.25 \pm 0.06\ keV \cdot b$ This value is about a factor 3 higher than the R-matrix fit [4] of the data from [3] alone.

For the total S-factor a contribution from the transition to the 6.18 MeV state of $S_{6.18}(0) = 0.06\ keV \cdot b$ from [4] has been added to obtain $S_{tot}(0) = 1.7 \pm 0.1$ (statistical) ± 0.2(systematic) $keV \cdot b$. Our value can be compared with $1.77 \pm 0.2\ keV \cdot b$ from the theoretical paper [4] and $1.70 \pm 0.22\ keV \cdot b$ from [8], where the asymptotic normalization coefficients for $^{14}N + p \rightarrow ^{15} O$ have been determined by measuring the $^{14}N(^3He, d)^{15}O$ proton transfer reaction at an incident energy of 26.3 MeV.

We point out that the LUNA result is the only one obtained from a direct measurement of the cross section at low energy, down to 135 keV. It is smaller than the value given by the most recent compilations: $3.5^{+0.4}_{-1.6}\ keV \cdot b$ [9] and $3.2 \pm 0.8\ keV \cdot b$ [10]. Our result has deep astrophysical consequences: the CNO neutrino yield in the Sun is decreased by about a factor two [11] and the age of the oldest Globular Clusters is increased by 0.7-1 Gyr [11][12] with respect to the current estimates.

2 The gas target set-up

In order to reduce the region where the cross section is obtained by extrapolation, we have to explore the energy range below 135 keV. For this it is essential to have both a γ ray detector with very high efficiency, to compensate for the rapidly decreasing cross section, and a very pure and thin ^{14}N target, to suppress the beam induced background and to minimize the straggling on the energy loss. This has been achieved with the same 4π BGO summing detector (about 80% efficiency) [13] used in the measurement of $d(p,\gamma)^3He$ [2] and with a new windowless gas target. A schematic diagram of the gas target is shown in Fig. 3. The ion beam enters the target chamber through three apertures of high pass flow impedance (A_3–A_1, Fig. 3) and it is stopped in a beam calorimeter placed at the downstream part of the chamber. The chamber is designed to fit inside the central hole (diameter $\phi = 6\ cm$) of the BGO crystal detector.

The pressure inside the chamber is measured with a capacitance gauge, and it has been checked to be homogeneous to a 0.5 % accuracy [6]. On the other hand, because of the beam heating effect, the target nuclei density along the beam path itself can be different

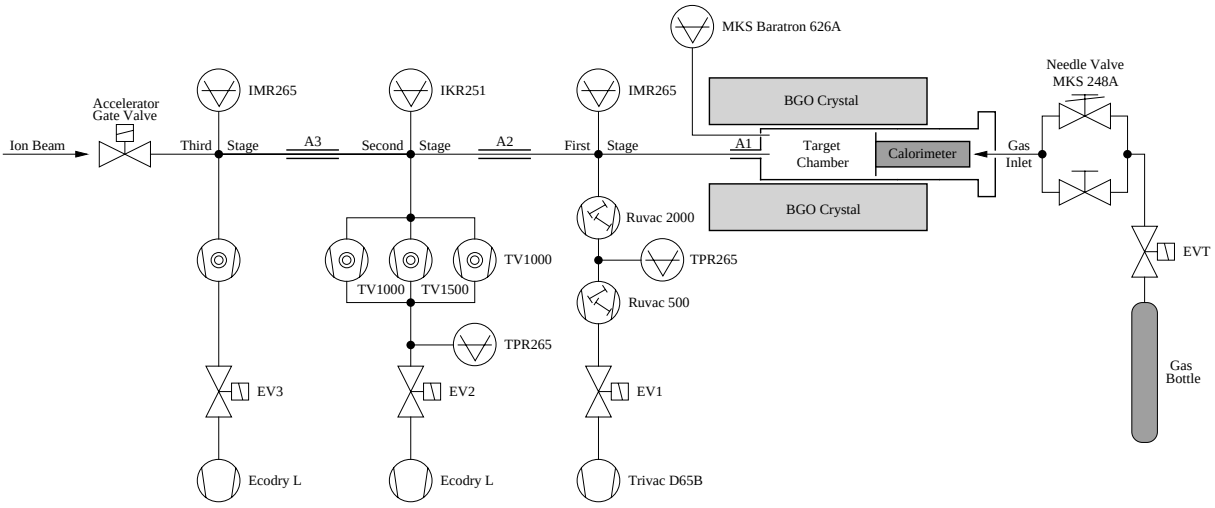

Figure 3: ^{14}N(p,γ)^{15}O windowless gas target schematic diagram.

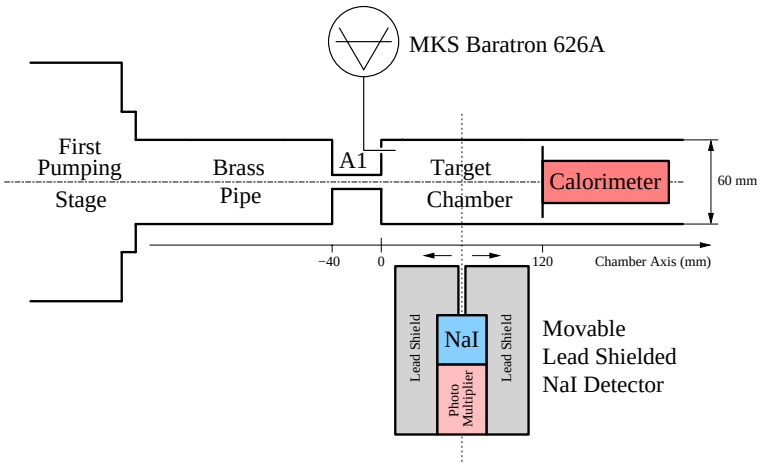

Figure 4: The set-up used to measure the beam heating effect.

[14] from the one given by the perfect gas law. Figure 4 shows the set-up we used to measure such effect in our experiment. The small NaI detector is movable along the beam axis and it is shielded with lead (hole diameter 5 mm, lead thickness 70 mm). From the position of the E$_R$=259 keV ^{14}N(p,γ)^{15}O resonance along the axis (and the beam energy at the target entrance) we obtain the energy loss and, from this, the target nuclei density. The correction factor is important in our running conditions. For instance, at the beam energy of 100 μA and a pressure in the target of 1 *mbar* we measured a density reduction along the beam of about 7% as compared to the one given by the perfect gas law.

The beginning of the experiment has been dedicated to the study of the background. Thanks to the strong muon suppression provided by the underground laboratory, the beam-induced background (Tab. 1) becomes the dominant one in the gamma energy region above 4 MeV. One of the first spectra obtained with our 4 π BGO summing detector is shown in figure 5. At the lowest energies the background due to the ^{2}D(p,γ)^{3}He reaction

Table 1: Principal sources of beam-induced background in the LUNA gas target system and their respective Q values [15] and relevant γ lines.

Reaction	**Q value [MeV]**	**γ lines above 4 MeV**	**location**
^{2}D(p,γ)^{3}He	5.493	5.493+E_{CM}	beam stop
^{11}B(p,γ)^{12}C	15.96	4.44, 11.54+E_{CM}, 12.71	collimator
^{12}C(p,γ)^{13}N	1.94	1.94+E_{CM}	beam stop
^{13}C(p,γ)^{14}N	7.55	7.55+E_{CM}	beam stop
^{18}O(p,γ)^{19}F	7.99	7.88+E_{CM}, 4.08+E_{CM}	not sign. outside resonance
^{19}F(p,$\alpha\gamma$)^{16}O	8.11	6.13	not sign. below E_p = 220 keV

is clear. The source of this background could be localized using the energy shift of the ^{2}D(p,γ)^{3}He line due to the recoil and the Doppler effects (such measurements have been made with a germanium detector). As a matter of fact, the ^{2}D was found to be implanted on the surface of the beam stopper. In the energy region of interest also the ^{11}B(p,γ)^{12}C reaction was a significant problem. The source of this background was localized on a collimator (using a NaI detector) and eliminated.

When completed the background suppression phase, we started the data taking for the $^{14}N(p,\gamma)^{15}O$ cross section measurement. The preliminary results are in good agreement with the solid target ones in the overlapping region above 135 keV. We have already reached the energy E=80 keV, with a rate of about 40 events/day: half coming from the reaction and half from the natural background (the beam induced background is completely suppressed at such energies). The experiment will last a few more months to measure in the energy region below 80 keV.

3 Other activities

$^{3}He(\alpha,\gamma)^{7}Be$ is the next reaction which will be studied in LUNA. $^{3}He(\alpha,\gamma)^{7}Be$ (Q-value: 1.6 MeV) is the key reaction for the production of ^{7}Be and ^{8}B neutrinos in the Sun. The joint effort of all experiments on solar neutrinos and solar physics has finally cast light on the long-standing solar neutrino puzzle. As a consequence, we can now go back to the original motivation of solar neutrino detection: the study of the Sun. The error on $S_{3,4}$, about 16%, is, at the moment, the main limitation to the extraction of physics from the ^{8}B neutrino flux measurement. For instance, a 5% determination of $S_{3,4}$ would allow a study of the central region of the Sun with an accuracy better than the one given by helioseismology [16].

During the year we have designed the set-up to measure $^{3}He(\alpha,\gamma)^{7}Be$ at low energies and we are now starting its construction. Very briefly, the detector will be a 150 % efficiency ultra-low background germanium heavily shielded and placed at close distance from the ^{3}He windowless gas target.

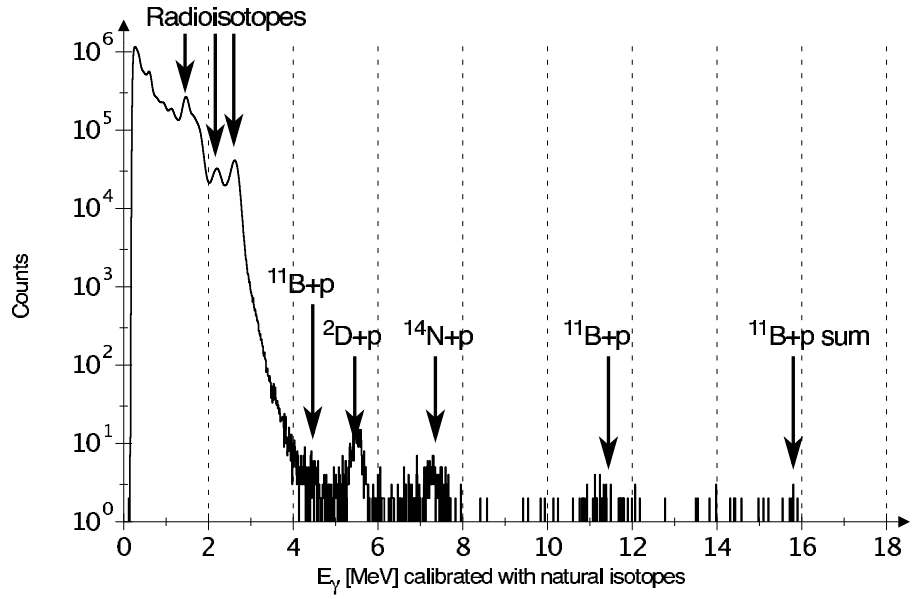

Figure 5: BGO spectrum at $E_p = 100$ keV with 86 C of proton beam on the N_2 gas target at 1 *mbar* pressure.

3.1 Electron screening for deuterated metals

For nuclear reactions studied in the laboratory the target nuclei and the projectiles are usually in the form of neutral atoms or molecules and ions, respectively. The electron clouds surrounding the interacting nuclei reduce the height of the Coulomb barrier and lead to a higher cross section, $\sigma_{\rm s}(E)$, than would be the case for bare nuclei, $\sigma_{\rm b}(E)$, with an exponential enhancement factor:

$$f_{\rm lab}(E) = \sigma_{\rm s}(E)/\sigma_{\rm b}(E) \simeq E(E+U_{\rm e})^{-1} \exp(\pi\eta\, U_{\rm e}/E), \qquad (2)$$

where $U_{\rm e}$ is an electron screening potential energy and η is the Sommerfeld parameter.

Recently, the electron screening effect on the $d(d,p)t$ reaction has been studied with deuterium implanted in various metals [17] [18]. The resulting $S(E)$ data show an exponential enhancement, however the extracted U_e values are about one order of magnitude larger than the value U_e =25±5 eV found in the corresponding gas target experiment [19]. In order to test these surprising results, we started already two years ago a complete experimental program at the 100 kV accelerator of the Bochum Tandem Laboratory [20][21]. With the data collected in 2002 we reached the number of 58 measurements. As compared to measurements performed with a gaseous deuterium target, a large effect has been observed in most metals, while a small (gaseous) effect is found for the insulators, semiconductors and lanthanides [22]. The periodic table provides the ordering of the observed small and large effects. An explanation of the large effects in metals is possibly provided by the classical plasma screening of Debye applied to the quasi-free metallic electrons. We have now built a set-up which will allow the study of the temperature dependence of the effect for temperature up to 400 degrees Celsius.

References

[1] R. Bonetti et al. (LUNA Coll.), Phys. Rev. Lett. 82(1999)5205

[2] C. Casella et al. (LUNA Coll.), Nucl. Phys. A 706(2002)203

[3] U. Schroeder et al., Nucl. Phys. A 467(1987)240.

[4] C. Angulo and P. Descouvemont, Nucl. Phys. A 690(2001)755

[5] A. Formicola et al. (LUNA Coll.), Nucl. Instr. Meth. A 507(2003)609

[6] LUNA Coll., Annual Report LNGS 2002

[7] A. Formicola et al. (LUNA Coll.), submitted to Phys. Lett. B, nucl-ex/0312015

[8] A.M. Mukhamedzhanov et al., Phys. Rev. C 67(2003)065804

[9] E.G. Adelberger et al., Rev. Mod. Phys. 70(1998)1265

[10] C. Angulo et al. (NACRE Coll.), Nucl. Phys. A 656(1999)3

[11] S. Degl'Innocentiet al., astro-ph/0312559

[12] G. Imbriani et al. (LUNA Coll.), sub. to Astr.and Astrophys. Lett.

[13] C. Casella et al. (LUNA Coll.), Nucl. Instr. Meth. A 489(2002)160

[14] J.Gorres et al., Nucl. Instr. Meth. 177(1980)295

[15] D.R. Tilley et al.: Energy Levels of Light

[16] G. Fiorentini et al., astro-ph/0310753

[17] H. Yuki et al., JETP Lett. 68(1998)823

[18] K. Czerski et al., Europhys. Lett. 54(2001)449

[19] U. Greife et al., Phys. A 351(1995)107

[20] F. Raiola et al., Eur. Phys. J. A 13(2002)377

[21] F. Raiola et al., Phys. Lett. B 547(2002)193

[22] F. Raiola et al., Eur. Phys. J. A, in press

4 Publications and Conferences

1. A. Formicola et al., "The LUNA II 400 kV accelerator", Nucl. Instr. Meth. A 507(2003)609
2. A. Formicola et al., "Astrophysical S-factor of $^{14}N(p,\gamma)^{15}O$", submitted to Phys. Lett. B, nucl-ex/0312015
3. G. Imbriani et al., "The bottleneck of the CNO burning and the age of the Globular Clusters", submitted to Astronomy and Astrophysics Letters
4. F. Raiola et al., "Enhanced electron screening in $d(d,p)t$ for deuterated metals", Eur. Phys. J. A, in press
5. C. Broggini, invited talk at the Physics in Collision Conference, Zeuthen
6. C. Broggini, invited talk at the Italian Physical Society Conference, Parma
7. C. Broggini, LOWNU Workshop, Paris
8. A. Formicola, TAUP 2003, Seattle
9. G. Imbriani, Meeting between Astrophysicists and Nuclear Physicists, Brussels
10. A. Lemut, Italian Physical Society Conference, Parma
11. A. Lemut, Meeting between Astrophysicists and Nuclear Physicists, Brussels
12. P. Prati, Work. on Underground Accelerator for Nuclear Astrophysics, Tucson
13. C. Rolfs, invited talk at the FUSION03 Conference, Matsushima
14. F. Strieder, Annual Spring Meeting of the German Physical Society, Tubingen
15. F. Strieder, Work. on Underground Accelerator for Nuclear Astrophysics, Tucson

LVD. Large Volume Detector

LVD COLLABORATION

N.Y.Agafonova[9], M.Aglietta[14], E.D.Alyea[7], P.Antonioli[1], G.Badino[14], G.Bari[1], M.Basile[1], V.S.Berezinsky[9], M.Bertaina[14], R.Bertoni[14], G.Bruni[1], G.Cara Romeo[1], C.Castagnoli[14], A.Chiavassa[14], J.A.Chinellato[3], L.Cifarelli[1], F.Cindolo[1], A.Contin[1], V.L.Dadykin[9], E.A. Dobrynina[9], L.G.Dos Santos[3], R.I.Enikeev[9], W.Fulgione[14], P.Galeotti[14], M.Garbini[1], P.L.Ghia[5,14], P.Giusti[1], F.Gomez[14], F.Grianti[4], G.Iacobucci[1], E.Kemp[3], E.V.Korolkova[9], V.B.Korchaguin[9], V.V.Kuznetsov[9], M.Luvisetto[1], A.S.Malguin[9], H.Menghetti[1], N.Mengotti Silva[3], C.Morello[14], R.Nania[1], G.Navarra[14], K.Okei[10], L.Periale[14], A.Pesci[1], P.Picchi[14], I.A.Pless[8], A.Porta[14], A.Romero[14], V.G.Ryasny[9], O.G.Ryazhskaya[9], O.Saavedra[14], K.Saitoh[13], G.Sartorelli[1], M.Selvi[1], N.Taborgna[5], N.Takahashi[12], V.P.Talochkin[9], G.C.Trinchero[14], S.Tsuji[11], A.Turtelli[3], P.Vallania[14], S.Vernetto[14], C.Vigorito[14], L.Votano[4], T.Wada[10], R.Weinstein[6], M.Widgoff[2], V.F.Yakushev[9], G.T.Zatsepin[9], A.Zichichi[1]

[1] *University of Bologna and INFN-Bologna, Italy*
[2] *Brown University, Providence, USA*
[3] *University of Campinas, Campinas, Brazil*
[4] *INFN-LNF, Frascati, Italy*
[5] *INFN-LNGS, Assergi, Italy*
[6] *University of Houston, Houston, USA*
[7] *Indiana University, Bloomington, USA*
[8] *Massachusetts Institute of Technology, Cambridge, USA*
[9] *Institute for Nuclear Research, Russian Academy of Sciences, Moscow, Russia*
[10] *Okayama University, Okayama, Japan*
[11] *Kawasaki Medical School, Kurashiki, Japan*
[12] *Hirosaki University, Hirosaki, Japan*
[13] *Ashikaga Institute of Technology, Ashikaga, Japan*
[14] *CNR-IFSI, Torino; University of Torino and INFN-Torino, Italy*

Abstract

The Large Volume Detector (LVD) in the INFN Gran Sasso National Laboratory, Italy, is a ν observatory mainly designed to study low energy neutrinos from the gravitational collapse of galactic objects.

The experiment has been monitoring the Galaxy since June 1992, under increasing larger configurations: in January 2001 it has reached its final active mass $M = 1$ kt. After ten years of running, LVD still remains one of the largest liquid scintillator apparatus for the detection of stellar collapses and, togheter with SNO and SuperKamiokande, it is part of the SNEWS network.

1 Introduction

LVD, located in Hall A of the INFN Gran Sasso National Laboratory, is a multipurpose detector consisting of a large volume of liquid scintillator inter leaved with limited streamer tubes in a compact geometry. The major purpose of the LVD experiment is the search for neutrinos from Gravitational Stellar Collapses (GSC) in our Galaxy [1].

In spite of the lack of a "standard" model of the gravitational collapse of a massive star, the correlated neutrino emission appear to be well established. At the end of its burning phase a massive star ($M > 8M_{\odot}$) explodes into a supernova (SN), originating a neutron star which cools emitting its binding energy $E_B \sim 3 \cdot 10^{53}$ erg mostly in neutrinos.

The largest part of this energy, almost equipartitioned among neutrino and antineutrino species, is emitted in the cooling phase: $E_{\bar{\nu}_e} \sim E_{\nu_e} \sim E_{\nu_x} \sim E_B/6$ (where ν_x denotes generically $\nu_\mu, \bar{\nu}_\mu, \nu_\tau, \bar{\nu}_\tau$ flavors). The energy spectra are approximatively a Fermi-Dirac distribution, but with different mean temperatures, since ν_e, $\bar{\nu}_e$ and ν_x have different couplings with the stellar matter: $T_{\nu_e} < T_{\bar{\nu}_e} < T_{\nu_x}$. LVD is able to detect $\bar{\nu}_e$ interactions with protons, which give the main signal of supernova neutrinos, with a very good signature. Moreover, it can detect ν_e through the elastic scattering reactions with electrons, and it is also sensitive to neutrinos of all flavors detectable through neutral and charged currents interactions with the carbon nuclei of the scintillator. The iron support structure of the detector can also act as a target for electron neutrinos and antineutrinos. The products of the interaction can exit iron and be detected in the liquid scintillator. The amount of neutrino-iron interaction can be as high as about 20% of the total number of interactions.

The described features of stellar collapses are in fact common to all existing models and lead to rather model independent expectations for supernova neutrinos. Thus, the signal observable in LVD, in different reactions and due to different kinds of neutrinos, besides providing astrophysical informations on the nature of the collapse, is sensitive to intrinsic ν properties, as oscillation of massive neutrinos and can give a contribution to define some of the neutrino oscillation properties still missing.

2 The LVD experiment

2.1 The detector

The LVD experiment has been in operation since 1992, under different increasing configurations. During 2001 the final upgrade took place: LVD became fully operational, with

an active scintillator mass $M = 1000$ t. LVD now consists of an array of 840 scintillator counters, 1.5 m^3 each, arranged in a compact and modular geometry. There are two subsets of counters: the external ones (43%), operated at energy threshold $\mathcal{E}_h \simeq 7$ MeV, and inner ones (57%), better shielded from rock radioactivity and operated at $\mathcal{E}_h \simeq 4$ MeV. In order to tag the delayed γ pulse due to n-capture, all counters are equipped with an additional discrimination channel, set at a lower threshold, $\mathcal{E}_l \simeq 1$ MeV.

The top level counters, more exposed to the tunnel walls, and thus characterized by a higher background counting rate and a minor capability to disentangle $\bar{\nu}_e$ interactions, have been shielded by a 2 cm thick iron layer. With respect to the neutron background, the 72 counters which belonged to the Mont Blanc LSD telescope, have been placed as a shield on the top of LVD. In figure 1 you can see a view of the ν telescope.

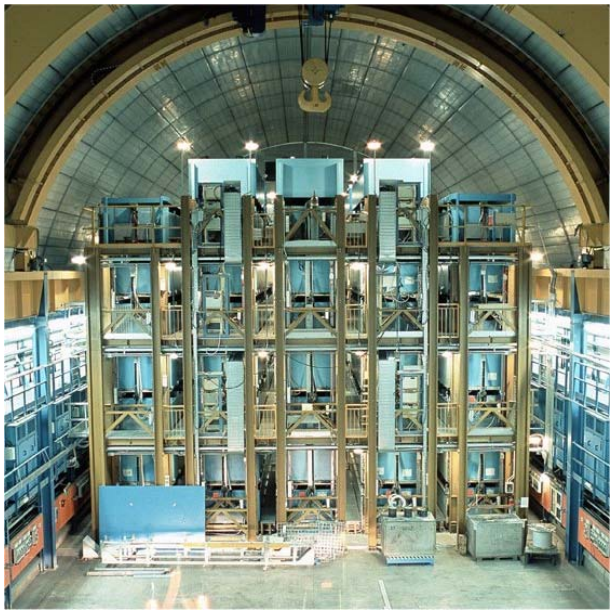

Figure 1: LVD

Relevant features of the detector are:

- (i) good event localization and muon tagging;
- (ii) accurate absolute and relative timing: $\Delta t_{abs} = 1\,\mu s$, $\Delta t_{rel} = 12.5\,ns$;
- (iii) energy resolution: $\sigma_E/E = 0.07 + 0.23 \cdot (E/\mathrm{MeV})^{-0.5}$;
- (iv) very high duty cycle, i.e. 99.7% in the last year;
- (v) fast event recognition.

2.2 SN neutrino interactions

The observable neutrino reactions in the liquid scintillator (LS) are:

- *(1)* $\bar{\nu}_e p, e^+ n$, (physical threshold $E_{\bar{\nu}_e} > 1.8\ MeV$) observed through a prompt signal from e^+ above threshold $\mathcal{E}_h$ (detectable energy $E_d \simeq E_{\bar{\nu}_e} - 1.8$ MeV $+2m_e c^2$), followed by the signal from the $np, d\gamma$ capture ($E_\gamma = 2.2$ MeV), above $\mathcal{E}_l$ and with a mean delay $\Delta t \simeq 180\ \mu$s. The cross section for this reaction has been recently recalculated [2] with a better treatment of the $10 - 100$ MeV region, i.e. the SN neutrino energy. The efficiency for the prompt signal is $\epsilon_{\bar{\nu}_e\, p, e^+\, n} = 95\%$, while for the neutron capture is 50%.

- *(2)* ν_e ^{12}C,^{12}N e^-, (physical threshold $E_{\nu_e} > 17.3\ MeV$) observed through two signals: the prompt one due to the e^- above $\mathcal{E}_h$ (detectable energy $E_d \simeq E_{\nu_e} - 17.3$ MeV) followed by the signal, above $\mathcal{E}_h$, from the β^+ decay of ^{12}N (mean life time $\tau = 15.9$ ms). The efficiency for the detection of the ^{12}N beta decay product is 90%.

- *(3)* $\bar{\nu}_e$ ^{12}C,^{12}B e^+, (physical threshold $E_{\bar{\nu}_e} > 14.4\ MeV$) observed through two signals: the prompt one due to the e^+ (detectable energy $E_d \simeq E_{\bar{\nu}_e} - 14.4\,\text{MeV} + 2m_e c^2$) followed by the signal from the β^- decay of ^{12}B (mean life time $\tau = 29.4$ ms). As for reaction *(2)*, the second signal is detected above the threshold $\mathcal{E}_h$ and the efficiency for the detection of the ^{12}B beta decay product is 75%.

- *(4)* $\overset{(-)}{\nu}_\ell$ ^{12}C, $\overset{(-)}{\nu}_\ell$ ^{12}C* ($\ell = e, \mu, \tau$), (physical threshold $E_\nu > 15.1\ MeV$), whose signature is the monochromatic photon from carbon de-excitation ($E_\gamma = 15.1$ MeV), above $\mathcal{E}_h$, detected with a 55% efficiency. Cross sections for reactions (2), (3) and (4) are taken from [15].

- *(5)* $\overset{(-)}{\nu}_\ell$ e^-, $\overset{(-)}{\nu}_\ell$ e^-, which yields a single signal, above $\mathcal{E}_h$, due to the recoil electron.

The LVD detector presents an iron support structure made basically by two components: the tank (mean thickness: $0.4\ cm$) which contains the LS and the portatank (mean thickness: $1.5\ cm$) which hosts a cluster of 8 tanks. Indeed, the higher energy part of the ν flux could be detected also with the $\nu(\bar{\nu})$Fe interaction, which results in an electron (positron) that could exit iron and release energy in the LS.

The considered reactions are:

- *(6)* ν_e ^{56}Fe,^{56}Co e^-. The mass difference between the nuclei is $\Delta_{m_n} = m_n^{\text{Co}} - m_n^{\text{Fe}} = 4.055$ MeV; moreover the first Co allowed state is at 3.589 MeV. Other higher energy allowed states are present in Cobaltum 56, indeed we consider $E_{e^-}^{\text{kin}} = E_{\nu_e} - \Delta_{m_n} - E_{\text{level}} - m_e$ MeV, where E_{level} is the energy difference between the excitation level and the ground state level: it can take values: $3.589, 4.589, 7.589, 10.589\ MeV$. A number of gammas are produced in the interaction, depending on the excitation level considered.

  A full simulation of the LVD support structure and LS geometry has been developed in order to get the efficiency for electron and gammas, generated randomly in the iron structure, to reach the LS with energy higher than $\mathcal{E}_h$. It is greater than 20%

for $E_\nu > 30$ MeV and grows up to 70% for $E_\nu > 100$ MeV. On average, the electron energy detectable in LS is $E_d \simeq 0.45 \times E_\nu$.

- *(7)* $\bar{\nu}_e$ ^{56}Fe,^{56}Mn e^+, the energy threshold is very similar to reaction *(6)* and the same efficiency is considered.

The cross section for reactions *(6),(7)* are taken respectively from [16] and [17].

The number of all the possible targets present in the LVD detector is listed in table 1

Table 1: Number of targets in the LVD detector.

Target Type	Contained in	Mass	Number of targets
Free protons	Liquid Scintillator	1000 t	9.34 10^{31}
Electrons	LS	1000 t	3.47 10^{32}
C Nuclei	LS	1000 t	4.23 10^{31}
Fe Nuclei	Support Structure	710 t	7.63 10^{30}

3 Supernova and ν physics

3.1 Monitoring

LVD has been continuously monitoring the Galaxy since 1992 in the search for neutrino bursts from GSC [1]. Its active mass has been progressively increased from about 330 t in 1992 to the present 1000 t, always guaranteeing a sensitivity to GSC up to distances $d = 20$ kpc from the Earth, even for the lowest ν-sphere temperature.

The telescope duty cycle has been continuously improving since 1992. As it can be seen in Fig.2, in the last year the average duty cycle was 99%.

The reliability of LVD to detect and recognize ν-bursts with different characteristics, has been tested by inducing clusters of pulses - with different multiplicity and duration - in the LVD counters. The cluster injector, consisting of a generator of light pulses in a certain number of counters, was realized during 2001 and allowed us to evaluate the system efficiency on detecting and disentangling bursts from the background, even with different background conditions.

3.2 Effect of neutrino oscillations

The observation of a neutrino burst due to the explosion of a galactic supernova can add precious informations about neutrino mass and mixing scenarios, in a complementary way with respect to solar, atmospheric and terrestrial ν experiments.

The signal at LVD from a SN exploding at $D = 10$ kpc for 3-flavor ν oscillation, assuming the LMA-MSW solution for solar ν, and normal or inverted mass hierarchy has been calculated [9] [10] [11]. When $U_{e3}^2 \geq 5 \cdot 10^{-4}$ the conversion at the high density

[1] The results of this search have been periodically updated and published[3, 4, 5, 6, 7, 8]

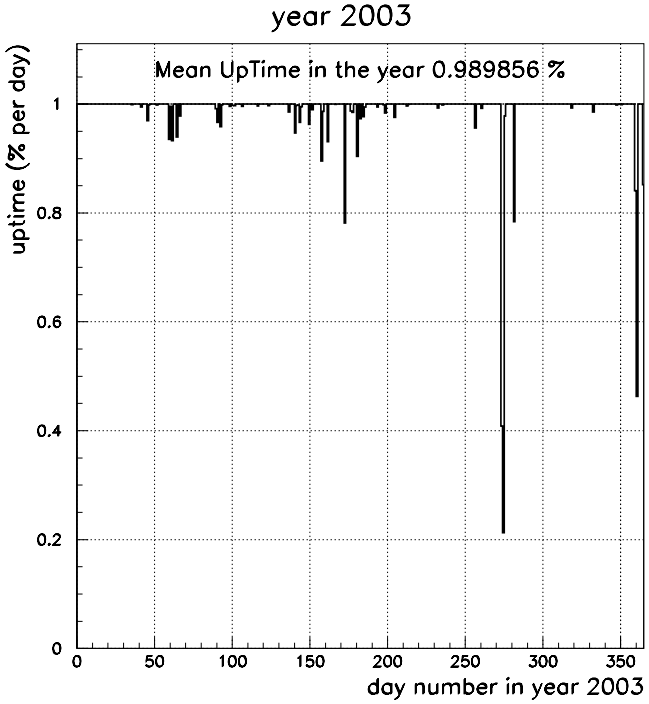

Figure 2: LVD duty cycle during 2003.

resonance ($\sim 10^3\ g/cm^3$) completely adiabatic, meaning that the flip probability between two adiacent mass eigenstates is null ($P_h = 0$). In the adiabatic case and normal mass hierarchy, the $\bar{\nu}_e$ produced in the SN core arrive at Earth as ν_1, and they have a high ($U^2_{e1} \simeq cos^2\theta_{12} \simeq 0.7$) probability to be detected as $\bar{\nu}_e$. On the other hand, the original $\bar{\nu}_x$ arrive at Earth as ν_2 and ν_3 and are detected as $\bar{\nu}_e$ with probability $U^2_{e2} \simeq sin^2\theta_{12}$. Given the higher energy spectrum of $\bar{\nu}_x$ this configuration results in a larger number of interactions, with respect to the no-oscillation case, due to the increasing cross sections with energy. In the adiabatic, inverted hierarchy case the detected $\bar{\nu}_e$ completely come from the original $\bar{\nu}_x$ flux in the star and the number of interaction is still greater, as shown in figure 3, where we take into account the contribution of both inverse beta decay and neutrino-iron interactions and we assume as neutrinosphere temperatures: $T_{\nu_e} = 4$ MeV, $T_{\bar{\nu}_e} = 5$ MeV and $T_{\nu_x} = 7.5$ MeV.

The contribution of the neutrino-iron interactions is better shown in figure 4. For the chosen SN and oscillation parameters they can be as large as about 18% of the inverse beta decay signal and they are due to higher energy neutrinos ($E_\nu > 20\ MeV$).

4 SNEWS

The SNEWS (SuperNova Early Warning System) is a collaboration among experiments of several major neutrino detectors with sensitivity to supernova neutrinos. The primary goal of SNEWS is to provide the astronomical community with a completely automated

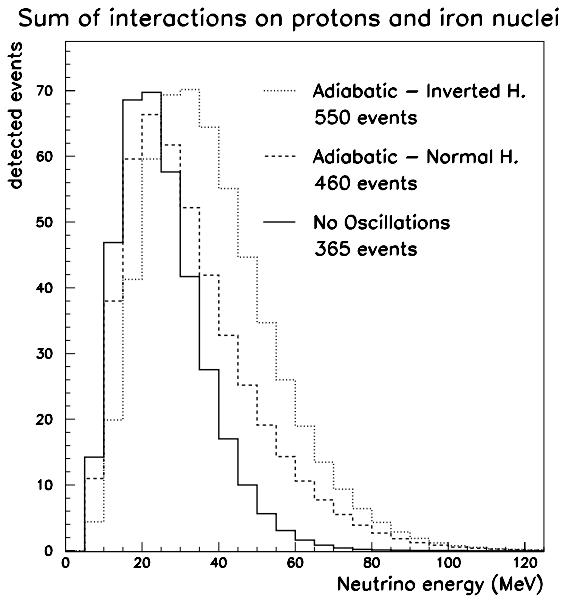

Figure 3: Effect of neutrino oscillations in the signal detected in LVD.

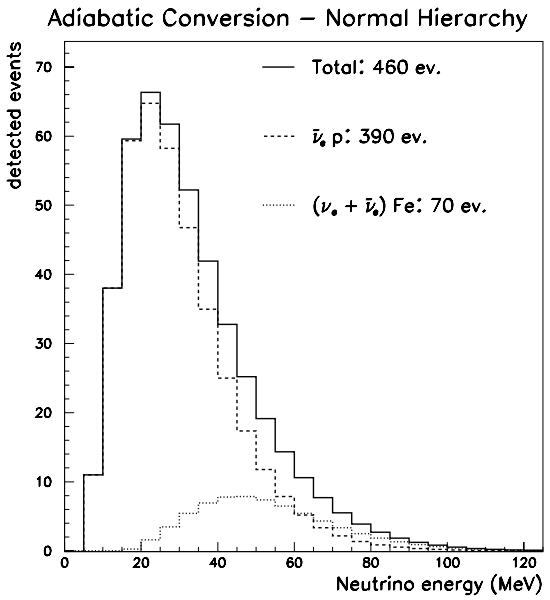

Figure 4: Impact of iron interactions in the global neutrino signal in LVD.

alert[13]. At present Super-K, SNO and LVD are charter members of the SNEWS network. Representative of AMANDA, KamLAND, Borexino, and OMNIS are members of the SNEWS Working Group, and will eventually join the active members of the network.

Two coincidence machines are currently on line, at the Kamioka site and at Gran Sasso. Additional machines will be deployed in the future. These machines continuously run coincidence programs, which wait for alarm signals from the experiments and provide an alert if there is a coincidence within a specified time window (10 seconds for normal running).

At present, the SNEWS network is in a test phase, to ensure the continued reliability of operations.

5 Search for correlations with Gravitational Wave Detector events

A recent analysis of the data collected in coincidence by the gravitational wave bar detectors EXPLORER and NAUTILUS during the year 2001 [18] shows an excess (8 events against 2.6 expected from the background) when the two detectors are favorably oriented with respect to the Galactic Disc. Moreover, this result comes from the present day most sensitive experiments for the detection of gravitational wave bursts and a search for neutrino bursts in correlation with the 8 GWD events is, therefore, appropriate.

A few astrophysical transient sources are indeed expected to produce associated bursts of neutrinos and gravitational waves. It is well known that most of the energy (99%) released in the gravitational core collapse of a massive star is carried away by neutrino originated both from the matter accretion in the shock and from the cooling of the proto-

neutron star (see for example [19]). Depending on the collapse dynamics, some fraction of the total energy is emitted in GW [20, 21], asymmetric supernovae in our Galaxy being the best candidate sources for GW bar detectors. Two coalescing neutron stars would also constitute a source for both neutrinos and gravitational waves. From the point of view of GW emission, it is likely that the merging event would produce powerful gravitational wave bursts, and, even if the physics of the merger is not known, there are estimates that, for binary systems of large mass, coalescence waves are likely to be stronger than the inspiral ones. Some amount of the kinetic energy is converted in thermal energy so that the hot remnant would probably emits thermal neutrinos.

5.1 The Analysis

The scintillator counting rate is continuously monitored: all the events are examined on-line on the basis of their time sequence. Neutrino burst candidates are identified as clusters of scintillator counter pulses with an imitation frequency less than a predefined threshold [22]. During the year 2001, no neutrino burst candidate has been evidenced, thus allowing to conclude that no ν signal from gravitational stellar collapse in the Galaxy has been detected [8].
However, the absence of candidates in the LVD detector taken alone does not preclude the possibility of positive effects, when combining it with another detector, since the joint measurement allows to increase the sensitivity. The analysis in correlation with the 8 candidate events has then been conducted, in four steps described in the following.

Step 1. Check of the detector stability.

First of all, the LVD detector performance at the occurrence of the 8 GW events (see the list in [18]) has been checked by studying the behavior of the counting rate in a 24 hours interval around the time of each of them.

For each event, the 24 hr average of the number of counts every 15 minutes, $\langle n_{15} \rangle$, is evaluated. The LVD counting rate, for all the 8 events and all the data classes, is then well understood in terms of Poissonian statistics: this sets a firm base for the following steps.

Step 2. Search in a sliding window.

The search for a possible ν burst has been conducted in a 24 hours interval T around the occurrence of each of the 8 events. The 8 intervals have been scanned through a "sliding window" of variable duration: more in detail, they have been divided into $N_{\delta t} = 2 \cdot \frac{T}{\delta t} - 1$ intervals of different duration δt, each one starting at the middle of the previous one. The multiplicity distributions of clusters (i.e., the number of events within each δt) have then been studied for the three classes of data and for $\delta t = 1, 5, 10, 20, 50, 100$ s, and have been compared with the expectations from Poissonian fluctuations of the background.

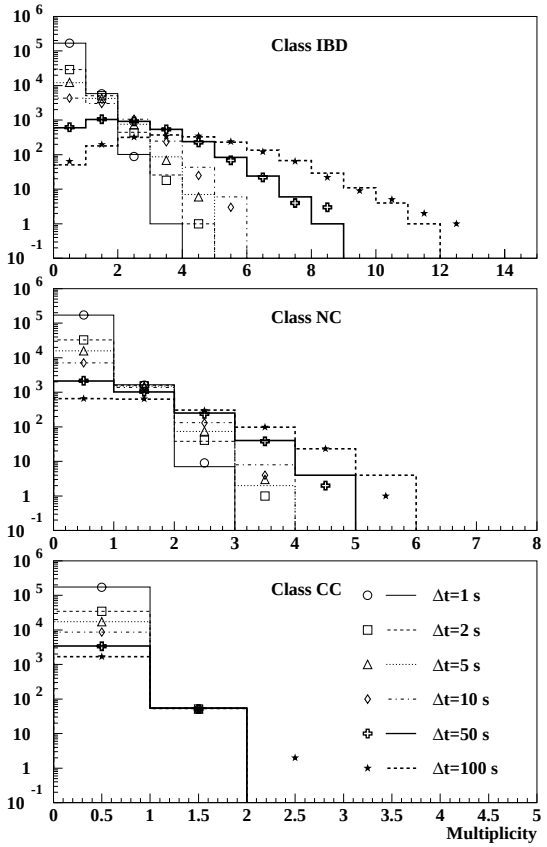

Figure 5: Distributions of cluster multiplicities, for IBD class events (top), NC class (medium), CC class (bottom), together with expectations from Poissonian fluctuations, in the case of GW event n.5.

We show as an example the case of GW event n.5: the distributions of cluster multiplicity, for events of IBD class (top), NC class (middle) and CC class (bottom), in the case of the 6 different δt, can be seen in fig. 5, together with the expectations from Poissonian fluctuations of the background, the relative reduced χ^2 values ranging from 0.1 to 1.2. The agreement between data and expectations holds also in the case of the other seven events. This, together with the check of the Poissonian probabilities associated to each measured multiplicity, in each class and for each event, allows to state that there is no evidence for any detectable ν signal in correspondence of any of the considered events.

Step 3. Search in a fixed window.

The search for a ν signal in coincidence with every GW event has been further conducted using a "fixed window" centered at the time of each of them. In particular, for each data class, we compare the number of pulses ($N_{\rm d}$), recorded during time windows of different duration δt, centered on each event time, with the average number of pulses expected from background, $N_{\rm bk}$. The value of $N_{\rm bk}$ is evaluated by using the rate in the 24 hours around each event, excluding the contribution of the central portion of time to avoid the

contamination due to a possible signal.

The differences between $N_{\rm d}$ and $N_{\rm bk}$ are within the statistical fluctuations, for all data classes and for all the events.

Step 4. Time distribution of pulses.

We have studied the time distribution of LVD pulses around each GW event: no particular time structure is present. Finally, for IBD class data, we have also checked the time distribution of secondary pulses (i.e., those possibly due to neutron capture) with respect to the prompt ones. The measured distribution is uniform and compatible with the one expected in the case of pure background, where delayed and prompt signals are uncorrelated and the distribution of the differences in time is flat (On the contrary, if the pulses were due to $\bar{\nu}_e$ interactions with protons, the distribution of time delays should show an exponential behavior, with $\tau \sim 180\ \mu s$, corresponding to the average capture time of neutrons in the LVD counters).

5.2 Calculation of upper limits on neutrino fluence

No evidence for any statistically relevant signal in LVD, in the three considered reaction channels (corresponding to different neutrino species) and over a wide range of time durations, has been found in correspondence of any of the 8 excess events detected in coincidence by NAUTILUS and EXPLORER.

In the absence of any ν signal, we calculate 90% C.L. neutrino fluence upper limits at the detector without assuming particular energy spectra, i.e., on monoenergetic neutrinos at different energies:

$$\Phi(E_\nu) = \frac{N_{90}}{M \cdot N_t \cdot \sigma(E_\nu) \cdot \epsilon(E_\nu)} \tag{1}$$

where: N_{90} is the 90% c.l. upper limit on the number of LVD signals per GW event, obtained following [23] in the case of Poisson processes with background. The considered background value represents the total number of expected background events for all the 8 GWD events; the signal value, as well, is the total number of detected events for all the 8 GWD events. M is the detector active mass in ton (summed over the 8 events); N_t is the number of targets per ton (either protons or ^{12}C nuclei); ε is the detection efficiency; $\sigma(E_\nu)$ is the appropriate cross section.

Results are shown in table 2 for $\delta t = 100 s$.

Table 2: Fluence upper limits (90% C.L.) for neutrinos of different energies, obtained from IBD and NC classes of events.

E_ν	$\Phi_{\bar{\nu}_e}\ cm^{-2}$	$\Phi_{\nu_i}\ cm^{-2}$
10 MeV	$9.81 \cdot 10^9$	–
15 MeV	$4.07 \cdot 10^9$	$2.30 \cdot 10^{15}$
20 MeV	$2.27 \cdot 10^9$	$3.32 \cdot 10^{11}$
30 MeV	$1.04 \cdot 10^9$	$3.90 \cdot 10^{10}$
40 MeV	$6.17 \cdot 10^8$	$1.56 \cdot 10^{10}$
50 MeV	$4.20 \cdot 10^8$	$9.10 \cdot 10^9$
60 MeV	$3.11 \cdot 10^8$	$6.44 \cdot 10^9$
70 MeV	$2.44 \cdot 10^8$	$5.18 \cdot 10^9$
80 MeV	$1.99 \cdot 10^8$	$4.48 \cdot 10^9$
90 MeV	$1.64 \cdot 10^8$	$4.12 \cdot 10^9$
100 MeV	$1.44 \cdot 10^8$	$3.93 \cdot 10^9$

5.3 Conclusions

We have found no evidence for any statistically relevant signal in LVD, in three different reaction channels (inverse beta decay, charged current and neutral current interactions with ^{12}C) corresponding to different neutrino species, over a wide range of time durations, for any of the 8 events. Consequently, we have derived 90% fluence upper limits to antineutrino and neutrino emission from an average GW event, at different energies in the range of sensitivity of the LVD detector.
We have then related the result of the search with two possible simplified models for neutrino emission, i.e., "cooling" and "accretion", deriving limits, on the one side, to the total energy emitted in neutrinos at the source, and, on the other, to the amount of accreting mass. Assuming a source distance $d = 10$ kpc, possible candidates as new-born and colliding neutron stars have been excluded by this analysis. This makes even more challenging and interesting the search for a likely astrophysical source for the reported GWD events.

6 Search for correlations with solar flares

During large solar flares protons of the solar atmosphere can be accelerated at several tens of GeV; from theirs interaction with the solar matter pions and kaons are produced which decay into neutrinos:

$$\pi \rightarrow \mu + \nu_\mu$$

$$k \rightarrow \mu + \nu_\mu$$

$$\mu \rightarrow e + \nu_e + \nu_\mu$$

Theoretical calculation of neutrino and antineutrino production during solar flares are affected by large uncertainties [24]. They are presented as a function of the proton energy spectrum, which varies from flare to flare, and as a function of the neutrino emission angle with respect to the proton beam axis.

During 2000, 2001 and 2002 the Sun has reached a maximum in the activity of its 23^o cycle; we select 23 events with a high proton flux to search for an excess of neutrino events in the LVD experiment.
Premilinary results were presented at the latest ICRC [25].

7 List of pubblications in 2003

- *CNGS beam monitor with the LVD detector at LNGS.*
  Proc. of the XX International Conference on Neutrino Physics and Astrophysics, Munich, Germany, 25-30 May 2002.
  Nuclear Physics B (Proc. Suppl.) 118, 507 (2003)

- *CNGS beam monitor with the LVD detector at LNGS.*
  LNGS/EXP-05/03 *March 03*

- *The Study of Elemental Species or the Primary Cosmic Rays at Energies* $10^{13} - 10^{16}$ *eV by the LVD Experiment*
  Proc. 28 ICRC, Tsukuba, HE 2.1, 1135, (2003).

- *The Evidence for the Variation of the Mass Composition with Energy in the Region of the Knee by the LVD Experiment*
  Proc. 28 ICRC, Tsukuba, HE 2.1, 1139, (2003).

- *Analysis of the Events Recorded by the LVD Neutrino Detector from Large Solar Flares during High Solar Activity*
  Proc. 28 ICRC, Tsukuba, HE 2.2, 1251, (2003).

- *CNGS Beam Monitor with the LVD Detector*
  Proc. 28 ICRC, Tsukuba, HE 2.2, 1279, (2003).

- *Study of the Effect of Neutrino Oscillation on the SuperNova Neutrino Signal with the LVD Detector*
  Proc. 28 ICRC, Tsukuba, HE 2.3, 1297, (2003).

- *10 Years Search for Neutrino Bursts with LVD*
  Proc. 28 ICRC, Tsukuba, HE 2.3, 1333, (2003).

- *Search for Correlations between GW Detectors and the LVD Neutrino Telescope*
  Proc. 28 ICRC, Tsukuba, OG 3.5, 3149, (2003).

References

[1] LVD Collaboration, Il Nuovo Cimento **A105** (1992) 1793

[2] A. Strumia, F. Vissani, `astro-ph/0302055`.

[3] LVD Collaboration, 23th ICRC Conf.Proc.,HE 5.1.1,Vol.4,468,1993

[4] LVD Collaboration, 24th ICRC Conf.Proc., HE 5.3.6,Vol.1,1035,1995

[5] LVD Collaboration, 25th ICRC Conf.Proc., HE 4.1.12,1997

[6] LVD Collaboration, 26th ICRC Conf.Proc., HE 4.2.08,Vol.2,223,1999

[7] LVD Collaboration, 27th ICRC Conf.Proc., HE230,1093,2001

[8] LVD Collaboration, 28th ICRC Conf.Proc., HE2.3,1333,2003

[9] LVD Collaboration, Nucl. Phys. B Proc. Sup. 110 (2002) pp 410-413, astro-ph/0112312

[10] A. Zichichi, *The most powerful scintillator supernova neutrino detector*, talk presented at the symposium *LVD: the First Ten Years*, LNGS, 28-29 October, 2002).

[11] LVD Collaboration, 28th ICRC Conf.Proc., HE2.3,1297,2003

[12] C.Lunardini and A.Yu.Smirnov, hep-ph/0106149

[13] http://hep.bu.edu/∼snnet/

[14] SNEWS Subgroup "Proposal for an Automated Supernova Alert for the Astronomical Community"

[15] M. Fukugita, Phys. Lett. B 212:139 , (1988)

[16] E. Kolbe, K. Langanke, `nucl-th/0003060`.

[17] J. Toivanen et al., *Nuclear Physics A* **694** (2001), 395-408.

[18] Astone P., Babusci D., Bassan M., et al., 2002, Class. Quant. Grav. 19, 5449

[19] Burrows A., Klein D., Gandhi R. 1992, Phys. Rev. D, 45, 3361

[20] Thorne, K.S., 1988, "Gravitational radiation", Cambridge Univ. Press, Cambridge (MA)

[21] Muller, E. Class. Quant. Grav. 1997, 14, 1455

[22] Fulgione, W., Mengotti-Silva, N., & Panaro, L. 1996, Nucl. Instr. Meth., A, 368, 512

[23] Montanet, L., et al., 1994, Phys. Rev., D, 50, 1173

[24] Kocharov et al., Il Nuovo Cimento C **14** (1991) 417.

[25] LVD collaboration, Proc. 28 ICRC, Tsukuba, HE 2.2, 1251, (2003).

OPERA

METU, Ankara, Turkey
M. Guler, M. Serin-Zeyrek, P. Tolun, M.T. Zeyrek

LAPP, IN2P3-CNRS and Université de Savoie, Annecy, France
A. Degre, J.Damet, D. Duchesneau, J. Favier, M. Lavy, H. Pessard

L'AQUILA University and INFN,'LAquila, Italy
P. Monacelli

Bari University and INFN, Bari, Italy
M. Ieva, M.T. Muciaccia, M. De Serio, S. Simone

IHEP, Beijing, China PR
S.L. Lu, J. Ren, S.J. Zhou

Humboldt University, Berlin, Germany
K. Winter

Bern University, Bern, Switzerland
K. Borer, M. Hess, U. Moser, K. Pretzl, T. Waelchli, M. Weber

Bologna University and INFN, Bologna, Italy
G. Giacomelli, G. Mandrioli, L. Patrizii, P. Serra, M. Sioli, G. Sirri

IIHE (ULB-VUB), Brussels, Belgium
G. Van Beek, P. Vilain, G. Wilquet

JINR, Dubna, Russia
D. Bardin, I. Boudagov, G. Chelkov, Y. Gornouchkine, Z. Kroumchtein, A. Nozdrin, A. Olchevski, A. Sadovski.

LNF, Frascati, Italy
F. Bersani Greggio, B. Dulach, A. Franceschi, F. Grianti, A. Paoloni, M. Spinetti, F. Terranova, L. Votano

LNGS, Assergi, Italy
C. Gustavino

Toho University, Funabashi, Japan
S. Ogawa, H. Shibuya

Märkische Fachhochschule FB Elektrotechnik, Hagen, Germany
K. Schauties, H. Sohlbach, H. Woltersdorf

Israeli group c/o Technion, Haifa, Israel
J. Goldberg

Hamburg University, Hamburg, Germany
C. Ballhausen, F.W. Buesser, J. Ebert, B. Koppitz, B. Naroska, W. Schmidt-Parzefall, R. van Staa, R. Zimmermann

Shandong University, Jinan, Shandong, China PR
C.F. Feng, Y. Fu, M. He, J.Y. Li, L. Xue

Aichi Educational University, Kariya, Japan
K. Kodama, N. Ushida

Kobe University, Kobe, Japan
S. Aoki, T. Hara

IPNL, IN2P3-CNRS and Université C. Bernard Lyon I, Villeurbanne, France
A.Autiero,L. Chaussard, Y. Déclais, C. Heritier,I. Laktineh, J. Marteau, P. Royole-Degieux

Münster University, Münster, Germany
P. Boschan, N. Bruski, D. Frekers

Nagoya University, Nagoya, Japan
K. Hoshino, M. Komatsu, M. Miyanishi, M. Nakamura, T. Nakano, K. Niwa, O. Sato, T. Toshito

"Federico II" University and INFN, Naples, Italy
M. Ambrosio, S. Buontempo, N. D'Ambrosio, G. De Lellis, G. De Rosa, F. Di Capua, P. Migliozzi, C. Pistillo, L. Scotto Lavina, G. Sorrentino, P. Strolin, V. Tioukov

Neuchatel University, Neuchatel, Switzerland
J. Busto, M. Hauger, J. Janiscko, F. Juget, J-L. Vuilleumier, J-M. Vuilleumier

Institute of Nuclear Power Engineering, Obninsk, Russia
S. Aplin, V. Galkine, V. Saveliev, M. Zaboudko

LAL, IN2P3-CNRS and Université Paris-Sud, Orsay, France
J. Boucrot, J.E. Campagne, A. Cazes, A. Lucotte, J.P. Repellin

Padova University and INFN, Padova, Italy
R. Brugnera, F. Dal Corso, S. Dusini, C. Fanin, A. Garfagnini, L. Stanco

"La Sapienza" University and INFN, Rome, Italy
P. Righini, G. Rosa

Fachbereich Physik der Universitaet Rostock, Rostock, Germany
M. Beyer, H. Schroeder, R. Waldi, R. Zimmermann

Salerno University and INFN, Salerno, Italy
E. Barbuto, C. Bozza, G. Grella, G. Romano, S. Sorrentino

Sofia University, Sofia, Bulgaria
D. Kolev, R.Tsenov

IRES, IN2P3-CNRS and Université Louis Pasteur, Strasbourg, France
R. Arnold, E. Baussan, M. Dracos, J.L. Guyonnet, J.P. Engel, B. Dorion

Utsunomiya University, Utsunomiya, Japan
Y. Sato, I. Tezuka

Rudjer Boskovic Institute (IRB), Zagreb, Croatia
K. Jakovcic, A. Ljubicic, M. Stipcevic

Abstract

The OPERA experiment has been designed for an appearance search of $\nu_\mu \leftarrow \nu_\tau$ oscillations in the parameter region indicated by Super-Kamiokande as the explanation of the zenith dependence of the atmospheric neutrino deficit. OPERA is a long baseline experiment being constructed at the Gran Sasso Laboratory in the CNGS neutrino beam from the CERN SPS. The detector design is based on a massive lead/nuclear emulsion target. Nuclear emulsion are used as high resolution tracking devices, for the direct observation of the decay of the τ leptons produced in ν_τ charged-current interactions. Electronic detectors are used to locate the event in the emulsions. Magnetized iron spectrometers measure charge and momentum of muons. The discovery potential of OPERA originates from the observation of a ν_τ signal with very low background level. The direct observation of $\nu_\mu \leftarrow \nu_\tau$ appearance will constitute a milestone in the study of neutrino oscillations. The OPERA experiment will also search for $\nu_\mu \leftarrow \nu_e$ with a sensitivity a factor two better than current limits from CHOOZ. During 2003 the OPERA collaboration made important progresses on the construction of the detector components and the installation in tha Hall C of LNGS.

1 Design Principles

The OPERA experiment [1] is designed for the direct observation of ν_τ appearance from $\nu_\mu \rightarrow \nu_\tau$ oscillations in the CNGS long-baseline beam from the CERN SPS to the Gran

Sasso laboratory.

The measurements of atmospheric neutrino fluxes performed by the Super-Kamiokande experiment indicate a deficit of muon neutrinos with a zenith angle distribution consistent with $\nu_\mu \rightarrow \nu_\tau$ oscillations with $\Delta m^2_{23} = 1.3 - 3.0 \times 10^{-3} eV^2$ (90% C.L.) and full mixing.

The Soudan2 and MACRO and K2K experiments also made observations compatible with this result. Therefore the primary goal of OPERA is to obtain direct evidence for ν_τ appearance, which would confirm the oscillation hypothesis and its nature. An important byproduct is the search for $\nu_\mu \rightarrow \nu_e$ oscillations which could lead to a first measurement of the mixing angle θ_{13}.

A long baseline of 732 Km is used between the neutrino source (the CERN beam line) and the detector (located in the Gran Sasso underground laboratory), in order to be sensitive to the oscillation parameters indicated by the Super-Kamiokande data. The CNGS neutrino beam has been optimized for the detection of ν_τ charged current (CC) interactions and provides an average ν_μ energy of about 20 GeV. For the evaluation of the performance of the experiment an integrated fluence of 2.25×10^{20} protons on target is assumed, corresponding to 5 years SPS operation in shared mode. However, ongoing studies at CERN aim to obtain a beam intensity upgrade equivalent to a factor 1.5.

The main principle of the ν_τ search is the direct detection of the decay of the τ lepton produced by CC interactions. This is achieved by a massive (about 1.8 Kton) neutrino target based on the Emulsion Cloud Chamber (ECC) design which combines, in a sandwich-like cell, the high-precision tracking capabilities of nuclear emulsions (two 40 μm layers on both sides of 200 μm plastic base) and the large target mass provided by the lead plates (1 mm thick). This technique has been recently demonstrated to be effective for τ detection by the DONUT Collaboration.

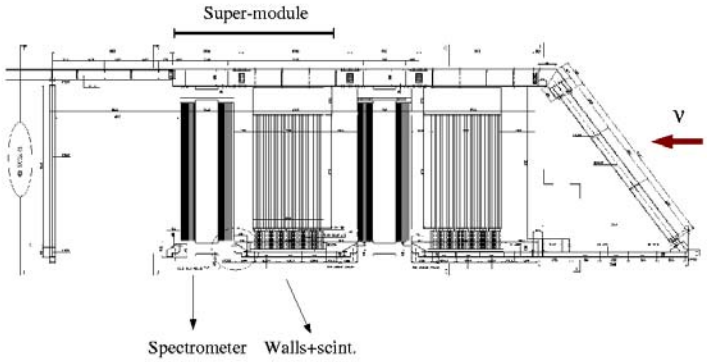

Figure 1: Side view of the OPERA detector

The basic element of the target structure is the brick, made out of consecutive series of ECC cells with transverse dimensions of 10.2×12.7 cm^2. Bricks are arranged in planar structures (walls), which are interleaved with electronic tracker planes (fig. 1). These planes are built from vertical and horizontal strips of extruded plastic scintillator 2.6 cm wide, read out by wavelength-shifting fibers coupled with photodetectors at both ends. The main purposes of the target tracker are to provide a trigger for neutrino

interactions, localize the particular brick in which the neutrino interacted and perform a first muon tracking within the target. The selected brick is then extracted from the target for the emulsion development and scanning in a quasi-online sequence. Large emulsion areas can be scanned with automatic microscopes equipped with fast track-recognition processors. This technique allows for the search of the tau decay topology and, at the same time, for the measurement of the event kinematic. Tracks momenta are measured from their multiple scattering in the brick and electron and gamma energies from showers development. The total number of bricks amounts to 206,336 resulting in a target mass of 1766 tons.

Figure 1 shows the target and the tracker sections, which are further arranged in two independent supermodules. Each supermodule includes a block of 31 walls+scintillator planes, followed downstream by a magnetized iron spectrometer. The spectrometers are used for the identification of muons and to measure their charge and momentum. Each spectrometer consists of a dipolar magnet made of two iron walls interleaved with pairs of precision trackers. Particle trajectories are measured by these trackers, consisting of vertical drift tube planes. Resistive Plate Chambers (RPC) with inclined strips, called XPC, are combined with the precision trackers to provide unambiguous track reconstruction in space. Moreover, planes of RPCs (Inner Tracker) are inserted between the magnet iron plates. They allow a coarse tracking inside the magnet to identify muons and ease track matching between the precision trackers. They also provide a measurement of the tail of the hadronic energy leaking from the target and of the range of muons which stop in the iron.

The OPERA design is optimized to achieve low background levels for the tau appearance search. The experiment aims at the analysis of all the single-prong tau decay modes (e,μ,h). Signal events are classified as long or short decays depending on whether the tau track traverses an emulsion sheet or not. The main background sources are charm production in CC interactions, hadronic interactions in lead and large-angle muon Coulombian scatterings. These events are rejected by the identification of the primary lepton in CC interactions and either by requiring the presence of a tau-like kink topology (long decays) or by an impact parameter method (short decays). In addition a kinematic analysis is used to enhance the signal-to-background ratio. Overall a total background of 0.7 events is expected. If $\nu_\mu \rightarrow \nu_\tau$ oscillations occur, the average number of detected signal events ranges from 3.1 (at $\Delta m^2 = 1.3 \times 10^{-3} eV^2$) to 16.4 (at $\Delta m^2 = 3.0 \times 10^{-3} eV^2$) and corresponds to 7.3 events for the Super-Kamiokande best fit value ($\Delta m^2 = 2.0 \times 10^{-3} eV^2$, full mixing).

For what concerns the search for $\nu_\mu \rightarrow \nu_e$ oscillations, still after a five years run, OPERA will be able to constrain the θ_{13} mixing angle at the level $\theta_{13} < 0.06$ at 90% C.L. (for $\Delta m^2 = 2.5 \times 10^{-3} eV^2$, $\sin^2 2\theta_{23} = 1$).

2 Detector construction progress in 2003

The OPERA experiment was approved in 2001. During 2002 the Collaboration completed the detector design, tests and optimization phase resulting in a two supermodules configuration. Important progresses were made in 2003, as foreseen by the construction schedule,

in order to finalize the design for the industrial production and enter in the construction phase of several parts of the detector. The production chain for the target tracker modules was completely setup in Strasbourg. The design of the Brick Assembly Machine (BAM) was completed and a tendering procedure has been recently accomplished in order to select the industry which will build the BAM. The target walls tendering and ordering have been completed as well in 2003 after final definition of the brick dimensions. Their first delivery at LNGS is expected in September 2004. The prototyping phase for the general DAQ electronics and the front end electronics for the target tracker has been completed in 2003. A prototype of the Brick Manipulator System was fully tested. The production of many components of the detector (magnets, RPC, target tracker strips, mechanics and readout electronics) was started.

The mass production of nuclear emulsions started in April 2003 and will end in spring 2005. About 15% of the emulsion films have been produced so far. An underground facility for their refreshing (the erasure of the cosmic ray tracks accumulated during the production) was setup in the Tono mine in Japan. After production at Fuji Inc., the emulsion sheets are refreshed and sent to Gran Sasso where an emulsion storage area, located in the hall B of LNGS, was built in summer 2003. The development of the scanning systems has improved significantly. A peak scanning power of 20 cm^2/h has been reached by the european laboratories while the current scanning speed at 90% efficiency is of the order of 10 cm^2/h. The development of the Japanese scanning system is also well in progress.

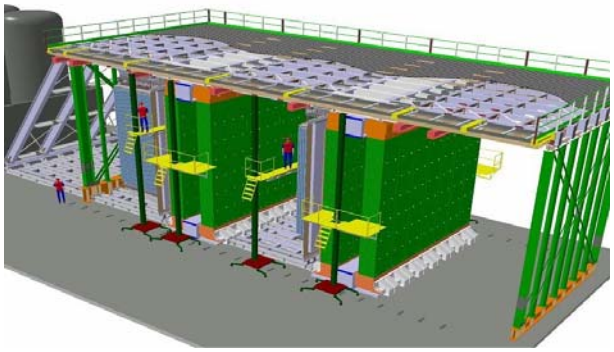

Figure 2: Artist view of the installation setup in Hall C

Since February 2003 the detector installation (fig. 2)in the Hall C of the LNGS underground laboratory has been going on with the assembly of the magnetic spectrometers and the RPC system. It was temporarily halted in May, after sealing of the experimental hall due to the investigations on the accidental Borexino pseudocumene discharge in summer 2002 and it has been restored in August. At the time of writing (January 2004), the lower return yokes of the two magnets have been installed together with the connecting support structure. Two vertical walls have been positioned and fully instrumented with Resistive Plate chambers (see fig. 3).

The mass production of the RPC started in January 2003. All the chambers for the construction of the first spectrometer have been already produced. Before being inserted

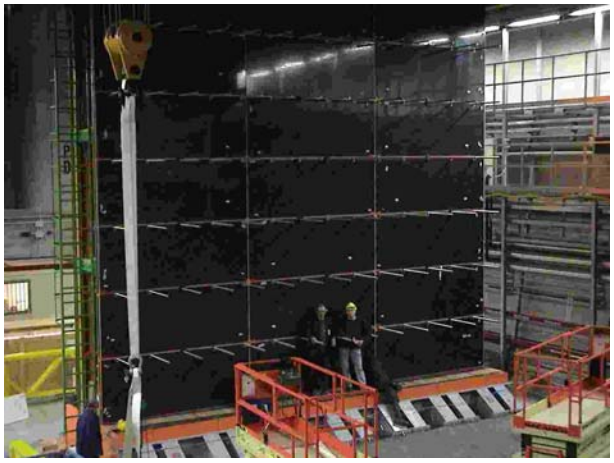

Figure 3: Installation of the first RPC plane in the OPERA spectrometer at LNGS

in the magnet they undergo a full test procedure (including mechanical tests, electrical tests and efficiency measurements with cosmic muons) in a facility setup at LNGS in 2003. The completion of the first spectrometer is foreseen in June 2004 while the installation of the target tracker will start in fall 2004.

The OPERA installation will end in 2006, when the first neutrinos from the CNGS beam are expected.

3 The OPERA RPC system

The RPC (Resistive Plate Chamber) system for the OPERA Spectrometers reached fully functionality during the year 2004. The major results were the start in April 2003 of the mass production test inside the Lab2 building and the beginning of the installation in the underground area Hall C. The RPC are produced at the external company General Tecnica in Colli (Frosinone) with a rate of roughly 20 detectors per week. Each detector consists of two plate of high resistivity ($\geq 10^{11}$ Ω/cm) of bakelite, each 2mm thick, and an air gap of 2 mm. The size is 291x114 cm^2 to optimize the iron wall of the spectrometer (875x800 cm^2). Each iron wall is then overlayed by 21 detectors, in total being 22 walls of RPCs. The installation of RPC in Hall C started in November. At the present time, more than 1/3 of the first Spectrometer of OPERA has been assembled (see picture 3). Only 2 detectors had some brokening during installation time and 1 detector had further the gas outlet broken (to be restored by an expert of the General Tecnica). Only 6 detectors over 160 showed some electrical problems eventually solved. The electronics for RPC was developed during 2003. The final prototype of the Front-End boards was setup, together with a controller board and the first ideas for a trigger board. The full electronic system is going to be settled in Naples in the next months while the installation is foreseen for the beginning of 2005 when the floor on the top of the Spectrometers will be completed.

3.1 The Gran Sasso RPC test facility

Before the installation in the OPERA experiment, bakelite RPCs are subjected to a chain of quality tests performed at the Gran Sasso Laboratories [2]. Mechanical properties are first investigated in a fully automatized station, measuring the gas leakage and checking the gluing of the internal spacers. Then electrical properties are tested: current vs voltage characteristics are measured both with pure argon and with gas mixture filling; moreover the short term behavior of the current is monitored. Finally the response uniformity is tested, measuring the efficiency on the entire detector surface at cosmic rays fluxes.

- The aim of the mechanical tests is to verify RPC gas tightness and check for proper gluing of the spacers between the electrodes. The "leakage" test consists in connecting the RPC gas outlets to the gas system and monitoring the variation of the internal pressure with respect to the atmospheric pressure. Once an overpressure of 6 mbar is reached, the gas circuit is closed and the RPC pressure is monitored: since the sensor is sensitive to small pressure variations, few minutes are enough to detect small gas leakages. The "push" test is used to verify the proper gluing of the spacers. It is based on the fact that a small RPC overpressure will produce a local deformation when a spacer is not glued to the electrodes. Applying a small pressure on the spacer from outside, it is possible to "push" the electrode back to the spacer: this will decrease the RPC gap volume resulting in a pressure increase. The test is performed by means of small cylinders mounted on a bar which can be moved over the table where the RPC lays. The bar moves automatically over the RPC rows of spacers and tests them all. If a faulty row is found, each spacer is tested independently. All the movements are controlled with a PLC which is interfaced with a linux PC running Labview.

- The electrical tests have been designed to measure:

  1. current - voltage characteristics in pure argon;
  2. current - voltage characteristics in gas mixture (Ar: i-C_4H_{10} : $C_2H_2F_4$: 76 : 4 : 20 with additional 0.5% of SF_6);
  3. short term behaviour of the RPC at a fixed voltage.

  The test setup allows to test 48 RPCs at once. The currents are measured independently on the negative poles with nanoamperometers embedded in the distributors and on the positive channels using the current-meters of the power supply. At last, a short term test is performed (for minimum 24 hours up to few days). The RPC is kept at a fixed voltage (below the operational voltage) and the current is monitored versus time. Only RPCs with low and stable currents pass the test.

- Cosmic ray test. The last test is dedicated to study the performance in detecting cosmic rays. The cosmics test stand is made of two vertical and parallel planes (4×4 m^2) with glass RPCs, placed at a distance of 3.15 m. These two planes are used for trigger and tracking purposes. A picture of the cosmic ray test facility is shown in figure 4 The RPCs under tests are placed inside 3 boxes, (12 RPCs/box),

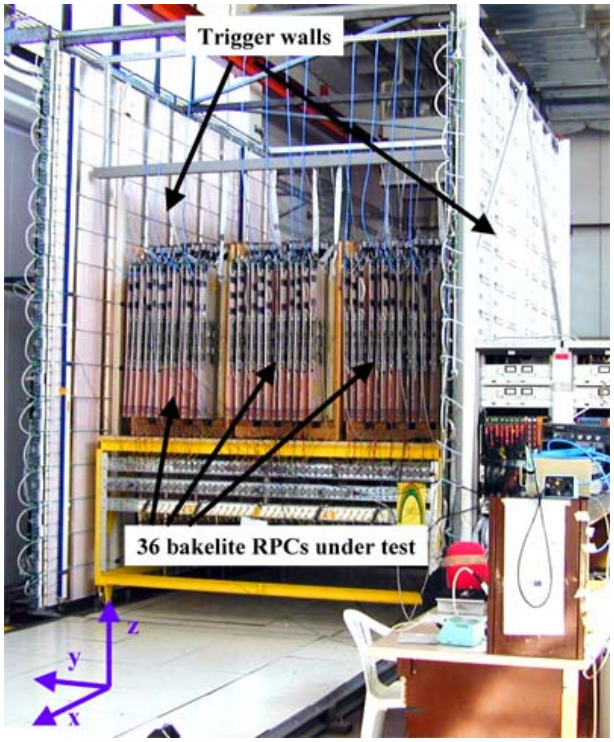

Figure 4: The cosmic ray test facility at the LNGS.

in vertical position. They are read out by two planes of orthogonal strips with a 3.5 cm pitch (32 horizontal channels and 96 vertical), using digital Front End (FE)cards developed for the MACRO experiment. Each FE card generates also a digital OR of the input channels which is sent to a scaler and used to measure the RPC's single rate. The test program is divided into three steps:

1. average efficiency and single rate as a function of gap voltage;
2. local RPC efficiency (chamber radiography) at the nominal working voltage;
3. local noise map of the RPC.

The local RPC efficiency is measured in bins of 10×10 cm^2 and is used to check the chamber response uniformity; the uncertainty on the efficiency is less than 1%. In case of local inefficiencies the RPC is rejected.

4 List of Publications

1. P. Migliozzi and F. Terranova, *Next generation long baseline experiments on the path to leptonic CP violation Phys. Lett. B563 (2003) 73.*

2. D. Autiero et al., *The synergy of the golden and silver channels at the neutrino factory*, hep-ph/0305185, to appear in Eur. Phys. J.

3. A. Garfagnini et al., *Quality control tests on RPCs for the OPERA experiment* , Proceedings of the VII Workshop on Resistive Plate Chambers and Related Detectors (Clermont-Ferrand, France, 20-22 Oct. 2003), to appear in Nucl. Instrum. Meth.

4. C. Gustavino et al., *The OPERA test facility at the Gran Sasso*, Proceedings of the VII Workshop on Resistive Plate Chambers and Related Detectors (Clermont-Ferrand, France, 20-22 Oct. 2003), to appear in Nucl. Instrum. Meth.

5. G. Sorrentino et al., *The OPERA muon spectrometer tracking electronics*, Proceedings of the VII Workshop on Resistive Plate Chambers and Related Detectors (Clermont-Ferrand, France, 20-22 Oct. 2003), to appear in Nucl. Instrum. Meth.

References

[1] M. Guler *et al.*, OPERA proposal, CERN/SPSC 2000-028, SPSC/P318, LNGS P25/2000.

[2] S. Dusini *et al.*, "Design And Prototype Tests Of The Rpc System For The Opera Spectrometers," NIM A 508 (2003) 175.

THEORY GROUP

R.Aloisio, Z.Berezhiani, V.Berezinsky, P. Ciarcelluti, G. Di Carlo, A.F.Grillo, A.Galante, L. Gianfagna, F.Mendez, M. Narayan, A. Sakharov, F.Vissani.

The activity of the group in year 2003 has concerned research in the fields: Astroparticle Physics (mainly in Iniziativa Specifica FA51), Particle Phenomenology (mainly in IS PI21) and Computer simulations of Lattice Gauge Theory (in IS GS11). In addition, a research activity on Planck Scale Kinematics and Phenomenology is continuing, also partly included in year 2003 in IS GS11. The activities are more specifically reported below.

1 Astroparticle Physics

The Astroparticle group of LNGS in 2003 included R.Aloisio, V.Berezinsky, M.Narayan, F.Vissani and visitors V.Dokuchaev (Institute for Nuclear Research, Moscow), Yu.Eroshenko (Institute for Nuclear Research, Moscow), B.Hnatyk (Lviv University, Ukraine) ,S.Grigorieva (Institute for Nuclear Research, Moscow) and A.Gazizov (DESY, Germany). The group worked in close collaboration with A.Vilenkin (Tufts University, USA), M.Kachelriess (CERN), P.Blasi (Fermilab), G.Senjanovich (ICTP), A.Strumia (Pisa University) and others

Scientific work

The main field of the work is astroparticle physics, including solar neutrinos, physics in underground detectors, massive neutrinos, ultra high energy cosmic rays, topological defects, and relativistic astrophysics. From several works finished in 2003 two following results can be mentioned

B. Bajc, G. Senjanovic and F. Vissani demonstrated that neutrino masses led to reconsider SO(10), in its minimal renormalizable form. In Phys.Rev.Lett. 90 051802 (2003) was outlined the link, due to non-canonical (type II) form of the see-saw, between large atmospheric neutrino mixing and b-tau unification. The consistency of a supersymmetric version of this theory has further been explored in hep-ph/0306242.

V.Berezinsky, V.Dokuchaev and Yu.Eroshenko studied production and evolution of small-scale dark matter clumps in the standard cosmological scenario with inflation produced primeval fluctuation spectrum. The mass spectrum of small clumps with $M \leq 10^3 M_\odot$ is calculated with tidal destruction of the clumps taken into account. Only 0.1 - 0.5 % of clumps survive the stage of tidal destruction. The mass distribution of clumps has a cutoff at $M_{\rm min}$ due to free streaming. In case of neutralino (bino) $M_{\rm min} \sim 10^{-8} M_\odot$. The evolution of density profile does not result in the singularity because of the formation of the core under influence of the tidal interaction. The radius of the core is $R_c \sim R$, where

R is radius of the clump. The enhanacement of annihilation signal due to clumpiness for the halo DM is calculated. Despite small survival probability, the annihilation signal is dominated by the clumps.
The work is published in Phys.Rev. **D68**,103003 (2003).

Conferences, seminars and other activities

V.Berezinsky works as an editor of Int. Journal "Astroparticle Physics"

F.Vissani works (together with O.Palamara) as the organizer of the LNGS seminar

V.Berezinsky served as convener at TAUP 2003 in Seattle, USA

, F.Vissani was one of the organizers of Conference on Hierarchy Problems in Four and More Dimensions ICTP, Trieste, October 2003

R.Aloisio presented two invited talks at the 10th Marcel Grossman Meeting (Rio de Janeiro, July 2003

V.Berezinsky presented invited talks at TAUP 2003 (Seattle USA), at 6th RESCEU International Conference "Frontiers in Astroparticle Conference and Cosmology" (Tokyo, Japan), at Int. Workshop "Neutrino Oscillations" (Venice, Italy) and at Int. Workshop " Cosmology and DM" (Sorrento, Italy) and served as a lecturer at Summer school on Particle and Nuclear Astrophysics in Nijmegen (Holland).

F'Vissani presented invited talks at 17th Rencontres De Physique De La Vallee D'Aoste "Results And Perspectives In Particle Physics" March 2003, La Thuile,Italy, and at International Europhysics Conference On High-Energy Physics (HEP 2003), July 2003, Aachen, Germany.

Journal and Proceedings publications in 2003

1. V. Berezinsky, V. Dokuchaev, Yu. Eroshenko
SMALL-SCALE CLUMPS IN THE GALACTIC HALO AND DARK MATTER ANNIHILATION
Phys.Rev. **D68**, 103003 (2003)

2. V. Berezinsky, M. Narayan, F. Vissani
MIRROR MODEL FOR STERILE NEUTRINOS
Nucl.Phys. **B658**, 254 (2003)

3. LVD Collaboration (M. Aglietta,.. V.Berezinsky et al.)
STUDY OF SINGLE MUONS WITH THE LARGE VOLUME DETECTOR AT GRAN SASSO LABORATORY
Phys.Atom.Nucl.**66**, 123 (2003), Yad.Fiz.**66**, 125 (2003)

4. V.Berezinsky
SUPERGZK NEUTRINOS: TESTING PHYSICS BEYOND THE STANDARD MODEL

Proc. 21 Symp. on Relativ. Astrophysics (eds, R.Bandiera, R.Maiolino, F.Mannucci), World Scientific, 379 (2003)

5. V.Berezinsky, A.Gazizov, S.Grigorieva
SIGNATURES OF PROTONS IN UHECR
Proc. of Workshop "Extremely High Energy Cosmic Rays" (eds M.Teshima and T.Ebisuzaki) Universal Academy Press (Japan), 63 (2003)

6.F. Vissani, M. Narayan, V.S. Berezinsky
U(E3) FROM PHYSICS ABOVE THE GUT SCALE
Phys.Lett. **B571**, 209 (2003)

7. B. Bajc, G. Senjanovic, F. Vissani
B - TAU UNIFICATION AND LARGE ATMOSPHERIC MIXING: A CASE FOR NON-CANONICAL SEESAW
Phys.Rev.Lett. **90** 051802 (2003)

8. A. Strumia, F. Vissani
PRECISE QUASIELASTIC NEUTRINO/NUCLEON CROSS-SECTION
Phys.Lett. **B564**, 42 (2003)

9. F. Vissani
PERSPECTIVES IN NEUTRINO PHYSICS
Frascati Physics Series, Volume XXX Special Issue (2003) Les Rencontres de Physique de la Valle d'Aoste RESULTS AND PERSPECTIVES IN PARTICLE PHYSICS La Thuile, Aosta Valley, March 9-15, 2003, pp. 103-144

10. F. Vissani
NEUTRINO MASSES AND MIXINGS: WHAT DO THEY MEAN?
The European Physical Journal C - Particles and Fields, online publication: 28 October 2003, DOI: 10.1140/epjcd/s2003-03-918-1

11. F. Feruglio, A. Strumia, F.Vissani
NEUTRINO OSCILLATIONS AND SIGNALS IN BETA AND 0NU2BETA EXPERIMENTS
Nucl.Phys. **B659** (Addendum) 359-362,2003

12. F. Cavanna, M.Costantini, O. Palamara, F. Vissani
NEUTRINOS AS ASTROPHYSICAL PROBES
"Astroparticle physics and cosmology", 415 (2003) Trieste

Preprints of 2003

1. R. Aloisio, V. Berezinsky, M. Kachelriess
FRAGMENTATION FUNCTIONS IN SUSY QCD AND UHECR SPECTRA PRODUCED IN TOP - DOWN MODELS
e-Print Archive: hep-ph/0307279 (submitted Phys. Rev. D)

2. V. Berezinsky
SUPERGZK NEUTRINOS: TESTING PHYSICS BEYOND THE STANDARD MODEL

e-Print Archive: hep-ph/0303091

3. V. Berezinsky, A. Gazizov, S. Grigorieva
SIGNATURES OF PROTONS IN UHECR
e-Print Archive: astro-ph/0302483

4. C.S. Aulakh, B. Bajc, A. Melfo, G. Senjanovic, F. Vissani
THE MINIMAL SUPERSYMMETRIC GRAND UNIFIED THEORY
e-Print Archive: hep-ph/0306242

5. F. Cavanna, M.L. Costantini, O. Palamara, F. Vissani
NEUTRINOS AS ASTROPHYSICAL PROBES
e-Print Archive: astro-ph/0311256

2 Particle Phenomenology

During this year the activity of the group, which included Z. Berezhiani, P. Ciarcellutti, L. Gianfagna, A. Galante and A. Sakharov, was mainly devoted to different problems of particle astrophysics and cosmology. The following results can be mentioned.

Z. Berezhiani and P. Ciarcelluti in collaboration with D. Comelli and F. Villante (Ferrara) have studied cosmological implications of the mirror dark matter. The hidden mirror Universe is considered as an identical copy of the observed particle world interacting with the latter only gravitationally, and its existence can be motivated in the context of string or brane world theories. The primordial nucleosynthesis bounds demand that at the Big Bang the mirror particle sector is born with a lower temperature than the ordinary one. In this case mirror baryogenesis should be more effective than ordinary one, and the mirror baryons can constitute dark matter of the universe, with specific implications for for the large scale structure (LSS) of the Universe and the cosmic microwave background (CMB), etc. It was given a complete numerical calculations by a special computational code for the LSS power spectrum and the CMB angular anisotropies in the cases of dark matter entirely constituted by mirror baryons, and for the case of mixed cold dark matter and mirror dark mater.

Z. Berezhiani and A. Dolgov (INFN Ferrara) have suggested that the large scale cosmic magnetic field could be generated in the primeval plasma slightly before hydrogen recombination. Non-zero vorticity, necessary for that, might be created by the photon diffusion in the second order in the temperature fluctuations or by isocurvature perturbations. The spectrum of resulting seed fields was calculated and it was concluded that a reasonable galactic dynamo is needed to amplify the seed fields by 8-9 orders of magnitude in order to explain the magnitudes of coherent magnetic fields in galaxies.

Z. Berezhiani in collaboration with I. Bombaci (Pisa) A. Drago, F. Frontera (Ferrara) and A. Lavagno (Turin) proposed a model to explain the Gamma Rays Burst via the conversion of a pure hadronic star (neutron star) into a quark star constituted, at least in part, of deconfined quark matter. The conversion process can be delayed if the surface tension at the interface between hadronic and deconfined-quark-matter phases is taken into account. The nucleation time (i.e. the time to form a critical-size drop of quark

matter) can be extremely long if the mass of the star is small. Via mass accretion the nucleation time can be dramaticaly reduced and the star is finally converted into the stable configuration, releasing the binding energy of the order 10-100 foe during the conversion process and thus produce a Gamma Ray Burst. The delay between the supernova explosion generating the metastable neutron star and the new collapse can explain the delay proposed in GRB990705 and in GRB011211.

A. Sakharov, in collaboration with J. Ellis (CERN), N.E. Mavromatos (London) and D.V. Napopoulos (Texas) have discussed that the interactions of different particle species with the foamy space-time fluctuations expected in quantum gravity theories may not be universal, in which case different types of energetic particles may violate Lorentz invariance by varying amounts, violating the equivalence principle. This possibility was illustrated in two different models of space-time foam based on D-particle fluctuations in either flat Minkowski space or a stack of intersecting D-branes. These models suggest that Lorentz invariance could be violated for energetic particles that do not carry conserved charges, such as photons, whereas charged particles such electrons would propagate in a Lorentz-invariant way. The phenomenological implications of these phenomena have been discussed.

Participation in conferences

Vietri Meeting "Problemi Attuali di Fisica Teorica", IIASS "E.R.Caianiello", Vietri sul Mare, Salerno, 11-16 apr 2003: invited talk of Z. Berezhiani "Baryogenesis"

XII Int. Baksan School "Particles and Cosmology", Baksan Valley, Russia, 20-27 Apr 2003: invited lectures of Z. Berezhiani "Gamma Ray Bursts beyond the Standard Model" and "Overview of SUSY GUTs"

Int. Conf. on "Hierarchy Problems in Four and More Dimensions", ICTP, Trieste, 1-4 Oct. 2003: invited talk of Z. Berezhiani "Hierarchy of GUTs and fermion masses"

Journal and Proceedings publications in 2003

1 Z. Berezhiani, I. Bombaci, A. Drago, F. Frontera, A. Lavagno, GAMMA-RAY BURSTS FROM DELAYED COLLAPSE OF NEUTRON STARS TO QUARK MATTER STARS, Astrophys.J. 586, 1250-1253 (2003)

2. Z. Berezhiani, A.D. Dolgov, GENERATION OF LARGE SCALE MAGNETIC FIELDS AT RECOMBINATION EPOCH. May 2003. 19pp. e-Print Archive: astro-ph/0305595, accepted for publication in Astropart. Phys.

3. Z. Berezhiani, MIRROR WORLD AND ITS COSMOLOGICAL CONSEQUENCES, Dec. 2003, 35 pp. e-Print Archive: hep-ph/0312335, accepted for publication in Int. J. Mod. Phys. A

4. Z. Berezhiani, P. Ciarcelluti, D. Comelli, F.L. Villante, STRUCTURE FORMATION WITH MIRROR DARK MATTER: CMB AND LSS, Dec 2003. 11pp. e-Print Archive: astro-ph/0312605, submitted to Phys. Lett. B

5. J. Ellis, N.E. Mavromatos, D.V. Nanopoulos, A.S. Sakharov, SYNCHROTRON RADIATION AND QUANTUM GRAVITY, Sep 2003, 4pp., e-Print Archive: astro-ph/0309144, submitted to Nature

6. J. Ellis, N.E. Mavromatos, D.V. Nanopoulos, A.S. Sakharov, SPACE-TIME FOAM MAY VIOLATE THE PRINCIPLE OF EQUIVALENCE, Dec 2003, 21pp., e-Print Archive: gr-qc/0312044, submitted to Int. J. Mod. Phys. A

3 Computer Simulations of Lattice Gauge theories

The activity performed during 2003 is a continuation of earlier studies and concerned, in particular, new methods for simulations of systems with complex actions, in particular models with a topological term (theta term) and non-zero baryon density QCD. With reference to theta term actions, we have introduced a second method[1] in addition to the one developed in 2002[2]; having two independent methods, which both can in principle suffer of unknown systematics, we can have a better understanding of our results, in particular when the two methods give results compatible within statistical errors. In this case we have a strong indication of having the systematics well under control.

This is the case of our results for CP^9 model with theta term; the results reported in [3] show that no sensible differences can be obtained using the two different (and independent) methods [1][2] in the whole space for the parameter theta (0-pi).

We are now analysing the results from the simulations of other 2-dimensional models of the CP(N-1) family, with N ranging from 2 to 8; these results will be presented to the community during 2004. A contributions on this subject have been presented to the Lattice 2003 Conference by A. Galante[4].

With reference to non-zero baryon density QCD simulations we have introduced a new variant of the well known Hasenfratz-Karsch action that allows some step forward the determination of the critical line in the plane Temperature-Baryon density. A preliminary study in two dimensional Nambu-Jona Lasinio model have produced encouraging results and we are now moving the the more physically interesting case of 2 Flavours QCD.

Following previous studies in 2 and 3 Colours QCD at non zero baryonic density, we have also studied the phenomenon of Diquark Condensation in the framework of Strong Coupling expansion[5]. In the paper is shown that even if a vacuum with non zero diquark condensate do exist in 3 Colours theory, the corrisponding minimum in the energy density remains a local one, while the global minimum is the standard one for any value of the chemical potential.

Finally we are performing a study of the chiral transition in QCD at finite temperature with staggered dynamical fermions using the approach of the probability distribution function of the order parameter. To this end a fairly large number of gauge field configuration has been generated on the APE machine, using a TAO code for dynamical fermions borrowed from the Pisa APE group. These configurations have been fully diagonalised on the PC cluster of LNGS-GrIV and the final analysis is under way.

Journal and Proceedings publications in 2003

1. V. Azcoiti, G. Di Carlo, A. Galante, V. Laliena; "Theta-vacuum systems via real action simulations". Phys.Lett. B563 (2003) 117-122. 2. V. Azcoiti, G. Di Carlo, A. Galante, V. Laliena; "New proposal for numerical simulations of theta-vacuum like systems". Phys.Rev.Lett. 89 (2002) 141601. 3. V. Azcoiti, G. Di Carlo, A. Galante, V. Laliena; "Theta dependence of CP^9 model". To appear in Phys Rev D. 4. V. Azcoiti, G. Di Carlo, A. Galante, V. Laliena; "New advances in numerical simulations of theta-vacuum systems" Lattice2003 Proceedings. 5. V. Azcoiti, G. Di Carlo, A. Galante, V. Laliena; "Diquark condensation at strong coupling" JHEP 0309 (2003) 014

4 Planck Scale Kinematics and Phenomenology

This activity is now included in IS GS11 and concerned the analysys of phenomenological consequences, in particular in Ultra High Energy Cosmic Ray Physics, of possible departures from (special) relativistic invariance at energy-momentum scales near the Planck Mass. The persons involved are R. Aloisio, A. Galante, A. Grillo and F. Mendez, in collaboration with P. Blasi (IAF, Arcetri) and P.L. Ghia (IFSI and INFN Torino).

In particular it has been discussed in detail the effect of spacetime (*i.e.* metric) fluctuations on the propagation of Ultra High particles. It has been found that in a fluctuating metric, being the sign of the fluctuation of mass-shell relation generally undefined, the net result is a *decrease* of threshold energy for absorption of UHE CRs, with possible important phenomenological consequences [1]. However a more striking consequence is that essentially any stable particle could decay ate relatively high energy, in blatant contraddiction with experiments. This is discussed in [2] where also possible ways to alleviate the problem have been discussed.

R. Aloisio has given on the subject an invited talk at the Marcell Grossmann Meeting in Rio De Janeiro (Brazil) in July 2003.

Journal and Proceedings publications in 2003

1. R. Aloisio, P. Blasi, A. Galante, P.L. Ghia, A.F. Grillo
SPACE TIME FLUCTUATIONS AND ULTRAHIGH-ENERGY COSMIC RAY INTERACTIONS
Astropart.Phys. **19**,127 (2003)

2. R. Aloisio, P. Blasi, A. Galante, A.F. Grillo
A FLUCTUATING ENERGY-MOMENTUM MAY PRODUCE AN UNSTABLE WORLD
Astropart.Phys. **20**, 369 (2003)

ERMES

Wolfango Plastino[a,b], Matthias Laubenstein[c],
Giuseppe Etiope[d], Paolo Favali[d]

[a] Department of Physics, University of Roma Tre,
via della Vasca Navale, 84, I-00146, Rome (Italy)
[b] National Institute for Nuclear Physics, Section Rome III,
via della Vasca Navale, 84, I-00146, Rome (Italy)
[c] National Institute for Nuclear Physics, Underground Laboratories of Gran Sasso,
S.S.17bis km 18+910, I-67010, Assergi (AQ) (Italy)
[d] National Institute for Geophysics and Volcanology, RIDGE unit
Roma 2 Department, via di Vigna Murata, 605, I-00143, Rome (Italy)

Abstract

Oceanographic data, acquired throughout 6 months by the GEOSTAR-2 benthic observatory in southern Tyrrhenian Sea, evidenced ocean-lithosphere interactions in the 1900 m deep Benthic Boundary Layer (BBL), distinguishing two water masses with different origin and, possibly, benthic residence time. Environmental radioactivity analyses [1] shown a BBL characterised by a colder western water (WW), which is episodically displaced by the cascading of the warmer Eastern Overflow Water (EOW).

1 Introduction

GEOSTAR-2 (GEophysical and Oceanographic STation for Abyssal Research) is the first European deep-sea observatory for geophysical and environmental monitoring at seabed becoming operative in 2000. It was deployed in September 2000 from the Italian R/V Urania, in the southern Tyrrhenian Sea, between the Sicilian coast and the island of Ustica, at a depth of about 1900 m. After 206 days, in April 2001, the observatory was recovered. More than 4100 hours of data were recorded continuously. This mission represented the longest lasting experiment using a complex module, with an intelligent unit, deployed at great depth. The environmental radioactivity analyses of seawater samples, obtained from the automatic water sampler, has been performed in the framework of ERMES research project (Environmental Radioactivity Monitoring for Earth Sciences) to trace environmental changes in the benthic boundary seawater [1]. The analysis of radionuclides was carried out by means of gamma spectrometry with coaxial high purity Germanium (HPGe) detectors having volumes ranging from 200 to 500 cm^3 and a total background rate in the energy range [(60÷2700) keV] varying from (221±2) to (980±10)

counts/days depending on the detector [2]. Each seawater sample has been measured for about ten days using a polystyrene box of 70 mm diameter and 30 mm height [1].

2 Results

The most remarkable characteristics regarding the temperature and salinity records resides in the almost regular occurrence, roughly every 2-3 weeks, of sharp peaks deviating from the background (T:13.05 °C, S: 38.51 psu) with values up to 13.45 °C and 38.63 psu, respectively. On the basis of T-S peak height, duration and density variations we recognise seven major events occurring on 24 October 2000, 14 and 30 November 2000, 9 and 25 January 2001, 10 and 26 February 2001 [4]. The variation of helium concentration and its isotopic ratio ($^3He/^4He$) has been detected, and although He isotopes were measured only in 11 samples, the $^3He/^4He$ ratio coupled with He/Ne ratio suggested clearly the distinction of two different waters, as shown in figure 1.

Five water samples showed a significant enrichment of radiogenic He (low ^3He content) and these samples have also higher He mass concentration (mean of 3.2 ppmv) respect to the others (2 ppmv). The lower ^3He content is also indicative of lower tritiogenic ^3He, produced by tritium decay within the water column [4]. The radioactivity data are coherent with this pattern (figure 2 and 3). The same group of samples having lower gas content and less radiogenic helium display drops of radioactivity for all radionuclides with typical values of standard seawater [3]. The main result of these analyses is the sharp distinction of two geochemically different water masses, as suggested by He isotopes and radionuclides. Anyway, it is possible to argue that during or close to the major events of T-S variation the gas and radionuclide content decreases and the He isotopic ratio increases. Events of lower He, radionuclides and higher R/Ra (closer to the atmospheric ratio) would reflect the sinking of a less deep water (EOW). The deeper water (WW), likely with higher residence time, has higher gas content and radioactivity and a lower He isotopic ratio, with more significant radiogenic component. The enrichment of radionuclides such as ^{226}Ra in deep-sea waters due to diffusion from sediments is a well known phenomenon [4].

3 Conclusions

The GEOSTAR 2 data-set represents the first long-term and multidisciplinary monitoring of deep BBL. The oceanographic data and the environmental radioactivity analyses are basically coeherent converging towards the indication of a BBL mainly characterised by a colder western water which is episodically displaced by the cascading of a warmer eastern water. GEOSTAR-2 demonstrated the potential of long-term, continuous and multiparametric monitoring in providing unique information which cannot be acquired by traditional, short-term or single-sensor investigations.

Acknowledgements The authors are grateful to Prof. Eugenio Coccia for his kind collaboration and Eng. Marco Balata, Mr. Massimiliano De Deo, and Mr. Stefano Nisi of the LNGS for their very useful and precious assistance.

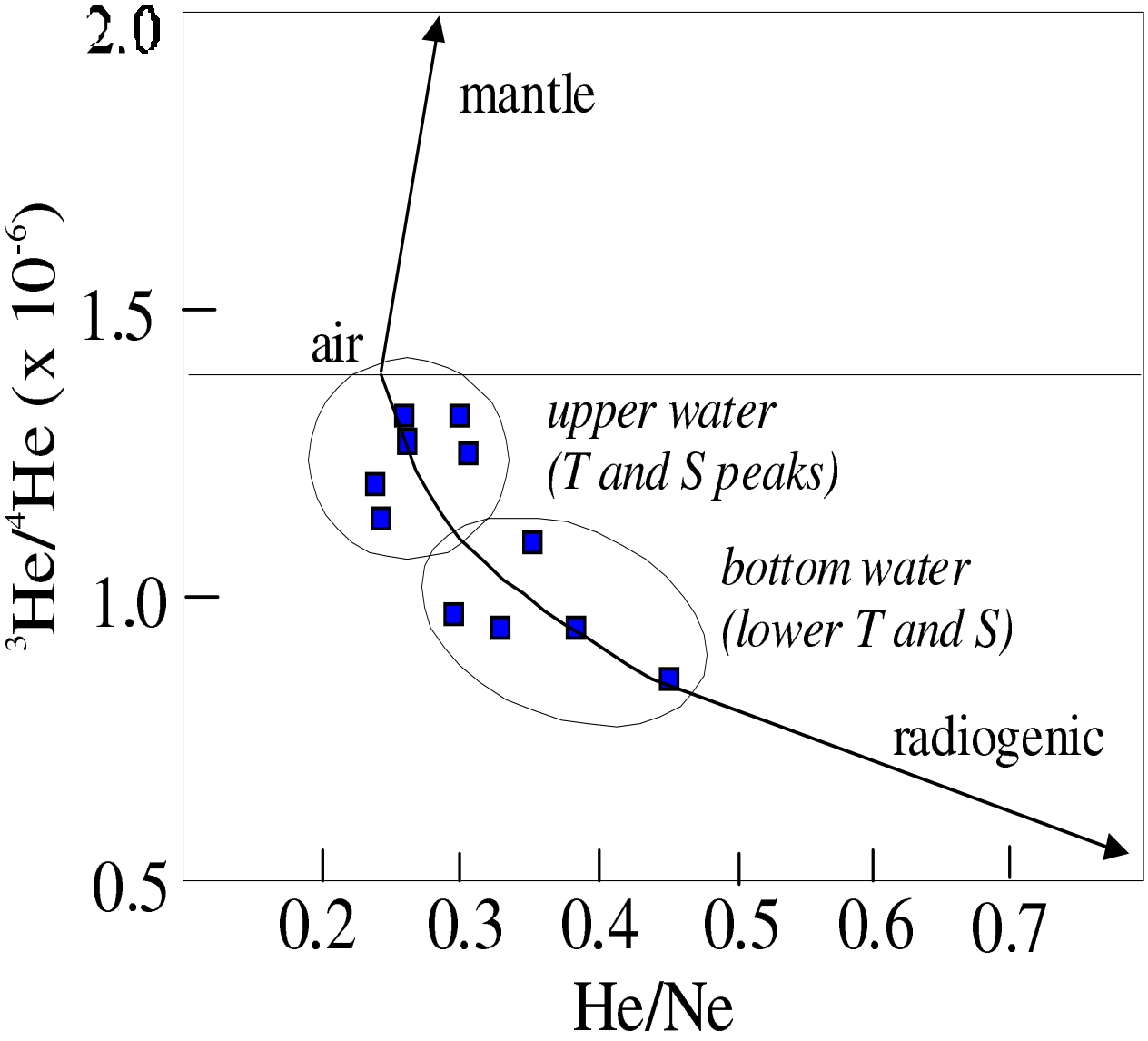

Figure 1: Helium isotope ratio vs He/Ne. The plot indicates two different waters probably linked to the different water masses whose interface oscillates producing T/S peaks. The isotope ratio of 1.4×10^{-6} is that of the atmosphere. Samples closer to this ratio indicate major atmospheric signal (shallower water). Lower ratios are along the mixing line with crustal (radiogenic) sources, and this can be indicative of bottom water, closer to seafloor, with higher residence time.

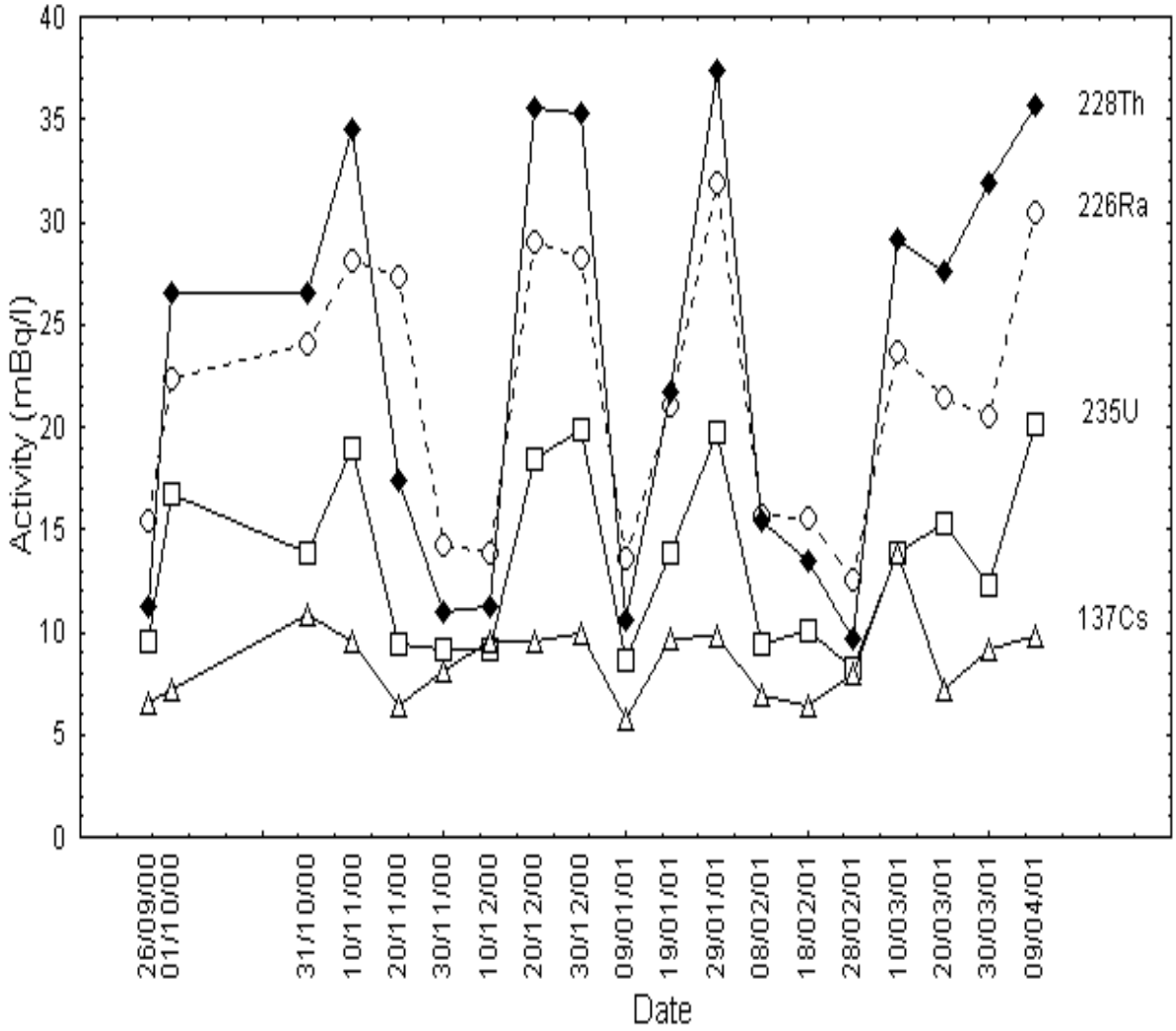

Figure 2: Variation of activity of some radionuclides. Lower activities correspond to T/S peaks and are indicative of shallower water mass, as suggested by helium and its isotopic ratio.

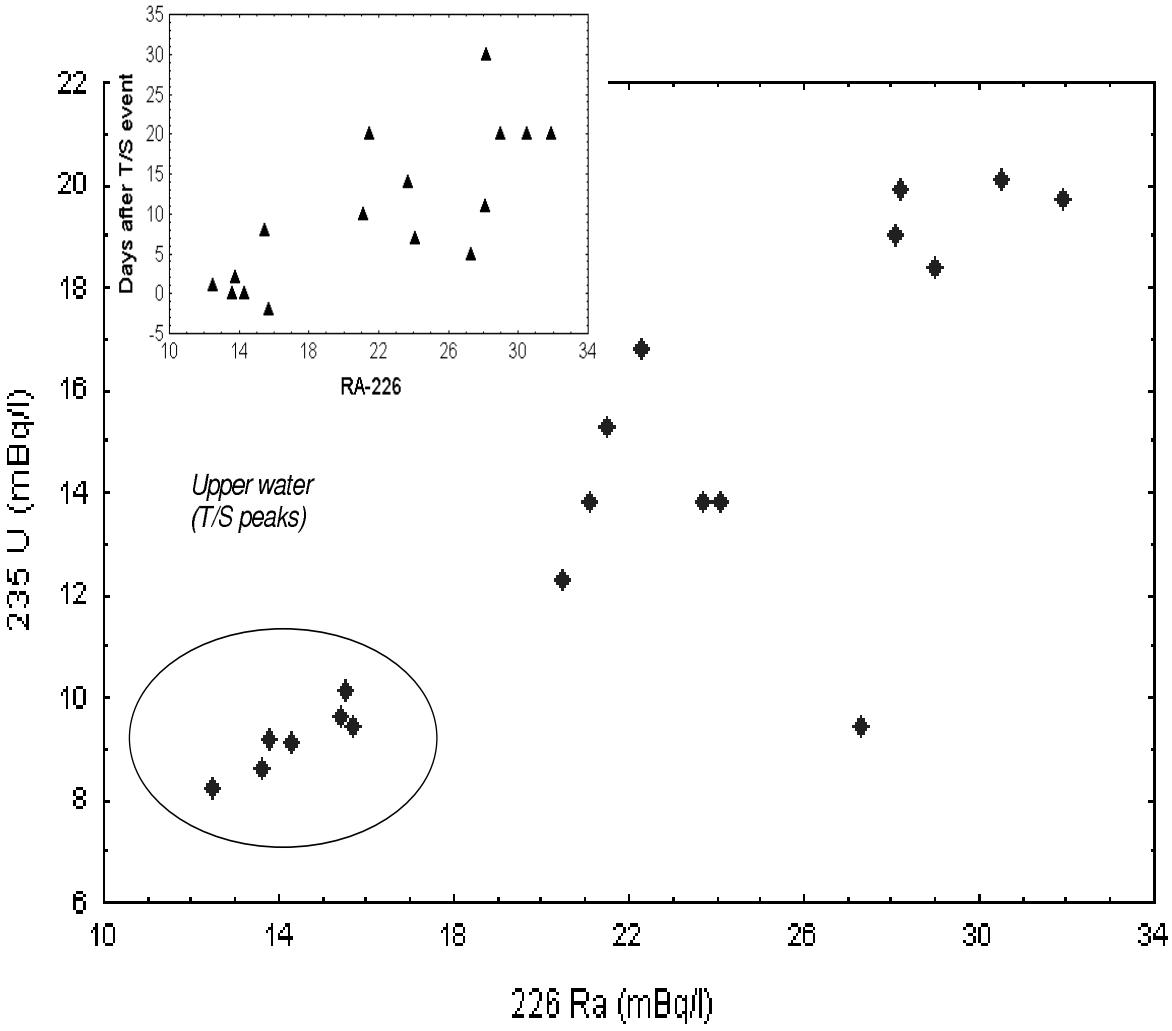

Figure 3: ^{235}U vs ^{226}Ra. A group of lower activity is distinguished, referring to samples closer to T/S peaks. The smaller plot shows the clustering in relation to the temporal distance (in days) of water sampling after a T/S event.

References

[1] Plastino, W., Laubenstein, M., Etiope, G. and Favali, P., 2003, Environmental radioactivity analysis in sea-water samples collected by GEOSTAR deep-sea observatory, Istituto Nazionale di Fisica Nucleare, Laboratori Nazionali del Gran Sasso, Annual Report 2002, 201-206.

[2] Arpesella, C., 1996, A low background counting facility at Laboratori Nazionali del Gran Sasso, Appl. Rad. Isot., 47, 991-996.

[3] Inn, K.G.W., Zhichao Lin, Zhongyu Wu, McMahon, C., Filliben, J.J., Krey, P., Feiner, M., Chung-King Liu, Holloway, R., Harvey, J., Larsen, L., Beasley, T., Huh, C.A., Morton, S., McCurdy, D., Germain, P., Handl, J., Yamamoto, M., Warren, B., Bates, T.H., Holms, A., Harvey, B.R., Popplewell, D.S., Woods, M.J., Jerome, S., Odell, K.J., Young, P. and Croudace, I., 2001. The NIST natural-matrix radionuclide standard reference material program for ocean studies, J. Radioanal. Nucl. Chem., 248,1 227-231.

[4] Etiope, G., Favali, P., Fuda, J.L., Italiano, F., Laubenstein, M., Millot, C. and Plastino, W., Annals of Geophysics, submitted.

GIGS. The Interferometric Station at LNGS

Antonella Amoruso[a,c], Luca Crescentini[b,d,e]

[a] Dip.to di Fisica Univ. dell'Aquila, L'Aquila - Italy
[b] Dip.to di Scienze della Terra Univ. di Camerino, Camerino (MC) - Italy
[c] INFN - Gruppo collegato dell'Aquila, L'Aquila - Italy
[d] INFN - LNGS, L'Aquila - Italy
[e] Spokeperson

Abstract

During 2003 strain data have been recorded continuously. Several months of tidal records have been analyzed and modelling is in progress. We are also carrying on a joint analysis of strain data recorded by the interferometers and of particle velocity data recorded by the very-broad-band seimometer installed inside the interferometric station, in an attempt to detect seismic wave phase velocity changes during stress build-up.

1 Introduction

The interferometric station at LNGS consists of two 90-m long laser interferometers designed for geophysical purposes. Their azimuth are N66E and N24W, i.e. approximately perpendicular and parallel to the local direction of the Apennines. Instrumental configuration has changed since their first start up in 1994. From May 1994 to October 1995 we have monitored the extension of a 90-m long baseline (azimuth = N66E), using a 20-cm long reference baseline (unequal-arm configuration). Since laser frequency fluctuations can give spurious signals whose amplitude depends on the difference in length between the two baselines, in order to check for their effects from December 1995 to October 1998 both arms were 90-m long and one component of shear strain was measured (equal-arm configuration). Some instrumental changes in 1999 allowed to measure extensions of the two baselines independently, so that now also areal strain can be obtained. Recording rate is 5 data per second.

In what follows, extensions are expressed as dimensionless strain, $\Delta l/l$, where l is instrumental baselength; Δl is positive for extension. We use the symbol nϵ, nanostrain, for $\Delta l/l = 10^{-9}$.

The instruments are characterized by very high sensitivity ($\approx 3 \times 10^{-3}$nϵ), wide frequency band (from d.c. up to hundreds of Hz), large dynamic range (unbounded in

principle), and good reliability. During the transit of teleseismic waves it recorded signals as large as 600 nϵ and as fast as 100 nϵ/s without any nonlinearity or abnormal behavior. The experiment has been planned for a better knowledge of crustal deformation processes, due to tectonic processes (strain accumulation and release, aseismic slips, coseismic steps and earthquakes - regular and slow) as well as to earth tides.

From October 2002, a three-component very-broad-band seismometer (installed and managed by researchers of INGV - Istituto Nazionale di Geofisica e Vulcanologia), flat in velocity down to 360 sec, is at work inside the interferometric station.

Since last year, the project is carried on in the framework of an Accordo di Programma between INFN and INGV.

2 Earth tides

Several-month records of tidal strain had already been analyzed and compared with theoretical predictions in the case of an elliptic rotating Earth and taking into account ocean loading effects, during year 2001. Theoretical predictions had been generated by using the GOTIC2 code [1] and satellite altimetric data from TOPEX/POSEIDON. Ocean loading effects accounted for about 10% of total expected tidal signal, in the case of a reference layered Earth. Both areal and shear strain were about 20% smaller than predicted. Since the release of GOTIC2 available at that time had a severe bug which resulted in erroneous loading estimation, further work was considered necessary (see 2001 Annual Report).

Preliminary results obtained using the upgraded version of Gotic are similar to those previously mentioned. Discrepancy between predicted and measured Earth tides could be due to elastic properties of nearby lithosphere, a very important topic extremely difficult to study, as well as to unproper ocean tide models or to local effects (e. g. small-scale geological inhomogeneity or topography) that cross couple remote areal/shear strain into measured areal/shear strain. Cross coupling can be described using three unknown coefficients for each measured strain component. Each of the above mentioned topics are of some relevance in geophysics. Remote areal/shear strain given by Earth tides can be compared with measured tides. Since predicted values of the three independent plane strain components do not scale homogeneously when considering diurnal and semidiurnal tides, and, to a less extent, when considering different diurnal or semidiurnal tidal harmonics, comparison between predicted and measured Earth tides could lead to simultaneous estimates of local effects and of the most correct ocean tide model.

As a first step, ocean loading effects have been computed in the Gran Sasso area, but also in the whole Italy and in the whole Europe, using three different ocean tide models (CSR4.0, got99, and nao99) and two different Earth models (GB and 1066A), in order to state how different predictions are. As a second step, detailed tidal analysis of about three years of recorded strain will be carried out. We aim to obtain the first results in few months.

3 Joint analysis of interferometric and seismometric data

As mentioned in the 2002 Anuual Report, a three-component very-broad-band seismometer, flat in velocity down to 360 sec, is operating since October 2002 inside the interferometric station. The seismometer has been installed by researchers of INGV (Istituto Nazionale di Geofisica e Vulcanologia). The ratio between particle velocity and strain gives local phase velocity, thus a suitable joint analysis of strain data and of particle velocity data for large teleseismic waves from various sources could permit detection of possible anisotropies and temporal changes during stress build-up.

For now, few recordings of large teleseismic waves are available, and we are performing preliminary joint analysis of strain data and of particle velocity data.

References

[1] Matsumoto, K., T. Sato, T. Takanezawa, and M. Ooe, GOTIC2: A Program for Computation of Oceanic Tidal Loading Effect, *J. Geod. Soc. Japan*, *47*, 243-248, 2001.

[2] Crampin, S., Calculable fluid-rock interactions, *J. Geol. Soc.*, *156*, 501-514, 1999.

LNGS-EXP 20/99. Measurement of the Radon concentration in the water from the Gran Sasso fault

G. Colombo[c], M. De Deo[a], L. Degli Esposti[b], R. Fresca Fantoni[c], D. Di Ferdinando[b], G. Giacomelli[b], G. Mandrioli[b], F. Materazzi[c], D. Matteuzzi[b], G. Scarpanti[c], G. Sirri[b], L. Snidero[b]

[a]*INFN, Laboratori Nazionali del Gran Sasso, Assergi*
[b]*Dipartimento di Fisica dell'Università di Bologna and INFN Bologna*
[c]*Eni S.p.A. Agip Division, Radiation Protection Department, San Donato Milanese*

Abstract

We describe an experiment designed to monitor the ^{222}Rn concentration in the water from the fault in the underground Gran Sasso Laboratory. The water is directly collected from the fault and radon gas is extracted from the water by nitrogen bubbling. The main goal of the experiment is to investigate possible correlations between variations in radon concentration in the water and seismic phenomena. The data, collected from the beginning of 2000 till the middle of 2003, are presented and discussed.

1 Introduction

Radon contents in groundwaters are being monitored by several experiments with the aim of studying possible correlations between radon concentration variations and seismic phenomena [1 - 8].

We developed and implemented an automatic instrument for monitoring the radon concentration in groundwater. Since the beginning of 2000 till the middle of 2003 this apparatus was collecting data in the interferometric tunnel of the underground Gran Sasso Laboratory. The sampling rate was two measurements per day. Water was collected from the fractured rock in the fault, which is one of the most important features of the Gran Sasso Massif. The apparatus complements other instruments that are monitoring seismic activities in the underground laboratory: a geodetic interferometer [9], tiltmeters and the apparatus for groundwater measurements of the University of Roma Tre [10, 11, 12].

2 The apparatus

A photograph of the apparatus is shown in Fig. 1; it consists of three sections: the system for the extraction of radon from water, the detecting system and the data acquisition and control system.

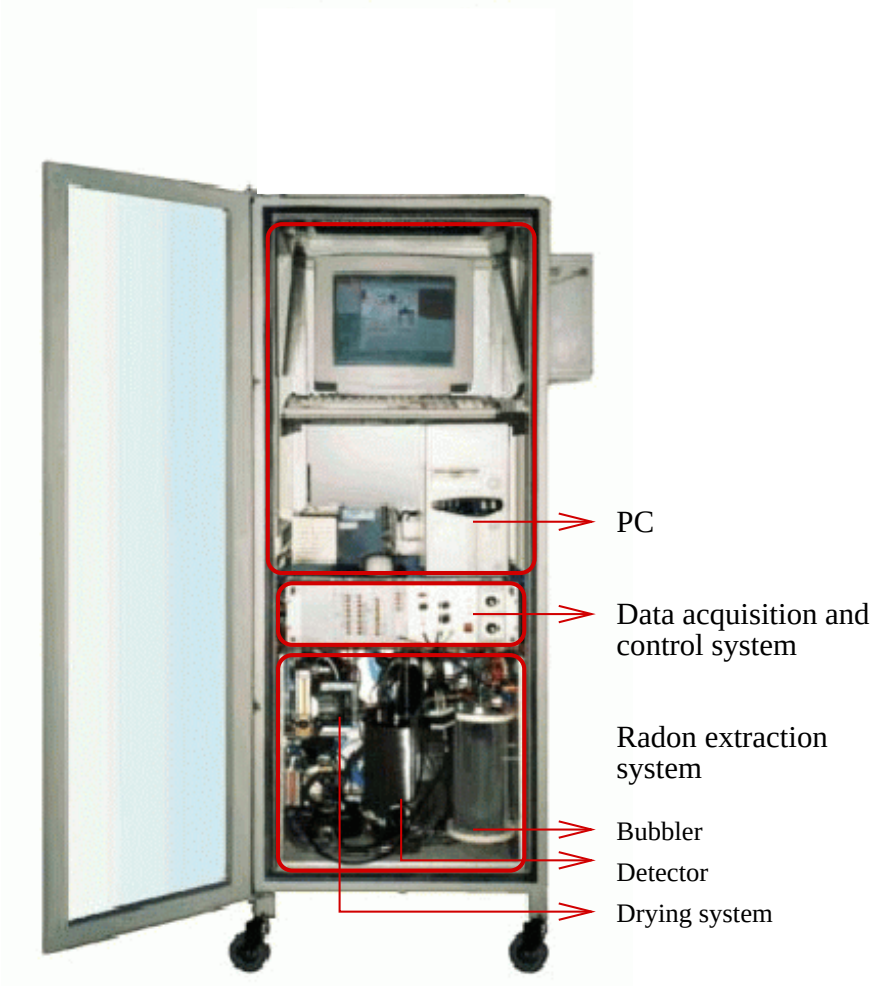

Figure 1: *Photograph of the apparatus for monitoring the radon concentration in the Gran Sasso groundwater from the fault.*

2.1 Radon extraction system

The layout of the extraction system is shown in Fig. 2. It is located in the bottom part of the rack in Fig. 1. The process starts by flushing the radon extraction system with nitrogen gas (in order to clean the circuit); immediately after, the background measurement is started. Then a sample of 1.9 liters of water collected directly from the rock fault is pumped into the bubbler.

Radon gas is then extracted from the water by nitrogen bubbling. The bubbling circuit includes the bubbler, the drying system, the detector chamber, the air flow sensor, the air

pump and the valves V3, V4, V9, V11 of Fig. 2. At the end of the extraction, the radon concentration in the bubbling gas is in equilibrium with the radon concentration in the water, according to the Henry's law.

After radon extraction all valves are closed and radon counting is started. At the end of counting, the water is pumped out, and the process restarts.

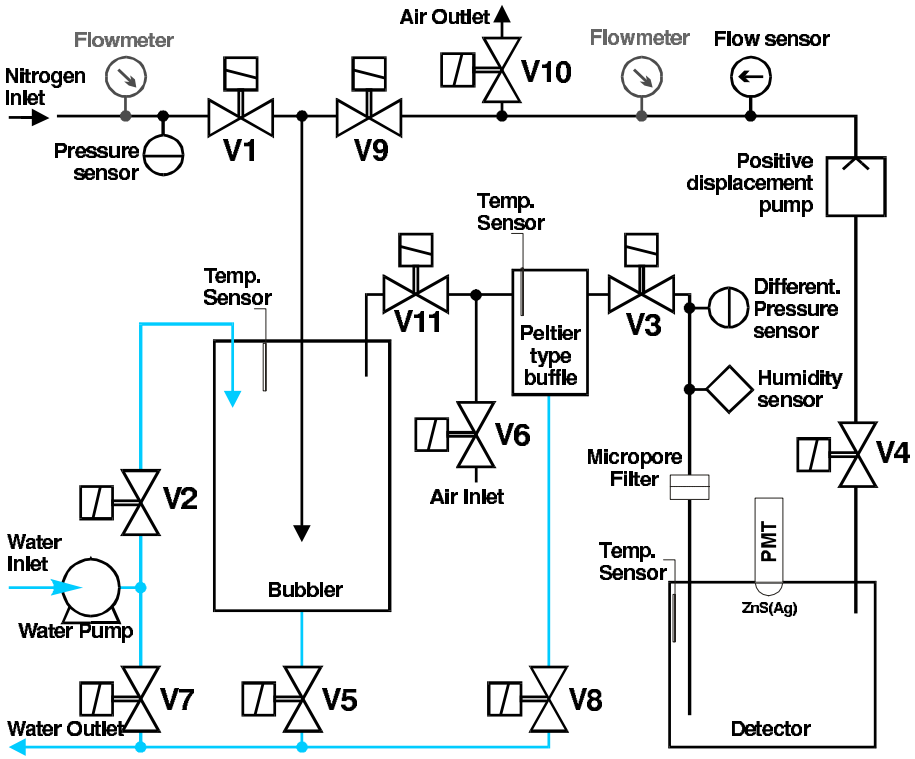

Figure 2: *Layout of the radon extraction system.*

2.2 Detection system

A scheme of the detecting system is shown in Fig. 3. The detector is a Pylon mod. PMT - EL, which consists of a silver activated zinc sulfide scintillator ZnS(Ag) located into a 5 litre electrostatic chamber. The scintillator is covered by an aluminized mylar foil that acts as cathode of the electrostatic chamber and collects the positively charged radon daughters. A power supply polarizes the chamber creating a voltage difference of about 1000 Volts between the cathode and the chamber walls.

The ^{222}Rn nuclei in the gas pumped inside the detector decays into ^{218}Po, which is attracted to the negatively charged aluminium cathode. ^{218}Po decays into ^{214}Bi, which decays in ^{214}Pb and then into ^{214}Po, as indicated below:

$$\underset{3.82\ \mathrm{d}}{^{222}\mathrm{Rn}} \overset{\alpha}{\Longrightarrow} \underset{3.05\ \mathrm{min}}{^{218}\mathrm{Po}} \overset{\alpha}{\Longrightarrow} \underset{26.8\ \mathrm{min}}{^{214}\mathrm{Pb}} \overset{\beta}{\longrightarrow} \underset{19.7\ \mathrm{min}}{^{214}\mathrm{Bi}} \overset{\beta}{\longrightarrow} \underset{164\ \mu\mathrm{s}}{^{214}\mathrm{Po}} \overset{\alpha}{\Longrightarrow} {}^{210}\mathrm{Pb}$$

(the time intervals quoted above are half-lives, $t_{1/2}$). The ^{222}Rn nuclei emit alpha particles; a fraction of these impacts the scintillator and produces light pulses that are transmitted through the light pipe to the photomultiplier (PMT). The subsequent decays of the daughter nuclei, collected by the cathode, increase the instrumental efficiency. The electric pulses produced by the PMT are amplified and sent to the data acquisition system (Fig. 3 a). Fig. 3 b shows details concerning the collection of ^{222}Rn daughters.

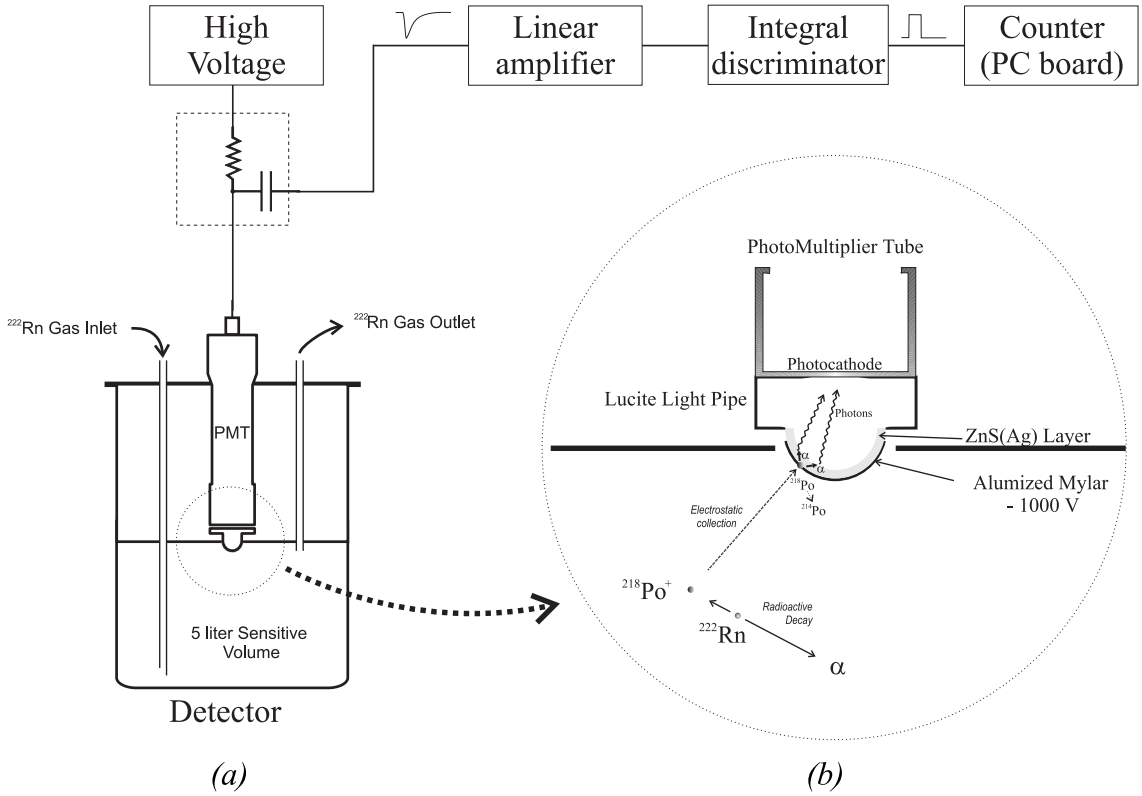

Figure 3: *(a) Scheme of the detection system; (b) scheme of the collection of radon daughters.*

2.3 Data acquisition system

The process control and data acquisition are made by a PC with a Pentium processor and two acquisition boards. The system, located above the crate in the rack shown in Fig. 1, allows to control the various devices, such as the water pump, the air pump, the electrovalves and the Peltier cells placed in the drying system; at the same time it monitors the water level in the bubbler, the pressure in the nitrogen gas system, the air flow and the pressure in the circuit, the temperature of different devices and finally the radon counting.

The computer is remotely controlled via Internet; tests and measurements are displayed on web pages.

3 Measurements

Examples of background and of radon concentration measurements performed over a 12 hours period are shown in Fig. 4. Even if the aim of this experiment is to monitor the variations of the radon concentration, an absolute calibration of the detector was performed by cross-calibration with another calibrated instrument (Genitron Alphaguard).

Plots of the radon concentration in water versus time in the periods July 2000 - May 2003 are shown in Figs. 5 and 6 a. Atmospheric pressure and bubbling temperature are shown in Fig. 6 b.

The Dobrovolsky parameter ε [13] was computed from the seismic informations from the National Institute of Geophysics and Vulcanology (INGV) [14]; the data recorded within a distance of 100 km from the Gran Sasso Laboratory were used. The ε parameter for the period June 2001 - May 2003 is shown in Fig. 6 c. Normally one considers relevant the events with $\varepsilon > 10^{-9}$ (indicated by the horizontal dashed line in Fig. 6 c). In the period during which we have radon data there was some seismic activity, in particular around September - November 2001 and August 2002. There seem to be some variations of radon concentration during the period September 2001 - January 2002. Unfortunately there were some power failures at the beginning and in the middle of this period; therefore possible correlations between variations of radon concentration and seismic activities are not considered to be of sufficient reliability.

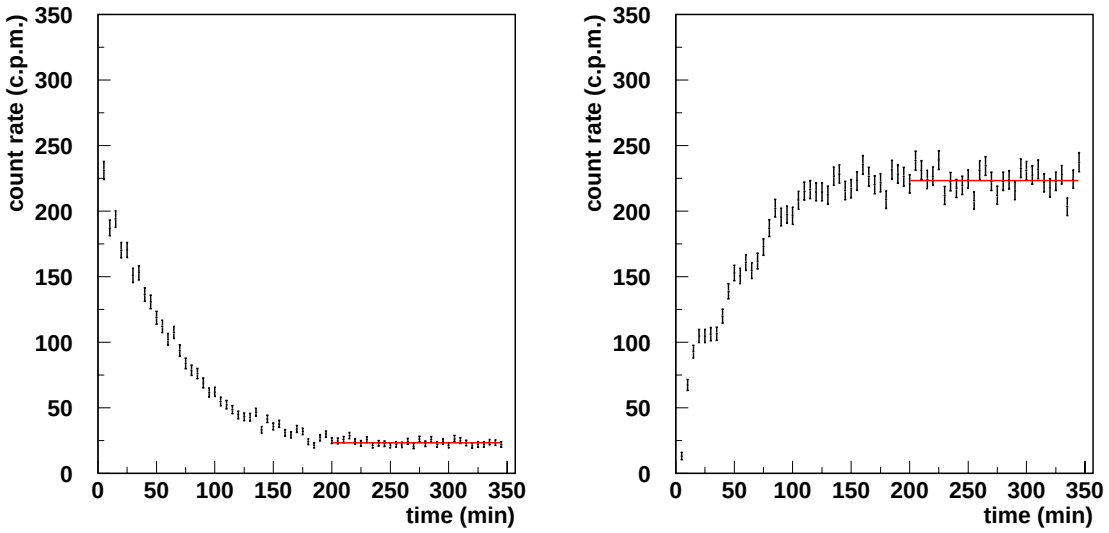

Figure 4: *Examples of background (left) and of radon concentration measurements (right). The final counting rates are obtained from a fit of the data over 350 minutes, or simply by taking the average rates from 200 to 350 minutes, as indicated by the solid horizontal lines.*

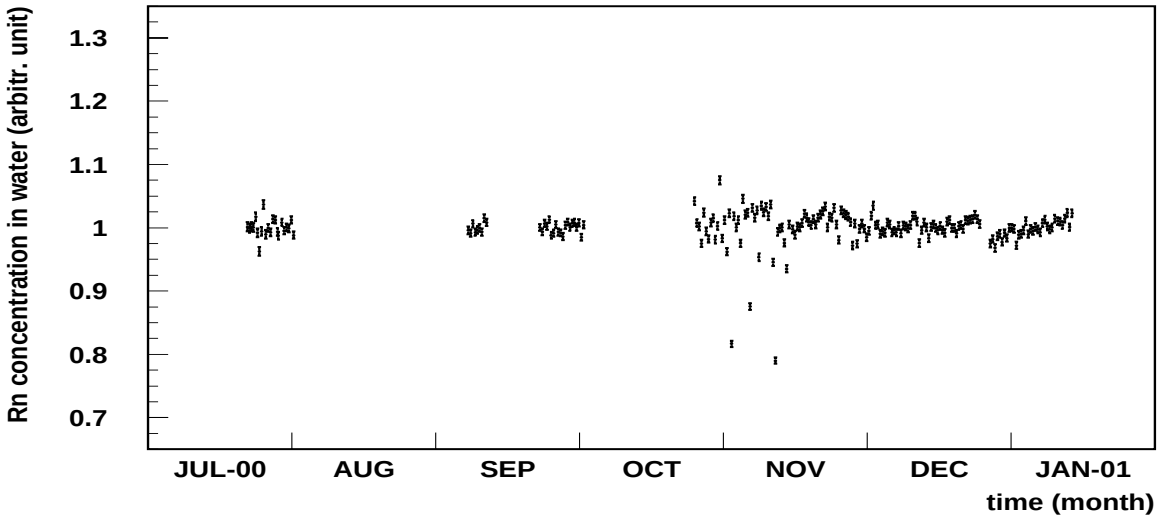

Figure 5: *Corrected radon concentrations made during the period July 2000 - Jan 2001.*

4 Conclusions

An apparatus for monitoring radon concentration in the water from the Gran Sasso fault has been designed and implemented. The extraction technique and the detector system allow a good reproducibility and a good signal to background ratio.

Data have been taken from July 2000 till May 2003 with some interruptions, see Figs. 5 and 6 a.

During these years there were some periods of sismicity in the area (Fig. 6 c); the data seem to indicate some possible correlations between sismicity and radon concentration in the water from the Gran Sasso fault, but unfortunely the power failures which occurred during these periods make the stability of the radon data not completely reliable.

Future improvements should concern the stability and the reliability of the apparatus.

Acknowledgments

We acknowledge the support of the Director and of the Staff of the Gran Sasso Laboratory and of the Institutions partecipating in the experiment. We acknowledge discussions with F. Bella and W. Plastino.

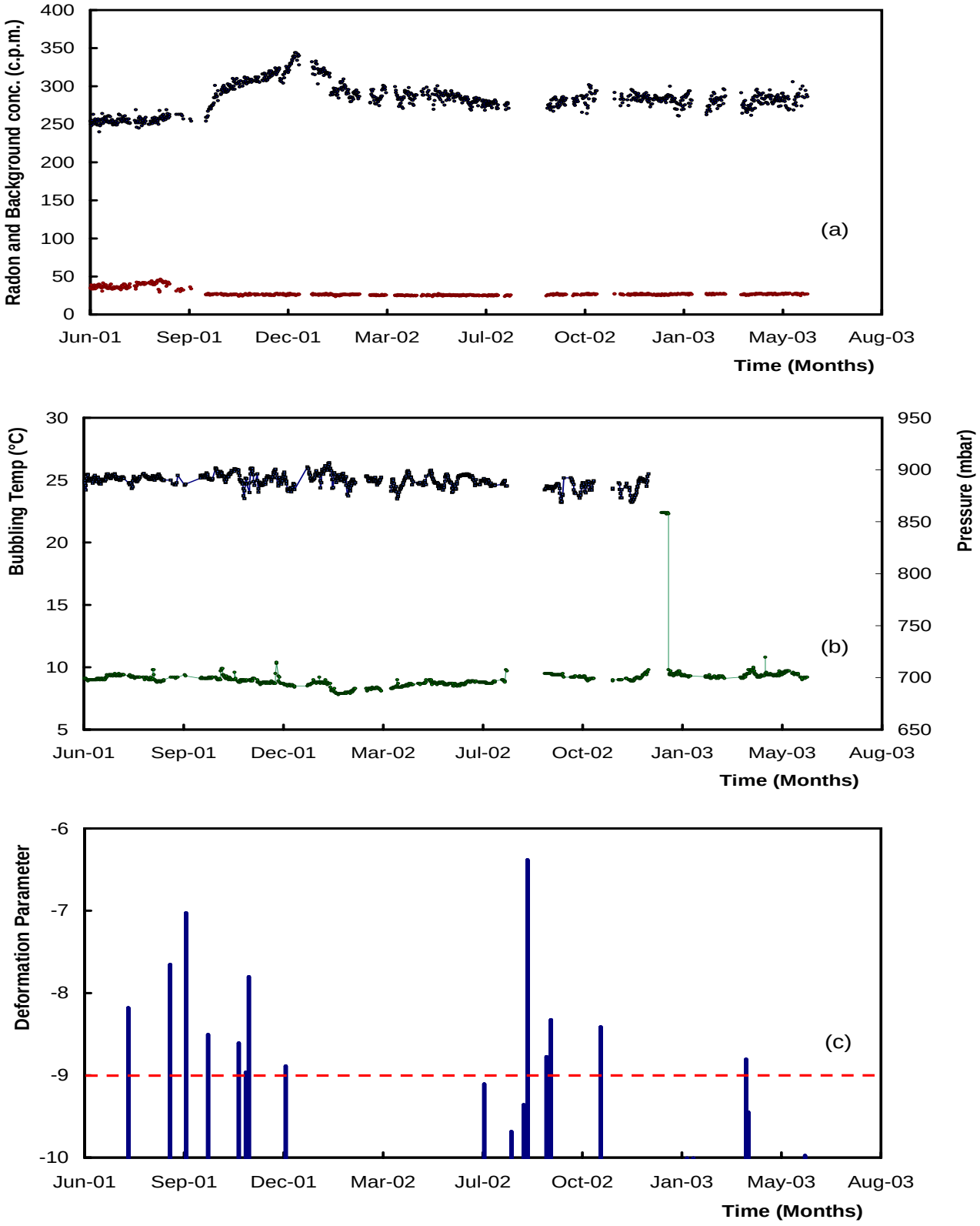

Figure 6: *(a) Corrected radon and background concentrations, (b) bubbling temperature and atmospheric pressure, (c) Dobrovolsky parameter during the period June 2001 - May 2003.*

References

[1] M. Noguchi and H. Wakita, A method for Continous Measurement of Radon in Groundwater for Earthquake Prediction, Jou. Geoph. Res. 82 (1977) 1353.

[2] Chi-Yu-King, Radon monitoring for Earthquake Prediction in China, Earthq. Predict. Res. 3 (1985) 47.

[3] E. Haukkson, Radon content of groundwater as an earthquake precursor: evaluation of worldwide data and physical basis, 1981, J. Geophys. Res. 86 9397 9410.

[4] A. A. Qureshi et al., Radon measurements for use in earthquakes prediction and location for geological faults in Pakistan, Proc. of 2nd Workshop on Radon Monitoring in Radioprotection, Trieste (1991) 532.

[5] Natsumoto, Regression Analysis for anamalous changes of ground water level due to earthquakes, Geoph. Res. Lett. 19 (1992) 1193.

[6] U. Facchini et al., Study on Radon Emission in a fault located in the Bergamasc Prealps, Atti Colloquio scientifico sulla protezione sismica (1993).

[7] M.M. Monnin and J.L. Seidel, Physical models related to radon emission in connection with dynamic manifestations in the upper terrestrial crust: a review, Radiation Measurements 28 (1997) 703.

[8] M. Singh et al., Radon in ground water related to seismic events, Radiation Measurements 30 (1999) 465.

[9] A. Amoruso et al., GIGS. The Interferometric Station at LNGS, LNGS Annual Reports 1997, 1998, 2001.

[10] F. Bella, W. Plastino et al., Tectonic deformation events and local seismicity in the Gran Sasso area of the Central Appennines, LNGS Annual Reports from 1997 to 2001.

[11] W. Plastino and F. Bella, Radon groundwater monitoring at underground Laboratory of Gran Sasso, Geophysical Research Lett. 28 (2001) 2675.

[12] F. Bella et al., Radiocarbon and Radon analysis for geophysical monitoring of Gran Sasso acquifer, LNGS Annual Report (2000) 187.
F. Bella et al., ENVARD, Radongroundwater analysis, LNGS Annual Report (2001) 233.

[13] Dobrovolsky et al., Estimation of the size of earthquake preparation zones, Pure and Appl. Geophys. 117 (1979) 1025.

[14] Istituto Nazionale di Geofisica e Vulcanologia, website: *http://www.ingv.it.*

TELLUS. Ground Deformations and their Effects in the near-Earth Space

V. Sgrigna[a], A. Buzzi[a], A. Cirella[a], L. Conti[a], V. Malvezzi[a]

[a] Dipartimento di Fisica, Universitá degli Studi di Roma "Roma Tre", Italy

The aim of the TELLUS (Telluric Emissions and Local Lithospheric Uppermost Strains) experiment is to carry out a continuous tilt monitoring at three tilt sites of LNGS in order to detect aseismic creep strain episodes associated with the earthquake preparation. Observations of numerous seismic precursors and consequent development of theoretical models on this subject aim at seeing in perspective the phenomenon "earthquake" within the framework of a unique theory able to explain the causes of its genesis, and the dynamics, rheology, and micro-physics of its preparation, occurrence, post-seismic relaxation, and inter-seismic phases. More in general, seismo-associated phenomena also include electromagnetic, acoustic and gas emissions from the Earth's surface which perturb the surrounding medium and can reach large distances up to the ionosphere and magnetosphere. Therefore, in our investigation of local deformation processes we also decided to include the study of possible electromagnetic perturbations and instabilities in the near-Earth space as a consequence of such local ground processes. In doing this, both ground monitoring, atmosphere radio-sounding and satellite EME wave and plasma observations are necessary. Two space missions (ARINA and ESPERIA) are under study. They have been described in the previous LNGS Annual Report 2002. ARINA experiment is devoted to measure particle precipitation from the Van Allen Radiation belt induced by seismo-electromagnetic perturbation in the lower magnetosphere. Within the framework of the PAMELA-ARINA collaboration, the ARINA detector will be installed on board of the RESURS-DK1 satellite of the Russian Space Agency which launch is scheduled for end year 2004. The scientific space mission ESPERIA (Earthquake investigation by Satellite and Physics of the Environment Related to the Ionosphere and Atmosphere) based on a low-orbit micro-satellite is planned with strong emphasis on coordinated ground-based and space observations. On board the satellite ULFHF electromagnetic fields, charged particle fluxes, and ionospheric plasma parameters will be detected. Simultaneous ground-based measurements of mechanical and electromagnetic fields will be carried out in several test areas one of which is the Central Apennines where an instrumental network is operational. The LNGS tilt sites constitute one point of this network. Then, the TELLUS experiment gives a contribution to a more general scientific project devoted to study ionospheric and magnetospheric perturbations caused by seismicity, and in particular, to develop a method to reveal short-term earthquake precursors.

The results obtained with regards to year 2003 consist of :

- a continuous ground tilt data collection at LNGS
- a model for propagation of electromagnetic preseismic emissions into the lithosphere and the atmophere
- development of magnetic sensors for ground based and space based measurements

Tiltmeters experimental apparatus

Tiltmeters are located at three different sites of the LNGS. In each site are installed two-component-tiltmeters with relative analog detecting and digital acquisition systems. Tilt sensors consist of horizontal-pendulum tiltmeters with Zöllner bifilar suspension realised in super Invar. The analog detecting system is constituted by an infrared laser beam and a 1024-photodiodes linear array of 0.5 inch long. The resolution is 0.05 mrad. The digital acquisition system allows the tilt data to be collected hourly. The tiltmeter apparatus is illustrated in figure (1).
The study of deformation processes related to earthquakes demands for a long time series of tilt data (a few years). For the period 1996-2000 results concerning aseismic creep strain episodes and their numerical modeling have been shown in the LNGS Annual Report 2001. Since then, a continuous tilt monitoring is in progress to perform a study on more recent seismo-associated phenomena.

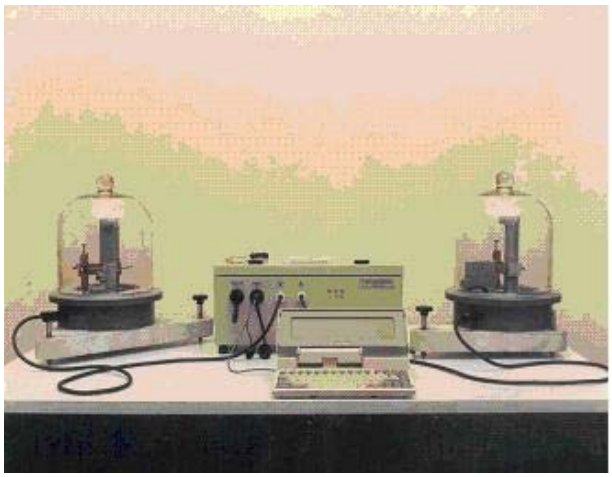

Figure 1: Ground tilt station consisting of two-component-horizontal-pendulum tiltmeters with Zöllner bifilar suspension, and relative analog detecting and digital acquisition systems.

Magnetic sensors development

During 2003 an instrumental activity has been carried out:

- to develop magnetic sensors for the magnetic field mapping at the ground surface

- to modify existing magnetometers for their application on board of satellites.

In particular a preliminary study has been carried out for realizing:

- a new magnetometer which allows to cover the whole frequency band actually covered by using two different instruments (flux-gate and search-coil ones (fig.2)
- a multi-probe system useful to detect electric and magnetic fields

We also designed and checked a digital acquisition system (fig.3)

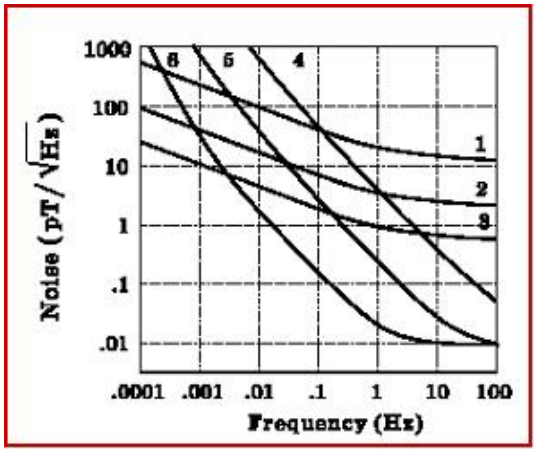

Figure 2: Threshold sensitivity for flux-gate magnetometer with core length from 15mm to 150 mm (curves 1,2,3) and low-frequency search-coil magnetometer with core length from 150mm to 1.5m (curves 4,5,6).

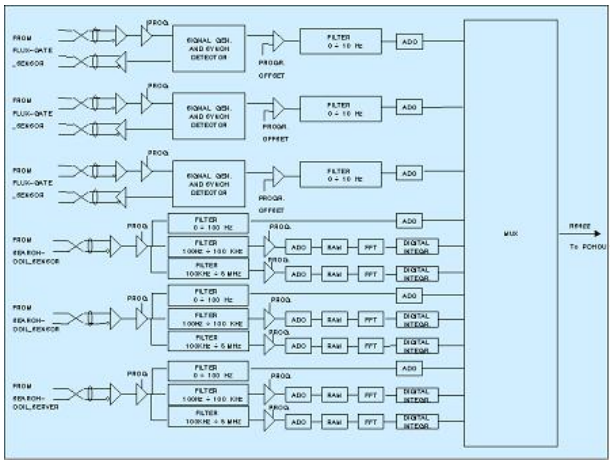

Figure 3: Digital acquisition system link between magnetic probes and PDHCU via RS422 interface.

Theoretical model for pre-earthquake electromagnetic waves propagation from the underground seismic source to the Earth's surface

Within the framework of the TELLUS project a model is proposed to describe the propagation of pre-seismic electromagnetic emissions from the preparation focal area to the near Earth space. Two seismoelectromagnetic sources have been considered. First one is a point-like source constituted by electric or magnetic oscillating dipoles with several orientations. In the second case a more realistic volumetric source, based on dilatancy models, has been taken into account. It is represented by a spatial distribution of elementary emitters filling the source volume. The model describes the propagation of electric and magnetic fields through layered lithospheric and atmospheric media with assigned vertical conductivity profiles. The lithospheric and atmospheric layering has been assumed on a realistic basis as well as the associated characteristic physical parametes. No limits have been applied a priori to the frequency spectrum of the electromagnetic source in order to determine the real attenuation of electromagnetic waves caused by the conductive layers. The model allows to determine the electric and magnetic fields in each layer.

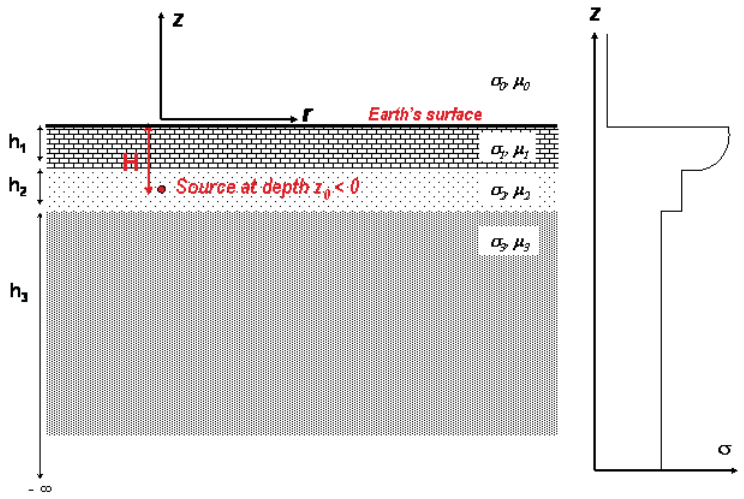

Figure 4: Stratified upper lithosphere with different conductivity layers.

– The upper lithosphere layering and the location of the earthquake preparation focal volume are defined from seismic data and assumed to be: $h_1 = 5km; h_2 = 10km, H = |z_0| = 10km$.

– The electric conductivity σ and magnetic permittivity μ are considered in two different cases:

- σ constant values but different for each layer;
- σ varying exponentially with depth.

– Displacement currents have been taken into account.

– Dilatancy preseismic source dimensions are defined as a function of the earthquake magnitude from the Dobrovolsky et al. (1989) model, and the volume shape is assumed to be ellipsoidal.

– Electric and magnetic fields have been obtained at any layer by applying the potential theory to the conductive stratified medium with appropriate gauge, initial, and boundary conditions.

Maxwell's equations:

$$\vec{\nabla} \wedge \vec{E}(\vec{R},t) = -\frac{\partial \vec{B}(\vec{R},t)}{\partial t} \qquad \vec{\nabla} \cdot \vec{B}(\vec{R},t) = 0$$
$$\vec{\nabla} \wedge \vec{H}(\vec{R},t) = \vec{J}(\vec{R},t) + \frac{\partial \vec{D}(\vec{R},t)}{\partial t} \qquad \vec{\nabla} \cdot \vec{D}(\vec{R},t) = 0$$

Scalar and vector potential:

$$\vec{B} = \vec{\nabla} \wedge \vec{A} \qquad \vec{E} = \vec{\nabla} \wedge \vec{A}$$
$$\vec{E} = -\frac{\partial \vec{A}}{\partial t} - \nabla\psi \qquad \vec{H} = \epsilon\frac{\partial \vec{A}}{\partial t} + \sigma\vec{A} - \nabla\psi$$

Fields and potentials are assumed to have an harmonic time dependency:

$$\vec{f}(\vec{R},t) = \vec{f_0}(\vec{R})e^{-i\omega t}$$

Wave equation in cylindrical coordinates is:

$$\frac{\partial^2 A_i}{\partial r^2} + \frac{1}{r}\frac{\partial A_i}{\partial r} + \frac{\partial^2 A_i}{\partial z^2} + k^2 A_i = 0$$

where $k^2 = i\omega\mu(\sigma - i\omega\epsilon) = i\omega\mu\sigma'$, and $\frac{\partial}{\partial\phi} = 0$.
If $A_i = U(r)V(z)$, then wave equation reduces to:

$$\frac{1}{U}\frac{d^2U}{dr^2} + \frac{1}{Ur}\frac{dU}{dr} + \frac{1}{V}\frac{d^2V}{dz^2} + k^2 = 0$$

Point-like source: the case of a single vertical oscillating electric dipole

Primary potential:

$$A_z^{(s)} = \mu p_0 \sigma \frac{e^{ikR}}{R} = \mu p_0 \sigma \int_0^\infty \frac{\lambda}{m} e^{-m|z+H|} J_0(\lambda r) d\lambda$$

where $m = \sqrt{\lambda^2 - i\omega\mu(\sigma - i\omega\epsilon}$ and p_0 is the dipole moment.
When $\sigma_1 = \sigma_e^{\beta(z+h_1)}$ and $\sigma_0 \neq \sigma_2 \neq \sigma_3 = const$:

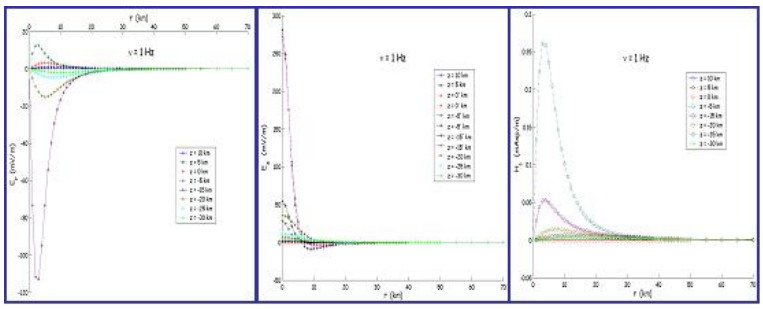

Figure 5: Electric and magnetic field components vs. r at different depths for an oscillating electric vertical dipole (p=10^4 C m). Conductivity values assumed for the upper lithosphere and atmosphere are: $\sigma_0 = 10^{-14}$ S/m, $\sigma_d = 10^{-2}$ S/m, $\sigma_2 = 10^{-3}$ S/m, $\sigma_3 = 210^{-4}$ S/m, and $\mu_0 = \mu_1 = \mu_2 = \mu_3 = 4\pi 10^{-7}$ h/m.

$$
\begin{aligned}
A_{z_0}(r,z,H) =& \mu_0 p_0 \sigma_2 \int_0^\infty C_0(\lambda) e^{-m_0 z} J_0(\lambda r) d\lambda \\
A_{z_1}(r,z,H) =& \mu_1 p_0 \sigma_2 \int_0^\infty \left[C_1(\lambda) J_{-\nu}(v) + C_1'(\lambda) J_\nu(v) \right] J_0(\lambda r) d\lambda \\
A_{z_2}(r,z,H) =& \mu_2 p_0 \sigma_2 \int_0^\infty \left[\frac{\lambda}{m_2} e^{-m_2|z+H|} + C_2(\lambda) e^{m_2(z+H)} + C_2'(\lambda) e^{-m_2(z+H)} \right] J_0(\lambda r) d\lambda \\
A_{z_3}(r,z,H) =& \mu_3 p_0 \sigma_2 \int_0^\infty C_3(\lambda) e^{m_3 z} J_0(\lambda r) d\lambda
\end{aligned}
$$

Volumetric source: the case of a distribution of vertical oscillating electric dipoles

Normalized distribution function:

$$
\rho(x_0, y_0, z_0) = \rho(r_0)\, \rho(z_0) = \frac{1}{4\pi} \frac{L_r^2}{\left(L_r^2 + r_0^2\right)^2} \cdot \frac{2L_z}{\pi} \frac{L_z^2}{\left(L_z^2 + z_0^2\right)^2}
$$

Primary potential:

$$
A^{(s)}(r', z') = p_0 \sigma \mu \int_\infty^0 d\lambda \frac{\lambda}{m} e^{\mp m z'} \left(\cos L_z m + L_z m \sin L_z m \right) \frac{\pi\, L_r}{2}\, \lambda\, K_1(L_r \lambda)\, J_0(\lambda r')
$$

Conclusions

Fields amplitudes calculated using our model are comparable with observations. The upper lithospheric layers behaves as a low-pass filter with cut-off frequency depending on the layer conductivity. The extension of the model to the ionospheric and magnetospheric layers is in progress.

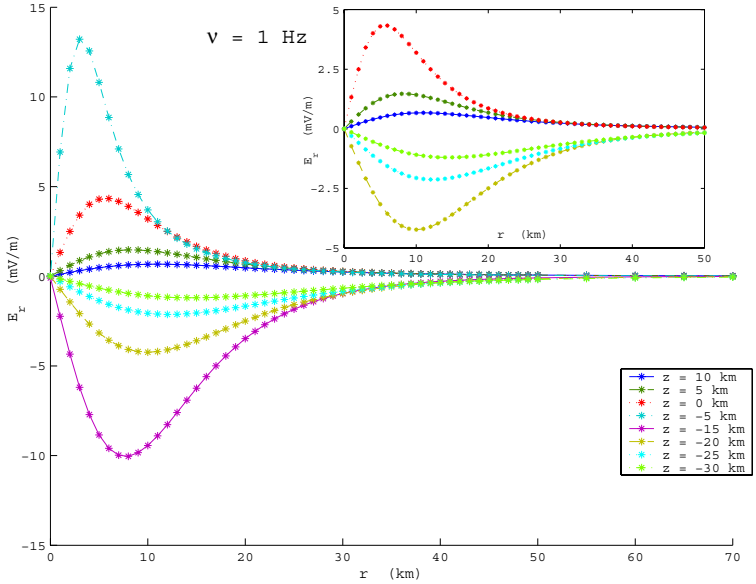

Figure 6: The case of a distribution of vertical oscillating electric dipoles: radial electric field component vs r at different depths

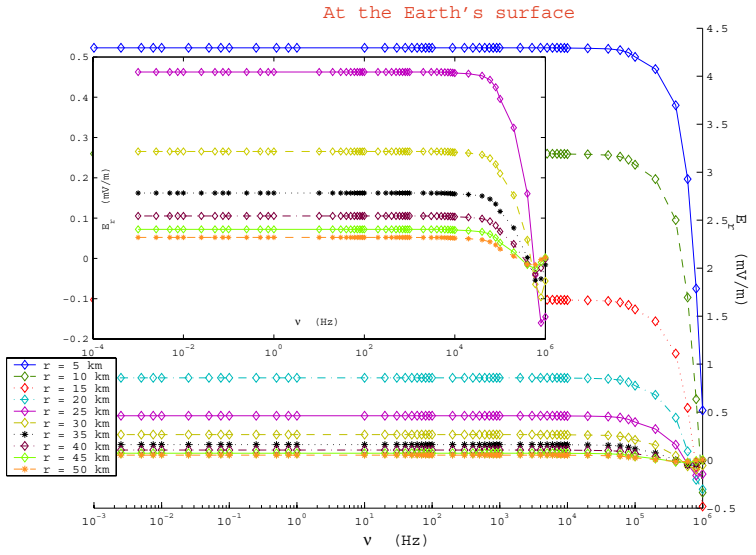

Figure 7: The case of a distribution of vertical oscillating electric dipoles: radial electric field spectrum at different distances for the source ($10^{-2} \leq \sigma \leq 10$ S/m)

References

[1] Sgrigna, V., Conti, L., Malvezzi, V., 2001. TELLUS. Ground deformations and their effects on the near-Earth space, Laboratori Nazionali del Gran Sasso, INFN, Annual report, 2001, pp.247-264.

[2] Sgrigna, V., Conti, L., Malvezzi, V., 2002. TELLUS. Ground deformations and their effects in the near-Earth space, Laboratori Nazionali del Gran sasso, INFN, Annual Report, 2002, pp. 217-232.

[3] Sgrigna, V., R.Console, L.Conti, A.M.Galper, V.Malvezzi, M.Parrot, P.Picozza, R.Scrimaglio, P.Spillantini and D.Zilpimiani, 2002. Natural and anthropogenic emissions from the earth's surface and their effects in the near earth space, Eur. Geophys. Soc.(EGS), EGS02-A-05730; ST068, Nice, France, p. 250.

[4] Sgrigna, V., Console, R., Conti, L., Galper, A., Malvezzi, V., Parrot. M., Picozza, P., Scrimaglio, R., Spillantini, P., Zilpimiani, D., 2002. Preseismic Natural Emissions from the Earth's Surface and their effects in the near Earth Space. A project for monitoring Earthquakes from Space, EOS Trans., AGU, vol. 83, T22B-10, n.19, S356.

[5] Conti, L., A. Buzzi, A.M.Galper, S.V.Koldashov, V.Malvezzi, M.Murashov, P.Picozza, R.Scrimaglio, V.Sgrigna, and L.Stagni, 2003. A Possible Correlation between Seismic Events and Trapped Particles Precipitation, Proc. ISEC2003 "Radiation Belt Science Meeting", September 2-5, 2003, Toulouse (France), p.45.

[6] Sgrigna V., R. Console, L. Conti, A.M. Galper, V. Malvezzi, M. Parrot, P. Picozza, R. Scrimaglio, P. Spillantini, D. Zilpimiani, 2003. The ESPERIA space project: a mission for monitoring preseismic emissions and anthropogenic effects in the near-Earth space, and for defoining the near-Earth magnetic environment, Proc. 2nd CHAMP Science Meeting, September 1-4, 2003, GeoForschungsZentrum, Potsdam, Germany, p 20.

[7] Sgrigna, V., L.Conti, V.Malvezzi, A.V.Guglielmi, and O.A.Pokhotelov, 2003.Electromagnetic Signals Produced by Elastic Waves in the Earth's Crust, Nuovo Cimento, C , submitted.

[8] Sgrigna, V., L.Carota, L.Conti, M.Corsi, A.Galper, V.Malvezzi, P.Picozza, R. Scrimaglio and L.Stagni, 2003. Temporal correlations between earthquakes and anomalous particle burst from SAMPEX/PET satellite observations, J. Geophys. Res., submitted.

[9] Sgrigna, V., Conti, L., Malvezzi, V., Picozza, P. et al.(ESPERIA Collaboration), 2003. The multi-instrument ESPERIA space mission, Nucl. Instr. Meth. Phys. Res. A, submitted.

[10] Sgrigna, V., Conti, L., Malvezzi, V., Picozza, P. et al.(ESPERIA Collaboration), 2003. Physics of the LEO ESPERIA satellite, J. Geodyn., submitted.

[11] Sgrigna, V., A. Buzzi, L. Conti, V.Malvezzi, P. Picozza, 2003. Study of seismo-associated phenomena from space, J. Indian Soc. Remote Sensing, submitted.

UNDERSEIS
Underground Seismic Array

M. Abril[a], G. Alguacil[a], W. De Cesare[b], C. Fischione[c], M. Martini[b], R. Muscente[d], P. Rotella[c], R. Scarpa[e], F. Tronca[d]

[a] Istituto Andaluz de Geofisica - Granada, Spain
[b] Osservatorio Vesuviano, INGV - Napoli, Italy
[c] Dipartimento di Fisica, Università dell'Aquila - Italy
[d] Parco Scientifico e Tecnologico d'Abruzzo - L'Aquila, Italy
[e] Dipartimento di Fisica, Università di Salerno - Italy

Abstract

This report describes a geophysical instrument under installation in the underground physics laboratories of Gran Sasso (LNGS-INFN), located in the seismic zone of central Apennines, Italy. This instrument is aimed to monitor seismic radiation with very high sensitivity; it is a small aperture seismic array composed by 20 three-components short period seismomenters (Mark L4C-3D). The installation started in May 2002 and will be completed during 2004.

1 Introduction

The physics of earthquakes is based on the measurements of radiated seismic waves and ground displacement associated with this phenomena. The inertial pendulum is the oldest and most diffused instrument used to measure the main features of seismic waves. The advantages of this instrument are the simplicity of the theory, the high sensitivity, the robust design and the simple calibration methods, in spite of the quite reduced frequency band and linearity (Wielandt, 1983). Other instruments based on different physical principles, such as strainmeters and gyroscopes, are only partially used by seismologists (Benioff, 1935; Farrell, 1969, Aki and Richards, 1980). Networks of short period seismometers are as far the most diffused system to monitor local and regional seismicity (Lee and Stewart, 1981). Broad-band instruments make up a powerful system to study the details of seismic sources and also to study large earthquakes at global scale (Lee and Wallace, 1995). Moreover arrays of seismometers and accelerometers are used to study the details of sources and radiation patterns of earthquakes, nuclear underground explosions and volcanic activity (Bolt, 1976; Chouet, 1996). Strainmeters and tiltmeters (Agnew, 1986) are used to study the lower frequencies radiated from seismic sources and allow to detect

slow earthquakes and strain steps (i.e. anelastic deformations around seismic sources). At present, the seismic activity of central Apennines, and in particular of the Gran Sasso massif, is relatively low, as compared to other seismically active areas of Europe such as Turkey or central Greece. Three seismic swarms were monitored in August 1992, June 1994 and October 1996, with the largest earthquake having $M_L = 4.2$. These swarms are the largest events occurred since 1985 in this region. However, this area experienced destructive earthquakes in the past: a magnitude 7 event occurred in 1703. Close to this region, the 1915 Avezzano earthquake ($M_S = 6.8$) occurred, causing more than 15,000 victims. On average, about 1 microearthquake per day above $M_L = 1$ occurs, within 20 Km radius from LNGS-INFN. The facilities existing in the laboratories, and the seismotectonics features of the Gran Sasso massif, make them an excellent site for studies related to the physics of earthquake source, wave propagation in a complex medium and seismic monitoring.

2 The Underground Seismic Array

A seismic array is a set of seismographs distributed over an area of the Earth's surface at spacing narrow enough so that the signal waveform may be correlated between adjacent seismometers (Aki and Richards, 1980).

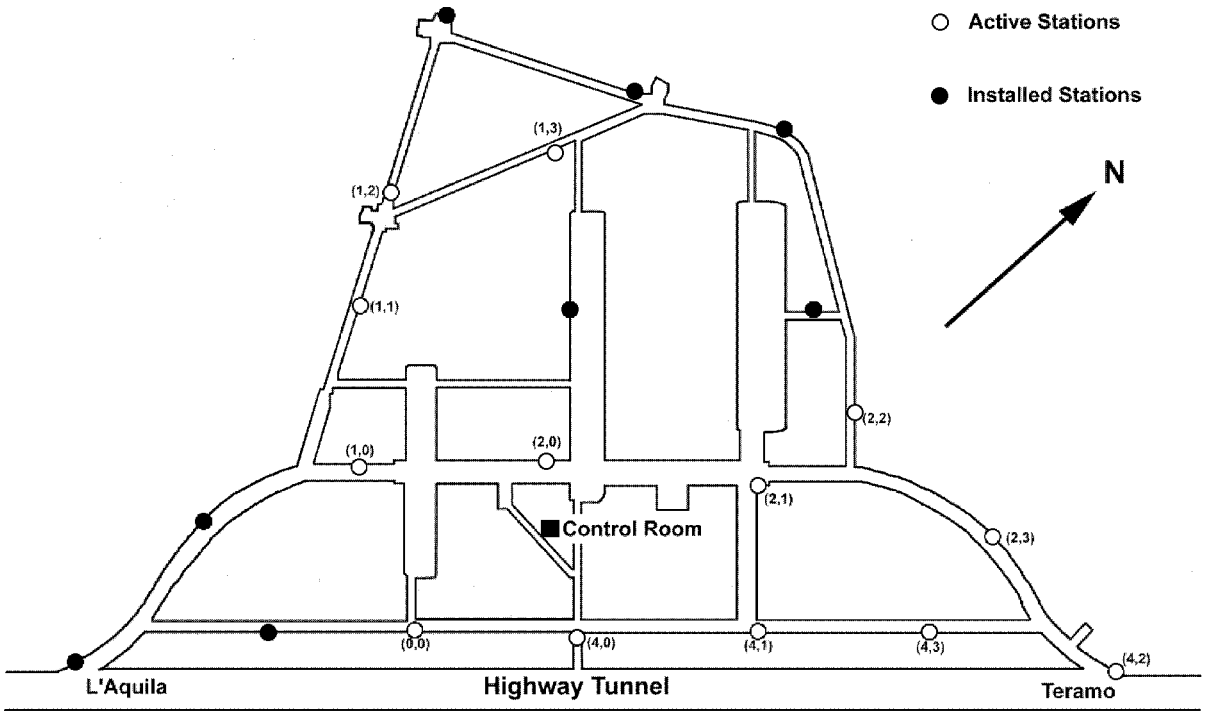

Figure 1: Map of the Underground Seismic Array. The notation (n,m) shows the line number (n) and the station number (m).

The main advantages of such geometrical configurations are the improvement of signal-

to-noise ratio and the possibility to perform a detailed analysis of wave propagation and composition. The development of large aperture seismic arrays such as LASA in Montana, USA (Green et al., 1965) and NORSAR in Norway (Kedrov and Ovtchinnikov, 1990) led to many improvements in the knowledge of Earth's structure (Aki et al., 1977) other than to monitor underground nuclear explosions. More recent developments of these arrays make use of low number of sensors and smaller apertures in order to reduce the effects of lateral inhomogeneities (Mykkeltveit, 1985). The need to monitor local seismicity in the very large underground physics laboratories of LNGS-INFN led to some preliminary experiments to understand the site response; a L-shaped array along the way to access the LNGS, having spatial extension of 10.5 km, was deployed in 1993. This array was formed by 17 three component short period digital seismic stations spaced 600 m (De Luca et al., 1997). In the same region, from 1992 to 2001, a digital seismic network equipped with a maximum of 18 3D short period seismic stations was installed.

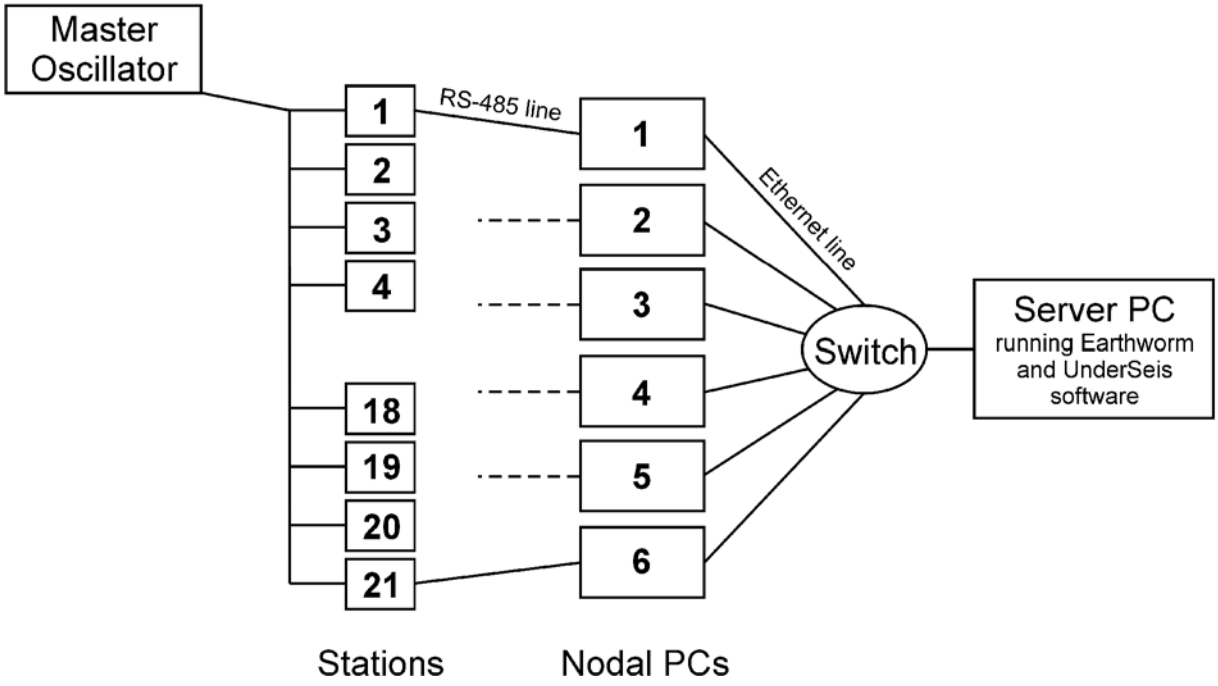

Figure 2: Block scheme of the Underground Seismic Array.

Two important features of seismic response in the region have been observed: a substantial homogeneity of spectral response from underground linear array and, for S waves, an average decrease of amplitudes with respect to the data recorded at the surface, in the band 1-8 Hz. In particular the horizontal components are reduced by a factor 4, while the vertical one is reduced by a factor 2. Strain monitoring, in the same region, through GPS, EDM, levellings and microgravimetry has been also carried out. The optimal array configuration is generally obtained through a compromise between the need of sampling coherent portions of wavefield and the need for adequate azimuthal resolution, which requires a large antenna aperture. However we were limited by the geometry of the underground laboratories, so we decided to start with 21 receivers. In consequence, the

underground seismic array has a small aperture (400 m x 600 m) and the average spacing between the short period seismographs is about 90 m (Fig. 1), thus allowing to resolve wavelenghts in the range $180 - 500m$ which correspond to phase velocity $0.2 - 10\frac{km}{sec}$ (the frequency response is in the range $1 - 20Hz$).

Figure 3: Underground Seismic Array components and control room.

At present, we have completely developed the electronics and the data acquisition system, which constitute an original project. The installation started in May 2002 and will be completed during 2004. Each seismometer is linked, through a 24 bits A/D board, to an industrial PC which is, in its turn, connected to a serial communication line via a RS-485 standard. The PCs placed at the head of each serial line (nodal PCs) transmit data to a server through an ethernet network. Time syncronization is provided by a Master Oscillator controlled by an atomic clock (Fig. 4). Earthworm package is used for real time data processing and transmission. High quality data have been recorded since May 2002, including local and regional earthquakes. In particular the 31 October, 2002, Molise ($M_W = 5.8$ earthquake) and its aftershocks have been recorded at this array. Array

techniques such as polarization and frequency-slowness analyses with the ZLCC algorithm indicate the high performance of this array, as compared to the national seismic network, for analyzing the main source parameters of earthquakes located up to distances of few hundreds of km.

Figure 4: The Underground Array seismic stations acquire data simultaneously. The time syncronization is controlled by a Master Oscillator: it takes a 1 pps input signal from an atomic clock located in the labs and generates codified time signals which are send to the single stations in order to provide simultaneous data acquisition.

3 Preliminary data analysis.

3.1 Polarization analysis Molise earthquake, ($M_W = 5.8$) October 31, 2002.

A preliminary polarization analysis was performed on data from the Molise October 31 mainshock (only 4 stations active at the moment). The location results are in good agreement with the National network location.

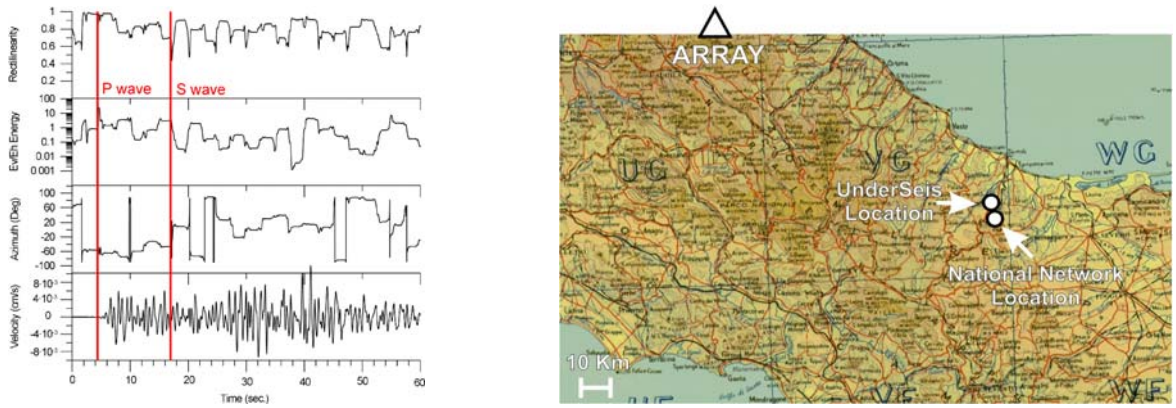

Figure 5: Polarization analysis results and location map.

3.2 ZLCC analysis local earthquake, ($M = 2.4$) November 20, 2002.

A preliminary ZLCC analysis was performed on data from a local earthquake, November 20, 2002 (13 stations active at the moment). The location results are in good agreement with the National network location.

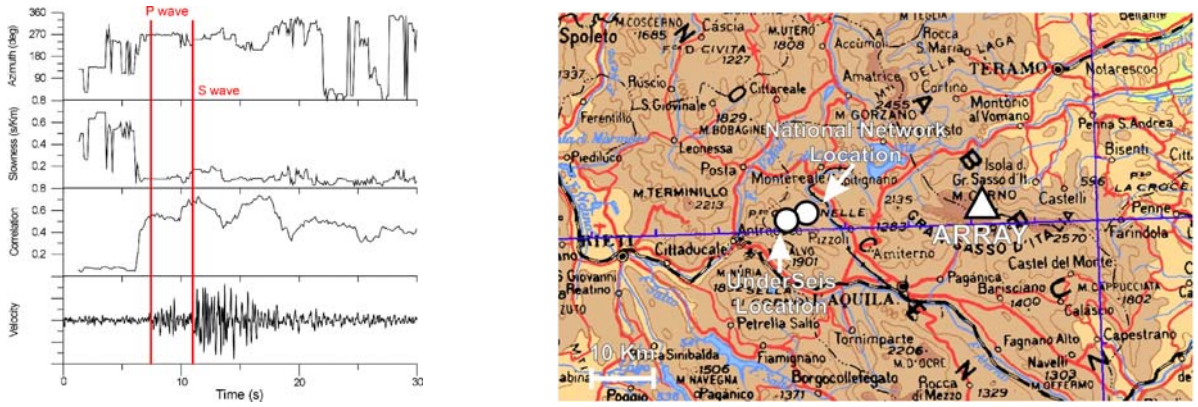

Figure 6: ZLCC analysis results and location map.

4 Conclusions.

The dense small-aperture seismic array is a powerful high-sensitivity instrument designed and presently under realization and installation. The underground location beneath Gran Sasso has been proved to be an ideal site, in spite of the local noise sources due to human activity, to record seismic waves from regional and local microearthquakes. Its location is rather unique in the world, due to the close distance from active fault segments of the seismogenetic zone of central Apennines. The scientific goals of this multichannel seismic observational system are an improvement of the seismotectonical knowledge of a high potential seismogenetic region of Italy, and a very detailed study of the physical processes leading to seismic ruptures in the area. Moreover the installation of this underground seismic array will allow an experimental study of wave propagation phenomena within a complex medium, leading to results of relevant interest for seismic hazard evaluation in areas of complex geology, for physics of earthquake process, with particular reference to the study of rupture preparation and for all relevant precursory phenomena, seismic radiation and earthquake waveform modeling for hazard reduction.

References

[1] Agnew D. C., 1986. *Strainmeters and tiltmeters*. Rev. Geophys. 24, 579-624.

[2] Aki K. and Richards P., 1980. *Quantitative seismology: Theory and methods*. Freeman, San Francisco, California, 932 pp.

[3] Aki K., Christoffersson A. and Husebye E. S., 1977. *Determination of the three dimensional seismic structure of the lithosphere*. J. Geophys. Res. 82, 277-296.

[4] Benioff H., 1935. *A linear strain seismographs*. Bull. Seism. Soc. Am. 25, 283-309.

[5] Bolt B. A., 1976. *Nuclear explosions and earthquakes. The parted veil*. Freeman, San Francisco.

[6] Capon J., 1969. *High resolution frequency-wavenumber spectrum analysis*. Proc. IEEE 57, 1408-1418.

[7] Chouet B., 1996. *New methods and future trends in seismological volcano monitoring*. In "Monitoring and mitigation of volcano hazards", R. Scarpa and R. Tilling (Eds.), Springer-Verlag, New York.

[8] Chouet B., G. Saccorotti, M. Martini, P. Dawson, G. De Luca, G. Milana and R. Scarpa (1997). *Source and path effects in the wavefields of tremar and explosions at Stromboli Volcano, Italy*. J. Geophys. Res., 102, 15,129-15,150.

[9] De Luca G., Scarpa R., Del Pezzo E. and Simini M., 1997. *Shallow structure of Mt. Vesuvius volcano, Italy, from seismic array analysis*. Geophys. Res. Lett. 24,481-484.

[10] De Luca G., Del Pezzo E., Di Luccio F., Margheriti L., Milana G. and Scarpa R., 1998. *Site response study in Abruzzo (centraI Italy): underground array versus surface stations*. J. Seismol., 2, 223-226.

[11] Farrell W. E., 1969. *A gyroscopic seismometer: measurements during the Borrego earthquake*. Bull. Seism. Soc. Am. 59, 1239-1245.

[12] Green Jr., Frosh B. A. and Romney C. F., 1965. *Principles of an experimental large aperture seismic array*. Proc. IEEE 53, 1821-1833.

[13] Kedrov O. K. and V. M. Ovtchinnikov, 1990. *An on-line analysis system for three component seismic data: method and preliminary results*. Bull. Seism. Soc. Am. 80, 2053-2071.

[14] Lee W. H. K. and Stewart S. W., 1981. *Principles and applications of microearthquake networks*. Academic Press, New York, 293 pp.

[15] Lay T. and Wallace T. C., 1995. *Modern Global Seismology*. Academic Press, New York, 517 pp.

[16] Mikkeltveit S., 1985. *A new regional array in Norway: design, work and results from analysis of data from a provisional installation, in The Vela Program*. A twenty- Five Review of Basic Research, edited by U. A. Kerr (Defence Advanced Research Project Agency), 546-553.

[17] Milana G., Barba S., Del Pezzo E. and Zambonelli E., 1996. *Site response from ambient noise measurements: new perspectives from an array study in CentraI Italy.* Bull. Seism. Soc. Am. 86, 1-9.

[18] Schmidt R. O., 1986. *Multiple emitter location and signal parameter estimation.* IEEE Trans Antennas Propagation 34, 276-280.

[19] Wielandt E., 1983. *Design principles of electronic inertial seismometers.* In H. Kanamori and E. Boschi (Eds.) "Earthquakes: Observation, Theory and Interpretation". Proc. Int. School of Phys. "E. Fermi", North Holland, Amsterdam.